POLYMER NANOCOMPOSITES FOR PHTHALATE DETECTION, REMEDIATION AND METAMATERIAL APPLICATIONS

Thesis submitted to
the University of Calicut for the partial fulfillment of
the requirements for the award of the degree of

DOCTOR OF PHILOSOPHY IN PHYSICS

Under the faculty of science

by

ANJU. K

\

DEPARTMENT OF PHYSICS
UNIVERSITY OF CALICUT
KERALA, INDIA 673635

JULY 2024

POLYMER NANOCOMPOSITES FOR PHTHALATE DETECTION, REMEDIATION AND METAMATERIAL APPLICATIONS.

Ph.D. Thesis in Physics

Author:

ANJU. K
Department of Physics
University of Calicut
Calicut University (P.O)
673635, Kerala, India
Email: abhanjanak@gmail.com

Under the guidance of

Dr. Libu K. Alexander
Associate Professor
Department of Physics
University of Calicut
Calicut University (P.O)
673635, Kerala, India
Email: lka@uoc.ac.in

Dr. Libu K. Alexander
Associate Professor
Department of Physics

Calicut University (P.O)
673635, Kerala, India
+919446376861 (M)
Email: lka@uoc.ac.in

CERTIFICATE

Certified that the work presented in the thesis, entitled **"POLYMER NANOCOMPOSITES FOR PHTHALATE DETECTION, REMEDIATION AND METAMATERIAL APPLICATIONS"** is based on the authentic record of research carried out by **Ms. ANJU. K** under my guidance in Department of Physics, University of Calicut, Calicut University (P.O), Kerala-673635 and this work has not been included in any other thesis submitted previously for the award of any degree.

Calicut University
11 July 2024

Dr. Libu K. Alexander

Dr. Libu K. Alexander
Associate Professor
Department of Physics

Calicut University (P.O)
673635, Kerala, India
+919446376861 (M)
Email: lka@uoc.ac.in

CERTIFICATE

Certified that the work presented in the thesis, entitled **“POLYMER NANOCOMPOSITES FOR PHTHALATE DETECTION, REMEDIATION AND METAMATERIAL APPLICATIONS”** is based on the authentic record of research carried out by **Ms. ANJU. K** under my guidance in Department of Physics, University of Calicut, Calicut University (P.O), Kerala-673635 and this work has not been included in any other thesis submitted previously for the award of any degree. Also certified that the corrections suggested by the adjudicators have been incorporated in the revised thesis.

Calicut University
05 June 2025

Dr. Libu K. Alexander

DECLARATION

Certified that the work presented in this thesis, entitled **“POLYMER NANOCOMPOSITES FOR PHTHALATE DETECTION, REMEDIATION AND METAMATERIAL APPLICATIONS”** is based on the original research work done by me under the supervision and guidance of Dr. Libu K. Alexander, Associate Professor, Department of Physics, University of Calicut, Calicut university (P.O), Kerala-673635 and has not been included in any other thesis submitted previously for the award of any degree. The contents of the thesis are undergone plagiarism check using iThenticate software at C.H.M.K. Library, University of Calicut, and the similarity index found within the permissible limit. I also declare that the thesis is free from AI generated contents.

Calicut University
11 July 2024

ANJU. K

ACKNOWLEDGEMENT

I find it difficult to express in writing the depth of my thankfulness, affection, and admiration for the incredible individuals in my life who have played a crucial role in bringing my Ph.D. thesis to life. I am fortunate to have been surrounded by numerous exceptional individuals who have woven a tapestry of affection, concern, and assistance around me. The journey to reach this point of acknowledgment would have been significantly more challenging without their presence.

At the outset, I want to convey my profound appreciation and affection towards my mentor, Dr. Libu K. Alexander. Throughout the various phases of my work, he has consistently shown immense care, creative assistance, and unwavering attention to detail. His thoughtful and innovative approach to thinking has played a pivotal role in shaping the concepts presented in this thesis. I am sincerely grateful for his continuous motivation and assistance, which played a vital role in successfully bringing this research to fruition. I am always surprised with his extraordinary ability to think outside the box has not only driven innovative approaches but also transformed complex results into elegant solutions. Working with him has been an immensely gratifying experience that has enriched my understanding and knowledge. His effective guidance and unwavering support have consistently steered me towards professionalism and ethical conduct, especially during challenging periods.

I would like to extend my special acknowledgments to Dr. Muhammed Shahin Thayyil, the Head of the Department of Physics at the University of Calicut, for giving me the opportunity to carry out BDS analysis in his laboratory. His support and generosity in providing access to the lab facilities are deeply appreciated. Along with former department heads Dr. M.M Musthafa, Dr. P.P Pradyumnan, Dr. A.M Vinodkumar and Dr. C.D Ravikumar. Their assistance in providing essential resources during my Ph.D. program is highly appreciated. Additionally, I offer my sincere gratitude to the current faculty members of our department for their support. I am forever indebted to all my former teachers as they built the foundation for this achievement. Especially, it gives me immense pleasure to acknowledge professor Dr. Vishnu Mayya Bannur, former and Dr. Antony Joseph *former Faculties at Department of Physics, University of Calicut, my beloved teachers during My M. Sc period. I am immensely grateful for their invaluable academic guidance and hold them in high esteem for their unmatched kindness. I take immense delight in recognizing the swift and efficient assistance provided by the non-teaching personnel in our department. I extend my regards to both the current and past administrative staff and the department's Librarian for their timely assistance.*

I wish to express my deep appreciation to CSIF at the University of Calicut, STIC Cochin, Karunya Institute of Technology in Tamil Nadu, the Department of Chemistry at the University of Calicut, and the Department of Nanoscience and Technology for conducting the essential analyses for my research project. I also acknowledge the financial assistance received from University of Calicut.

My most sincere and heartiest thanks go to my esteemed seniors: Dr. Vidyarajan N, Dr. Ahammed Raseen Nnnakkal and Dr. Bintu Thomas. The friendly and lovable atmosphere I received from my groupmates, namely Sravandas P, Reeja G. Nair and Aruna U, overwhelmed me. Beyond the words I express my deepest love from the bottom of my heart to my brother, Sravandas for his care, love and holding my hands during my up and downs. I would also grateful to the care and support provided by my M. Phil and M. Sc project students in our group for contributing to a positive laboratory environment.

I found myself at a loss for words as I began this paragraph. My appreciation and love run deep for my dear friends within my department, and I must give special mention to Ntthu Ashok, Sanila, Nicemon Thomas, Prasanth, Seban, Jemshihas, Hajara, Salma, Usha, Vinod K.T, Shabeeba P, Mohammed shan and Mohammed Shabeer for their invaluable support, love and care. I also want to express my gratitude to Parvathi P and Vineetha V S for their joy, enthusiasm, love, and care were a constant source of inspiration for me. I look back with a joyful smile on every moment spent with them, and these cherished memories will always remain vivid in my heart. Words fall short in capturing the depth of my love and fondness for my close friends, Varsha Raveendran P T, Aswin, Sreelakshmi, Manu, Nabeela, Divya, Aswathi and Lijesh. They have been a steady pillar of support, love, and care in my life since my school days.

"My family is my life, and everything else comes second as far as what's important to me" My dear family and beloved parents, words cannot fully convey

the depth of love and gratitude I hold in my heart for all of you. You are the pillars of my life, the ones who have stood by me through thick and thin, and your unwavering support means the world to me. Your sacrifices, guidance, and unconditional love have shaped me into the person I am today, and I am eternally grateful. Each day, I cherish the moments we share, and I am committed to making you proud. Please know that my love for you knows no bounds, and I am here for you, just as you have always been there for me. Thank you for being my rock and the source of endless warmth and comfort in my life. I present this thesis as a tribute to them, especially my ***'AMMA'****, to whom I owe a profound debt of gratitude. Her unwavering support, warmth, and fortitude have empowered me to pursue my aspirations. Words are insufficient to capture my appreciation for her. My* ***'ACHA'****, a paragon of honesty, dedication, and selflessness, has been my foremost mentor. I express my gratitude to my father for always standing steadfastly beside me and for instilling trust and confidence in my journey. I wish to express my deep fondness love and care for my younger sister,* ***'KUNJATTA'*** *(Arunaja), for her unwavering support and affection. She is my dearest friend, and a true angel who appears when I need her most. The continuous love and care from my family, have been pivotal in accomplishing this task in the manner it has been achieved.*

Verbal expressions fall short in adequately conveying the depth of my love and affection for a truly exceptional person in my life, my soulmate, friend and life partner, ***Vishnu****. His boundless love, patience, support, care, and steadfast belief in me, played an integral role in the successful culmination of my thesis.*

To my little one **Praan V Niranj,** *As I wrote these pages, you kicked gently within me, reminding me that life, in all its beauty, was unfolding both on paper and within my womb. This thesis is not just mine it carries the heartbeat of our shared resilience, late nights, quiet prayers, and deep love. One day, even before your first breath, you inspired me to finish what I started.*

I consider myself fortunate to have been welcomed into the family of two genuinely affectionate individuals. The love, backing, and motivation extended by my mother-in-law and father-in-law are deeply cherished. While some may not have been specifically named, no one has been left out of remembrance.

I humbly offer everything at the feet of the Almighty.

Anju. K

Dedicated to

Achan and Amma
For their infinite love, steadfast support,
and continual encouragement.

CONTENTS

LIST OF TABLES

LIST OF FIGURES

LIST OF SCHEMES

ABBREVIATIONS

PNC	Polymer Nanocomposutes
PCB	Polychlorinated Biphenyles
MOF	Metal Organic Framework
EMI	Electromagnetic Interference
RF	Radio Frequency
MW	Microwave
DMP	Dimethyl Phthalate
DEP	Diethyl Phthalate
DBP	Bibutyl Phthalate
DEHP	Di (2-Ethylhexyl) Phthalate
GC-MS	Gas Chromatography-Mass Spectrometry
HPLC	High Performance Liquid Chromatography
ELISA	Enzyme- Linked Immunosorbent Assay
CE	Capillary Electrophoresis
SERS	Surface Enhanced Raman Spectroscopy
EF	Enhancement Factor
EM	Electromagnetic Enhancement
CM	Chemical Enhancement
LSPR	Localised Surface Plasmon Resonance
AOP	Advanced Oxidation Process
UV	Ultra Violet
MF	Microfiltration

UF	Ultrafiltration
RO	Reverse Osmosis
ELF	Extremely Low Frequency
XRD	X-Ray Diffraction Analysis (Xrd)
FESEM	Field Emission Scanning Electron Microscope (Fesem)
BET	Brunauer-Emett-Teller (Bet) Technique
BDS	Broadband Dielectric Spectroscopy (Bds)
UV-VIS &DRS	Ultraviolet-Visible Diffuse Reflectance Spectroscopy
PMMA	Polymethyl Methacrylate
$BaTiO_3$	Barium Titanate
BT	Barium Titanate
PMMA_BT	Polymethyl Methacrylate_ Barium Titanate
PBT	PMMA_BT Film
ST	Strontium Titanate
$SrTiO_3$	Strontium Titanate
PMMA_ST	Polymethyl Methacrylate_ Strontium Titanate
PST	PMMA_ST Film
EPA	Environmental Protection Agency
PPy	Polypyrrole
ZnO	Zinc Oxide
PPy _ ZnO	Polypyrrole_Zinc Oxide Composite
PAE	Phthalic Acid Ester
AC	Activated Carbon
G	Graphite

PMMA_ZnO_AC	Polymethyl Methacrylate_Zinc Oxide_Activated Carbon Composite System
PMMA_$CaTiO_3$_GRAPHITE	Polymethyl Methacrylate_Calcium Titanate_Graphite Composite System
PZA	Polymethyl Methacrylate_Zinc Oxide_Activated Carbon Composite System
PCG	Polymethyl Methacrylate_Calcium Titanate_Graphite Composite System

PUBLICATIONS

International Journals/Proceedings (Published/Communicated):

1. *'Extremely low frequency plasmonic state achieved in AC-ZnO polymer composite for tuned negative permittivity applications.'*, Anju K and Libu K. Alexander, *Materials Research Bulletin 172 (2024) 112649.*
2. *'BaTiO$_3$ SERS substrate for Dimethyl phthalate detection.'*, Anju K, K. Roopitha and L. K. Alexander, *Materials Today: Proceedings 46 (2021) 3044-3050.*
3. *'Surface-engineered flexible PMMA-SrTiO$_3$ as a SERS substrate for ultrasensitive detection of Di(2-ethylhexyl) phthalate.',* Anju K and Libu K. Alexander, *Composites Communications (Under Review/Accepted).*
4. *'A novel polymer nanocomposite system for rapid Dimethyl phthalate toxicity removal.',* Anju K and Libu K. Alexander, *Polymer Bulletin (2025) 82:147–163.*
5. *'Polymer Based noble metal free SERS substrates for Diethyl phthalate detection.'*, Anju K and L. K. Alexander, *Proceedings book: ISBN 978-81-950313-5-1 (AMALIT-2022).*
6. *'Removal of plasticizer from water by polymer-based nanocomposites.'*, K. Anju and L. K. Alexander, *Proceedings book: ISBN NO: 978-81-942768-0-7 (2020, KSCSTE).*
7. *'Polymer metal oxide nanocomposites as active materials for energy storage application.'* K. Anju and L. K. Alexander, *Proceedings book (ICSEA-2019 C-MET).*

Papers presented in International/National conferences

1. *‘Polymer based nanocomposites for advanced chemical sensors*.’ K. Anju and L. K. Alexander, in the Indian Nanoelectronics Users Program Centre for Nano Science and Engineering (CeNSE), IISc. Bangalore, on 28-30 November 2017.

2. *‘Polymers for solar cell applications*.’, K. Anju and L. K. Alexander, in the international monsoon course on polymer and hybrid electronics: Physics and device applications. (GIAN) organized by NIT Calicut,

3. *‘Polymer metal oxide nanocomposites as active materials for energy storage application.’* K. Anju and L. K. Alexander, in the international conference on Supercapacitors, Energy storage and Applications (ICSEA-2019), organized by Centre for Materials for Electronics Technology (C-MET), Govt. of India, 8-10 March 2019.

4. *‘Polymer Based noble metal free SERS substrates for Diethyl phthalate detection.’*, Anju K and L. K. Alexander, in the 32nd Kerala Science Congress organized by KSCSTE, Government of Kerala held at Yuvakshetra Institute of Management Studies, Mundur, Palakkad, Kerala, India on 25-27 January 2020.

5. *BaTiO3 SERS substrate for Dimethyl phthalate detection.*’, Anju K, K. Roopitha and L. K. Alexander, in the International Conference on Advances in Material Science and Chemistry (ICAMSC-2020), organized by Department of Chemistry, Amrita Vishwa Vidyapeetham, Amritapuri campus, Kerala on 10-12 August 2020.

6. *‘Polymer Based noble metal free SERS substrates for Diethyl phthalate detection.’*, Anju K and L. K. Alexander, in the international conference on The New Normal: Crisis Resilience and Re-Invention (AMALIT 2022) organized by Amal college of advanced studies, Nilambur on 15-17 February 2022.

7. *‘Polymer-based noble metal-free SERS substrates for Diethyl Phthalate Detection.’,* Anju K and L. K. Alexander, in the 7th International Conference on Nanoscience and Nanotechnology (ICONN-2023), organized by SRM Institute of Science and Technology, Kattankulathur - 603 203, Tamil Nadu, India on March 27 - 29, 2023.

ABSTRACT

The thesis, titled ***"Polymer Nanocomposites for Phthalate Detection, Remediation, and Metamaterial Applications,"*** is a product of our strong motivation to expand the structure-defining capabilities of polymers for environmental and dielectric applications. The central objective was to address phthalate detection and remediation issues and fill critical gaps in metamaterial technology for extremely low-frequency applications. The thesis comprises eight chapters, beginning with an introductory overview in Chapter 1 and an overview of experimental techniques in Chapter 2. Chapters 3 to 7 are working chapters, presenting findings and conclusions. Chapter 8 provides a comprehensive summary, and Chapter 9 gives our recommendations for future research works on the thesis topic.

One of the significant advancements made in this thesis is phthalate detection using flexible noble metal-free SERS substrates. The substrates based on $BaTiO_3$, PMMA_$BaTiO_3$, and PMMA_$SrTiO_3$ have been engineered and customized to detect dimethyl phthalate (DMP), diethyl phthalate (DEP), and Di(2-ethylhexyl) phthalate (DEHP), respectively. Innovative synthesis methods, combining modified low-temperature sol-gel routes with in-situ polymerization, produced substrates with the essential "hotspots" for amplifying Raman signals. Microstructuring within the substrates facilitates the trapping of probe molecules and enhances charge transfer-mediated chemical enhancement in Raman signals. The findings underscore the substrates' ability to detect accurately without spectral interference, essential for differentiating between substrate and probe molecules.

In the realm of water remediation, this thesis focuses on removing Dimethyl Phthalate (DMP) using Zinc Oxide-incorporated Polypyrrole (PPy_ZnO) polymer nanocomposites synthesized via oxidative polymerization. The structural integrity, cooperative effect of slit-like micropores and the conjugated benzene rings of

PPy_ZnO led to effective removal of DMP across a wide range of concentrations in aquatic environments.

In the domain of metamaterial applications, this research addresses the gap in metamaterials suitable for the extremely low-frequency regime. Two ternary composites were crafted by integrating a PMMA matrix with two distinct filler combinations: AC_ZnO and Graphite_$CaTiO_3$. Microstructuring mediated by the PMMA voids beyond the percolation threshold facilitated the formation of interconnected 3D conducting networks, enabling the transition to negative permittivity. Interestingly, replacing metallic fillers with ceramic counterparts drastically changes the order of magnitude of permittivity values from 10^4 to 10^8. The selection of filler candidates and their concentrations played a crucial role in fine-tuning negative permittivity for the ELF regime.

In summary, this thesis has made scientific contributions to managing environmental pollutants through their detection and removal. Also, it could effectively place a nanocomposite, which could fill the need for metamaterials working in the ELF regime- catering to communication technologies. For its social significance, the developed composites and their scientific understanding contribute to sustainable development goals by promoting cleaner environments and safer living conditions, aligning with global efforts to mitigate pollution and enhance technological capabilities for societal benefit.

Keywords: Polymer Nanocomposites, Phthalate, SERS, Adsorption, Metamaterial, Extremely Low Frequency.

സംഗ്രഹം

"പോളിമർ നാനോകോമ്പോസിറ്റുകൾ ഉപയോഗിച്ച് താലേറ്റ് മലിനീകരണത്തിൻ്റെ അതിസൂക്ഷ്മ കണ്ടെത്തലും നീക്കം ചെയ്യലും കൂടാതെ മെറ്റാമെറ്റീരിയൽ പ്രയോഗങ്ങളും” എന്നതാണു ഈ ഗവേഷണപ്രബന്ധത്തിൻ്റെ തലക്കെട്ട്. പോളിമെറുകൾക്ക് പങ്ക്ചേരുന്ന നാനോകോമ്പോസിറ്റുകളുടെ ഘടനയെ നിർമ്മിക്കാനുള്ള പ്രത്യേകവും സവിശേഷവുമായ ശേഷിയെ പരിസ്ഥികമോ ഡൈഇലക്ട്രിക് പ്രയോഗങ്ങൾക്കായോ ഉപയോഗപെടുത്തുക എന്ന ഞങ്ങളുടെ ദീപ്തമായ പ്രചോദനത്തിൻ്റെ അനന്തരഫലമാണു ഈ പ്രബന്ധം. അധ്യായം 1-ലെ ആമുഖ അവലോകനവും അധ്യായം 2-ലെ പരീക്ഷണാത്മക സാങ്കേതിക വിദ്യകളുടെ അവലോകനവും തുടങ്ങി ഒമ്പത് അധ്യായങ്ങൾ അടങ്ങുന്നതാണ് ഗവേഷണ പ്രബന്ധം. അധ്യായം 3 മുത്തൽ 7 വര പ്രബന്ധത്തിൻ്റെ കേന്ദ്രലക്ഷ്യ സഫലീകരണം സാദ്ധ്യമാക്കുന്ന രീതിയിൽ, ഗഹനമായി ഞങ്ങൾ നടത്തിയ പരീക്ഷണ നിരീക്ഷണങ്ങൾ റിപ്പോർട്ട് ചെയ്യുന്നു. അധ്യായം 8 സമഗ്രമായ ഒരു സംഗ്രഹം നൽകുന്നു, കൂടാതെ അധ്യായം 9 ഗവേഷണ വിഷയത്തെക്കുറിച്ചുള്ള ഭാവി പഠനങ്ങൾക്കായുള്ള ഞങ്ങളുടെ ശുപാർശകൾ നൽകുന്നു.

ഈ ഗവേഷണപ്രബന്ധത്തിൽ വരുത്തിയ സുപ്രധാന മുന്നേറ്റങ്ങളിലൊന്ന് ഫ്ലെക്സിബിൾ കുലീന ലോഹ രഹിത SERS സബ്സ്ട്രേറ്റുകൾ ഉപയോഗിച്ച് താലേറ്റുകളേ കണ്ടെത്തലാണ്. $BaTiO_3$, PMMA_$BaTiO_3$, PMMA_$SrTiO_3$ എന്നിവയെ അടിസ്ഥാനമാക്കിയുള്ള സബ്സ്ട്രേറ്റുകൾ യഥാക്രമം ഡൈമീഥൈൽ താലേറ്റ് (ഡിഎംപി), ഡൈ ഈഥൈൽ താലേറ്റ് (ഡിഇപി), ഡി(2-ഈഥൈൽഹെക്സൈൽ) താലേറ്റ് (DEHP) എന്നിവ

കണ്ടെത്തുന്നതിനായി രൂപകൽപ്പന ചെയ്തിരിക്കുന്നു. നവീനമായ സിന്തസിസ് രീതികൾ, പരിഷ്ക്കരിച്ച താഴ്ന്ന-താപനില സോൾ-ജെൽ രീതികളേ ഇൻ-സിറ്റു പോളിമറൈസേഷനുമായി സംയോജിപ്പിച്ച്, രാമൻ സിഗ്നലുകൾ വർദ്ധിപ്പിക്കുന്നതിന് ആവശ്യമായ "ഹോട്ട്സ്പോട്ടുകൾ" ഉള്ള സബ്സ്ട്രേറ്റുകൾ നിർമ്മിച്ചു. സബ്സ്ട്രേറ്റുകൾക്കുള്ളിലെ മൈക്രോ സ്ട്രക്ചറിംഗ് അന്വേഷണ തന്മാത്രകളുടെ ട്രാപ്പിംഗ് സുഗമമാക്കുകയും രാമൻ സിഗ്നലുകളിൽ ചാർജ് കൈമാറ്റം വഴിയുള്ള കെമിക്കൽ മെച്ചപ്പെടുത്തൽ വർദ്ധിപ്പിക്കുകയും ചെയ്യുന്നു. സ്പെക്ട്രൽ ഇടപെടലുകളില്ലാതെ കൃത്യമായി തൻമാത്രകളേ കണ്ടെത്താനുള്ള സബ്സ്ട്രേറ്റുകളുടെ കഴിവ് പ്രശംസനീയവും അത്യന്താപേക്ഷിതവുമാണ്

ജല ശുദ്ധീകരണ മേഖലയിൽ, ഓക്സിഡേറ്റീവ് പോളിമറൈസേഷൻ വഴി സമന്വയിപ്പിച്ച സിങ്ക് ഓക്സൈഡ്-ഇൻകോർപ്പറേറ്റഡ് പോളിപൈറോൾ (PPy_ZnO) പോളിമർ നാനോ കോമ്പോസിറ്റുകൾ ഉപയോഗിച്ച് ഡൈമീഥൈൽ താലേറ്റ് (DMP) നീക്കം ചെയ്യുന്നതിലാണ് മറ്റൊരു ശ്രദ്ധാ കേന്ദ്രം. ഘടനാപരമായ സമഗ്രത, സ്ലിറ്റ് പോലെയുള്ള മൈക്രോപോറുകളുടെ സഹകരണ പ്രഭാവം, PPy_ZnO യുടെ സംയോജിത ബെൻസീൻ വളയങ്ങൾ എന്നിവ ജല പരിതസ്ഥിതികളിലെ വിശാലമായ ശ്രേണിയിൽ നിന്ന് DMP ഫലപ്രദമായി നീക്കംചെയ്യുന്നതിന് കാരണമായി.

മെറ്റാമെറ്റീരിയൽ ആപ്ലിക്കേഷനുകളുടെ മേഖലയിൽ, ഈ ഗവേഷണം വളരെ കുറഞ്ഞ ആവൃത്തിക്ക് അനുയോജ്യമായ മെറ്റാമെറ്റീരിയലുകളുടെ വിടവ് പരിഹരിക്കുന്നു. രണ്ട് വ്യത്യസ്ത ഫില്ലർ കോമ്പിനേഷനുകളുള്ള ഒരു PMMA മാട്രിക്സ് സംയോജിപ്പിച്ച് രണ്ട് ത്രിമാന സംയുക്തങ്ങൾ രൂപകല്പന ചെയ്തു: AC_ZnO, Graphite_CaTiO$_3$. പെർകോലേഷൻ പരിധിക്കപ്പുറമുള്ള PMMA ശൂന്യതകളുടെ മധ്യസ്ഥതയിലുള്ള മൈക്രോസ്ട്രക്ചറിംഗ് പരസ്പര ബന്ധിതമായ 3D ചാലക ശ്രേണികളുടെ രൂപീകരണത്തിന് സഹായകമായി, ഇത് നെഗറ്റീവ്

പെർമിറ്റിവിറ്റിയിലേക്കുള്ള പരിവർത്തനം സാധ്യമാക്കി. രസകരമെന്നു പറയട്ടെ, മെറ്റാലിക് ഫില്ലറുകൾക്ക് പകരം സെറാമിക് ഫില്ലറുകൾ ഉപയോഗിക്കുക വഴി പെർമിറ്റിവിറ്റി മൂല്യങ്ങളുടെ ക്രമം 10^4 നിന്നൂ10^8 വരെ ഗണ്യമായി മാറ്റുന്നു. ഫില്ലർ തിരഞ്ഞെടുപ്പും അവരുടെ സാന്ദ്രതയും ELF നെഗറ്റീവ് പെർമിറ്റിവിറ്റി മികച്ചതാക്കുന്നതിൽ നിർണായക പങ്ക് വഹിച്ചു.

ചുരുക്കത്തിൽ, ഈ ഗവേഷണ പ്രബന്ധം പരിസ്ഥിതി മലിനീകരണം കണ്ടെത്തൽ, നീക്കംചെയ്യൽ എന്നിവയിൽ ശാസ്ത്രീയ സംഭാവനകൾ നൽകിയിട്ടുണ്ട്. ELF മേഖലയിൽ പ്രവർത്തിക്കുന്ന മെറ്റാമെറ്റീരിയലുകളുടെ ആവശ്യകത നികത്തുന്നതിന് നാനോകോമ്പോസിറ്റുകൾ വികസിപ്പിച്ചു. ഈ പ്രബന്ധത്തിൽ റിപ്പോർട്ട് ചെയ്യപ്പെട്ട പരീക്ഷണ നിരീക്ഷണങ്ങൾ സുസ്ഥിര വികസന ലക്ഷ്യങ്ങൾക്ക് ഗണ്യമായ സംഭാവനകൾ പ്രദാനം ചെയ്യുന്നു. അതുകൂടാതെ ശക്തമായ ശാസ്ത്രത്തിൻ്റെ പിൻബലത്തിൽ സാമൂഹിക നേട്ടങ്ങൾക്കായി സാങ്കേതിക കഴിവുകൾ വർധിപ്പിക്കാനുള്ള ആഗോള ശ്രമങ്ങൾക്ക് ഈ പ്രബന്ധം ഊർജം പകരുന്നു.

സൂചകപദങ്ങൾ: പോളിമർ നാനോകോമ്പോസിറ്റുകൾ, താലേറ്റ്, SERS, അധിശോഷണം, മെറ്റാമെറ്റീരിയൽ, വളരെ കുറഞ്ഞ ആവൃത്തി.

PREFACE

The field of material science has seen tremendous advancements, particularly with the development of polymer nanocomposites, which combine the advantageous properties of polymers as a platform and the unique characteristics of nanomaterials. These hybrid materials exhibit remarkable mechanical, thermal, electrical, surface and barrier properties, making them highly versatile for various applications. This Ph.D. thesis explores the potential of polymer to act as a structure-defining factor in polymer nanocomposites driving specific environmental and dielectric applications.

Polymer nanocomposites offer unique properties that make them ideal for detecting and removing pollutants, viz. (i). The high surface area and tunable surface chemistry of nanomaterials within the composites could enhance sensitivity and selectivity, enabling the accurate identification of low concentrations of phthalates. (ii) The exceptional adsorption capacity and chemical functionality of polymer nanocomposites could facilitate the efficient capture and removal of phthalate molecules. Utilising those properties of polymer nanocomposites, our research has developed advanced composites capable of detecting or removing phthalates, contributing to cleaner water sources and improved environmental health.

For dielectric applications, we identified a significant gap in the availability of suitable metamaterials for extremely low-frequency applications. 10^1 to 10^{-2} Hz electromagnetic waves belonging to the extremely low frequency (ELF) regime are the lowest frequency waves regularly utilised for wireless transmission and communication. Polymer nanocomposites possess properties that make them excellent candidates for filling this gap. Their ability to be engineered at the nanoscale allows for precise control over electromagnetic properties, essential for creating practical metamaterials. The structure-defining capability to create interconnected networks and the high dielectric constant and tunable electrical conductivity of polymer nanocomposites enable the design of materials with unique electromagnetic responses tailored to the extra-low frequency range. By leveraging these properties, our research aimed to develop advanced polymer nanocomposite-based metamaterials that can address the current limitations and meet the demands of dielectric materials for the specific frequency regime, 10^1 to 10^{-2} Hz.

The thesis work is based on five connected objectives:

(i) Synthesise certain innovative nanocomposite materials that utilise the unique structure-defining features of polymers.

(ii) To address environmental or dielectric material challenges using the synthesised polymer nanocomposites.

(iii) Develop polymer nanocomposite-based noble metal-free SERS substrates with high surface area and tunable surface chemistry to enhance the sensitivity and selectivity of detecting low concentrations of phthalates in water sources.

(iv) Utilise the exceptional adsorption capacity and chemical functionality of polymer nanocomposites to facilitate the efficient capture and removal of phthalate molecules from contaminated water.

(v) Identify and fill the gap in the availability of suitable metamaterials for applications in extra-low frequency regions (10^1 to 10^{-2} Hz) using polymer nanocomposites.

The thesis entitled **"Polymer Nanocomposites for Phthalate Detection, Remediation and Metamaterial Applications."** is organised into eight chapters. Chapter 1 provides a brief introduction to the topics covered in the thesis. Chapter 2 outlines the synthesis methods and characterisation techniques employed in the research. Chapters 3 through 7 present the results and conclusions for specific applications. Finally, Chapter 8 discusses the overall summary and future prospects of the research work.

Chapter 1 provides a general introduction to polymer nanocomposites, emphasising their structure-defining and structure-tuning capabilities. It discusses the significance of detecting and remediating phthalates from the environment and the need for dielectric metamaterials. The chapter also reviews various strategies for phthalate detection and removal. Finally, it highlights the motivation and objectives of the reported thesis work.

Chapter 2 introduces the experimental techniques employed in the thesis. Structural characterisation utilises X-ray diffraction (XRD) to analyse crystalline structures. Field Emission Scanning Electron Microscopy (FE-SEM) investigates morphology, structure, and particle size. Optical and adsorption studies employ ultraviolet-visible diffuse reflectance spectroscopy (UV-Vis DRS) and Raman spectroscopy. Surface area and porosity analysis utilise Brunauer–Emmett–Teller (BET) and Barrer–Joyner–Halenda (BJH) techniques. Raman spectroscopy further examines functional groups and vibrational modes. Dielectric properties are studied using broadband dielectric spectroscopy.

Chapter 3 deals with the applicability of $BaTiO_3$ and the polymer nanocomposites PMMA_$BaTiO_3$ based SERS substrate for the detection of dimethyl and diethyl phthalate impurities (DMP and DEP), respectively, from the water system. The synthesis, characterisation studies, adsorption-based affinity studies, and surface-enhanced Raman spectroscopic (SERS) investigations of the composites are discussed in the chapter. The Surface Enhanced Raman Spectroscopy (SERS) technique can amplify the Raman signals of target molecules, providing high sensitivity and specific identification of phthalate molecules. Developing noble metal-free SERS substrates with high selectivity and sensitivity is an emerging area of research. Semiconductor-based SERS substrates with tunable shape and size, elevated specific surface area, and fresh active sites enhance the affinity between the substrate and probe molecules. These active sites act as the "hotspots" for charge transfer, increasing the intensity of the Raman signals. We have synthesised $BaTiO_3$ using a novel, modified low-temperature sol-gel route. The $BaTiO_3$ (BT) was incorporated into a PMMA polymer matrix resulting in PMMA_BT SERS substrates. The PMMA promoted microstructural evolution, leading to the formation of hotspots. We have demonstrated the utilisation of the synthesised

SERS substrate to sensitively detect two different phthalates, viz. DMP and DEP. We have shown that the substrate design has created hotspots from the morphology tuning, ensuring distinct Raman bands and precise detection without spectral overlap. These hotspots enhanced the weak Raman signals of DMP and DEP, driven by a charge transfer resonance mechanism - originating from strong interactions between phthalates and BT and PMMA_BT substrates, respectively. Thus, Chapter 3 presents the $BaTiO_3$ and PMMA_$BaTiO_3$ composites as novel noble metal-free SERS substrates for detecting DMP and DEP, offering significant advancements in environmental remediation applications.

Chapter 4 introduces a novel detection method for Di(2-ethylhexyl) phthalate (DEHP), a widely used industrial chemical with significant health risks. Traditional DEHP detectors often fail to provide cost-effective and real-time detection. In contrast, Surface-Enhanced Raman Spectroscopy offers excellent potential for identifying environmental pollutants. This study presents a compelling, sensitive detection tool for DEHP using a flexible, noble metal-free polymer-based SERS substrate. The innovative design of the SERS substrate relies on hotspots created in the pores of semiconductor $SrTiO_3$, which is coated onto a PMMA polymer matrix. Unlike conventional high-temperature synthesis methods (above 1000°C), a low-temperature sol-gel route was employed to produce $SrTiO_3$. The PMMA platform mediated dense arrangement of micro spherical porous hotspots significantly enhances the weak Raman peaks of DEHP. Additionally, the chosen SERS element and platform ensure no overlap between the Raman bands of the substrate and the probe molecule. The primary mechanism driving the SERS activity is charge transfer resonance, facilitated by the strong affinity between $SrTiO_3$ and DEHP. Unlike conventional chromatographic techniques, this cost-effective, real-time, and sensitive detection method using a noble metal-free flexible SERS substrate provides an efficient approach for sensing DEHP.

Chapter 5 focuses on the efficient adsorptive removal of Dimethyl Phthalate (DMP) using facilely synthesised Zinc Oxide-incorporated Polypyrrole (PPy_ZnO) polymer nanocomposites. The high-yield synthesis of PPy_ZnO was achieved through the oxidative polymerisation method. The synthesised samples were characterised using various techniques, including XRD, FESEM, and BET-BJH. The study identified the PPy_ZnO composite with 0.03g of ZnO as a novel adsorbent for DMP. Batch adsorption experiments, utilising UV-Vis spectroscopy, examined the effects of contact time, adsorbate concentrations, and adsorbent dose. Results showed that PPy_ZnO removed 91.84% of DMP (1 ppm) molecules within 10 minutes, highlighting its potential for environmental remediation. Under optimised conditions, the removal efficiency of DMP by PPy_ZnO was 99.15% for 1 ppm and 99.78% for 20 ppm, demonstrating its effectiveness for both high and low concentrations of plasticisers in aquatic systems. The enhanced DMP adsorption is attributed to the synergistic effects of slit-like micropores and conjugated benzene rings in the PPy_ZnO, where DMP molecules are trapped and held primarily by electrostatic attraction, hydrogen bonding, and π-π interactions. This research underscores that engineered surface functional groups in polymer nanocomposites can be utilised to develop high-performance phthalate adsorbents, offering a promising solution for water pollution.

Chapter 6 delves into the intriguing realm of flexible composites exhibiting negative permittivity behaviour, which have garnered significant attention for their potential applications in the electromagnetic field and innovative capacitance. This chapter focuses on designing and exploring surface microstructure-induced negative permittivity in flexible composites, emphasising their metamaterial properties. The composites were synthesised using Poly (methyl methacrylate) (PMMA), Activated carbon (AC), and Zinc Oxide (ZnO) through an in-situ polymerisation process. With the synthesised composite, we have achieved negative permittivity in the extremely low-frequency (ELF) regime by varying the content of AC and ZnO fillers. Detailed investigations were conducted on the composite's microstructure formation, real permittivity, and AC conductivity. The results revealed that the negative permittivity with high order and its magnitude could be effectively controlled by adjusting the filler content of AC and ZnO. This tunability is crucial for creating flexible composites with suitable permittivity values tailored for ELF applications, which could meet the heavy industrial demand and lack of suitable metamaterial for the ELF regime.

Chapter 7 also focuses on flexible composites with negative permittivity for the ELF region. The composites, synthesised through an in-situ polymerisation process, consist of Poly (methyl methacrylate) (PMMA), Graphite (G), and Calcium titanate ($CaTiO_3$). The inherent properties of ceramics, $CaTiO_3$, including their high dielectric constant and ability to maintain stable permittivity over a wide frequency range, have augmented the composite's overall capacity to exhibit negative permittivity in the desired frequency regimes. This synergy between the polymer matrix and ceramic fillers facilitated precise control and enhancement of the composite's electromagnetic characteristics, making them suitable for applications requiring tailored permittivity behaviours. By varying the concentrations of graphite and $CaTiO_3$ fillers, the composites were engineered to exhibit a high value of negative permittivity ($\sim 10^8$) in the extremely low-frequency (ELF) range. Investigations into their microstructural formation, real permittivity, and AC conductivity demonstrated that the presence and degree of negative permittivity could be finely tuned by adjusting the filler content. This tunability makes these flexible composites highly attractive for industrial applications that require specific permittivity values in the ELF range.

Chapter 8 comprehensively summarises the thesis and chapter 9 talks about future prospects for the work discussed in the thesis.

Throughout the thesis, diverse categories of polymer nanocomposites were synthesised using different polymeric matrices and fillers, resulting in novel materials with enhanced surface properties ideally suited to achieve our primary research goals. Chapters 3, 4, 5, 6, and 7 collectively address the objectives mentioned at the beginning of this synopsis. Chapters 3 and 4 specifically contribute to the third objective, while Chapter 5 complements our fourth objective. Chapters 6 and 7 fulfil the fifth objective by focusing on the development of metamaterials. Thus, the thesis, "Polymer Nanocomposites for Phthalate Detection, Remediation, and Metamaterial Applications", presents a cohesive body of relevant and robust studies to enhance the application of polymer-based nanocomposites through their structure-defining properties. Moreover, our research delves into the mechanisms underpinning SERS enhancement, adsorption-based removal, and the formation of interconnected networks driving negative permittivity in metamaterials for ELF region. The insights provided by the thesis are poised to play a crucial role in advancing the utilisation of polymer nanocomposites in environmental and dielectric applications.

CHAPTER 1

INTRODUCTION

Contents

Abstract: *This chapter aims to provide a concise overview of the thesis and an introduction to its general aspects. The chapter offers a general introduction to the main topics of discussion in this thesis, viz., polymer nanocomposites, phthalates, and metamaterials. The importance of and ways to detect and remediate phthalates are also discussed. This chapter also highlights the significance of SERS substrates and metamaterials based on polymer nanocomposites. Towards the end of the chapter, the motivation, objectives, and a brief overview of the thesis - providing a chapter-wise division of the thesis is presented.*

In this thesis, titled "**Polymer Nanocomposites for Phthalate Detection, Remediation, and Metamaterial Applications.**" we work to utilise the structure-defining capability of polymers, especially when they drive the formation of nanocomposites. The resultant polymer nanocomposites were tested for environmental and electronic applications. With this in mind, we have synthesised various categories of polymer nanocomposites for the following three applications:

(a) Phthalate detection,

(b) Phthalate removal, and

(c) Metamaterial application.

The thesis consists of five different working chapters, each addressing one of the above applications.

In the realm of advanced materials, polymer composites have emerged as versatile and transformative solutions, driving innovation across diverse scientific domains. With their unique blend of properties, these composites offer remarkable potential in phthalate detection, environmental remediation, and developing cutting-edge metamaterials. Phthalates, ubiquitous in plastic products, pose significant health and environmental risks due to their endocrine-disrupting characteristics [1]. Traditional detection methods often fall short in sensitivity and specificity. In contrast, polymer composites, with their tunable chemical structures and high surface area, provide an unprecedented platform for precisely and efficiently detecting phthalates, ensuring safer consumer products and environments. Beyond detection, polymer composites could play a crucial role in the remediation of phthalate-contaminated sites. Their ability to adsorb and degrade phthalates through tailored surface functionalities enables effective water and soil purification, mitigating the adverse impacts of these hazardous chemicals. This dual capability of detection and remediation underscores the multifunctionality of polymer composites in addressing complex environmental challenges.

In the burgeoning field of metamaterials, polymer composites are pioneering new frontiers. Their customisable dielectric properties and flexible nature make them ideal candidates for constructing metamaterials with unique electromagnetic characteristics, such as negative permittivity and permeability. These composites pave the way for revolutionary applications in electromagnetic wave manipulation, stealth technology, and beyond.

Thus, polymer composites stand at the confluence of environmental science and material engineering, offering innovative solutions for phthalate detection and remediation while also unlocking new possibilities in the realm of metamaterials. This exploration into their multifaceted applications highlights their scientific significance and profoundly underscores their potential to impact various technological advancements.

1.1 Polymer Nanocomposites

Using nanoparticles directly in various applications is limited due to their instability, which stems from their large surface area-to-volume ratio, leading to quick oxidation, contamination, and handling difficulties [2]. Encapsulating nanostructures within a suitable matrix mitigates these issues, stabilising the nanoparticles and allowing for the modification of their morphology and arrangement. These encapsulated materials, known as nanocomposites, combine the properties of the host material with those of the nanostructures, making them superior to their individual components. Nanocomposites, multiphase materials with at least one phase in the nanometre range, offer the ability to fine-tune properties by adjusting the quantities of the host material and nanoparticles [3]. Depending on the host material, nanocomposites can be classified into ceramic, metal, and polymer nanocomposites. Despite ceramics' brittleness, ceramic nanocomposites can achieve quasi-ductility with appropriate fillers and retain advantages such as toughness, lightness, and high-temperature resistance, making them suitable for automotive and aerospace industries [4]. Metal and polymer nanocomposites leverage the intrinsic properties of their respective matrices, enhanced by the unique characteristics of the nanostructures [5].

1.1.1 Introduction to Polymer Nanocomposites

Polymer nanocomposites represent a groundbreaking advancement in materials science, combining the versatility of polymers with the exceptional properties of nanoscale fillers. Polymer nanocomposites are advanced composite materials characterised by a polymer matrix integrated with nanofillers with at least one dimension smaller than 100 nanometres. These nanofillers, which can be particles, fibres, or platelets, significantly enhance the properties of the polymer matrix due to their nanoscale dimensions and high surface area-to-volume ratio [5]. Incorporating these nanoscale fillers leads to remarkable improvements in mechanical strength, thermal stability, electrical conductivity, and barrier properties compared to conventional composites. By leveraging the unique interactions at the nanoscale, polymer nanocomposites offer tailored functionalities for diverse applications, ranging from automotive and aerospace components to electronics, packaging, and biomedical devices. This ability to fine-tune material properties through nanoscale engineering positions polymer nanocomposites as vital materials in modern technology and industrial applications.

1.1.2 Classification of Polymer Nanocomposites

(a) Polymer/ Ceramic Nanocomposites

Nanocomposites comprise single ceramic layers (1nm thick) homogeneously scattered in a persistent matrix. Integrating ceramic particles into a polymer matrix results in a material that exhibits superior mechanical properties, such as increased stiffness, toughness, and wear resistance. Additionally, the thermal stability and insulating properties of ceramics enhance the composite's ability to withstand high temperatures and improve its thermal management capabilities. One of the critical benefits of polymer-ceramic composites is their ability to be tailored for specific applications by adjusting the type and amount of ceramic filler and the polymer matrix used. This customisation allows for the design of materials with specific properties required for various industrial applications, such as in aerospace, automotive, electronics, and biomedical fields. *In the Polymer/ Ceramic Nanocomposites category, we have studied PMMA_ST and PMMA_BT as SERS* *substrates for phthalate detection applications.*

(b) Inorganic/Organic Polymer nanocomposites

Inorganic/organic polymer nanocomposites are advanced materials that synergistically combine the properties of inorganic nanoparticles with organic polymer matrices. These nanocomposites leverage the high strength, thermal stability, and unique optical or electrical properties of inorganic components with the flexibility, processability, and lightweight nature of organic polymers. Integrating inorganic nanoparticles, such as metal oxides, clays, or carbon-based materials, into polymer matrices results in enhanced mechanical strength, improved thermal and chemical resistance, and novel functional properties. This combination allows for developing materials with tailored functionalities for specific applications, ranging from high-performance structural components to smart materials in electronics, energy storage, and biomedical devices. *PPy_ZnO composites, which belong to this category, were prepared and utilised to remove phthalates from aqueous solutions.*

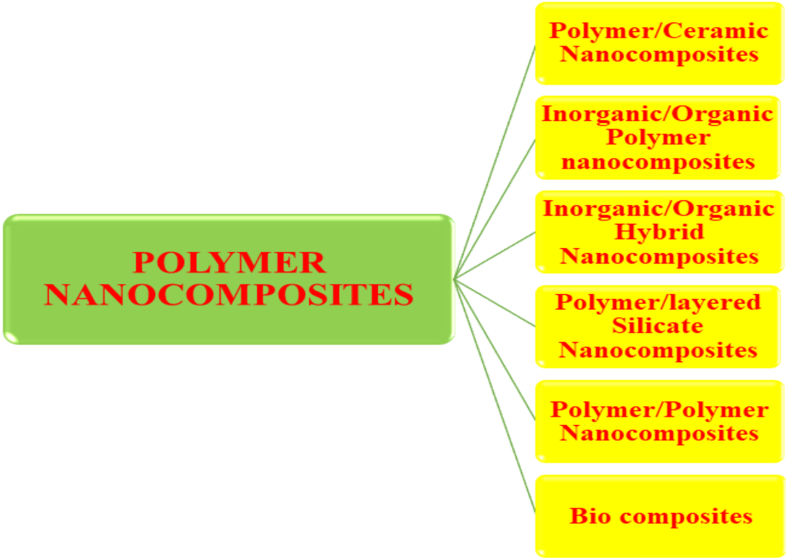

Fig 1.1 Diagram representing Classification polymer nanocomposites

(c)Inorganic/Organic Hybrid Nanocomposites

Hybrid inorganic/organic materials transcend simple physical mixtures and can be broadly defined as nanocomposites where organic and inorganic components are intimately blended. These hybrids can manifest as homogeneous systems formed from monomers and compatible organic/inorganic elements or as heterogeneous systems (nanocomposites) in which at least one component is on the nanometre scale. *In this class of polymer nanocomposites, we have prepared PMMA_ZnO_AC and PMMA_ Graphite_*$CaTiO_3$ *systems intended for metamaterial applications.*

(d)Polymer/layered Silicate Nanocomposites

Polymer/layered silicate nanocomposites are advanced materials composed of a polymer matrix intercalated or exfoliated with layered silicate nanoparticles. These nanocomposites exhibit superior properties to conventional composites due to the high aspect ratio and large surface area of the silicate layers. These layers can significantly enhance mechanical strength, thermal stability, and barrier properties when uniformly dispersed within the polymer matrix. The synergistic combination of the polymer's flexibility and the silicate's rigidity creates a composite material with remarkable performance characteristics, making them highly desirable for automotive, aerospace, packaging, and biomedical applications.

(e)Polymer/Polymer Nanocomposites

Polymer/polymer nanocomposites are innovative materials created by combining two or more distinct polymeric phases, with at least one phase dispersed at the nanoscale. This unique structure enhances various properties, such as mechanical strength, thermal stability, and optical characteristics. The nanoscale dispersion of one polymer within another can significantly improve the composite material's performance, providing a balance of flexibility, toughness, and durability. These nanocomposites are particularly advantageous in applications where traditional polymer blends fall short, such as high-performance coatings, advanced packaging materials, and next-generation electronic devices. By carefully selecting and engineering the constituent polymers, scientists and engineers can tailor the properties of polymer/polymer nanocomposites to meet specific functional requirements, paving the way for their widespread use in cutting-edge technologies.

(f)Biocomposites

Biocomposites are materials composed of natural fibres or bio-based polymers combined with synthetic or natural matrices to create environmentally friendly and sustainable alternatives to traditional composites. These materials leverage the strength and renewability of natural components such as plant fibres (e.g., flax, hemp, or jute) and bio-resins derived from renewable resources. Biocomposites offer several advantages, including reduced environmental impact, biodegradability, and lightweight properties, making them ideal for various automotive, construction, packaging, and consumer goods applications. The development and use of biocomposites support the move towards greener manufacturing practices and contribute to reducing carbon footprints, fostering a more sustainable future.

1.1.3 Enhancement in Properties

Polymer nanocomposites have demonstrated significant enhancements in properties due to the inclusion of nanomaterial additives, offering substantial advantages over conventional fillers and base polymers. These enhancements include remarkable improvements in mechanical properties such as strength, modulus, and dimensional stability, making the materials more robust and reliable for various applications. Additionally, polymer nanocomposites exhibit superior solvent and heat resistance and decreased flammability, enhancing their safety and durability under challenging conditions. Their reduced permeability to gases, water, and hydrocarbons further extends their utility in barrier applications. Thermal stability and heat distortion temperature are also notably increased, contributing to better performance at elevated temperatures. The flame retardancy and reduced smoke emissions of polymer nanocomposites make them safer in fire-prone environments. Furthermore, these materials show enhanced chemical resistance, ensuring longevity and resilience against corrosive substances. Surface appearance improvements, increased electrical conductivity and optical clarity compared to conventionally filled polymers make polymer nanocomposites versatile and suitable for a wide range of high-performance applications.

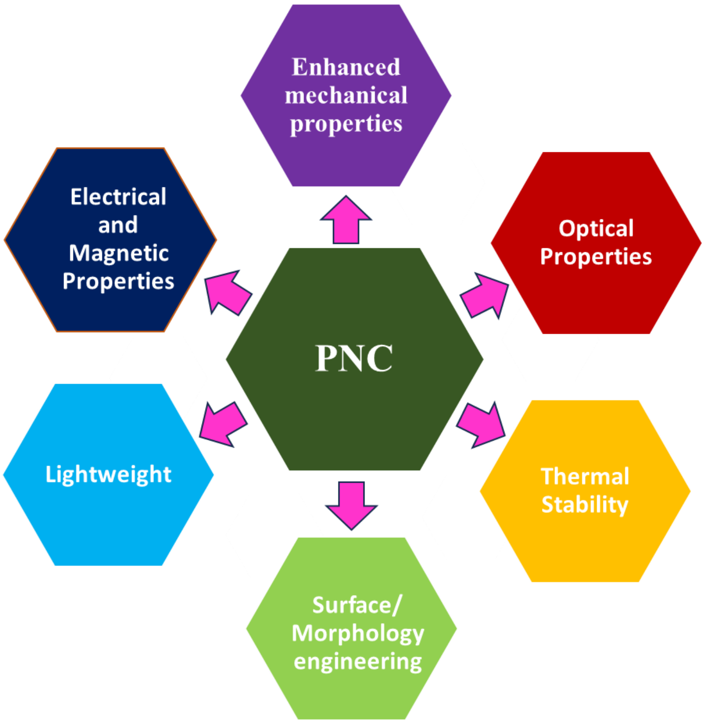

Fig 1.2 Representation of polymer nanocomposites (PNC) properties. The structure-defining capability of polymers can enhance the PNC properties.

1.1.4 Applications of Polymer Nanocomposites

Due to their enhanced properties, polymer nanocomposites have found diverse applications across various fields. Here are some critical applications:

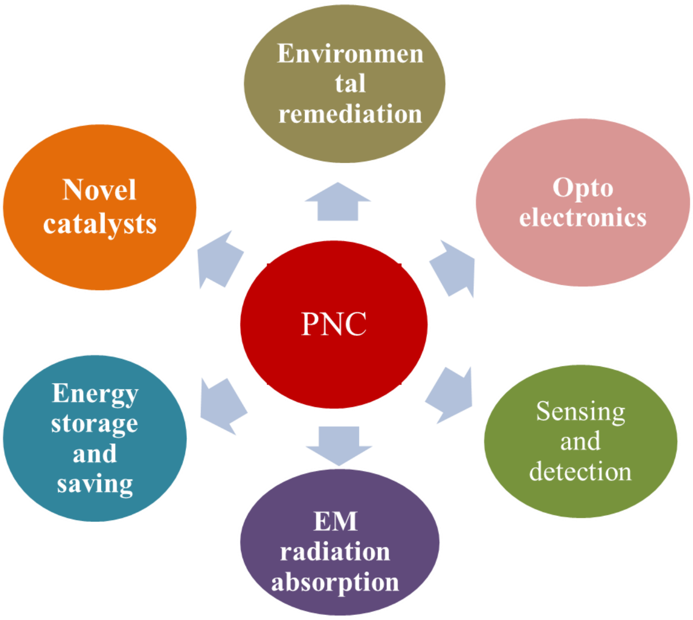

Fig 1.3 Diagram representing applications of polymer nanocomposites

(a) Environmental Remediation

Recently, polymer nanocomposites (PNCs) have garnered significant attention in the realm of wastewater treatment and remediation. The decline in the quantity and quality of freshwater sources, mainly due to human activities, poses a critical challenge. Water is vital for humans, agriculture, and industrial processes, but rapid industrialisation has increased wastewater discharge, introducing diverse pollutants into the environment with detrimental effects on ecosystems and human health. PNCs offer a promising solution as they are efficient and cost-effective materials for treating wastewater [6,7]. These composites, combining polymers with nanomaterials, exhibit enhanced properties, including improved resistance to fouling, thermal stability, membrane permeability, mechanical strength, photocatalytic activity, and adsorption capabilities [8]. The efficacy of PNCs in water treatment depends on factors such as the type, size, and shape of nanoparticles used, their interaction with the polymer matrix, and their concentration. Furthermore, the method of PNC modification influences their reusability, remediation efficiency, and selectivity in water treatment applications. PNCs are particularly effective in removing dyes, metal ions, and microorganisms from water, [9] highlighting their versatile role in addressing various environmental challenges.

Dyes are extensively utilised in textiles, papermaking, and cosmetics to impart colour to products. However, their discharge in wastewater poses severe environmental challenges due to their carcinogenic and toxic nature. Efficient removal of dyes is crucial to render wastewater suitable for reuse and prevent ecological harm. Polymer nanocomposites (PNCs) have emerged as practical materials for dye removal from polluted water, benefiting from the synergistic properties of polymers and nanomaterials [10]. For instance, cellulose/graphene oxide nanocomposites achieved 98% removal of methylene blue dye with an adsorption capacity of 334.19 mg/g within 135 minutes [11]. Similarly, cellulose/clay nanocomposites demonstrated up to 98% removal efficiency for methylene blue [12]. In another study, polyaniline/TiO_2 nanocomposites exhibited an adsorption capacity of 458.10 mg/gL for methylene blue, utilising mechanisms like membrane diffusion and chemical adsorption [13]. These examples illustrate the effectiveness of PNCs in addressing dye pollution in wastewater.

Polymer nanocomposites (PNCs) incorporating magnetic nanoparticles can serve as reusable magnetic adsorbents for dyes, leveraging the magnetic properties inherent in their nanoparticles. These PNC magnetic adsorbents possess a large surface area, porous structure, and small particle size, coupled with excellent magnetic characteristics that enable easy recovery via magnetic separation post-adsorption or regeneration. This addresses the challenges of separating PNC adsorbents and enhances their reusability in dye removal applications.

The effectiveness of dye removal using PNCs can be optimised by controlling several factors, such as the choice and characteristics of the polymer and the nanomaterial. Additionally, the methods used for preparing PNCs and their structural design are crucial in determining their performance in dye removal applications. Combining adsorption and photocatalytic degradation mechanisms in PNCs can enhance their efficiency compared to relying on either mechanism alone. PNCs with magnetic properties offer added benefits as they can be easily recovered and reused multiple times. Experimental conditions like dye concentration, PNC concentration, pH, temperature, and contact time also influence the dye removal process. Holistically addressing these factors would enable the development of PNCs that demonstrate superior performance in dye removal applications. However, scaling up production for industrial use remains a challenge that requires further research to reduce costs and enhance practical applicability. Issues such as toxicity, selective dye removal, regeneration capability, environmental friendliness, stability, and efficient separation from solutions also need careful consideration and exploration in future studies to maximise the potential of PNCs in large-scale applications.

Metal pollution has escalated globally due to rapid urbanisation and industrialisation, posing significant environmental threats. Consequently, removing metal ions from water sources has become crucial for safeguarding both the environment and human health. Polymer nanocomposites (PNCs) have emerged as effective materials for this purpose, utilising mechanisms such as adsorption to efficiently remove heavy metal ions like Cu (II), Cd (II), Pb (II), Co (II), Cr (VI), and Ni (II) from aqueous solutions. These composites offer advantages over traditional polymer adsorbents, including higher surface area, more active sites, enhanced stability, mechanical feasibility, and increased adsorption capacity [14]. For example, PNCs incorporating materials like polyaniline β-FeOOH, magnetite/poly (1-Naphthylamine), and poly (N-vinyl carbazole)/graphene oxide have demonstrated significant effectiveness in metal ion removal [15-17]. Moreover, PNCs with magnetic properties facilitate easy recovery and multiple reuses after adsorption, addressing challenges in separation and enhancing overall efficiency in water treatment applications. Due to their high adsorption capacity, excellent recycling performance, better mechanical strength, and ease of separation from solutions, polymer nanocomposites have been found to be extensively valuable for removing metal ions from wastewater. In these composites, the polymer matrix provides structural support and acts as a chelating agent, while the embedded nanoparticles contribute chelating sites, reducibility, and magnetic properties. PNCs exhibit rapid adsorption kinetics, efficient regeneration capabilities, and effective chelation of metal ions. However, challenges remain in scaling up production from laboratory to industrial scales, and research on cost-effective production methods and practical applications is limited. Further investigations are needed to evaluate adsorption capacities across different metal ions, develop reliable regeneration methods, and explore PNCs with enhanced long-term performance and regeneration capabilities. Advanced analytical techniques are also essential for better understanding the adsorption mechanisms and interaction processes at the molecular level [18,19].

(b) Optoelectronics

For most optical applications, conjugated polymers are essential in composite materials due to their wide range of band gap values and significant electrical conductivity, making them suitable for electronic devices like OLEDs and OPVs. Inorganic particles, selected to ensure transparency, enhance specific polymer characteristics without altering the optical properties. Typically smaller than 40 nm, these particles prevent optical scattering loss and aggregation, maintaining the composite's transparency [20]. Beyond enhancing specific traits, nanoparticles also improve the stability of the host polymer by protecting against atmospheric and light-induced degradation. This protection is crucial as traditional encapsulation with glass lids compromises the flexibility of polymer devices. Integrating small amounts of inorganic particles into the polymer matrix can preserve mechanical properties and provide resistance to degradation by absorbing energy and reducing organic structure defects [21].

(c) Novel catalyst

Nanoparticles exhibit significant potential as catalysts and redox-active media due to their high specific surface area, reactivity, and shape-dependent optical, electronic, and catalytic properties. These attributes have spurred extensive research into designing highly efficient photo- and chemo-catalytic materials for purifying contaminated water and gases. Common catalytic nanoparticles include nanosized semiconductor materials such as nano-TiO_2, ZnO, CdS, and WO_3, zero-valent metals like FeO, CuO, and ZnO, and bimetallic nanoparticles such as Fe/Pd, Fe/Ni, Fe/Al, and Zn/Pd [22]. These nanoparticles are effective in catalysing or acting as redox agents for the degradation of a wide range of environmental pollutants, including Polychlorinated Biphenyls (PCBs), azo dyes, halogenated aliphatic, organochlorine pesticides, halogenated herbicides, and nitroaromatics [23]. However, their use in aqueous suspensions is limited due to challenges in separating and recycling fine particles. Polymeric hosts are particularly attractive due to their controllable pore space, surface chemistry, and excellent mechanical strength, making them ideal for long-term use. The resulting polymer-based nanocomposites (PNCs) retain the inherent properties of the embedded nanoparticles while the polymer matrix provides enhanced stability, processability, and notable improvements stemming from nanoparticle-matrix interactions. Immobilising these nanoparticles onto polymer matrices, such as porous resins, ion exchangers, and polymeric membranes, has effectively mitigated these issues. This approach reduces particle loss, prevents agglomeration, and facilitates the application of convective flow by freestanding particles.

(d) Energy storage and saving

Polymer nanocomposites (PNCs) are emerging as vital materials for energy storage and saving applications, owing to their unique properties that enhance performance and efficiency. The integration of nanomaterials with polymers results in composites that exhibit superior mechanical strength, thermal stability, and electrical conductivity compared to their components. In energy storage, PNCs are utilised in advanced batteries and supercapacitors, where they improve the charge storage capacity, cycle stability, and rate performance. For instance, incorporating conductive nanoparticles like graphene or carbon nanotubes into polymer matrices significantly enhances the electrical conductivity and electrochemical properties of these devices. In terms of energy saving, PNCs play a crucial role in thermal insulation and lightweight construction materials. Nanoparticles such as silica aerogels and Metal-Organic Frameworks (MOFs) embedded in polymers can create materials with low thermal conductivity, which are essential for reducing energy consumption in buildings and industrial processes. Additionally, the high surface area and tailored pore structures of these composites contribute to better energy efficiency in various applications. Furthermore, PNCs are being explored for use in flexible and wearable electronics, where their mechanical flexibility and durability, combined with excellent electrical properties, open up new possibilities for energy harvesting and storage in portable and flexible devices. Overall, the development of polymer nanocomposites holds great promise for advancing energy storage technologies and improving energy efficiency across multiple sectors.

(e) Electromagnetic radiation absorption

Polymer nanocomposites (PNCs) are gaining significant attention for their potential in electromagnetic (EM) radiation absorption applications. These materials are designed to effectively absorb and dissipate EM waves, which is crucial for mitigating electromagnetic interference (EMI) and enhancing the performance of electronic devices. The integration of nanoparticles with polymers results in composites that combine the flexibility and processability of polymers with the unique electromagnetic properties of nanomaterials. One of the primary advantages of PNCs in EM radiation absorption is their ability to be tailored for specific applications through the choice of nanomaterials and polymer matrices. Commonly used nanoparticles include carbon-based materials like graphene and carbon nanotubes, metallic nanoparticles such as iron, nickel, and cobalt, and magnetic oxides like ferrites. These nanoparticles provide high electrical conductivity and magnetic permeability, essential for effective EM wave absorption. EM absorption in PNCs involves converting EM energy into thermal energy through dielectric loss, magnetic loss, and conductive loss. The high surface area and unique electronic properties of nanomaterials enhance these mechanisms, leading to improved absorption efficiency. Additionally, the polymer matrix offers mechanical flexibility and durability, making PNCs suitable for various applications, including coatings, films, and structural components. Recent advancements in the synthesis and processing of PNCs have led to the development of materials with tunable absorption properties across a wide frequency range, from Radiofrequency (RF) to Microwave (MW) bands. These materials are particularly useful in shielding sensitive electronic equipment from EMI, improving the performance of wireless communication systems, and reducing radar cross-sections in stealth technology.

Hence, continued research and development in this field are expected to lead to more efficient and cost-effective EMI shielding materials, benefiting a wide range of industries.

(f) Sensing and detection

Sensors find extensive applications in detecting chemicals, toxic gases, medical diagnostics, and defence. Key requirements for effective sensors include small size, multifunctionality, affordability, reliability, rapid response, high sensitivity, and selectivity. Achieving rapid response and high sensitivity often hinges on maximising specific surface area. Polymer nanocomposites (PNCs) have emerged as promising materials for sensor fabrication due to their cost-effectiveness, ease of fabrication, and versatile physicochemical properties [23]. PNCs allow convenient modification by incorporating side chains and inorganic materials into the polymer matrix, enhancing conductivity, electrolytic behaviour, dielectric properties, optical response, ion selectivity, and molecular recognition capabilities [24]. Nanofillers used in PNCs for sensor applications must possess unique electrochemical, optical, or magnetic properties to augment sensor sensitivity and detection rates. This synergy of polymeric matrices with tailored nanofillers underscores PNCs' growing role in advancing sensor technology across various fields. PNCs can be tailored to enhance sensor sensitivity and selectivity by incorporating functional nanoparticles like carbon nanotubes, graphene, metal oxides, and quantum dots, each offering specific attributes such as high surface area, conductivity, and catalytic or optical properties. This versatility allows PNCs to detect various analytes from gases and volatile compounds to biological molecules and environmental pollutants suiting applications in environmental monitoring, healthcare diagnostics, food safety, and industrial processes. Their rapid response time and real-time monitoring capabilities are precious in dynamic environments, providing timely feedback on analyte concentrations for swift interventions. Moreover, PNCs can be integrated into compact, portable devices and microfabricated sensor arrays, ensuring robust performance and durability in diverse and challenging conditions. Ongoing research aims to optimise PNC compositions, improve sensor selectivity, and enhance detection limits, addressing challenges such as reproducibility, interference management, and long-term stability. With continuous advancements, polymer nanocomposites are poised to drive innovations in healthcare, environmental monitoring, and industrial applications.

In this thesis, our focus has been on the design, application, and exploration of polymer nanocomposites for detecting and remediation of phthalates, as well as their use in metamaterial applications. Therefore, in the following sections 1.2 and 1.3, we provide an introduction to PNCs for phthalate detection and metamaterial applications.

1.2. Phthalate Detection and Removal.

We have employed Polymer Nanocomposites (PNCs) to detect and remove phthalates due to their versatile properties and effectiveness in environmental applications. PNCs combine the benefits of polymers with those of embedded nanoparticles, offering enhanced surface area and tailored functionalities crucial for efficient phthalate detection and remediation.

1.2.1 Introduction to Phthalates

Phthalates are esters derived from 1,2-dibenzene dicarboxylic acid, with their general structure depicted in Fig.1.4. They are created by reacting an excess of either branched or normal alcohols with phthalic anhydride in the presence of a catalyst. The initial reaction step produces a monoester, which is then transformed into a diester in the subsequent reaction step. This diverse group of industrial compounds is primarily used as plasticisers to enhance the flexibility and workability of high molecular weight polymers, making them the most widely produced plasticisers to date. Their low melting points and high boiling points also render them useful as heat-transfer fluids and carriers. Phthalates can make up to 50% of the total weight of certain plastics. Both linear and branched phthalate esters are utilised in plastic manufacturing, with linear esters offering superior flexibility at low temperatures and reduced volatility. However, due to volatility issues, phthalates with alkyl side chains shorter than C6 are rarely used as plasticisers. Phthalates are commonly found in products such as ink, paint, adhesives, vinyl flooring, food products, cosmetics, and pharmaceuticals. At ambient temperatures, phthalates are oily, colourless liquids with a slight Odor. The phthalates used in large quantities are insoluble in water, miscible with mineral oil and hexane, and soluble in most organic solvents. Table 1.1 provides an overview of commonly used phthalate esters. Their physicochemical properties vary significantly with the length of the alkyl chain. Volatility and water solubility can differ by up to four and twelve orders of magnitude, depending on the chain length. Generally, as the alkyl chain length (R and R') increases, volatility, plasticising efficiency, and water extraction decrease while lipophilicity and oil extraction increase.

Table.1.1 Names, acronyms, and Carbon numbers of some common phthalates.

Name	Abbreviation	Chain length (Carbon atoms)	
Linear Sidechain			
Dimethyl phthalate	DMP	C1/C1	[25]
Diethyl phthalate	DEP	C2/C2	[26]
Di-n-propyl phthalate	DPrP	C3/C3	[27]
Di-n-butyl phthalate	DBP	C4/C4	[28]
Di-n-pentyl phthalate	DPP	C5/C5	[29]
Di-n-hexyl phthalate	DNHP	C6/C6	[30]
Di-n-heptyl phthalate	DHP	C7/C7	[31]
Di-n-octyl phthalate	DOP	C8/C8	[32]
Di-n-undecyl phthalate	DUP	C11/C11	[33]
Di-n-tridecyl phthalate	DTDP	C13/C13	[34]
Branched side chain			
Diisobutyl phthalate	DIBP	C4/C4	[35]
Diisopentyl phthalate	DIPP	C5/C5	[36]
Diisoheptyl phthalate	DIHP	C7/C7	[37]
Di(2-ethylhexyl) phthalate	DEHP	C8/C8	[38]
Diisononyl phthalate	DINP	C8/C10	[39]
Dipropylheptyl phthalate	DPHP	C10/C10	[40]
Diisodecyl phthalate	DIDP	C9/C11	[41]
Diisoundecyl phthalate	DIUP	C11/C11	[42]
Diisotridecyl phthalate	DITP	C13/C13	[43]
Cyclic alkyl side chain			[44]
Dicyclohexyl phthalate	DCHP	C6/C6	[45]
Different side chain length			[46]
Benzyl butyl phthalate	BBP	C4/C6	[47]

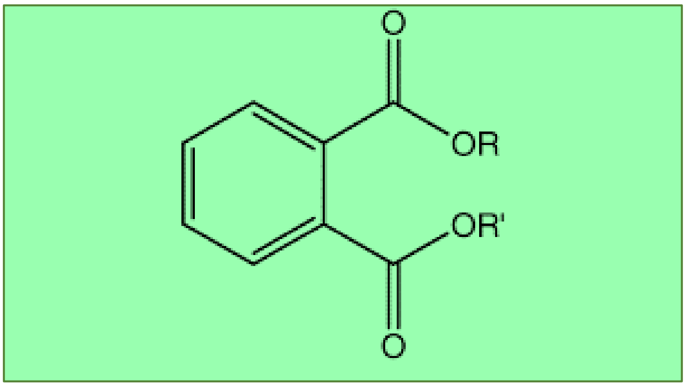

Fig. 1.4. General chemical structure of phthalates (where R and R' are linear or branched alkyl groups).

Lower molecular weight phthalates, such as dimethyl phthalate (DMP), diethyl phthalate (DEP), and dibutyl phthalate (DBP), are commonly used in cosmetics and personal care products, including fragrances, perfumes, bath preparations, and nail polishes [48,49]. In many industries, DEP is added to alcohol for denaturation purposes. On the other hand, higher molecular weight phthalates, particularly di ethylhexyl phthalate (DEHP), are extensively used as plasticisers in plastic products, including toys, where their contribution ranges from 10% to 40%. The plasticising effect of phthalates is primarily due to their low melting point below 25°C [50].

1.2.2 Phthalate exposure pathway and toxicity

Human exposure to phthalates is extensive and stems from numerous ubiquitous sources. Given the chemical and physical characteristics of phthalates and their distribution, multiple pathways for their entry into the body should be considered. Direct exposure to phthalate diesters can happen through inhaling air in both indoor and outdoor environments, unintentional ingestion of household dust, and consumption of drinking water and food. It is important to note that phthalates can leach into food during storage, packaging, and preparation. Additionally, medical treatments involving devices and pharmaceuticals and the use of toys, cosmetics, personal care products, and household items contribute to phthalate exposure. The human placenta does not effectively block phthalates, allowing these chemicals and metabolites to reach the foetus. Indirectly, Phthalates can also readily migrate through the food chain and find a way to all organisms throughout the pathway. This creates a complex exposure scenario, making it difficult to pinpoint the relative contribution of each source to overall human exposure.

Phthalates, widely used as plasticisers in various consumer products, have been linked to numerous adverse health effects. Studies have shown that exposure to phthalates can disrupt endocrine function, leading to hormonal imbalances. This disruption can affect reproductive health, causing reduced fertility, developmental abnormalities, and changes in sexual development. In particular, phthalates have been associated with lower sperm count and quality in men and early puberty in girls. Additionally, phthalates may contribute to metabolic disorders, such as obesity, fatal death, cancer, deformations, liver and kidney damage and insulin resistance, by interfering with lipid metabolism. They are also linked to respiratory issues, such as asthma and allergies, particularly in children. Furthermore, phthalate exposure during pregnancy has been connected to adverse outcomes, including low birth weight and preterm birth. Breast milk can transmit phthalates from maternal blood to the developing foetus and infants. These exposures can potentially impact the endocrine system, essential for various biological functions, including reproductive processes. Additionally, phthalates have been detected in seminal fluid and the placenta. The cumulative and pervasive nature of phthalate exposure, combined with its potential to accumulate in the body, raises significant public health concerns [51].

1.2.3. Different methods for phthalate detection.

Detecting phthalates in environmental samples requires various analytical methods tailored to their specific chemical properties and concentrations.

i. Gas Chromatography-Mass Spectrometry (GC-MS)

Gas Chromatography-Mass Spectrometry (GC-MS) is a highly effective analytical technique widely utilised for detecting and quantifying phthalates in various environmental and biological samples. The process involves first separating phthalate compounds based on their volatility and chemical characteristics using gas chromatography (GC), followed by precise identification and quantification through mass spectrometry (MS). GC-MS offers exceptional sensitivity, allowing the detection of phthalates even at low concentrations in complex matrices such as air, water, soil, and biological tissues. However, GC-MS also presents several challenges. Due to its complex instrumentation and data analysis requirements, it requires skilled personnel to operate and interpret results. Sample preparation for GC-MS can be time-consuming and labour-intensive, often involving extraction and purification steps to ensure accurate quantification. Additionally, GC-MS may not distinguish between different isomers of phthalates, which can affect specificity in identification.

ii. High-Performance Liquid Chromatography (HPLC)

High-Performance Liquid Chromatography (HPLC) is a powerful analytical technique widely used for detecting phthalates due to its ability to separate and quantify these compounds in various samples. In HPLC, a sample containing phthalates is injected into a column packed with a stationary phase, where the phthalates are separated based on their affinity for the stationary phase. Different phthalates elute from the column at different times (retention times), allowing for their identification and quantification. Detection is typically achieved using UV-visible spectroscopy or mass spectrometry, providing qualitative and quantitative information about phthalate concentrations. Despite its advantages in accuracy and sensitivity, HPLC has some limitations. It requires expensive equipment and consumables, skilled personnel for operation and maintenance, and relatively long analysis times compared to other rapid screening methods. Additionally, HPLC may struggle with separating structurally similar phthalates or present in complex matrices, requiring careful method development and optimisation.

iii. Solid-Phase Extraction

Solid-phase extraction (SPE) is a widely employed technique for detecting phthalates in various environmental samples due to its ability to concentrate analytes from complex matrices. In SPE, a solid sorbent material selectively retains phthalates from liquid samples while interfering compounds are washed away. This concentration step enhances the sensitivity of subsequent analytical methods like Gas Chromatography-Mass Spectrometry (GC-MS) or High-Performance Liquid Chromatography (HPLC), enabling detection at low concentrations. However, SPE has its limitations. It requires careful selection of sorbent materials and optimisation of extraction conditions to ensure efficient recovery of phthalates. Moreover, SPE can be time-consuming, especially when processing large sample volumes, and may suffer from variability in recovery efficiency depending on the sample matrix composition. The use of organic solvents in the elution step also raises concerns about environmental impact and disposal.

iv. Enzyme-Linked Immunosorbent Assay (ELISA)

Enzyme-linked immunosorbent Assay (ELISA) represents a valuable tool for detecting phthalates due to its specificity and rapidity. In this method, antibodies specific to phthalates are immobilised on a solid surface, such as a microtiter plate. When a sample containing phthalates is introduced, the target phthalates bind to the antibodies. This binding event is detected using an enzyme-conjugated secondary antibody that produces a measurable colour change or fluorescence signal upon substrate addition. ELISA is particularly advantageous for its simplicity, speed, and ability to screen many samples. However, ELISA also has limitations. It requires well-characterised antibodies specific to the phthalate of interest, which may not always be readily available for all phthalate compounds. Cross-reactivity with structurally similar compounds can lead to false-positive results, necessitating careful antibody specificity validation. Additionally, ELISA may not achieve the same level of sensitivity as instrumental methods like GC-MS or HPLC, particularly for detecting phthalates at very low concentrations in complex matrices.

v. Capillary Electrophoresis (CE)

Capillary Electrophoresis (CE) is a powerful analytical technique increasingly utilised for detecting phthalates due to its high separation efficiency and sensitivity. In CE, phthalate molecules are separated based on their charge-to-size ratio as they migrate through a narrow capillary filled with an electrolyte solution under the influence of an electric field. Detection typically occurs using UV absorption or fluorescence detection, providing precise quantification of phthalate concentrations in complex sample matrices such as environmental waters or biological fluids. CE offers advantages, including rapid analysis, minimal sample requirements, and the simultaneous analysis of multiple analytes. However, CE has some limitations. It can be challenging to optimise separation conditions for different phthalate species due to variations in their physicochemical properties. Moreover, CE requires specialised instrumentation and expertise, making it less accessible compared to some other analytical techniques.

vi. Electrochemical sensors

Electrochemical sensors represent a robust method for detecting phthalates due to their sensitivity, rapid response, and suitability for on-site monitoring applications. These sensors function by leveraging the changes in electrical properties that occur when phthalates interact with electrodes coated with specific materials. This interaction typically leads to current, voltage, or impedance alterations, which can be quantitatively measured to determine phthalate concentrations. Electrochemical sensors offer advantages such as portability, real-time monitoring capabilities, and relatively low cost compared to conventional analytical techniques. However, they also come with certain limitations. One drawback is their susceptibility to interference from other compounds present in complex sample matrices, which can affect the accuracy and specificity of measurements. Additionally, electrode fouling over time may reduce sensor performance, necessitating regular maintenance and calibration.

To tackle these challenges, we have chosen the Surface Enhanced Raman Spectroscopy (SERS) technique for detecting phthalates in diverse samples.

1.2.4 Surface Enhanced Raman Spectroscopy for phthalate detection.

Surface-enhanced Raman scattering (SERS) spectroscopy has been effectively employed as a spectroscopic method for identifying and detecting various biological and chemical species [52,53]. It is considered a surface-sensitive analytical technique. It can significantly enhance the Raman scattering cross-section of molecules adsorbed on the SERS substrate. In the presence of adsorbed molecules, the incident photon undergoes elastic Raman scattering, which involves the adsorption of incident photon energy, coupling to the internal molecular vibrations, and subsequent reemission of photons (Stokes and anti-stokes lines). The SERS technique stands out for its minimal sample preparation and high sensitivity, selectivity, compatibility, and reliability. The enhancement factor (EF) of Raman scattering in SERS can range from 10^8 to 10^{14}, enabling even a single molecule detection [54].

In surface-enhanced Raman scattering (SERS) spectroscopy, the choice of substrate plays a pivotal role in determining the sensitivity and effectiveness of the detection process. Traditionally, noble metal substrates, such as those made from Gold (Au), Silver (Ag), and Copper (Cu), have been the standard due to their superior plasmonic properties. When illuminated, these metals exhibit strong localised surface plasmon resonances (LSPRs), leading to significant enhancement of the Raman signal from molecules adsorbed on their surfaces. These substrates are known as noble metal SERS substrates. Noble metal substrates are known for their stability, high enhancement factors, and suitability for detecting various chemical and biological analytes. However, they can be expensive and sometimes lack specificity for specific applications.

In contrast, noble metal-free SERS substrates have been developed to overcome some limitations associated with noble metals, such as cost and material availability. These alternatives include substrates made from materials like graphene, transition metal dichalcogenides (e.g., MoS_2), metal oxides (e.g., TiO_2), or semiconductor nanostructures. Although these materials typically exhibit lower enhancement factors than noble metals, they offer unique advantages such as chemical tunability, biocompatibility, and potential for integration into various devices. For example, graphene-based substrates can provide uniform enhancement and possess unique electronic properties that can be tailored for specific sensing applications. Additionally, metal oxide substrates can be modified to enhance their plasmonic properties and provide stability under different environmental conditions. The development of noble metal-free SERS substrates is an active area of research aimed at broadening the applicability and affordability of SERS technology for diverse analytical applications.

1.2.4.1 Mechanism of SERS

The mechanism of SERS involves two primary enhancement effects: electromagnetic (EM) and chemical (CM).

(a) EM enhancement mechanism:

The electromagnetic (EM) enhancement in SERS is driven by surface plasmons, which are the resonant collective oscillations of electrons within the conduction band of metal nanostructures. These surface plasmons resonate with incident light at specific wavelengths, leading to increased electron oscillation, known as localised surface plasmon resonance (LSPR). This enhanced LSPR significantly boosts the Raman scattering cross-section of molecules adsorbed on the metal surface. The LSPR properties of metal nanostructures can be controlled and fine-tuned by adjusting their size, shape, morphology, and composition. Additionally, tuning the structural parameters of nanostructures can further modulate SERS enhancement. Plasmon energy remains bound to the surface on smooth surfaces, while on rough surfaces, it scatters, making surface roughness a critical factor for EM enhancement. This EM enhancement has a long-range effect, increasing the Raman scattering cross-section of analyte molecules located several nanometres from the nanostructure's hot spot. The enhancement mechanism of noble metal SERS substrates can be primarily explained by this EM enhancement process [55-57].

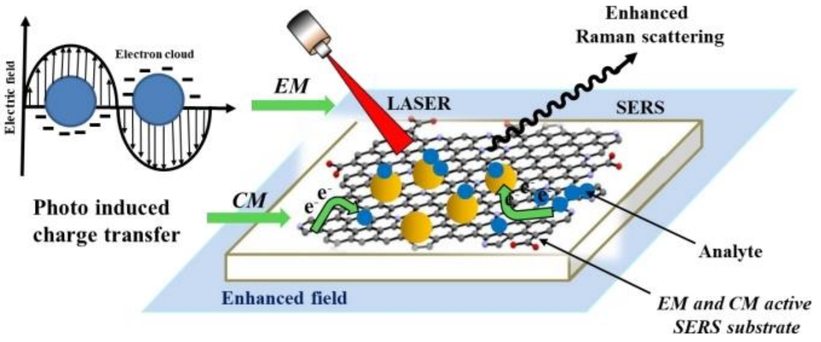

Fig. 1.5. Graphical representation for the mechanism of SERS-based detection of analyte (figure adapted from reference no 56)

(b) CM enhancement mechanism:

The chemical mechanism (CM) is another theory that explains the enhancement of Raman scattering cross-sections for analyte molecules adsorbed on SERS substrates. This theory was supported by observations from Moskovits et al. [58], who noted that the Raman peak enhancement for CO was about 200 times greater than that for N_2, indicating the presence of an additional mechanism beyond the electromagnetic (EM) mechanism, one that involves the chemical structure of the analyte. The CM mechanism involves chemical interactions and charge transfer between the metal nanostructure and the adsorbed analyte, enhancing Raman scattering. This enhancement requires direct interaction between the metal nanostructures and the analyte, making it a short-range effect, usually limited to the first layer of adsorbed molecules. The formation of a new surface complex through chemical interaction results in photo-induced charge transfer, which alters the polarizability of the adsorbed analyte molecule, thereby enhancing the Raman scattering cross-section [55-57]. EM and CM mechanisms can co-occur in highly sensitive SERS scenarios, with the EM mechanism generally playing a more prominent role. The CM mechanism is chemically selective, whereas the EM mechanism is nonselective [57].

Selectively detecting a specific analyte from mixtures containing multiple analytes poses a significant challenge. In SERS, the chemical mechanism (CM) provides selectivity, necessitating enhancements in the chemical interaction between the analyte and the SERS substrate to improve selectivity.

1.2.5. Different methods for phthalate removal.

(i) Advanced oxidation process (AOP)

Advanced Oxidation Processes (AOPs) are chemical treatment technologies that remove organic pollutants from water and wastewater. These processes generate highly reactive species, primarily hydroxyl radicals (•OH), which have a high oxidation potential and can effectively degrade a wide range of organic contaminants into harmless end products such as carbon dioxide and water. The fundamental principle of AOPs is the production of hydroxyl radicals, among the most potent oxidants available. These radicals react non-selectively with organic compounds, breaking them down through a series of reactions that ultimately lead to their mineralisation.

Common AOP Techniques:

❖ **Ozonation:**

- Process: Ozone (O_3) is dissolved in water, decomposing to produce hydroxyl radicals.
- Advantages: Effective against various pollutants and can operate in both gaseous and aqueous phases.
- Disadvantages: High operational costs are due to the need for ozone generation and the potential formation of by-products like bromate.

❖ **Photocatalysis:**

- Process: Utilises a semiconductor catalyst (e.g., titanium dioxide, TiO_2) activated by UV light to generate hydroxyl radicals.
- Advantages: Highly efficient and capable of degrading a wide range of contaminants.
- Disadvantages: UV light is required, which can increase energy costs and challenges related to catalyst recovery and deactivation.

❖ **Fenton and Photo-Fenton Processes:**

- Process: Involves the reaction of hydrogen peroxide (H_2O_2) with ferrous iron (Fe^{2+}) to produce hydroxyl radicals. The photo-Fenton process is an enhancement using UV or visible light.
- Advantages: Rapid and effective degradation of organic pollutants and can be enhanced by sunlight, reducing energy costs.
- Disadvantages: Generates iron sludge that needs disposal and requires acidic conditions (pH ~3).

❖ **Peroxone (O_3/H_2O_2):**

- Process: Combines ozone and hydrogen peroxide to enhance the production of hydroxyl radicals.
- Advantages: The synergistic effect increases the efficiency of pollutant degradation.
- Disadvantages: Requires careful control of the ozone to hydrogen peroxide ratio and may form secondary pollutants.

(ii) Biodegradation

Biodegradation is a natural process by which microorganisms such as bacteria, fungi, and algae break down complex organic compounds into simpler, non-toxic substances. This process is particularly relevant for the removal of phthalates. The biodegradation of phthalates involves a series of enzymatic reactions facilitated by microorganisms. The process can be aerobic (in the presence of oxygen) or anaerobic (in the absence of oxygen), depending on the environmental conditions and the microbial species involved. This process begins with ester hydrolysis, where esterases and lipases catalyse the conversion of phthalates into phthalic acid and alcohol. Subsequent degradation of phthalic acid occurs through pathways such as ortho-cleavage and meta-cleavage, facilitated by dioxygenases and monooxygenases, leading to complete mineralisation into carbon dioxide, water, and biomass by various catabolic enzymes involved in the Krebs cycle and beta-oxidation. Microorganisms capable of this process include bacteria like Pseudomonas spp., Bacillus spp., Rhodococcus spp., and Sphingomonas spp., fungi such as Aspergillus niger, Penicillium spp., and Phanerochaete chrysosporium, and certain species of algae. The efficiency of biodegradation is influenced by environmental conditions (temperature, pH, oxygen availability, nutrient levels), the presence and abundance of specific microbial species, and the concentration and chemical structure of phthalates. This eco-friendly and cost-effective method enhances the natural attenuation of contaminants without producing harmful by-products. However, biodegradation rates can vary, and sometimes intermediates or by-products persist in the environment, necessitating further treatment. Optimisation through bioaugmentation or bio stimulation may be required to enhance effectiveness.

(iii) Membrane filtration

Membrane filtration is an advanced separation technique that removes phthalates from water and wastewater. This method leverages semi-permeable membranes to selectively allow the passage of specific molecules while retaining others based on size, charge, and other properties. The process is highly effective for filtering out contaminants, including phthalates. The method utilises various membrane types with distinct pore sizes to target specific pollutants. Microfiltration (MF) with pore sizes from 0.1 to 10 micrometres removes larger particles and suspended solids, while Ultrafiltration (UF) with 0.01 to 0.1 micrometres retains macromolecules and colloids. Nanofiltration (NF) with 0.001 to 0.01 micrometres removes small organic molecules, including phthalates and divalent ions. Reverse Osmosis (RO) with pores smaller than 0.001 micrometres offers the highest filtration level, eliminating almost all dissolved salts, organic molecules, and contaminants. The process involves passing water through these membranes under varying pressures, where the membrane acts as a barrier, allowing only water molecules to pass while retaining phthalates and other contaminants. The filtered water, or permeate, is collected, while the retentate containing concentrated contaminants is discarded or treated. This method is highly efficient, scalable, environmentally friendly, and flexible, allowing for customisation based on specific removal needs. However, challenges include membrane fouling from organic matter or scaling, high costs associated with quality membranes and energy, and needing to properly dispose of or treat the retentate. Regular maintenance is essential to prevent fouling and ensure system longevity and performance.

(iv) Chemical precipitation

Chemical precipitation is a widely utilised method for phthalate removal from water, transforming soluble phthalates into insoluble forms for easy separation. This process involves adding chemicals like Aluminium sulphate, ferric chloride, or calcium hydroxide, which react with phthalates to form solid precipitates. These precipitates are aggregated using coagulants and flocculants, enhancing their size and settling speed. The solid particles are then separated via sedimentation, filtration, or centrifugation, resulting in a sludge that must be appropriately managed. The treated water may require further purification to remove residual chemicals, ensuring it is phthalate-free. This method is effective, straightforward, scalable, and suitable for various treatment volumes. However, it necessitates careful handling of chemicals, proper sludge disposal, and consideration of additional costs associated with chemical use and sludge management. Despite these challenges, chemical precipitation remains a potent technique for phthalate removal, balancing efficiency and environmental safety.

(v) Phytoremediation

Phytoremediation offers a promising approach for the remediation of phthalates from contaminated environments, leveraging the natural capabilities of plants to uptake, degrade, or immobilise pollutants like phthalates. Plants can absorb phthalates through their roots and translocate them to various plant tissues where they can be metabolised or stored. The remediation process typically involves selecting suitable plant species that can accumulate phthalates efficiently without compromising their growth. Once absorbed, phthalates may undergo biochemical transformations within the plant, facilitated by enzymes involved in detoxification pathways. Phytoremediation is particularly advantageous due to its environmental friendliness, as it minimises the need for extensive excavation chemical treatments. However, the efficacy of phytoremediation can vary based on factors such as plant species selection, environmental conditions, and the specific phthalate contaminants present. Continued research and optimisation of phytoremediation strategies hold promise for enhancing its effectiveness as a sustainable and cost-effective solution for phthalate contamination in soil and water systems.

Considering the challenges of the above-mentioned techniques, we opted for the adsorption technique to remove phthalates from water samples.

(vi) Adsorption

The adsorption technique for phthalate removal involves using adsorbent materials to capture and remove phthalate molecules from water or aqueous solutions. Adsorption is a surface-based process where phthalates adhere to the surface of solid materials, known as adsorbents, due to attractive forces such as Van der Waals interactions, hydrogen bonding, and electrostatic interactions. Commonly used adsorbents include activated carbon, zeolites, clay minerals, and various modified materials like graphene oxide and nanomaterials. This method passes the contaminated water through a bed or column packed with the adsorbent material. The phthalate molecules in the water adhere to the surface of the adsorbent, effectively reducing their concentration in the treated water. The efficiency of adsorption depends on factors such as the surface area and porosity of the adsorbent, pH of the solution, temperature, contact time, and initial concentration of phthalates. After adsorption, the adsorbent may be regenerated or disposed of, depending on the material and the level of contamination. Adsorption is favoured for its simplicity, cost-effectiveness, and ability to remove a wide range of contaminants from water.

In the present work, polymer nanocomposites are exploited for the adsorptive removal of phthalates. Polymer nanocomposites (PNCs) have emerged as promising materials for the adsorptive removal of phthalates from water due to their unique properties and structural flexibility. These composites comprise a polymer matrix embedded with nanoparticles, which can be tailored to enhance adsorption efficiency. The nanoparticles, such as activated carbon, metal oxides, or clay minerals, provide high surface area and specific binding sites that attract phthalate molecules from aqueous solutions. The polymer matrix in PNCs offers mechanical strength and stability and can be functionalised to improve adsorption properties further. The adsorption mechanism involves physical interactions (e.g., Van der Waals forces, π-π interactions) and chemical interactions (e.g., hydrogen bonding) between the phthalates and the composite material. Factors influencing adsorption include the type and concentration of nanoparticles, polymer matrix characteristics, pH, temperature, and the initial concentration of phthalates. PNCs offer advantages such as tunable properties, scalability, and potential for regeneration. Continued research aims to optimise PNCs for efficient and sustainable phthalate removal in water treatment applications.

1.3. Polymer Nanocomposites for Metamaterial Applications

Polymer nanocomposites (PNCs) have garnered significant interest for their potential applications in metamaterials, owing to their unique combination of properties derived from polymers and embedded nanoscale fillers. These materials offer tunable electromagnetic responses and structural flexibility, making them ideal candidates for designing metamaterials with unconventional optical, acoustic, and thermal properties. By integrating nanoparticles into polymer matrices, PNCs can achieve unusual functionalities. Their versatility and adaptability make PNCs promising for exploring new frontiers in metamaterial research.

1.3.1 Introduction to Metamaterials

Metamaterials represent a cutting-edge area of science that integrates physics, materials science, engineering, and chemistry to create artificial composite structures with extraordinary properties. The prefix 'meta-' signifies 'beyond,' indicating that metamaterials possess characteristics that surpass those found in natural materials. Unlike conventional materials, whose properties stem from their chemical composition, metamaterials derive their unique physical attributes from engineered internal structures. These structures interact with electromagnetic waves in precise ways, enabling the manifestation of remarkable properties that are not achievable with naturally occurring or conventionally synthesised materials. This distinct ability to manipulate electromagnetic waves distinguishes metamaterials as advanced composites that push beyond the limits of natural materials.

Victor Veselago's visionary ideas in 1967 laid the foundation for the field of metamaterials, particularly in exploring the concept of materials with a negative refractive index, as discussed in his seminal work in 1968. Such materials are characterised by effective medium parameters like dielectric permittivity ($\varepsilon(\omega)$) and magnetic permeability ($\mu(\omega)$), which are crucial for understanding their interaction with electromagnetic waves. Unlike natural materials, which typically lack significant magnetic responses at high frequencies, metamaterials can exhibit pronounced magnetic characteristics in these regimes, leading to the exploration of extraordinary phenomena. Permittivity and permeability describe how a material responds to electric and magnetic fields, respectively, influencing and being influenced by them. The conceptual framework, illustrated in Fig 1.6 as the "Material Parameter Space," categorises materials based on their electromagnetic properties. Region, I represent materials with positive permittivity and permeability, encompassing most dielectric materials. Region II includes metals, ferroelectric materials, and doped semiconductors capable of exhibiting negative permittivity under specific conditions, typically below the plasma frequency. Region IV involves certain ferrite materials with negative permeability, although this response diminishes above microwave frequencies. The most intriguing region, quadrant III, theoretically encompasses materials with negative permittivity and permeability simultaneously. It is a combination not found in nature but promising for its exceptional properties as originally theorised by Veselago over forty years ago.

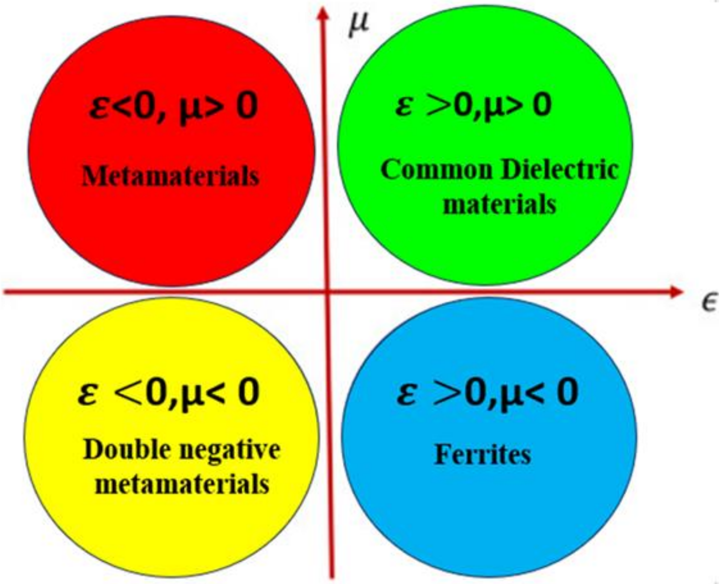

Fig 1.6. Material parameter space characterised by electric permittivity (ε) and magnetic permeability (μ).

1.3.2 Characteristics of metamaterials

Several distinct features characterise these materials:

- **Negative Refractive Index**: Metamaterials can achieve a negative refractive index, allowing them to bend light in unconventional ways. This property enables applications like superlenses and invisibility cloaks by manipulating how light interacts with the material.

- **Tailored Electromagnetic Properties**: Unlike natural materials, metamaterials can be designed with precise control over their electromagnetic responses. The controlling parameters include permittivity (electric field response) and permeability (magnetic field response), often achieving negative values, which are crucial for manipulating electromagnetic waves in desired ways.

- **Tunability**: Metamaterials offer tunable electromagnetic properties, allowing adjustments across different electromagnetic spectrum frequencies. This tunability is essential for applications in antennas, sensors, and imaging systems where specific frequency responses are required.

- **Anisotropic Properties**: Anisotropy in metamaterials means that their electromagnetic properties vary depending on the direction of the incident wave. This directional dependency enables precise control over wave propagation, polarisation, and other wave characteristics.

- **Broadband Performance**: Metamaterials can operate effectively over a broad range of frequencies, from microwave to optical wavelengths. This broadband capability is advantageous in applications such as telecommunications, where devices need to handle signals across multiple frequency bands.

- **Nonlinear Behavior**: Some metamaterials exhibit nonlinear responses to electromagnetic fields, meaning their properties change non-proportionally with the intensity of the incident wave. This nonlinear behaviour can be exploited for signal processing, frequency conversion, and nonlinear optics applications.

- **Negative permittivity**: Metamaterials are distinguished by their ability to exhibit negative permittivity, a property not found in natural materials. Permittivity refers to the ability of a material to respond to an electric field by polarising its molecules. In conventional materials, permittivity is typically positive, meaning they support the propagation of electromagnetic waves according to standard laws of physics. However, metamaterials are engineered to have negative permittivity at specific frequencies. This unique characteristic arises from their carefully designed subwavelength structures, which interact with electromagnetic waves in ways that lead to counterintuitive behaviours. Negative permittivity in metamaterials allows for unconventional manipulation of electromagnetic fields, enabling applications such as super lenses, electromagnetic cloaking devices, and antennas with enhanced performance. By harnessing negative permittivity, metamaterials pave the way for novel technologies that defy traditional electromagnetic principles and open new avenues in optics, telecommunications, and sensor development.

- **Negative permeability**: This unique property arises from the engineered structure of metamaterials rather than the inherent properties of their constituent materials. Negative permeability means that metamaterials can interact with magnetic fields in a manner opposite to conventional materials, effectively reversing the direction of magnetic flux when subjected to an external field. This phenomenon is crucial for manipulating electromagnetic waves at specific frequencies and wavelengths, enabling subwavelength imaging, electromagnetic cloaking, and antenna design applications. By controlling the internal geometries and configurations of metamaterials, engineers can tailor their magnetic responses across a wide range of frequencies, offering unprecedented flexibility in electromagnetic device design and functionality. The ability to achieve negative permeability marks metamaterials as pivotal in advancing technologies that rely on precise electromagnetic wave control and manipulation.

1.3.3 Negative permittivity and Metamaterials

Permittivity refers to the extent to which an electric field can penetrate a medium at a specific frequency. In materials where significant distances separate abundant free charges, this condition, akin to a plasma state, influences the permittivity and affects how electric fields interact with the medium.

$$\varepsilon = \varepsilon_0\left(1 - \frac{{\omega_p}^2}{\omega^2}\right) \qquad (1.1)$$

The expression for permittivity involving the plasma frequency (ω_p) is valid for ideal plasma across all frequencies, but for other materials, it holds only at high frequencies. Examples of plasmas include the ionosphere and electrically charged gases in laboratory settings. Notably, plasmas do not have an imaginary component in their dielectric constant. This implies that above the plasma frequency, the dielectric constant of plasma remains positive and real, resulting in a purely real wave number (k) and indicating no loss, allowing the wave to propagate unimpeded. Conversely, below the plasma frequency, the dielectric constant is always negative and real, leading to a purely imaginary wave number (k). As a result, a wave incident on a plasma below this frequency will be entirely reflected, with fields penetrating only slightly and decaying exponentially within the plasma. This phenomenon explains why radio waves are reflected by the ionosphere for low-bandwidth global communications, while higher-frequency microwaves pass through it and require satellite relays for high-bandwidth communications. The effective permittivity becomes negative when the frequency drops below the plasma frequency.

In this thesis, we have designed and fabricated metamaterials exhibiting negative permittivity.

1.4 Motivation for the work

The rapid advancements in material science have led to the development of innovative materials with unique properties, among which polymer nanocomposites stand out for their ability to combine the benefits of polymers and nanomaterials. The performance of these nanocomposites is critically dependent on their structure-defining capability, which can be tailored by controlling the dispersion, orientation, and interaction of nanomaterials within the polymer matrix. ***The motivation for this research work can be summarised as the need to expand the utility of the structure-defining capability of polymers for relevant environmental and dielectric applications.***

For environmental applications, we chose to focus on phthalate detection and removal due to the widespread use of phthalates in industrial products and their significant impact on human health and ecosystems. Phthalates are known endocrine disruptors, and their pervasive presence in water sources necessitates effective detection and removal methods. Polymer nanocomposites offer unique properties that make them ideal for this task.

(i) The high surface area and tunable surface chemistry of nanomaterials within the composites could enhance sensitivity and selectivity, enabling the accurate identification of low concentrations of phthalates.

(ii) The exceptional adsorption capacity and chemical functionality of polymer nanocomposites could facilitate the efficient capture and removal of phthalate molecules.

Utilising those properties of polymer nanocomposites, our research could develop advanced composites capable of detecting and removing phthalates, contributing to cleaner water sources and improved environmental health.

For dielectric applications, we identified a significant gap in the availability of suitable metamaterials for extremely low frequency applications. 10^1 to 10^{-2} Hz electromagnetic waves belonging to the extremely low frequency (ELF) regime are the lowest frequency waves regularly utilised for wireless transmission and communication. Polymer nanocomposites possess properties that make them excellent candidates for filling this gap. Their ability to be engineered at the nanoscale allows for precise control over electromagnetic properties, essential for creating practical metamaterials. The structure-defining capability to create interconnected networks and the high dielectric constant and tunable electrical conductivity of polymer nanocomposites enable the design of materials with unique electromagnetic responses tailored to the extra-low frequency range. By leveraging these properties, our research aims to develop advanced polymer nanocomposite-based metamaterials that can address the current limitations and meet the demands of dielectric materials for this specific frequency regime.

1.5 Objectives of the Work

The research conducted in this thesis is driven by the motivations outlined in the previous section (1.4). Based on those motivations, the objectives of the thesis can be listed as follows:

i. Synthesise certain innovative nanocomposite materials that utilise the unique structure-defining features of polymers.

ii. To address environmental or dielectric material challenges using the synthesised polymer nanocomposites.

iii. Develop polymer nanocomposite based noble metal-free SERS substrates with high surface area and tunable surface chemistry to enhance the sensitivity and selectivity for detecting low concentrations of phthalates in water sources.

iv. Utilise the exceptional adsorption capacity and chemical functionality of polymer nanocomposites to facilitate the efficient capture and removal of phthalate molecules from contaminated water.

v. Identify and fill the gap in the availability of suitable metamaterials for applications in extra-low frequency regions (10^1 to 10^{-2} Hz) using polymer nanocomposites.

1.6 Brief Outline of the Chapters in the Thesis.

The experimental work has been conducted in alignment with the thesis objectives. Chapter 2 provides a detailed overview of the various characterisation techniques and experimental procedures employed in the study. Chapters 3 to 7 present the detailed experiments and analysis of results. Chapter 3 primarily focuses on detecting DMP and DEP phthalates using suitable BT and PMMA_BT SERS substrates, addressing the underlying mechanisms. Chapter 4 discusses the study of a flexible, hotspot-engineered PMMA_ST SERS substrate for DEHP detection, providing insights into its mechanism. Chapter 5 highlights the removal of phthalates from aqueous solutions using PPy_ZnO polymer nanocomposites, explaining the adsorption-based mechanism behind the removal process. In Chapter 6, novel heterogeneous polymer nanocomposites based on PMMA_ZnO_AC are designed and synthesised for negative permittivity applications at extremely low frequencies, with a theoretical explanation rooted in plasma theory. Chapter 7 deals with the design of a ceramic hybrid polymer nanocomposite system, PMMA_$CaTiO_3$_Graphite, which exhibits a high value of negative permittivity. Finally, Chapter 8 presents the conclusions and chapter 9 provides the recommendations for future endeavours on the present study.

1.7 References

[1] NRC 2006 Human biomonitoring for environmental chemicals, pp. 167 –172. Washington, DC: National Research Council, National Academies Press.

[2] Khare H S and Burris D L A quantitative method for measuring nanocomposite dispersion Polymer 2010 , 51 719–29'

[3] Viswanathan V, Laha T, Balani K, Agarwal A and Seal S Challenges and advances in nanocomposite processing techniques Materials Science and Engineering: R: Reports 2006, 54 121–285.

[4] Li C, Sun W, Lu Z, Ao X and Li S Ceramic nanocomposite membranes and membrane fouling: A review Water Research, 2020 , 175 115674.

[5] Avasthi D K, Mishra Y K, Kabiraj D, Lalla N P and Pivin J C Synthesis of metal–polymer nanocomposite for optical applications Nanotechnology, 2007, 18 125604.

[6] Huang X and Jiang P Core–Shell Structured High-k Polymer Nanocomposites for Energy Storage and Dielectric Applications Advanced Materials, 2015, 27 546–5

[7] Akharame, M.O.; Fatoki, O.S.; Opeolu, B.O.; Olorunfemi, D.I.; Oputu, O.U. Polymeric Nanocomposites (PNCs) for Wastewater Remediation: An Overview. Polym. Technol. Eng. 2018, 57, 1801–1827.

[8] Wen, Y.; Yuan, J.; Ma, X.; Wang, S.; Liu, Y. Polymeric nanocomposite membranes for water treatment: A review. Environ. Chem. Lett. 2019, 17, 1539–1551.

[9] Mohammed, N.; Grishkewich, N.; Tam, K.C. Cellulose nanomaterials: Promising sustainable nanomaterials for application in water/wastewater treatment processes. Environ. Sci. Nano 2018, 5, 623–658.

[10] Khan, M.A.; Govindasamy, R.; Ahmad, A.; Siddiqui, M.; Alshareef, S.; Hakami, A.; Rafatullah, M. Carbon Based Polymeric Nanocomposites for Dye Adsorption: Synthesis, Characterisation, and Application. Polymers 2021, 13, 419.

[11] Zaman, A.; Orasugh, J.T.; Banerjee, P.; Dutta, S.; Ali, M.S.; Das, D.; Bhattacharya, A.; Chattopadhyay, D. Facile one-pot in-situ synthesis of novel graphene oxide-cellulose nanocomposite for enhanced azo dye adsorption at optimised conditions. Carbohydr. Polym. 2020, 246, 116661.

[12] Peng, N.; Hu, D.; Zeng, J.; Li, Y.; Liang, L.; Chang, C. Superabsorbent Cellulose–Clay Nanocomposite Hydrogels for Highly Efficient Removal of Dye in Water. ACS Sustain. Chem. Eng. 2016, 4, 7217–7224.

[13] Wang, N.; Chen, J.; Wang, J.; Feng, J.; Yan, W. Removal of methylene blue by Polyaniline/TiO2 hydrate: Adsorption kinetic, isotherm and mechanism studies. Powder Technol. 2019, 347, 93–102.

[14] Momina; Ahmad, K. Study of different polymer nanocomposites and their pollutant removal efficiency: Review. Polymers 2021, 217, 123453.

[15] Ebrahim, S.; Shokry, A.; Ibrahim, H.; Soliman, M. Polyaniline/akaganéite nanocomposite for detoxification of noxious Cr(VI) from aquatic environment. J. Polym. Res. 2016, 23, 79.

[16] Akl, Z.F.; El-Saeed, S.M.; Atta, A.M. In-situ synthesis of magnetite acrylamide amino-amidoxime nanocomposite adsorbent for highly efficient sorption of U(VI) ions. J. Ind. Eng. Chem. 2016, 34, 105–116.

[17] Tran, M.T.; Nguyen, T.H.T.; Vu, Q.T.; Nguyen, M.V. Properties of poly (1-naphthylamine)/Fe3O4 composites and arsenic adsorption capacity in wastewater. Front. Mater. Sci. 2016, 10, 56–65.

[18] Zhao, G.; Huang, X.; Tang, Z.; Huang, Q.; Niu, F.; Wang, X.-K. Polymer-based nanocomposites for heavy metal ions removal from aqueous solution: A review. Polym. Chem. 2018, 9, 3562–3582.

[19] Samiey, B.; Cheng, C.-H.; Wu, J. Organic-Inorganic Hybrid Polymers as Adsorbents for Removal of Heavy Metal Ions from Solutions: A Review. Materials 2014, 7, 673–726.

[20] H. Althues, J. Henle, S. Kaskel, Chem. Soc. Rev. 36 ,2007, 1454.

[21] C.W. Lee, C. Renaud, C.S. Hsu, T.P. Nguyen, Nanotechnology 19 ,2008, 455202.

[22] Xin Zhao, Lu Lv, Bingcai Pan, Weiming Zhang, Shujuan Zhang, Quanxing Zhang, Polymer-supported nanocomposites for environmental application: A review,Chemical Engineering Journal, Volume 170, Issues 2–3, 2011, Pages 381-394, ISSN 1385-8947, https://doi.org/10.1016/j.cej.2011.02.071.

[23] Shrivastava, S.; Jadon, N.; Jain, R. Next-generation polymer nanocomposite-based electrochemical sensors and biosensors: A review. TrAC Trends Anal. Chem. 2016, 82, 55–67.

[24] Luka, G.; Ahmadi, A.; Najjaran, H.; Alocilja, E.; DeRosa, M.; Wolthers, K.; Malki, A.; Aziz, H.; Althani, A.; Hoorfar, M. Microfluidics Integrated Biosensors: A Leading Technology towards Lab-on-a-Chip and Sensing Applications. Sensors 2015, 15, 30011–30031.

[25] Kamrin, M. A., and Mayor, G. H. (1991). Diethyl phthalate: a perspective. J. Clin Pharmacol, 31, 484–489.

26] Chen, B., Song, J., Yang, L. *et al.* Coupling UV–H_2O_2 to accelerate dimethyl phthalate (DMP) biodegradation and oxidation. *Biodegradation* 2015, 26, 431–441. https://doi.org/10.1007/s10532-015-9744-3

[27] Kushwaha M, Singh D, Akhter Y, Chatterjee S. Biodegradation of DEP, DIBP, and BBP by a psychrotolerant Sphingobium yanoikuyae strain P4: Degradation

potentiality and mechanism study. Arch Microbiol. 2024 May 10;206(6):254. doi: 10.1007/s00203-024-03977-7. PMID: 38727835.

[28] PubChem , https://pubchem.ncbi.nlm.nih.gov

[29] Tao HY, Shi J, Zhang J, Ge H, Zhang M, Li XY. Developmental toxicity and mechanism of dibutyl phthalate and alternative diisobutyl phthalate in the early life stages of zebrafish (Danio rerio). Aquat Toxicol. 2024 Jul;272:106962. doi: 10.1016/j.aquatox.2024.106962. Epub 2024 May 16. PMID: 38797068.

[30] Guo Z, Wang L, Li Y, Wu Z, Wang K, Duan J. Dust phase and window film phase phthalates in dormitories: profile characteristics, source screening, and estimated gas-phase concentration and dermal exposure comparison. Environ Sci Pollut Res Int. 2024 Feb;31(10):15257-15270. doi: 10.1007/s11356-024-32019-4. Epub 2024 Jan 30. PMID: 38291205.

[31] Ye J, Zhang K, Yuan X, Ji H, Hu M, Huang T, Ge RS. Di-n-hexyl phthalate causes Leydig cell hyperplasia in rats during puberty. Toxicol Lett. 2020 Oct 10;332:213-221. doi: 10.1016/j.toxlet.2020.07.018. Epub 2020 Jul 18. PMID: 32693021.

[32] Rushdi, A.I., Simoneit, B.R.T., Lijotra, L. *et al.* Phthalates, non-phthalates, polychlorinated biphenyls, and phenyl phosphates in atmospheric suspended particulate matter of Dhahran City, Saudi Arabia: levels and seasonal variation. *Int. J. Environ. Sci. Technol.* 2023, 20, 3561–3576. https://doi.org/10.1007/s13762-022-04247-z

[33] Shengnan Hu, Ronghui Wu, Ming Guo, Heterogeneous catalysis of di-n-octyl phthalate by pepsin based on an ionic coordination regulation strategy driving the evolution of MOF pore structure, Molecular Catalysis, Volume 564,2024,114285, ISSN 2468-8231, https://doi.org/10.1016/j.mcat.2024.114285.

[34] Derek Brown, Charlotte P. Croudace, Nicola J. Williams, Julian M. Shearing, Peter A. Johnson, The effect of phthalate ester plasticisers tested as surfactant stabilised dispersions on the reproduction of the Daphnia magna, Chemosphere, Volume 36, Issue 6, 1998, Pages 1367-1379, ISSN 0045-6535, https://doi.org/10.1016/S0045-6535(97)10018-2.

[35] Pace, A.; Vaglica, A.; Maccotta, A.; Savoca, D. The Origin of Phthalates in Algae: Biosynthesis and Environmental Bioaccumulation. *Environments* 2024, *11*, 78.https://doi.org/10.3390/environments11040078.

[36] rin E. Yost, Susan Y. Euling, James A. Weaver, Brandiese E.J. Beverly, Nagalakshmi Keshava, Anuradha Mudipalli, Xabier Arzuaga, Todd Blessinger, Laura Dishaw, Andrew Hotchkiss, Susan L. Makris,

[37] Hazards of diisobutyl phthalate (DIBP) exposure: A systematic review of animal toxicology studies, Environment International, Volume 125, 2019, Pages 579-594, ISSN 0160-4120, https://doi.org/10.1016/j.envint.2018.09.038.

[38] Michele Bertoncello Souza, Marcella Tapias Passoni, Claudia Pälmke, Katlyn Barp Meyer, Amanda Caroline Venturelli, Giulia Araújo, Bruno Sanches de Castilhos, Rosana Nogueira Morais, Paulo Roberto Dalsenter, Shanna Helen Swan, Holger Martin Koch, Anderson Joel Martino-Andrade,Unexpected, ubiquitous exposure of pregnant Brazilian women to diisopentyl phthalate, one of the most potent

antiandrogenic phthalates, Environment International, Volume 119, 2018, Pages 447-454, ISSN 0160-4120, https://doi.org/10.1016/j.envint.2018.06.042.

[39] Rama-Krishnan Poopal, Jingxuan Zhang, Ruibin Zhao, Mathan Ramesh, Zongming Ren, Biochemical and behavior effects induced by diheptyl phthalate (DHpP) and Diisodecyl phthalate (DIDP) exposed to zebrafish, Chemosphere, Volume 252, 2020, 126498, ISSN 0045-6535, https://doi.org/10.1016/j.chemosphere.2020.126498.

[40] Alejandra Martínez-Ibarra, Marco Cerbón, Luis Daniel Martínez-Razo, Miguel Morales-Pacheco, Iván Torre-Villalvazo, Simón Kawa, Mauricio Rodríguez-Dorantes, Impact of DEHP exposure on female reproductive health: Insights into uterine effects, Environmental Toxicology and Pharmacology,Volume 107, 2024, 104391, ISSN 1382-6689, https://doi.org/10.1016/j.etap.2024.104391.

[41] Bereketoglu, C., Häggblom, I., Turanlı, B., & Pradhan, A. (2024). Comparative analysis of diisononyl phthalate and di(isononyl)cyclohexane-1,2 dicarboxylate plasticisers in regulation of lipid metabolism in 3T3-L1 cells. *Environmental Toxicology*, *39*(3), 12451257. https://doi.org/10.1002/tox.24010.

[42] Jin, Y., Wang, J., Xu, H., Wang, C., Hu, Q., Hayat, K., … Liu, W. (2023). Ecological and human health risk of aryl-phosphate flame retardants (APFRs): Sources, distribution, and toxicity. *Critical Reviews in Environmental Science and Technology*, *54*(15), 1117–1137. https://doi.org/10.1080/10643389.2023.2293425.

[43] Lee, K. J., & Choi, K. (2023). Environmental occurrence, human exposure, and endocrine disruption of di-iso-nonyl phthalate and di-iso-decyl phthalate: A systematic review. *Critical Reviews in Environmental Science and Technology*, *54*(8), 603–640. https://doi.org/10.1080/10643389.2023.2261815.

[44] Hatzidaki, E.; Pagkalou, M.; Katsikantami, I.; Vakonaki, E.; Kavvalakis, M.; Tsatsakis, A.M.; Tzatzarakis, M.N. Endocrine-Disrupting Chemicals and Persistent Organic Pollutants in Infant Formulas and Baby Food: Legislation and Risk Assessments. *Foods* 2023, *12*, 1697. https://doi.org/10.3390/foods12081697

[45] Dongyang Li, Kushal Panchal, Roozbeh Mafi, and Li Xi, An Atomistic Evaluation of the Compatibility and Plasticization Efficacy of Phthalates in Poly(vinyl chloride) *Macromolecules* 2018 *51* (18), 6997-7012 DOI: 10.1021/acs.macromol.8b00756.

[46] Xiaolan Lv, Zheng Jiang, Guofang Zeng, Sujuan Zhao, Na Li, Fengping Chen, Xiaojian Huang, Jia Yao, Xun Tuo,Comprehensive insights into the interactions of dicyclohexyl phthalate and its metabolite to human serum albumin, Food and Chemical Toxicology, Volume 155, 2021, 112407, ISSN 0278-6915, https://doi.org/10.1016/j.fct.2021.112407.

[47] Evelyn Paquette, John Paul Giacalone, Michael Fumo, Nicole M. Roy, Butyl Benzyl Phthalate (BBP) disrupts neuromast development in embryonic zebrafish, Environmental Toxicology and Pharmacology, 2024, Volume 106, 2024, 104392, ISSN 1382-6689, https://doi.org/10.1016/j.etap.2024.104392.

[48] International Agency for Research on Cancer. (2000). Monographs on the evaluation of carcinogenic risks to humans. Some industrial chemicals., Lyon,

France: IAR

[49] Staples, C. A., Peterson, D. R., Parkerton, T. F., and Adams, W. J. The environmental fate of phthalate esters: a literature review. Chemosphere, 1997, 35, 667–749.

[50] Jan L. Lyche et al. (2016), Reproductive and Developmental Toxicity of Phthalates; Journal of Toxicology and Environmental Health, DOI: 10.1080/10937400903094091.

[51] M. Park, H. Jung, Y. Jeong, K.H. Jeong, Plasmonic schirmer strip for human tear-based gouty arthritis diagnosis using surface-enhanced raman scattering, ACS Nano 11 ,2017, 438–443.

[52] G. Bodelon, V. Montes-Garcia, E.H. Lopez-Puente, C. Hill, M.N. Sanz-Ortiz, L.M. Lizmarzan, Detection and imaging of quorum sensing in Pseudomonas aeruginosa biofilm communities by surface-enhanced resonance raman scattering, Nat. Mater. 2016, 15 , 1203–1211.

[53] Langer, J.; Jimenez de Aberasturi, D.; Aizpurua, J.; Alvarez-Puebla, R. A.; Auguié, B.; Baumberg, J. J.; Bazan, G. C.; Bell, S. E. J.; Boisen, A.; Brolo, A. G.; Choo, J.; Cialla-May, D.; Deckert, V.; Fabris, L.; Faulds, K.; García de Abajo, F. J.; Goodacre, R.; Graham, D.; Haes, A. J.; Haynes, C. L.; Huck, C.; Itoh, T.; Käll, M.; Kneipp, J.; Kotov, N. A.; Kuang, H.; Le Ru, E. C.; Lee, H. K.; Li, J.-F.; Ling, X. Y.; Maier, S. A.; Mayerhöfer, T.; Moskovits, M.; Murakoshi, K.; Nam, J.-M.; Nie, S.; Ozaki, Y.; Pastoriza-Santos, I.; Perez-Juste, J.; Popp, J.; Pucci, A.; Reich, S.; Ren, B.; Schatz, G. C.; Shegai, T.; Schlücker, S.; Tay, L.-L.; Thomas, K. G.; Tian, Z.-Q.; Van Duyne, R. P.; Vo-Dinh, T.; Wang, Y.; Willets, K. A.; Xu, C.; Xu, H.; Xu, Y.; Yamamoto, Y. S.; Zhao, B.; Liz-Marzán, L. M. Present and Future of Surface-Enhanced Raman Scattering. ACS Nano 2020, 14, 28-117.

[54] Cao, Y.; Zhang, J.; Yang, Y.; Huang, Z.; Long, N. V.; Fu, C. Engineering of SERS Substrates Based on Noble Metal Nanomaterials for Chemical and Biomedical Applications. Appl. Spectrosc. Rev. 2015, 50, 499-525.

[55] Luo, W.; Xiong, W.; Han, Y.; Yan, X.; Mai, L. Application of Two-dimensional Layered Materials in Surface-enhanced Raman Spectroscopy (SERS). Phys. Chem. Chem. Phys. 2022, 24, 26398-26412.

[56] Demirel, G.; Usta, H.; Yilmaz, M.; Celik, M.; Alidagi, H. A.; Buyukserin, F. SurfaceEnhanced Raman Spectroscopy (SERS): An Adventure from Plasmonic Metals to Organic Semiconductors as SERS Platforms. J. Mater. Chem. C 2018, 6, 5314-5335.

[57] M. Moskovits, Surface-enhanced Spectroscopy. Rev. Mod. Phys. 1985, 57, 783-826.

CHAPTER 2

EXPERIMENTAL TECHNIQUES

Contents

Abstract: *This chapter describes various Synthesis methods and experimental techniques adopted for for the synthesis and analysis of samples presented in this thesis. concise overview of the working principles of the instruments and their applications is provided. The discussed techniques include like XRD, FESEM, BET, BDS, RAMAN, and UV-Visible-DRS employed for characterization of fillers and its composites are discussed*

2.1 INTRODUCTION

The focus of this chapter revolves around the experimental methodologies utilised for synthesising and analysing the synthesised polymer nanocomposites. The synthesis mainly involves synthesising metal oxide nanoparticles via the solid-state reaction route and the insitu and oxidative polymerisation methods for fabricating polymer nanocomposites.

The structural characterisation was conducted utilising X-ray diffraction (XRD) techniques. Morphology, structure, and size were analysed using Field Emission Scanning Electron Microscopy (FE-SEM). Ultraviolet-visible diffuse reflectance spectroscopy (UV-Vis DRS) was employed for optical and adsorption studies. The Brunauer–Emmett–Teller (BET) technique accomplished surface area and porosity analysis. Raman spectroscopy was utilised for functional group identification, vibrational mode analysis, and Surface-Enhanced Raman Spectroscopy (SERS) studies. Broadband Dielectric spectroscopy was employed for dielectric spectroscopic studies.

2.2 SOLID STATE REACTION ROUTE

The solid-state reaction route for metal oxide synthesis involves the direct reaction of solid reactants to form metal oxides. This method typically entails heating the solid precursors, which could be metal salts, metal oxides, or other metal-containing compounds, to high temperatures in the presence of an oxidising agent or an oxygen-rich atmosphere. The reaction proceeds through solid-solid interactions between the reactants, forming the desired metal oxide product.

The solid-state reaction route offers several advantages, including simplicity, ease of scale-up, and the ability to produce high-purity metal oxides without needing solvents. Additionally, this method allows for precise control over reaction parameters such as temperature, heating rate, and duration, which can influence the phase composition, crystallinity, and morphology of the resulting metal oxide nanoparticles.

Muffle furnace: A muffle furnace plays a crucial role in the solid-state reaction route for synthesising metal oxides and various compounds. Solid precursors undergo direct solid-state interactions within the controlled environment of the furnace, where precise temperature regulation optimises reaction conditions. Typically housed in ceramic crucibles or boats to prevent direct contact with heating elements, the precursors are subjected to elevated temperatures, promoting solid-state reactions. This process facilitates the formation of desired metal oxides or compounds through the diffusion of reactant species, leading to the growth of crystalline phases and nanoparticles. The muffle furnace's utilisation in the solid-state reaction route offers notable advantages, including simplicity, scalability, and the ability to synthesise materials with controlled stoichiometry and morphology. The present study adopted a programmable muffle furnace for the synthesis process.

Fig. 2.1 Image of the muffle furnace used in the study (located at the Laboratory for Mesoscopic Sciences and Devices, Department of Physics, University of Calicut).

2.3 SOL GEL SYNTHESIS ROUTE

This approach is a highly adaptable and optimal method for producing a variety of oxide materials. It generally allows for precise control over the morphological properties, texture, and chemical stability of the solid produced. The primary advantages of the sol-gel method include the high purity of the precursors used, molecular-level mixing, and the homogeneity of the resulting sol-gel products, which exhibit high purity in their morphological, physical, and chemical properties. As indicated by its name, the method involves the formation of a sol, or colloidal suspension, through hydrolysis and subsequent condensation reactions of precursors, typically metal-organic compounds or inorganic metal salts. Factors influencing the properties of the gel, known as sol-gel parameters, include the type of solvent, type of precursor, precursor concentration, acid or base content, water content, and temperature. These parameters impact the initial gel. Gelation occurs when colloidal particles agglomerate to form precipitates. Following gelation, the resulting wet gel mixture, which is in a semi-solid state, undergoes drying and calcination to produce a dry powder. Aging, the total time between gel formation and drying, is also crucial. The resulting sol can have various structures, shapes, and dimensions, which, upon gelation and calcination, yield fine crystals with diverse structures such as nanoparticles, nanorods, nanowires, nanotubes, nanoflowers, and nanoflakes.

2.4 IN- SITU AND OXIDATIVE POLYMERISATION METHODS

We synthesised various polymer nanocomposites using the in-situ polymerisation method, including PMMA_$SrTiO_3$, PMMA_$BaTiO_3$, PMMA_AC_ZnO, and PMMA_$CaTiO_3$_Graphite. Additionally, the synthesis of the PPy_ZnO polymer nanocomposite was accomplished through the oxidative polymerisation method. The detailed synthesis procedures and properties of these corresponding composites are thoroughly discussed in the subsequent chapters of this thesis.

The **in-situ polymerisation method** is popular for synthesising polymer nanocomposites, wherein the polymer matrix is directly formed in nanofillers or nanoparticles. This method involves dispersing monomers and nanoparticles within a solvent or matrix and initiating polymerisation to generate the polymer matrix. Crucially, nanoparticles serve as nucleation sites during polymerisation, facilitating the uniform dispersion of nanoparticles within the polymer matrix. The process encompasses vital steps such as dispersion, where nanoparticles are evenly dispersed within a monomer solution or melt; initiation, initiated through suitable initiators like thermal initiators or catalysts; growth, where monomers polymerise and envelop nanoparticles, forming a polymer matrix with dispersed nanoparticles; and finally, termination, which occurs once the desired polymerisation degree is attained. Notably, the in situ polymerisation method provides numerous advantages for synthesising polymer nanocomposites, including precise control over nanoparticle dispersion and robust interfacial adhesion between nanoparticles and the polymer matrix. Additionally, it allows for incorporating a wide range of nanoparticles and monomers, enabling the customisation of nanocomposite properties to suit specific applications. The in-situ polymerisation method emerges as a versatile and extensively utilised approach for fabricating polymer nanocomposites endowed with improved mechanical, thermal, optical and electrical properties.

The **Oxidative polymerisation method** is another highly regarded technique for synthesising polymer nanocomposites, wherein the polymerisation process is initiated through the oxidation of monomers in the presence of nanoparticles or nanofillers. This method involves dispersing monomers and nanoparticles within a suitable solvent or matrix, followed by the initiation of polymerisation through oxidation reactions. Typically, this process includes crucial steps such as dispersion, where nanoparticles are uniformly dispersed within a monomer solution or melt; initiation, which is triggered by oxidising agents or catalysts, leading to the formation of radicals in the monomer molecules and subsequent polymerisation; growth, wherein monomers polymerise and encapsulate nanoparticles, resulting in the formation of a polymer matrix with dispersed nanoparticles; and termination, marking the conclusion of polymerisation once the desired degree of polymerisation is attained or when reactive sites are exhausted. The oxidative polymerisation method offers numerous advantages for synthesising polymer nanocomposites, including precise control over nanoparticle dispersion and the promotion of strong interfacial adhesion between nanoparticles and the polymer matrix. Moreover, it facilitates the incorporation of a diverse range of nanoparticles and monomers, thereby allowing for the customisation of nanocomposite properties to fulfil specific application requirements.

2.5 X-RAY DIFFRACTOMETRY (XRD)

We used X-ray Diffraction (XRD) for the structural analysis and phase identification of our polymer nanocomposites and metal oxides. XRD provided critical information about the crystallographic structure, phase composition, and crystallite size of the synthesised materials. This technique allowed us to confirm the successful incorporation of fillers like $SrTiO_3$, $BaTiO_3$, ZnO, and $CaTiO_3$ into the Polymer matrix and to study any changes in the crystalline phases that occurred due to the polymerisation process. The comprehensive analysis of XRD patterns enabled us to understand the structural integrity and morphological evolution of the polymer nanocomposites, which is essential for correlating their structural properties with their functional performance.

X-ray diffraction (XRD) is a rapid analytical technique reliant on the continuous interaction of monochromatic X-rays emitted from a cathode ray tube. These X-rays, filtered to produce monochromatic radiation, are directed onto a sample. When the X-rays hit the sample, they scatter in various directions depending on the atomic arrangement within the material. XRD is primarily utilised to determine the phase of crystalline substances and offers insights into their unit cell dimensions. By analysing the resulting XRD pattern, which serves as a unique "fingerprint" of the crystals in the sample, researchers can identify crystalline structures by comparing them to reference patterns [1].

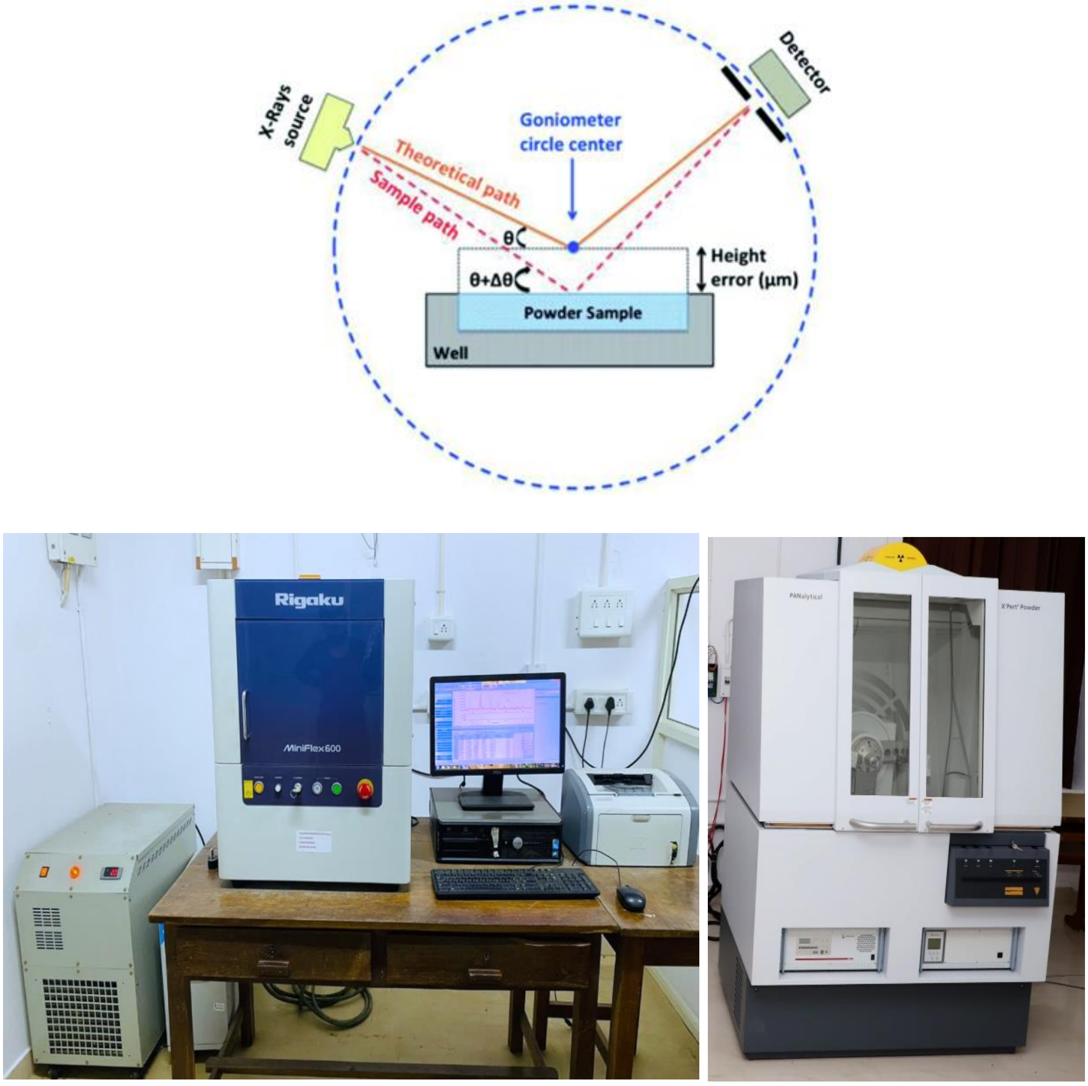

Fig.2.2 (a) Schematic diagram of XRD (image adapted from [2]). **(b)** Image of **Rigaku Miniflex 600** X-ray Diffractometer-Department of Physics, University of Calicut. **(c)** X'**pert^3 Powder** X-RAY Diffractometer-CSIF University of Calicut [3] (used for analysis in the thesis).

Understanding crystallinity is crucial as it often correlates with the properties and behaviour of materials, particularly in their development stages where specific crystalline forms may emerge. When the incident X-rays interact constructively with the sample's atomic arrangement according to Bragg's law, distinct diffraction patterns are generated, providing valuable information about the crystalline nature of the material.

$$n\lambda = 2dsin\theta \text{-------------} [2.1]$$

Bragg's law relates the wavelength of X-ray radiation (typically 0.154056 nm for a copper lamp) to the diffraction angle (θ) and lattice spacing of a crystalline sample. This law indicates that when X-rays interact with the atomic structure of a crystal, they undergo constructive interference, producing distorted X-rays, which are then identified, processed, and counted. Through scanning over a range of 2θ angles, representing all possible directions of the lattice due to the random orientation of the material, the XRD (X-ray diffraction) patterns can be obtained. Fig.2.2 (a) shows the schematic diagram of the XRD diffractometer.

Instrumentation: The X-ray diffractometer comprises three essential components: an X-ray tube, a sample holder, and a detector. X-rays are generated by directing electrons emitted from a heating filament towards a target material, where they are accelerated by applying a voltage, producing X-ray spectra. Copper is commonly used as the target material, providing X-rays with a wavelength of radiation (CuKα) of 1.5418 Å. These X-rays are collimated and directed onto the sample, and the intensity of the reflected X-rays is recorded as the sample and detector are rotated. In the instrumentation of an X-ray diffractometer, the sample rotates in the path of the X-ray beam at an angle θ, while the goniometer rotates at an angle of 2θ. When the incident X-rays satisfy the Bragg reflection condition upon striking the sample, constructive interference occurs, resulting in the observation of an intense peak. The schematic illustration in Fig 2.2 depicts the powder X-ray diffraction instrumentation using Bragg-Brentano geometry.

Applications: X-ray diffractometry identifies single or multiple phases within materials, providing valuable insights into the composition and arrangement of crystalline phases present. Additionally, it resolves crystal structures for known materials, unveiling atomic arrangements and bonding configurations. Moreover, the method aids in identifying amorphous components within partially crystalline mixtures, facilitating comprehensive material characterisation. Furthermore, X-ray diffractometry allows for structural analysis, stress-strain analysis and unit-cell parameter calculations for crystalline materials, elucidating lattice structures, loading properties and atomic arrangements. It also enables the determination of crystallite size through peak broadening analysis, offering essential information about the size and distribution of crystalline domains within materials.

Specifications: In this study, XRD patterns of all samples were acquired using a **Rigaku X-ray diffractometer** (Department of Physics, University of Calicut) **and X'pert^3 Powder X-ray diffractometer** (CSIF University of Calicut) [3] with CuKα radiation (λ = 1.5418 Å) within a Bragg angle (2θ) range from 0° to 80°.

2.6 FIELD EMISSION SCANNING ELECTRON MICROSCOPE (FESEM)

We used Field Emission Scanning Electron Microscopy (FESEM) for the detailed morphological and structural study of our polymer nanocomposites and metal oxides. FESEM provided high-resolution images that allowed us to examine the surface characteristics, particle size distribution, and the interaction between the polymer matrix and the embedded nanoparticles. This analysis was crucial for understanding the influence of nanomaterials on the overall properties of the composites. The insights gained from FESEM imaging contributed significantly to optimising the synthesis process and enhancing the performance of our polymer nanocomposites and metal oxides.

Field Emission Scanning Electron Microscopy (FESEM) is a cutting-edge imaging technique that offers unparalleled insights into material surface morphology and structure with extraordinary resolution. Its fundamental principle revolves around generating a focused electron beam using a field emission electron source, like a cold field emitter or a Schottky field emitter, which produces electrons of exceptional energy and brightness, thereby enhancing imaging capabilities. This highly focused electron beam is then directed onto the specimen surface using electromagnetic lenses, akin to conventional SEM, but with significantly heightened resolution and imaging detail. Upon interaction with the specimen's atoms, the high-energy electrons generate various signals [4,5], including secondary electrons (SE) and backscattered electrons (BSE), which carry crucial information about surface morphology and composition, forming the basis for creating detailed images. Secondary electrons, emitted from the specimen's surface upon interaction with the incident electron beam, furnish high-resolution images with intricate surface detail. In contrast, backscattered electrons deflected back from the specimen's nuclei provide insights into elemental composition variations and contrast. To produce an image, the electron beam traverses the specimen's surface in a meticulously orchestrated raster pattern, with signals generated during electron-specimen interaction meticulously collected and processed. The resulting images unveil detailed surface morphology, topography, and composition information at an exceptionally high spatial resolution, typically ranging from nanometres to sub-nanometre scales.

Instrumentation: A Field Emission Scanning Electron Microscope (FESEM) is an advanced imaging instrument renowned for revealing details about the elemental composition, electronic structure, and surface morphology of various samples. It represents a refined iteration of the conventional scanning electron microscope, employing electrons emitted from a field emission source to scan the targeted regions of a specimen in a zig-zag pattern. In the FESEM technique, electrons emitted from the field emission source undergo acceleration under a higher electric field gradient. Within a vacuum column, the pressure is reduced to an ultra-low level of around 10-8 torrs, ensuring optimal electron beam performance. These primary electrons are then focused and guided by electronic lenses to generate a tightly focused beam. Upon striking the sample material, the electron beam induces the emission of secondary electrons from each spot on the sample surface. The velocity and radiation angle of these secondary electrons correlate with the surface features of the sample. A detector captures the emitted secondary electrons, converting them into an electronic signal, which is subsequently amplified and translated into a video scan-image that is visible on a monitor. The schematic diagram of FESEM is shown in Fig. 2.3 (a).

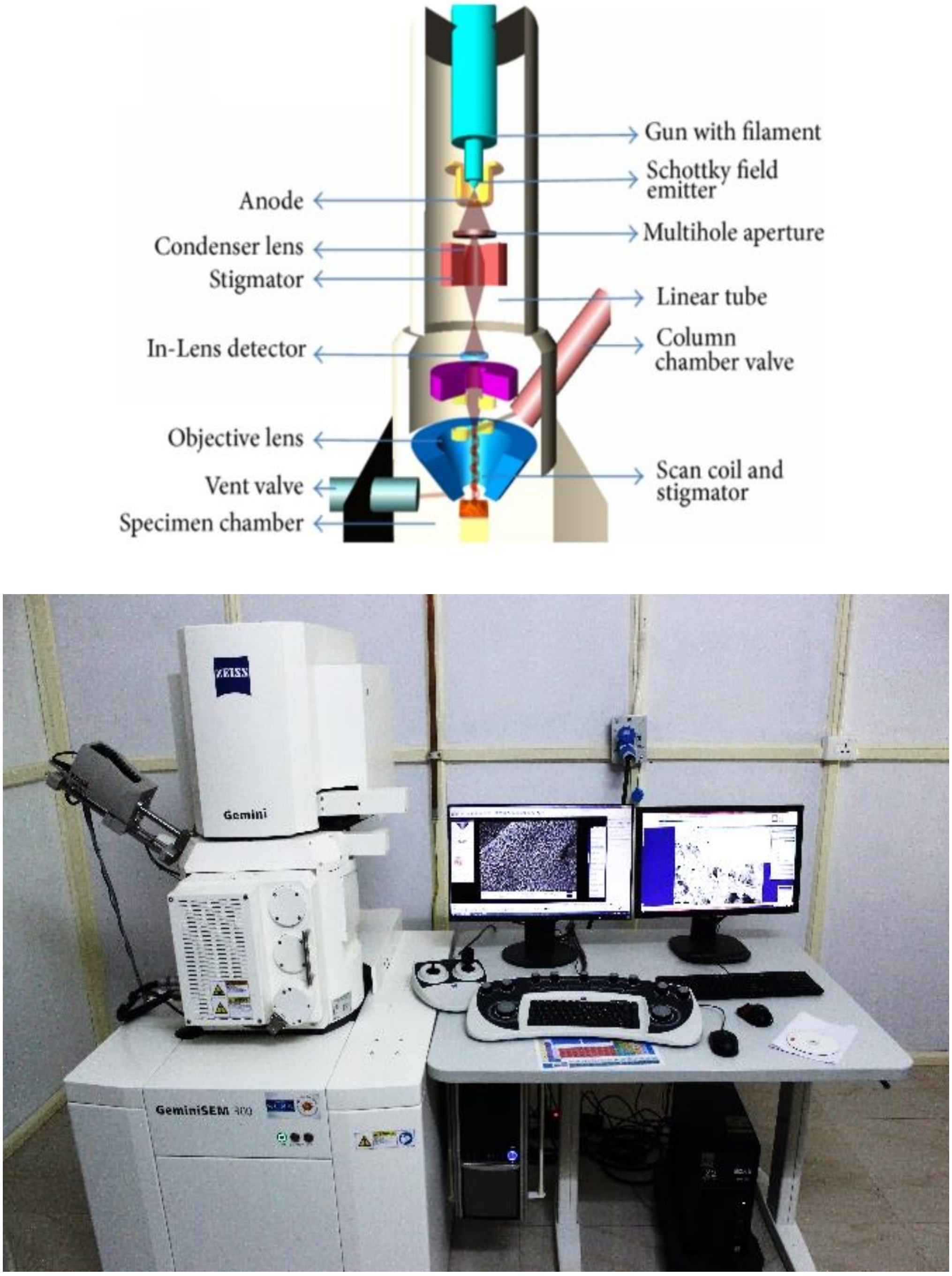

Fig. 2.3 (a) Schematic diagram of FESEM Setup [5] **(b)** Gemini SEM 300- CSIF University of Calicut [3] (used for analysis in the thesis).

Applications: In materials science, it is instrumental for investigating the surface morphology, microstructure, and composition of various materials ranging from metals to nanomaterials. Moreover, FESEM plays a pivotal role in nanotechnology research by imaging and characterising nanomaterials, essential for designing nanodevices. It facilitates the study of biological samples, providing insights into cellular morphology and biomolecular interactions. Additionally, FESEM finds applications in geology, forensic science, and materials failure analysis, contributing to geological mapping, crime scene investigations, and understanding the causes of material failures.

Specifications: In the current study, images of all prepared samples were captured using the Model **ZEISS Gemini SEM 300** (CSIF, University of Calicut) [3].

2.7 BRUNAUER-EMETT-TELLER (BET) TECHNIQUE

We used the BET technique for the surface area and porosity study in our polymer nanocomposites and metal oxides. This technique allowed us to characterise the specific surface area, pore volume, and pore size distribution of the materials, providing crucial insights into their structural properties. Understanding these parameters is essential for optimising the performance of the composites in various applications, such as adsorption, and detection. The BET analysis thus played a vital role in correlating the morphological characteristics with the functional properties of the synthesised nanocomposites and metal oxides.

The ratio of surface area to volume, which holds little significance in bulk materials, becomes highly significant when studying nanostructured materials. In nanomaterials, the increased surface area of particles contributes to numerous intriguing properties that are absent in their bulk counterparts. Accurately assessing the surface area of nanoparticles is crucial for various applications. Gas adsorption is one of the most effective methods for determining the surface area of particles at the atomic level. This technique enables the calculation of what is now known as the BET surface area, named after the scientists who developed the equation for its computation. The BET theory was formulated by Stephen Brunauer, Paul Emmett, and Edward Teller in 1938 [6].

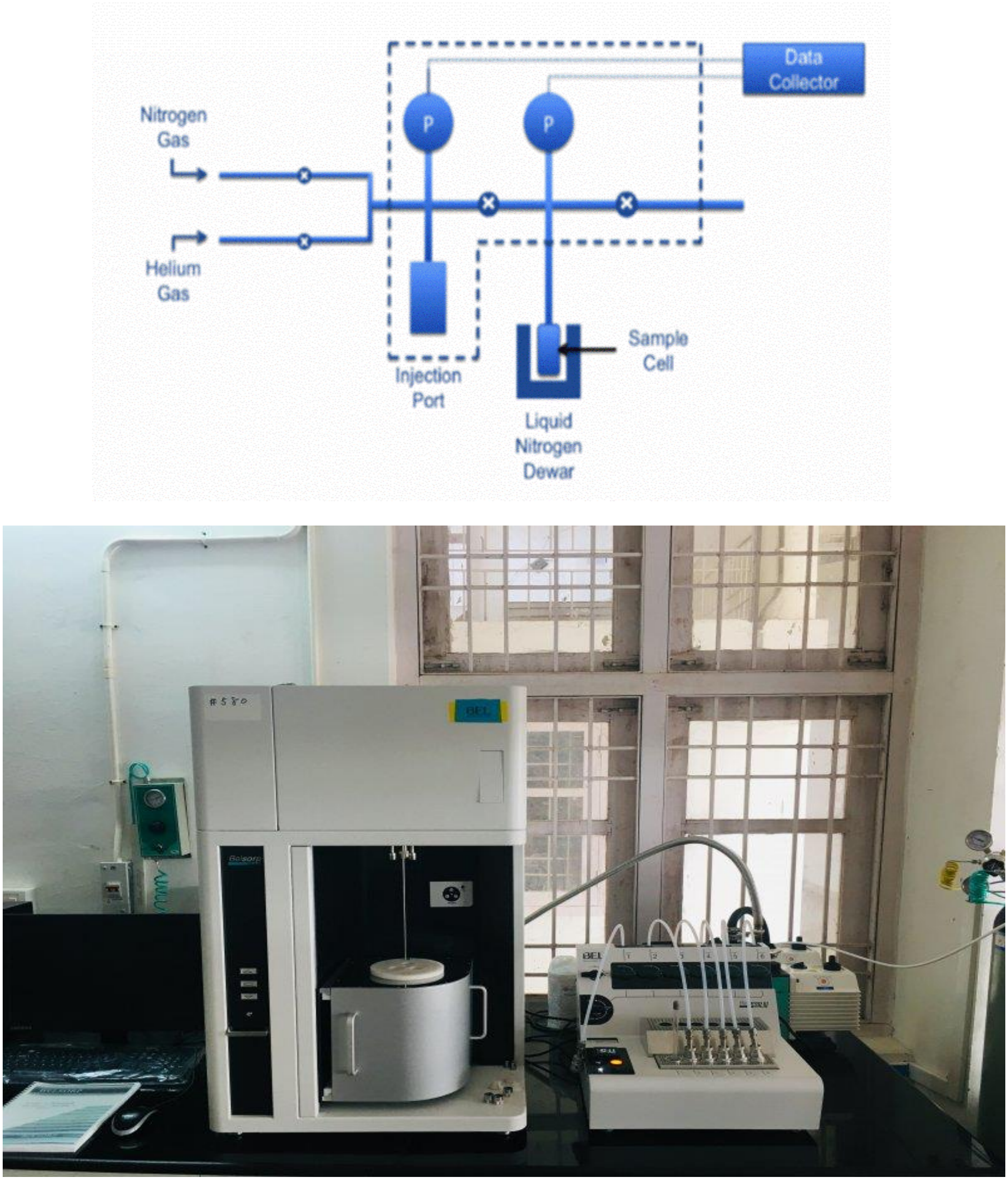

Fig. 2.4 (a) Schematic diagram of the BET surface area analyser [6], **(b)** Image of Model BELCAT-M– CSIF University of Calicut (used for analysis in the thesis) [3].

Surface area and porosity represent two critical physical attributes that significantly impact the quality and usability of solid-phase chemicals. Disparities in surface area and porosity among particles, even if they share similar physical dimensions, can profoundly affect the performance characteristics of a material, particularly in electrochemical applications. The BET theory, an extension of the

Langmuir theory devised by Irving Langmuir in 1916, is instrumental in understanding these phenomena. The Langmuir theory elucidates the monolayer adsorption of gas molecules, or adsorbates, onto a solid surface in relation to the gas pressure of a medium above the solid surface at a constant temperature.

Nitrogen is commonly employed for BET (Brunauer-Emmett-Teller) analysis due to its widespread availability in high purity and its strong interaction with most solids. Given the typically weak interaction between a solid surface and gaseous nitrogen, the surface is cooled using liquid nitrogen to facilitate adsorption. As the pressure is adjusted relative to atmospheric pressure, the adsorbed nitrogen is released into the sample cell through vacuum adjustments. The adsorption process ceases once the gas pressure reaches saturation. Pressure transducers of high accuracy monitor pressure changes resulting from the adsorption process. Subsequently, as adsorption layers form, the adsorbed nitrogen is released from the material and its quantity is measured [7]. The obtained data is presented in the form of a BET isotherm, illustrating the amount of gas adsorbed against relative pressure. A schematic diagram of the BET analyser is provided in Fig 2.4 (a).

Instrumentation: The instrumentation of a BET analyser encompasses several essential components working together to accurately measure the surface area and porosity of materials through gas adsorption. At the core lies the gas adsorption system, enabling precise dosing of adsorbate gases like nitrogen or argon onto the sample surface under varied pressures and temperatures. Housed within the sample chamber, the material sample, usually in powdered or porous solid form, is subjected to a controlled environment meticulously regulated for temperature and pressure during adsorption. The gas handling system, comprising gas cylinders, pressure regulators, and flow controllers, meticulously delivers the adsorbate gas to the sample chamber at precise flow rates and pressures [8]. Preceding the adsorption process, the vacuum system evacuates the sample chamber, eliminating residual gases or contaminants to ensure the accuracy and reliability of gas adsorption measurements. Crucial for monitoring the adsorption process, pressure transducers measure the adsorbate gas pressure within the sample chamber, facilitating the calculation of gas adsorption at different pressure points. Operating in tandem, the data acquisition and control system governs the BET analyser's operation, from setting experimental parameters to real-time monitoring of the adsorption process. Finally, specialised analysis software processes the collected raw data, applying mathematical models such as the BET equation to compute vital parameters like surface area, pore volume, and pore size distribution, offering comprehensive insights into the material's physical properties.

Applications: BET analysis, widely employed in diverse fields, is a cornerstone for understanding surface properties and porosity characteristics crucial for various applications. In adsorption studies, it offer valuable insights into gas and vapour adsorption behaviour on solid surfaces. These are vital for gas separation, pollutant removal, and drug delivery systems, where surface area and adsorption capacity are vital factors. Porous materials like zeolites, activated carbons, and MOFs benefit from BET analysis, providing crucial data on pore size distribution, volume, and surface area essential for adsorption, separation, and storage applications. In pharmaceuticals, BET analysis aids in assessing the surface area and porosity of drug particles, influencing dissolution rate, bioavailability, and stability, which is pivotal for formulation development in drug delivery systems. Moreover, in nanomaterial research, BET analysis characterises the surface area and porosity of nanoparticles, nanocomposites, and nanostructured materials, facilitating optimisation of material synthesis and evaluating performance in diverse applications like sensors, catalysts, and energy storage devices [9]. Lastly, in materials science, BET analysis contributes significantly by elucidating surface properties, pore structure, and textural characteristics of ceramics, polymers, metals, and composites, influencing their mechanical, thermal, and electrical properties.

Specifications: In this study, the surface area analysis were recorded by **BELCAT-M**– CSIF Calicut University using the N_2 gas adsorption method [3].

2.8 BROADBAND DIELECTRIC SPECTROSCOPY (BDS)

We used the Broadband Dielectric Spectroscopy (BDS) analyser to study the dielectric properties and relaxation behavior in our polymer nanocomposites and metal oxides. This comprehensive analysis allowed us to investigate the frequency-dependent dielectric response, conductivity, and molecular dynamics within these materials. By examining the interactions between the polymer matrix and the incorporated nanoparticles, as well as the influence of different metal oxides, we gained valuable insights into the mechanisms affecting the performance and potential applications of these advanced composites. The results obtained from the BDS analysis are discussed in detail in the respective chapters of this thesis.

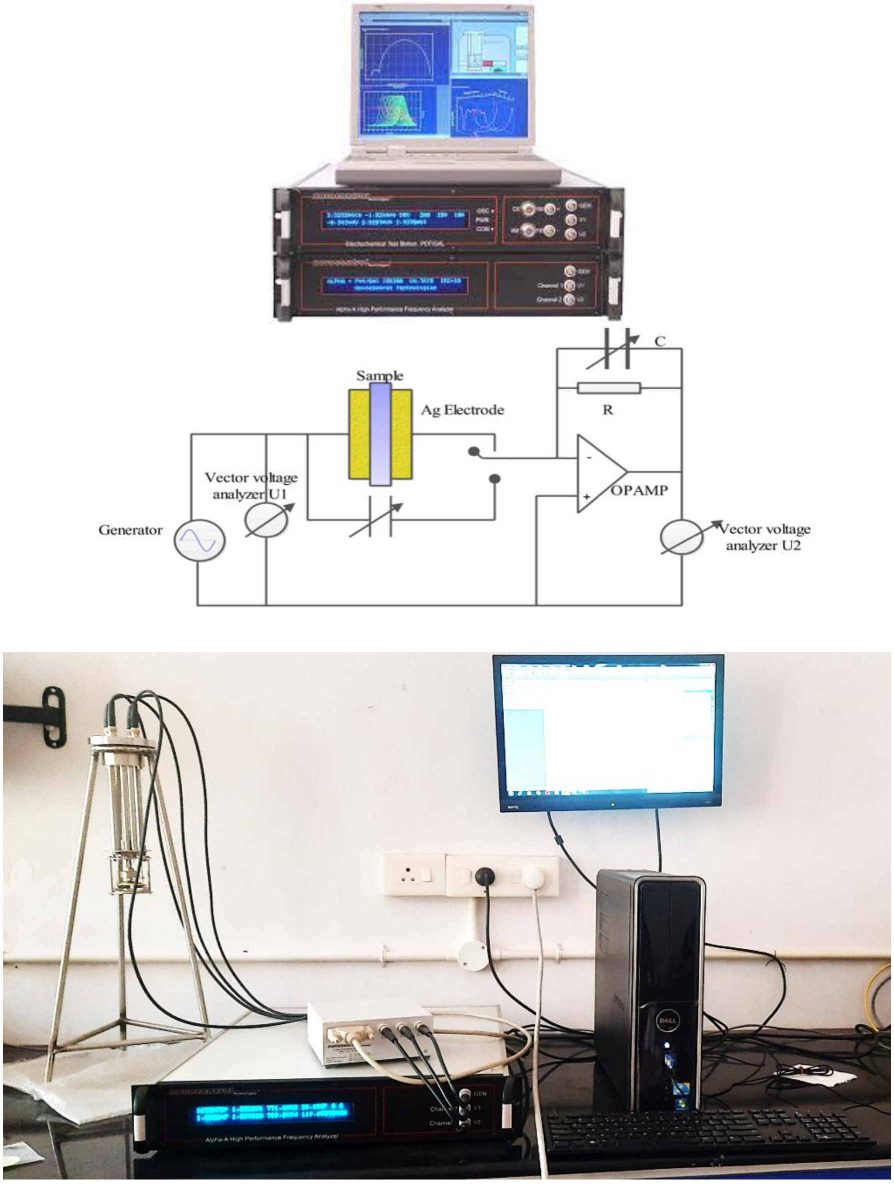

Fig. 2.5 (a) Schematic diagram of the BDS Analyzer [11] **(b)** Image of Model **Novocontrol BDS Analyser-** Department of Physics, University of Calicut (used for analysis in the thesis).

Broadband Dielectric Spectroscopy (BDS) is a valuable tool for probing molecular dynamics, encompassing rotational fluctuations of molecular dipoles, ion hopping, and charge transport. By extracting impedance data and analysing the dielectric function, comprehensive insights into molecular ensembles and their dynamics can be derived. Operating within the frequency range of $10^{\wedge -2}$ to $10^{\wedge 12}$ Hz, BDS explores a vast dynamic range, elucidating molecular and collective dipole fluctuations, charge transport phenomena, and polarisation effects at internal and external boundaries, thus revealing the dielectric properties of materials under investigation. This technique facilitates the acquisition of extensive information regarding dipole dynamics and mobile charge carriers tailored to the specifics of the molecular system. BDS measures the frequency response of systems, encompassing both energy storage and dissipation properties, making it an experimental approach for characterising electrochemical systems. It applies across various systems, from monomers to polymers in various states, including solids, liquids, and glasses [10]. The schematic diagram of the BDS set up shown in Fig. 2.5 (a).

Instrumentation: At its core, a frequency generator produces alternating electric fields spanning from millihertz to gigahertz, adapting to the desired analysis frequency range. The sample holder securely accommodates the material sample in various forms, ensuring consistent positioning for accurate measurements. Electrodes, typically crafted from conductive materials like metal, apply the electric field to the sample and capture its response, minimising interference with dielectric properties. An amplifier boosts the electrical signals generated by the sample, while a detector measures these signals, containing vital data about dielectric properties. A sophisticated data acquisition system records and processes signals, employing analog-to-digital converters for conversion into digital data for computer-based analysis. Controlled by specialised software, a computer manages the BDS instrument, setting parameters, visualising data, and extracting key dielectric properties such as permittivity and conductivity [12]. Temperature control systems are often integrated to regulate sample temperature, which is critical for ensuring accurate measurements due to temperature's influence on dielectric properties. Optionally, humidity control systems maintain stable humidity levels, particularly useful for moisture-sensitive materials, minimising their impact on dielectric property measurements.

Applications: In materials science, BDS is instrumental in comprehensively analysing polymers, ceramics, composites, and biomaterials, shedding light on their behaviour and structure-property relationships crucial for various applications. Specifically, in polymer research, BDS aids in understanding permittivity, conductivity, and relaxation dynamics, facilitating optimisation for applications ranging from insulation materials to electronic devices. BDS is indispensable for evaluating dielectric materials used in critical components like capacitors and insulators in the electronics and semiconductor sectors, ensuring device performance and reliability. Moreover, BDS enables thorough analysis of electrode materials and electrolytes in battery research and energy storage systems, contributing to the development of safer and more efficient energy storage solutions. BDS is a vital tool for studying the dielectric properties of biological tissues and biomaterials in biomedical engineering and biotechnology, advancing diagnostic and therapeutic applications. Furthermore, BDS is used extensively in the food and pharmaceutical industries for quality control and safety assessment, as well as in environmental monitoring for analysing pollutants and guiding remediation efforts [13].

Specification: In this study, conductivity spectra were analysed for all samples using the **Novocontrol BDS analyser**- Materials science lab of Dr. Mohamed Shahin Thayyil, Department of Physics, University of Calicut, within a frequency range of 10^{-2} to 10^{7} Hz at room temperature.

2.9 RAMAN SPECTROSCOPY

We used Raman spectroscopy to investigate the molecular structure, vibrational modes, surface enhanced raman spectroscopic analysis, and chemical interactions within our polymer nanocomposites and metal oxides. This technique provided detailed insights into the bonding characteristics and phase composition of the materials, allowing us to analyse the dispersion of nanoparticles within the polymer matrix and identify any structural changes induced by the incorporation of fillers. The Raman spectra helped us to understand the influence of different synthesis methods on the composites' properties, thereby enabling the optimisation of their performance for various applications. The comprehensive Raman study is elaborated in the following chapters of this thesis.

Raman spectroscopy is a potent characterisation method primarily reliant on vibrational information derived from samples' bulk mixed oxide molecular structures. In this technique, when radiation traverses a transparent medium, a portion of the beam scatters from the sample in all directions. Raman spectroscopy employs a robust laser source emitting visible or near-infrared monochromatic radiation to irradiate the sample. The emitted radiation primarily consists of three types,

1. Stokes scattering

2. Anti-stokes scattering

3. Rayleigh scattering

A crucial aspect of Raman spectroscopy is the wavenumber shift (ν), which refers to the disparity in wavenumbers (expressed in cm^$^{-1}$) between the observed radiation and the utilised light source. Raman spectra typically exhibit peaks on both sides of the Rayleigh peak, and the shift patterns on both sides mirror each other. Since anti-Stokes lines are generally less intense than the corresponding Stokes lines, the spectrum derived from Stokes lines alone is typically used for analysis. Raman spectroscopy is versatile and capable of operating across all phases, solid, liquid, and gas, and across a wide range of temperatures and pressures [14]. The strong Raman scattering from ordered crystalline lattice structures tends to dominate over signals from disordered amorphous surface phases in samples, emphasising the signal from crystalline materials. Unlike XRD, Raman spectra can detect amorphous phases alongside crystalline nanoparticles (less than 3 nm). The relative sharpness of peaks in Raman spectra facilitates the quantitative determination of the crystallinity of composite sample bulk phases. However, a significant limitation of Raman spectroscopy is sample fluorescence, although composite samples often yield dominant Raman signals.

Raman spectroscopy utilises a laser source emitting monochromatic light to irradiate samples. As the laser light interacts with the samples, it is absorbed and subsequently re-emitted. The Raman Effect causes a shift in the frequency of the re-emitted wave compared to the initial monochromatic wave frequency.

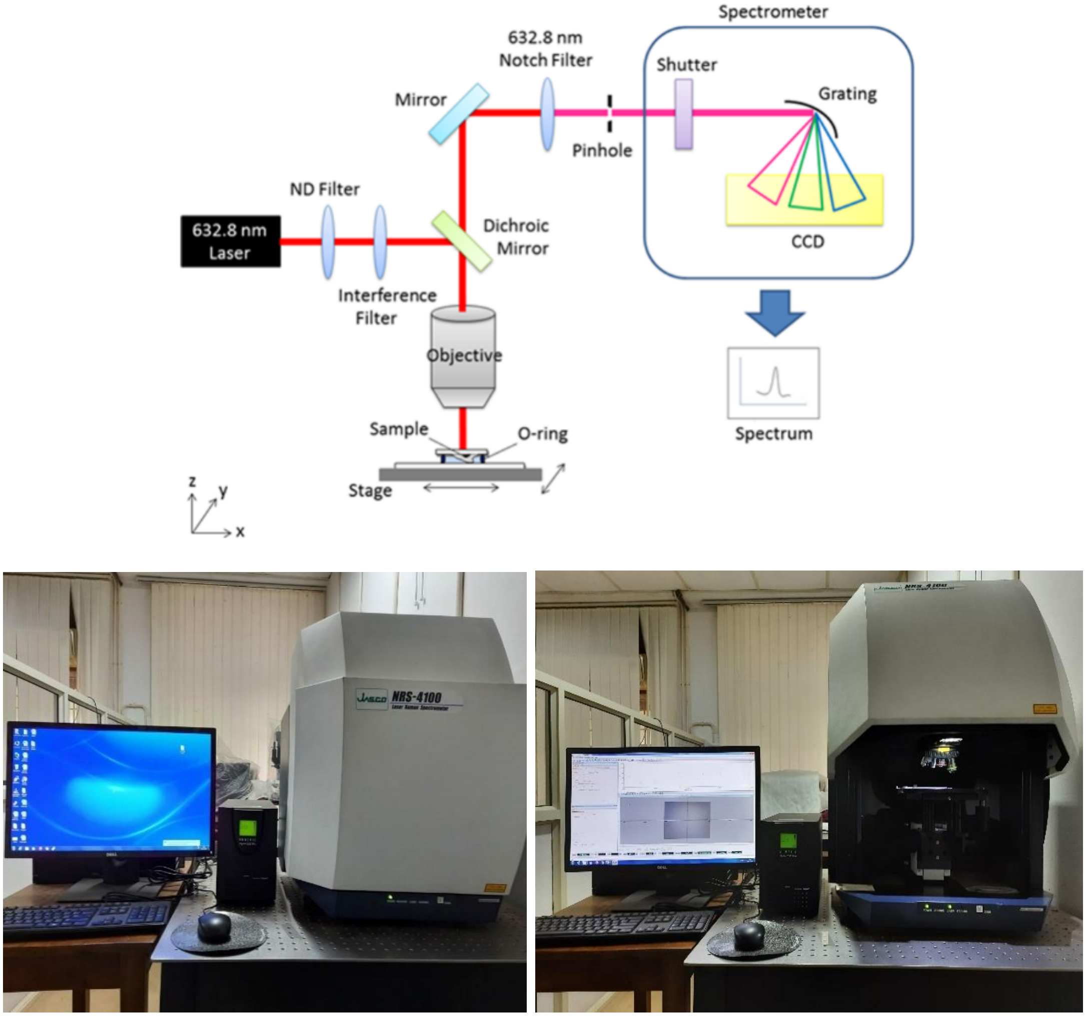

Fig. 2.6 (a) Schematic diagram of the Raman platform set-up [15], **(b)** Micro Raman instrument **Jasco NRS 4100** Department of Physics, Calicut University, (used in the analysis in the thesis).

Instrumentation: A Raman Spectrometer consists of several essential components that work together to enable the analysis of Raman scattering spectra of materials. At its core is the excitation source, typically a laser such as 532 nm and 785 nm (with selectable grating L 900, L 1800) laser, which emits light across the ultraviolet, visible, and near-infrared range. This laser beam is directed onto the specimen through a specimen illumination system and light collection optics. Once irradiated, the emitted light from the sample is collected and directed to a spectrophotometer equipped with appropriate filters and devices like tunable filters, notch filters, and laser stop apertures. These components are crucial for filtering out the Rayleigh signals and enhancing the quality of the Raman signals. The spectrophotometer is complemented by a detector, often a Charge Coupled Device (CCD) or photodiode array, which rapidly and precisely captures the Raman scattering data. Advanced features like Surface-Enhanced Raman Spectroscopy (SERS) and Resonance Raman Effect (RRE) enhance weak Raman signals, making them stronger and more detectable [16]. Micro Raman Spectrometers, equipped with a microscope, offer the advantage of analysing microscopic samples while minimising laser-induced sample damage by reducing the spot size of light on the sample.

Applications: Micro-Raman spectrometers serve as indispensable tools in various scientific fields, offering valuable insights into the chemical structure, defects, and properties of materials at the microscale. One of their primary uses is identifying the chemical structure and defects present in the sample, enabling researchers to characterise molecular compositions and understand material behaviour. Additionally, micro-Raman spectrometers are instrumental in studying phase transitions, allowing for the investigation of changes in material properties under different environmental conditions. Moreover, they find extensive application in the study of graphene materials, facilitating the determination of the number of layers and structural properties of graphene-based materials with high precision. Furthermore, micro-Raman spectrometers are employed to quantify polymer composition and investigate polymer degradation processes [17]. Analysing vibrational modes and molecular interactions provides valuable information about polymer composition, degradation mechanisms, and structural changes over time, contributing to developing advanced materials and quality control in polymer-based industries.

Specifications: In this study, Molecular vibrational analysis and SERS analysis were carried out using the Micro Raman spectrometer Model- **Jasco NRS 4100** (with 532 nm green laser) (Department of Physics, University of Calicut).

2.10 ULTRAVIOLET-VISIBLE (UV-VIS) DIFFUSE REFLECTANCE SPECTROSCOPY (DRS)

We used UV-visible spectroscopy and Diffuse Reflectance Spectroscopy (DRS) for the optical characterisation and bandgap analysis of our polymer nanocomposites and metal oxides. These techniques allowed us to investigate the materials' absorption properties and electronic transitions. By analysing the UV-visible and DRS spectra, we determined the optical bandgaps and adsorption characteristics critical for understanding the materials' potential applications in optoelectronic devices, adsorption, and sensing technologies.

UV-visible diffuse reflectance spectroscopy is a characterisation method reliant on two primary optical properties of the samples: their absorptive and light scattering properties upon light excitation within the range of 200-800 nm. The obtained sample absorbance is then compared against a $BaSO_4$ standard for reference. Reflectance data can be used to calculate the Kubulka-Munk function, aiding in the determination of the optical band gap for composite materials. This measured optical band gap offers insights into the photon energy required to excite an electron from the valence band to the conduction band, thus generating photoinduced electron-hole pairs within the bulk of graphene-based photocatalyst materials. Consequently, it delineates the requisite light source UV or visible light—for the photocatalytic application of graphene-based photocatalysts. Specifically, a band gap energy value below 3.0 eV indicates absorption in the visible light region, while values exceeding 3.0 eV render the photocatalyst active solely in the UV region. UV-Vis DRS leverages electronic transitions from ground to excited states in the sample to glean information on oxidation states, transitions, and coordination of metals within metal oxides. However, a notable limitation of UV-Vis DRS is its bulk nature, which provides averaged insights from all components of the nanocomposite system.

In addition, UV-visible spectrometry is an indispensable tool in adsorption studies, offering multifaceted capabilities crucial for comprehensive analysis. It enables precise quantification of adsorbate concentration, shedding light on the adsorption capacity and efficiency of the materials under scrutiny. Additionally, UV-visible spectroscopy aids in characterising adsorbent materials themselves, providing insights into their electronic structure, surface properties, and chemical composition. Its real-time monitoring capabilities facilitate the detection of adsorption kinetics, unveiling vital data on reaction rates and equilibrium times. Furthermore, through the construction of adsorption isotherms, UV-visible spectrometry elucidates the relationship between adsorbate concentration and adsorption onto the material's surface, unveiling crucial insights into adsorption capacity and affinity. Lastly, analysing changes in absorption spectra offers valuable clues regarding the mechanisms driving adsorption processes, thus contributing significantly to the advancement of efficient adsorbent materials and the comprehension of fundamental adsorption phenomena.

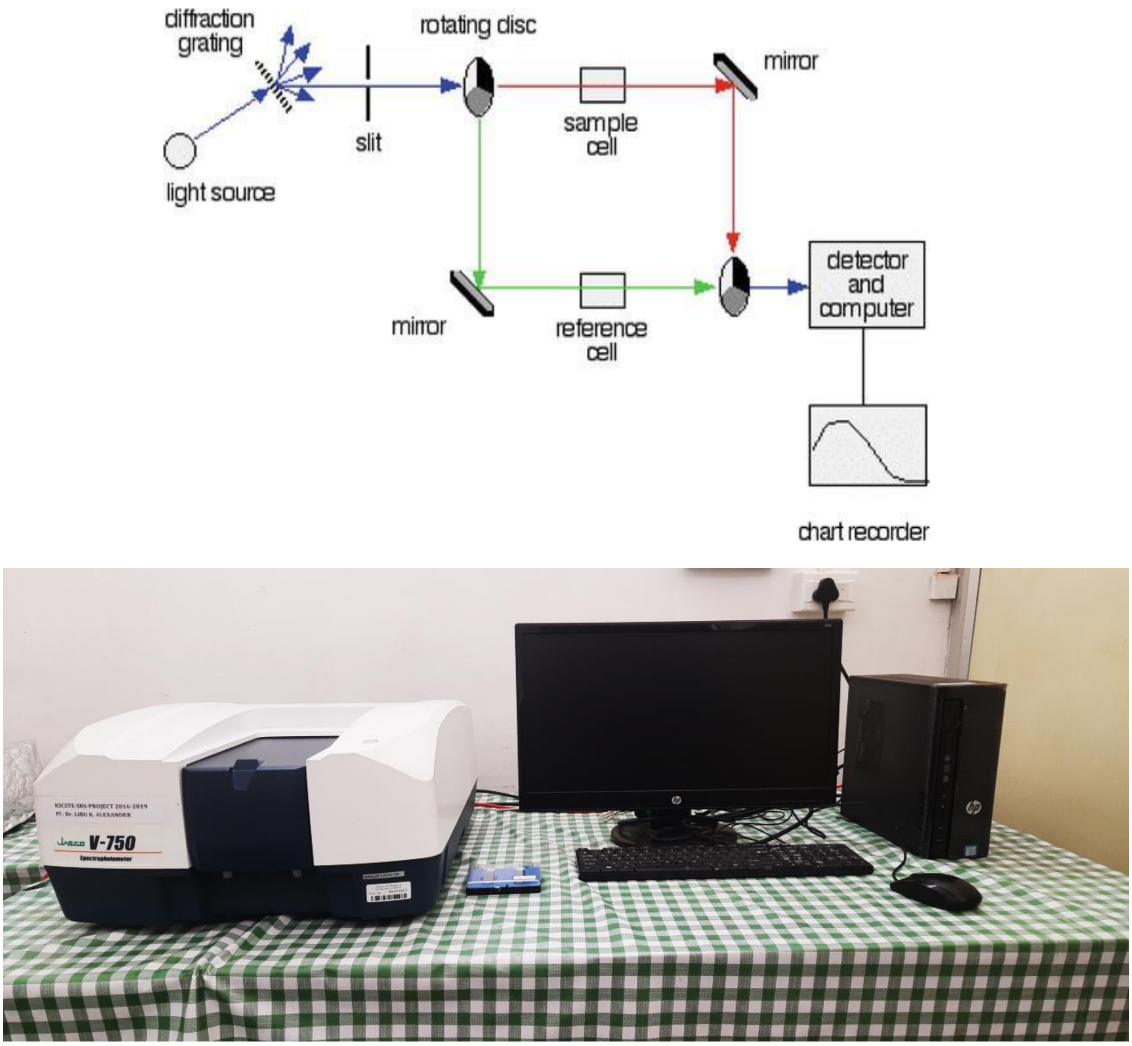

Fig. 2.7 (a) Schematic diagram of the UV-Visible Spectrometer set-up [18], **(b)** UV-Visible **Jasco V-750** spectrophotometer Department of Physics, University of Calicut (used in this study).

Instrumentation: A UV-Vis spectrophotometer comprises several essential components to analyse the absorption of light by a sample. Firstly, a stable light source, such as a tungsten filament, deuterium arc lamp, LED, or Xenon arc lamp, emits radiant energy within the desired wavelength range. The sample holder, typically a transparent cuvette made of quartz, securely contains the sample for analysis. The light beam is split by a diffraction grating or monochromator, directing one beam through the sample and the other through a reference cuvette. The absorbance of the sample is determined based on Beer-Lambert's law, which correlates absorbance (A) with the path length (l) and the concentration of absorbing species, represented by the absorptivity (ε). The intensity of light passing through the sample is measured by a detector, and the absorbance value is calculated using the logarithm of the ratio of the initial intensity of light (I_0) to the intensity of light after passing through the sample (I). This absorbance value is then displayed on the LCD screen, providing quantitative information about the sample's absorption characteristics [19].

Applications: One primary use is determining the concentration of unknown samples and studying reaction kinetics, which is essential in chemical analysis and reaction monitoring. UV-Vis spectrometers also enable quantitative and qualitative analysis of samples, offering insights into their composition and properties. They are also valuable tools for detecting impurities and functional groups in compounds, aiding in quality control and purity assessment. Spectrophotometric measurements of both inorganic and organic compounds are routinely performed, providing valuable information about their electronic structure and optical properties. Furthermore, UV-Vis spectrometers are utilised to measure band gaps from diffuse reflectance spectra (DRS), crucial for characterising semiconductor materials and understanding their optical behaviour [20].

Specifications: In this study, bandgap analysis and adsorption studies were carried out using a Jasco V-750 spectrometer, and a tungsten filament and deuterium arc lamp were used as the source. (Department of Physics, University of Calicut).

In this chapter, we have comprehensively explored a variety of experimental techniques pivotal to the synthesis, characterization, and analysis of advanced materials. Each technique provided critical insights into the structural, thermal, and optical properties of the materials, contributing significantly to our understanding of their performance and potential applications. The outcomes underscore the importance of selecting appropriate experimental techniques to tailor material properties for specific applications, ultimately paving the way for the development of suitable materials.

2.11 References

[1] A. A. Bunaciu and H. Y. Aboul-enein, "X-Ray Diffraction : Instrumentation and Applications Critical Reviews in Analytical Chemistry X-Ray Diffraction : Instrumentation and Applications,"J.*Critical Reviews in Analytical Chemistry* , 2015.

[2] M. Bennis, E. Heuson, P. Roussel, F. Dumeignil, and S. Paul, "Design of a multi-well plate for high-throughput characterization of heterogeneous catalysts by XRD, FT-IR, Raman and XRF spectroscopies," *RSC Advances*, pp. 40912–40920, 2018.

[3] https://csif.uoc.ac.in/index.php/2016-06-16-11-19-36.

[4] P. Gnanamoorthy, V. Karthikeyan, and V. A. Prabu, "Field Emission Scanning Electron Microscopy (FESEM) characterisation of the porous silica nanoparticulate structure of marine diatoms,"*J. Porous materials*, pp. 225–233, 2014.

[5] S. E. M. Edx, "Investigation of CPD and HMDS Sample Preparation Techniques for Cervical Cells in Developing Computer-Aided Screening System Based on FE-SEM / EDX," *NCBI*, 2014.

[6] "Website:" [Online]. Available: https://chem.libretexts.org/Bookshelves/Analytical.

[7] Anil Kumar (Cusat-Cochin), "Chapter 2 Relevant Experimental Techniques," pp. 29–47.https://shodhganga.inflibnet.ac .in/bitstream/10603/231902/8/08_chapter%202.pdf

[8] https://www.meritics.com/technologies/bet-surface-area-analysis/

[9] J. Rouquerol, F. Rouquerol, K. S. W. Sing, P. Llewellyn, G. Maurin. Adsorption by Powders and Porous Solids: Principles, Methodology and Applications, Academic Press (2014).

[10] F. Kremer · A. Schönhals, "Broadband Dielectric Spectroscopy" , *Springer book*, 2003.

[11] "Website:" https://www.novocontrol.de/php/index.php.

[12] W. H. Hunter Woodward, Broadband Dielectric Spectroscopy—A Practical Guide, Chapter 1pp 3-59, *ACS Symposium Series*Vol. 1375, DOI: 10.1021/bk-2021-1375.ch001.

[13] Fabio Fanari, Ciprian Iacob, Gianluca Carboni, Francesco Desogus, Massimiliano Grosso, Manfred Wilhelm, Broadband Dielectric Spectroscopy (BDS) investigation of molecular relaxations in durum wheat dough at low temperatures and their relationship with rheological properties, LWT,Volume 161, 2022, 113345, ISSN 0023-6438, https://doi.org/10.1016/j.lwt.2022.113345.

[14] R. R. Jones, D. C. Hooper, L. Zhang, D. Wolverson, and V. K. Valev, "Raman Techniques : Fundamentals and Frontiers",*Nanoscale Research Letters*, 2019.

[15] P. Hung, Y. Kuo, H. Chen, H. K. Chiang, and O. K. Lee, "Detection of Osteogenic Differentiation by Differential Mineralized Matrix Production in Mesenchymal

Stromal Cells by Raman Spectroscopy,"*PLoS One*, vol. 8, no. 5, pp. 1–7, 2013.

[16] Eshbekova, N., Sowndarya, A., Thangadurai, T. D., & Lee, Y. I. (2024). Recent advancements in Raman instrumentation and capabilities for pharmaceutical and biomedical applications. *Applied Spectroscopy Reviews*, 1–52. https://doi.org/ 10. 1080/05704928.2024.2355193.

[17] Andrzej Kudelski,Analytical applications of Raman spectroscopy,Talanta, Volume 76, Issue 1, 2008, Pages 1-8, ISSN 0039-9140, https://doi.org/ 10.1016/ j.talanta.2008.02.042.

[18] http://ecoursesonline.iasri.res.in/mod/page/view.php?id=42662.

[19] Pietro Morozzi, Barbara Ballarin, Sara Arcozzi, Erika Brattich, Franco Lucarelli, Silvia Nava, Pedro José Gómez-Cascales, J.A.G. Orza, Laura Tositti, Ultraviolet–Visible Diffuse Reflectance Spectroscopy (UV–Vis DRS), a rapid and non-destructive analytical tool for the identification of Saharan dust events in particulate matter filters,Atmospheric Environment, Volume 252, 2021, 118297, ISSN 1352-2310, https://doi.org/10.1016/j.atmosenv.2021.118297.

[20] M.A. Zanjanchi, H. Noei, M. Moghimi, Rapid determination of aluminum by UV–vis diffuse reflectance spectroscopy with application of suitable adsorbents, Talanta, Volume 70, Issue 5, 2006, Pages 933-939, ISSN 0039-9140, https://doi.org/ 10.1016/j.talanta.2006.05.056.

CHAPTER 3

$BaTiO_3$ and PMMA_$BaTiO_3$ SERS substrate for Dimethyl Phthalate and Diethyl Phthalate detection.

Contents

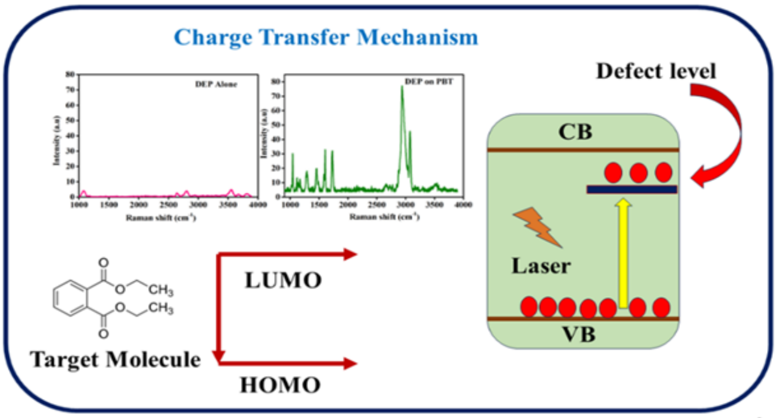

Abstract: *Dimethyl phthalate (DMP) and Diethyl phthalate (DEP) are low-density phthalates commonly used to manufacture various artificial products. These compounds migrate through the food chain, posing significant health risks. Current detectors for DMP and DEP lack cost-effective and real-time detection capabilities. Surface-enhanced Raman spectroscopy (SERS) offers substantial promise for detecting environmental pollutants. This study presents an effective tool for sensitively detecting DMP and DEP using noble metal-free SERS substrates. The successful design of the SERS substrates hinges on creating hotspots based on the morphology of the semiconductor* $BaTiO_3$ *and its incorporation into a PMMA polymer matrix. Unlike traditional high-temperature synthesis methods exceeding 1000 °C, a low-temperature sol-gel route was employed to synthesize* $BaTiO_3$*. The dense arrangement of cuboidal and tubular morphology hotspots on the substrate significantly enhances the weak Raman signals of DMP and DEP. Moreover, the design ensures that the Raman bands of the SERS substrate and the probe molecule do not coincide, enabling precise and unambiguous detection. The primary mechanism behind the SERS activity of* $BaTiO_3$ *(BT) and PMMA-* $BaTiO_3$ *films (PBT) is charge transfer resonance, bolstered by the strong affinity between BT and DMP and between PBT and DEP. This study demonstrates a cost-effective, real-time sensitive phthalate detection method using noble metal-free flexible SERS substrates. It can provide an efficient alternative to conventional chromatographic techniques - offering a potent route for detecting environmental pollutants.*

3.1 Introduction

Surface-enhanced Raman spectroscopy (SERS) is an excellent analytical tool widely used to detect trace substances. This technique is considered superior to all other detection methods because of its high selectivity and very short detection time[1]. SERS technique was introduced in detail in chapter 1- section 1.2.4. The past two decades have witnessed significant developments in noble metals-based SERS substrates with considerable sensitivity, selectivity, and reproducibility[2,3]. Still, this substrate has some limitations in the cost of fabrication and product price, as well as a lack of biocompatibility and poor stability. Recently, considerable attention has been paid to fabricating noble metal-free materials that exhibit SERS performance [2-7]. In particular, semiconductors exhibit more controllable physical and chemical properties such as bandgap, doping, resistance to corrosion, degradation, tunable morphology, and excellent surface properties, which meets a series of demands in SERS analysis [8].

The observation of SERS on the surface of semiconductors (metal oxides) can be traced back to the 1980s. The presence of the semiconductor responsible for enhanced Raman scattering is very important for the in-depth understanding of the SERS phenomenon. Due to the limitations in semiconductor synthesis and characterization technologies, this phenomenon was observed only for minor semiconductor surfaces, such as NiO, GaP, and TiO_2, with relatively small enhancement effects.[9-11]. The lack of sufficient experiments prevented a systematic examination of the validity of the proposed theoretical models. Thus, semiconductor-enhanced Raman scattering did not gain comprehensive attention in the early stages. With the recent progress in nanoscience and nanotechnology, the semiconductor-enhanced Raman scattering has developed remarkably. An increasing number of semiconductor materials have been demonstrated to be SERS-active substrates, such as metal oxides, metal sulfides, metal tellurides, metal halides, and some single-element semiconductors [2]. Various numerical methods have been developed to study the interaction of light with small particles, which helps obtain a theoretical understanding of the experimental phenomena [12].

However, it is challenging to compare the results from various studies owing to the diversity in material synthesis and properties.

Merits of semiconductor materials as SERS-active substrates include molecular specificity and *in situ* analysis capability. More importantly, semiconductor materials have some inherent physicochemical features that are attractive to theoretical studies and applied research. The essential qualities of the semiconductor-enhanced Raman scattering technique are as follows:

1 Surface properties: The semiconductor surfaces exhibit novel surface properties, such as better surface bonds to hold analytes. The superior biocompatibility of semiconductors has assured them an inherent advantage in biochemical and biomedical applications[13].

2 Chemical stability: Difficulties with the reproducibility of Raman signals related to substrate degradation have been a significant constraint on SERS applications. Semiconductor materials and their structures have superior thermal stability compared to conventional metals. This makes them suitable for detection in various environmental conditions[13].

3 Diversity of substrates: These semiconductor substrates show diversity in morphology-including quantum dots, nanowires, nanosheets, three-dimensional nanostructures, and multi-dimensional nanofilms, which could meet the different criteria for a particular purpose[13].

4 Optoelectrical properties: The SERS intensity can be borrowed from some allowed molecular transitions by the molecule-to-substrate or substrate-to-molecule transition through the Herzberg–Teller coupling term. The band structure of a semiconductor can be easily tuned by varying the nanoparticle's size, shape, material, and doping. Consequently, the charge transfer transition can be tailored based on the analyte, providing possible resonant contributions to the enhancement. In addition, the low-cost and novel synthetic techniques for semiconductor substrates also play an essential role in SERS application[13].

The enhancement in the Raman signal in SERS relies primarily on two different mechanisms, which were discussed in detail in Section 1.2.4.1. As mentioned in section 1.2.4, for noble metal substrates, the Raman signal enhancement is predominantly attributed to electromagnetic (EM) mechanisms, which are driven by the oscillations of free electrons on the metal surface, known as localized surface plasmon resonances (LSPR) [14]. These resonances amplify the local electromagnetic field, significantly increasing the Raman signal of the probe molecules. In contrast, for semiconductor substrates, the enhancement arises from the charge transfer mechanism [15]. This involves the transfer of electrons between the semiconductor substrate and the probe molecule, which modifies the electronic states of the molecule and enhances the Raman scattering. This distinct approach in semiconductors leverages the material's electronic properties to achieve signal amplification, offering a complementary method to the EM mechanism observed in noble metal substrates.

Regarding the design and development of SERS substrates for phthalate detection, we worked on three different samples. Two of these samples are discussed in detail in this section, highlighting their unique properties and applications. The fourth chapter will explore the analysis and SERS activity of the remaining sample, providing a comprehensive understanding of its significance and performance.

SERS Substrate	**Probe molecule**	**Chapter**
Barium Titanate (BT)	**Di Methyl Phthalate (DMP)**	**Chapter 3**
PMMA_Barium Titanate Polymer Nano Composite	**Di Ethyl Phthalate (DEP)**	**Chapter 3**
PMMA_Strontium Titanate Polymer Nano Composite	**Di (2-ethylhexyl) phthalate (DEHP)**	**Chapter 4**

Phthalates were introduced in detail in Chapter 1-sections 1.2.1 & 1.2.2. As mentioned in those sections, Pthalic acid esters have been well-known as potent carcinogens and endocrine disrupters, and their removal from aqueous solutions has recently been of considerable concern. Phthalic acid ester is widely used as an industrial compound to improve plastics' flexibility, durability, and workability for various applications. Most commonly, they are used in cosmetics, soaps, shampoos, toys, blood containers, medical tubing, plastic containers, food packing, and numerous other products[16]. The possible migration and bioaccumulation of these phthalic acid esters (PAEs) can cause serious adverse effects on human health due to their carcinogenic and endocrine-disrupting properties[17]. Dimethyl phthalate (DMP) and Diethyl phthalate (DEP) are two of the significant phthalate pollutants, and we have tried to detect them using polymer-based SERS substrates.

Dimethyl phthalate (DMP) is a versatile organic compound widely used as a plasticizer in manufacturing various consumer products. DMP is favoured for its ability to impart flexibility and durability to polymers. Its significance in industrial applications cannot be understated, as it enhances the mechanical properties of plastic products, making them more adaptable for various uses. However, DMP also poses significant health risks. It is known to be an endocrine disruptor, potentially leading to reproductive and developmental issues in humans. DMP is the most leached phthalic acid ester from mineral water containers and coolers. Its exposure to humans has been found to irritate sensing organs, and DNA damage has led to malformation[18]. Exposure to DMP, whether through ingestion, inhalation, or skin contact, has been linked to adverse health effects such as respiratory problems and skin irritation. Moreover, due to its widespread use, DMP has become a persistent environmental pollutant, capable of migrating through the food chain and accumulating in ecosystems, posing long-term risks to human health and the environment. Consequently, there is a growing need for effective detection and regulation of DMP to mitigate its harmful impacts. Dimethyl phthalate (DMP) is a typical example of an industrially crucial phthalic acid ester, which is extensively utilized in several plasticizing industries and has a menacing harmful effect on humans. Therefore, it is essential to detect the presence of trace DMP in aqueous solutions.

Diethyl phthalate (DEP) is another phthalic acid ester used as a plasticizer to increase the flexibility of plastics and as a solvent in various products, including personal care items like perfumes, lotions, and cosmetics. It is known for its excellent solubility and low volatility, making it a versatile ingredient in numerous industrial and consumer applications. Despite its widespread use, DEP has raised significant health and environmental concerns. It can easily migrate into the environment and enter the food chain, leading to potential human exposure. Studies have linked DEP exposure to endocrine disruption, reproductive toxicity, and developmental issues [19]. Prolonged contact with DEP may result in adverse health effects such as hormonal imbalances, fertility problems, and potential carcinogenicity. Consequently, the monitoring and regulation of DEP usage have become crucial to mitigate its harmful impacts on human health and the environment.

In this study, we developed two noble metal-free SERS substrates with morphologically customized hotspots through the low-temperature synthesis of $BaTiO_3$ - offering better characteristics than the one prepared through the conventional high-temperature route. The resulting substrate exhibits distinctive Raman peaks attributed to Barium titanate. These SERS substrates, adorned with cuboidal and tubular hotspots, show a pronounced chemical enhancement effect based on charge transfer resonance, which is particularly advantageous for detecting DMP and DEP.

3.2 Materials and methods

3.2.1 Low-temperature synthesis of Barium Titanate nanoparticles.

To synthesize $BaTiO_3$ nanoparticles, a modified two-step sol-gel method with stepwise sintering was employed. Acetic acid, deionized water, and 2-propanol were utilized for low-temperature hydrolysis. The modified acetate-derived $BaTiO_3$ sol was prepared using barium acetate, deionized water, titanium tetra isopropyl alkoxide (TTIP), 2-propanol, acetone, and glacial acetic acid as precursors.

Initially, barium acetate was dissolved in acetic acid at 65°C with constant stirring. The solution was then slowly cooled to room temperature, and a few drops of 2-propanol were added. In the subsequent step, Titanium Tetra Isopropyl Alkoxide dissolved in acetone was added to initiate partial hydrolysis. The prepared mixture was exposed to low-temperature treatment (5–10°C) while deionized water was gradually added simultaneously. A magnetic stirring was carried out throughout the sol preparation process to ensure proper agitation of the solution. Eventually, a colourless and transparent sol was formed. After gelation, the gel was dried at 100°C. The resulting xerogels were then calcined and sintered at various temperatures to obtain phase-pure, nanocrystalline tetragonal $BaTiO_3$. The fine powder was calcined at 900°C for 1 hour in a muffle furnace. After cooling to room temperature, the powder was ground using an agate mortar and sintered at 650°C to 850°C via a stepwise programmed sintering route.

3.2.2 Synthesis of PMMA_$BaTiO_3$ nanocomposite substrates.

Flexible self-standing polymer matrix films were prepared by dissolving PMMA crystals in an acetone solvent. As the PMMA dissolved and the solution transformed into a white, viscous consistency, $BaTiO_3$ nanoparticles were gradually introduced into the mixture while continuously stirring. This gradual addition ensures uniform dispersion of the $BaTiO_3$ nanoparticles within the polymer matrix. The stirring process was continued until a thick, homogeneous white gel was formed. This gel exhibited consistency that was suitable for moulding into various shapes. The resultant composite film, hereafter referred to as PBT film/substrate, was cast to achieve a thickness of approximately 100 microns. The PBT film's flexible and self-standing nature makes it an ideal candidate for applications requiring adaptable and durable materials. This method allows for precise control over the film's thickness and ensures the even distribution of nanoparticles, enhancing the film's mechanical and functional properties.

3.2.3 Dimethyl phthalate and Diethyl phthalate stock solution preparation.

A meticulous process is essential to prepare DMP and DEP stock solutions with ultra-low concentrations required for SERS investigation. A standard 100-ppm solution of Dimethyl phthalate ($C_{10}H_{10}O_4$), which has a molecular weight of 194.184 g/mol, is made with 8.4 µl of DMP. Similarly, Diethyl phthalate ($C_{12}H_{14}O_4$) with a molecular weight of 222.24 g/mol, or precisely 9.1 µl of DEP, is used to make a 100-ppm stock solution. This measurement is critical, as achieving the exact concentration is necessary for accurate experimental results. Given the desired ultra-low concentration, a one-ppm DMP and DEP solution was subsequently prepared. This process involves the careful dilution of the standard 100-ppm stock solution. Specifically, the stock solution is thoroughly mixed with distilled water in a calibrated standard flask, ensuring uniform dispersion of DMP and DEP throughout the solution.

3.2.4 Experimental procedure for adsorption

Adsorption experiments assessed the affinity between (i) DMP (Bis(2-ethylhexyl) phthalate) and the synthesized BT substrate and (ii) DEP and the synthesized PBT. A 30 mg of BT and 1 cm x 1 cm PBT film was immersed in 100 ml of 1 ppm DMP and DEP phthalate solution, and the mixture was stirred for 60 minutes at room temperature. Every 30 minutes, 30 ml of the solution was withdrawn for analysis. UV-Vis spectrophotometry (using a JASCO V-750 spectrometer) was employed to analyze the initial and post-adsorption solutions at the wavelength of maximum absorbance.

3.2.5 Raman and SERS property analysis

The micro-Raman measurements were performed using a Laser Micro Raman Spectrometer (532 nm excitation wavelength, ×50 L magnification, one mW excitation power) for precise Raman band detection of BT, PBT film, DMP and DEP. SERS sensitivity was measured using the DMP and DEP probe molecule stock solution coated onto a BT and PBT film aligned on a clean glass slide.

3.3 Results and Discussion

3.3.1 X-ray diffractogram Analysis

In the present study, tetragonal Barium Titanate nanoparticles synthesized at lower temperatures are utilized – as detailed in the previous section. When the xerogel was fired at 650 °C for 1-hour, peak splitting was observed around $2\theta = 45°$, indicating the formation of the tetragonal phase, as shown in Fig. 3.1. This peak splitting became more pronounced when the xerogels were sintered at various temperatures (650 °C, 700 °C, 750 °C, 800 °C, and 850 °C), suggesting an increase in the degree of polymorphic transformation. Notably, this transformation began at lower temperatures compared to previously reported sol-gel methods, highlighting the advantages of our modified synthesis and sintering process. Consequently, the diffraction peaks of the samples sintered at different temperatures were successfully indexed to $BaTiO_3$ with a tetragonal structure. Tetragonal barium titanate nanoparticles were formed at a lower sintering temperature of 650 °C. The average particle size, calculated using the Debye-Scherrer formula, was 27.32 ± 1.12 nm. Fig. 3.2 displays the XRD pattern of the synthesized $BaTiO_3$ samples at different sintering temperatures.

The synthesized BT nanoparticles are incorporated within the polymer matrix to form a PBT film. The X-ray diffractogram confirms the formation of the PBT film. The XRD pattern displays characteristic peaks corresponding to the tetragonal phase of $BaTiO_3$, indicating that the barium titanate nanoparticles are well-dispersed within the polymethyl methacrylate (PMMA) matrix. The presence of these peaks confirms the successful incorporation of $BaTiO_3$ into the PMMA matrix without altering its crystalline structure. Additionally, the broad, amorphous hump observed in the XRD pattern is attributed to the PMMA polymer – indicating the expected lack of long-range order. The intensity and sharpness of the $BaTiO_3$ peaks suggest that the nanoparticles retain their crystallinity even after being embedded in the polymer matrix.

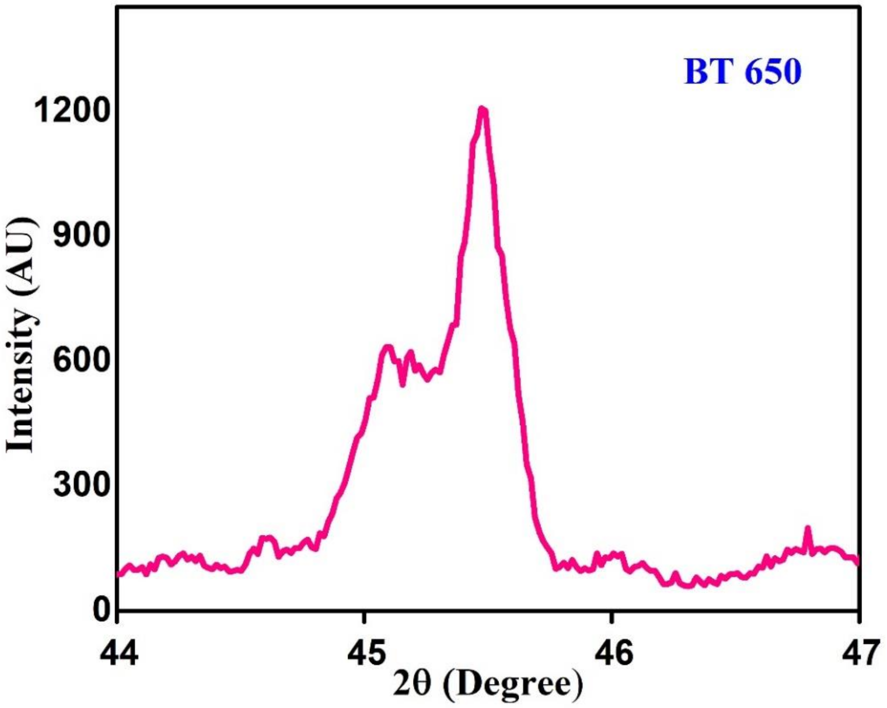

Fig. 3.1. XRD peak splitting of the sample BT 650 after calcination.

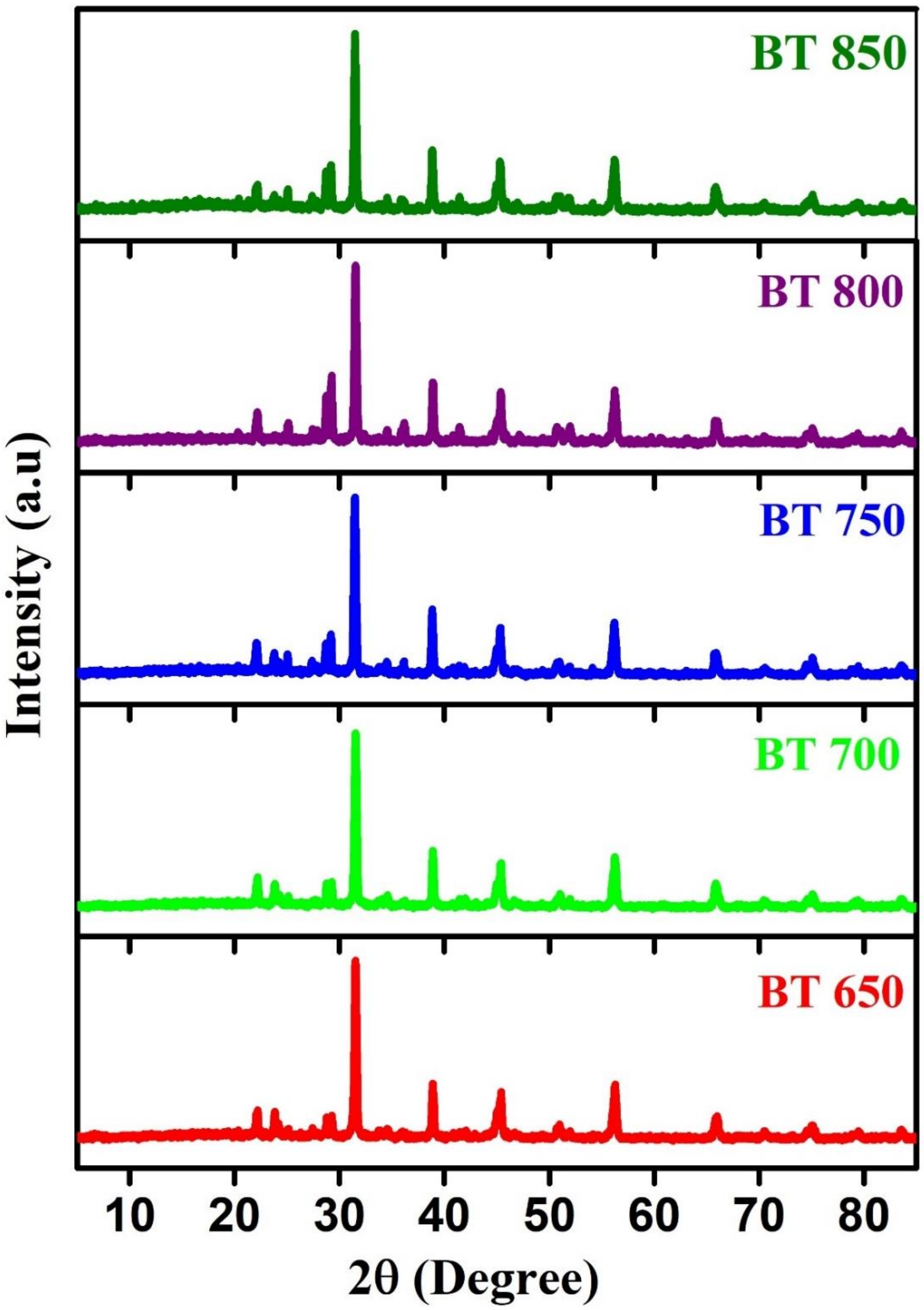

Fig.3.2. X-ray diffractogram of BT nanoparticles sintered at different temperatures.

3.3.2 Bandgap analysis

The importance of bandgap analysis of a Surface-Enhanced Raman Scattering (SERS) substrate lies in its profound impact on the substrate's optical and electronic properties, which directly influence the efficiency and sensitivity of SERS. The bandgap of a material determines its ability to interact with light, particularly in absorption and emission processes.

The diffuse reflectance spectra studies unveil the optical properties of the prepared Barium Titanate ($BaTiO_3$) samples. The optical band gap of $BaTiO_3$ nanoparticles is determined by considering the direct allowed inter-band transition occurring between the valence and conduction bands, using Tauc's Law:

$$(\alpha h\nu)^2 = A\,(h\nu - E_g)$$

where, α is the absorption coefficient ($\alpha=4\pi k/\lambda$; k is the absorbance, λ is the wavelength in nm), A is a constant, Eg is the optical bandgap, and hν is the photon energy. $BaTiO_3$, being a a semiconductor with a direct bandgap, has its bandgap Eg estimated by plotting $(\alpha h\nu)^2$ versus hν and extrapolating the linear portion of the plot to $(\alpha h\nu)^2 = 0$. The bandgap of the prepared $BaTiO_3$ is obtained as 3.23 ± 0.01 eV, as shown in Fig. 3.3. This precise bandgap determination is essential for optimizing the material's performance in SERS applications.

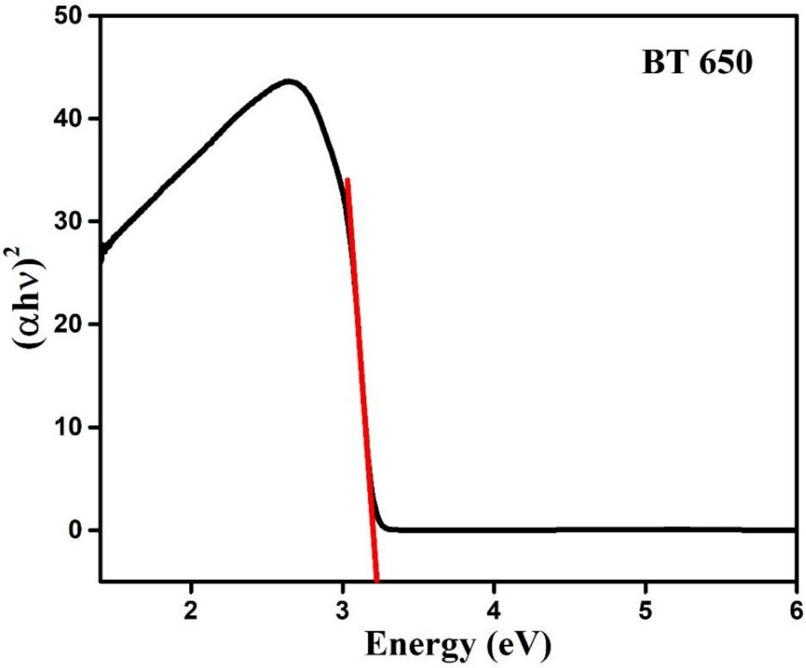

Fig. 3.3. Optical bandgap determination using Tauc plot for BT 650.

A bandgap of 3.2 eV corresponds to photon energy in the ultraviolet (UV) region (around 387 nm), allowing $BaTiO_3$ to effectively interact with UV light, which is beneficial for SERS applications using UV excitation sources. This ensures efficient light absorption and the generation of strong localized electromagnetic fields on the substrate's surface, which is essential for enhancing Raman signals of adsorbed molecules. Furthermore, when $BaTiO_3$ is combined with metallic nanoparticles, it enhances the local electromagnetic field generated by the metal, significantly boosting the Raman scattering cross-section of surface molecules, a phenomenon known as the electromagnetic enhancement mechanism. Additionally, the 3.2 eV bandgap facilitates the charge transfer mechanism between $BaTiO_3$ and adsorbed molecules, contributing to chemical enhancement in SERS. Upon illumination, electrons excited across the bandgap from the valence band to the conduction band can participate in charge transfer processes with the molecules, further enhancing the Raman signal.

3.3.3 Raman spectra analysis

Raman analysis is used for the structural analysis of barium titanate nanoparticles sintered at different temperatures. At ambient temperature, $BaTiO_3$ exhibit tetragonal with C4v symmetry. The frequency covered ranges from 0 cm^{-1} to 1200 cm^{-1}. Based on the crystallography, Raman-active modes for tetragonal $BaTiO_3$ (P4mm) are 4E (TO + LO) + 3A1(TO + LO) +B1(TO + LO), while no Raman-active mode is predicted for the cubic phase (Pm3m). Raman studies reveal the presence of peaks at frequencies around 133cm^{-1}, 261cm^{-1}, 303cm^{-1}, 517cm^{-1} and 712cm^{-1}. The intensity of the peaks varies slightly with the temperature. The optical phonon frequencies and their symmetries in tetragonal $BaTiO_3$ are reported[20]. As shown in Fig 3.4 (a) Raman spectrum of the samples sintered at different temperatures (650°C,700°C,750°C,800°C, and 850 °C) evince the characteristic peculiarities of the $BaTiO_3$ tetragonal phase: the broad peak at about 260 cm^{-1} corresponding to [A1 (TO)], a sharp peak at 303cm^{-1} corresponding to [B1 and E(TO+LO)], an asymmetric peak at 513 cm^{-1}corresponds to [A1 (TO), and E(TO)] and the peak at 712 cm^{-1} related to [A1(LO) and E(LO)] phonon modes[21-22].The peak at 303cm^{-1} assures the tetragonal phase of barium titanate particle formation.

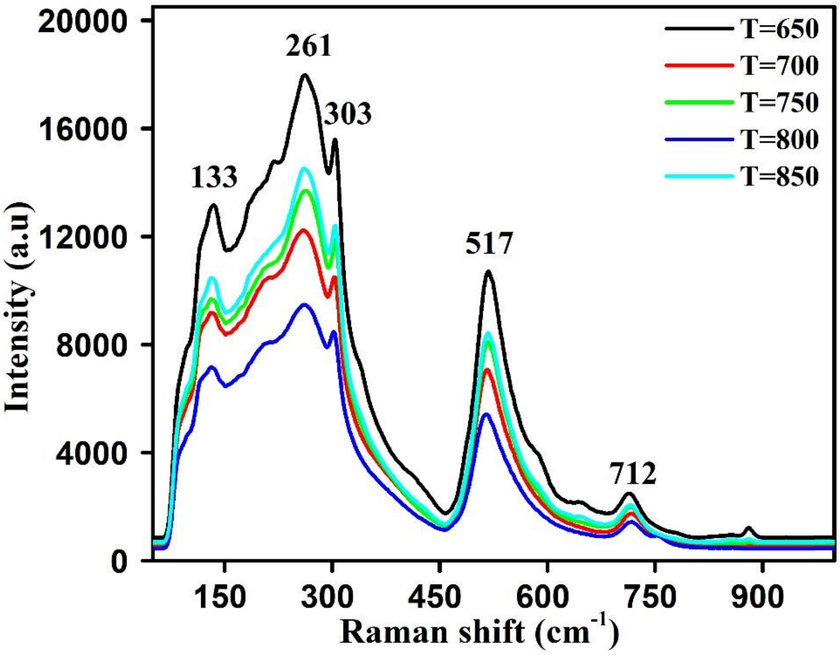

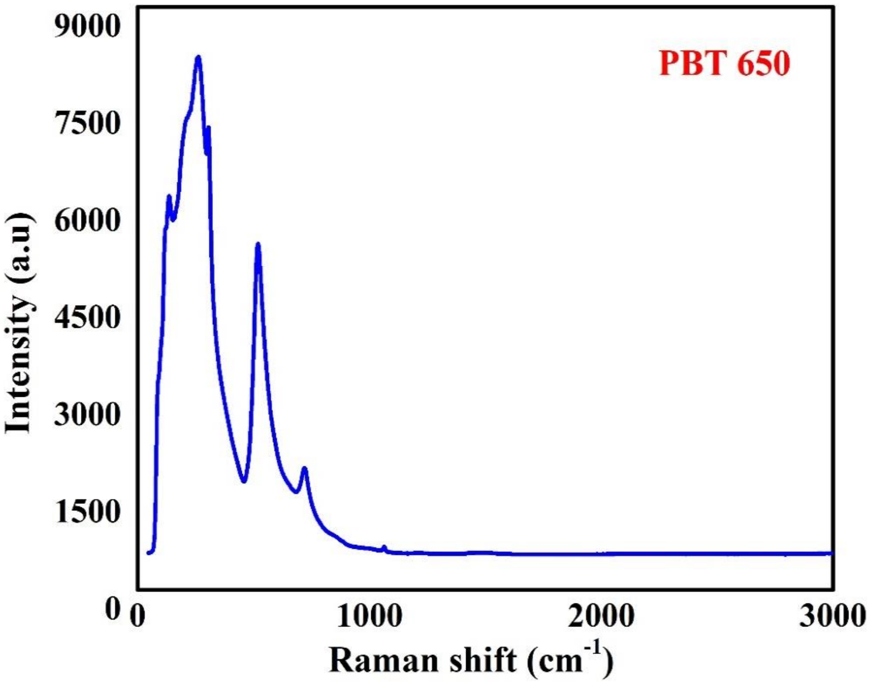

Fig. 3.4 (a). Raman spectra of Barium Titanate sintered at different sintering temperatures **(b)** The Raman spectra of PBT 650.

A slight dip at 180 cm^{-1} and 183 cm^{-1} of spectra of samples is attributed to the anharmonic coupling among the three A1 (TO) phonons [23-24]. The 133cm^{-1}, 303cm^{-1}, and the somewhat broader 712 cm^{-1} modes constitute the E(LO) modes. The intensity of the peak around 303 cm^{-1} was assigned to the overlap of E(3TO) +E(2LO) +B1, and the intensity of this characteristic peak decreased with an increase in sintering temperature. There are two E(TO) modes near 190cm^{-1} and 517 cm^{-1}, in which 190cm^{-1} becomes absent at a sintering temperature of 850°C. The E(TO) mode with frequency 517cm^{-1} shifts slightly towards the left until the sintering temperature is 800°C and then shifts towards the right. The presence of characteristic molecular vibration modes in Raman spectra confirms the formation of tetragonal phase Barium Titanate nanoparticles.

The Raman spectrum of the PMMA_$BaTiO_3$ (PBT) film, as depicted in Fig. 3.4(b), exhibits a composite profile characterized by distinct features from both PMMA and $BaTiO_3$. The PMMA-associated peaks are observable within the PBT spectrum alongside the characteristic peaks of $BaTiO_3$. Specifically, the signature peaks of PMMA are discernible at approximately 1700-1725 cm^{-1}, corresponding to the stretching vibrations of the carbonyl group (C=O). The mid-frequency range, from 1000 to 1500 cm^{-1}, also reveals peaks linked to the bending vibrations of methylene (CH_2) groups [25]. In the high-frequency region, vibrations associated with methyl (CH_3) groups are evident, with symmetric stretching occurring around 2950 cm^{-1} and asymmetric stretching around 2980 cm^{-1}.

3.3.4 Morphological characterization

FE-SEM micrographs of the Tetragonal phase Barium Titanate powder sintered at 650°C is shown in Fig.3.5. The powders appear to be closely packed polygonal structures caused primarily by the various processes occurring during the drying process. Moreover, small three-dimensional cuboid-like and irregular polygonal structures are embedded in each closely packed cluster, corresponding to the $BaTiO_3$ particles shown in Fig.3.5(a). SEM micrographs show excellent uniformity and narrow-sized distribution of Barium Titanate nanoparticles. The elemental composition of the prepared samples was analyzed using the EDX technique.

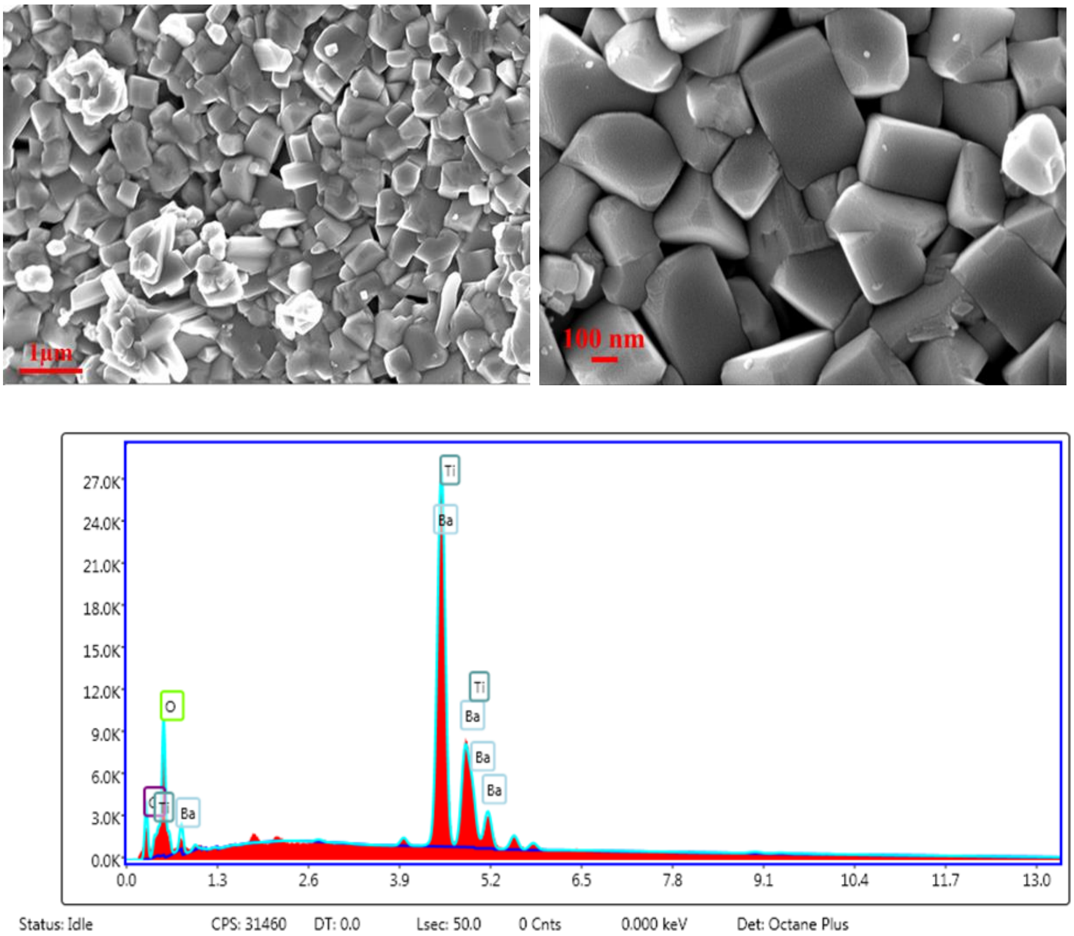

Fig. 3.5 (a). SEM images of nanostructured cuboidal hotspots provided by BT 650, **(b)** EDX spectra of nanostructured BT 650.

EDX also confirmed the formation of Barium Titanate. No impurity peaks corresponding to the precursors are present in the EDX spectra. The EDX spectra of the sample are shown in Fig.3.5 (b). Traditionally, Barium titanate is prepared by the conventional solid-state reaction, which involves high calcination temperatures of about 800°C -1200°C and sometimes at 1300°C. The Barium titanate prepared by this traditional method is highly agglomerated, with large particle size (2-5µm) and high impurity contents due to their inherent problems such as high reaction temperature heterogeneous solid-phase reaction [19]. By this modified synthesis method, we can generate highly pure, homogeneous, ultrafine Barium titanate powders at low temperatures.

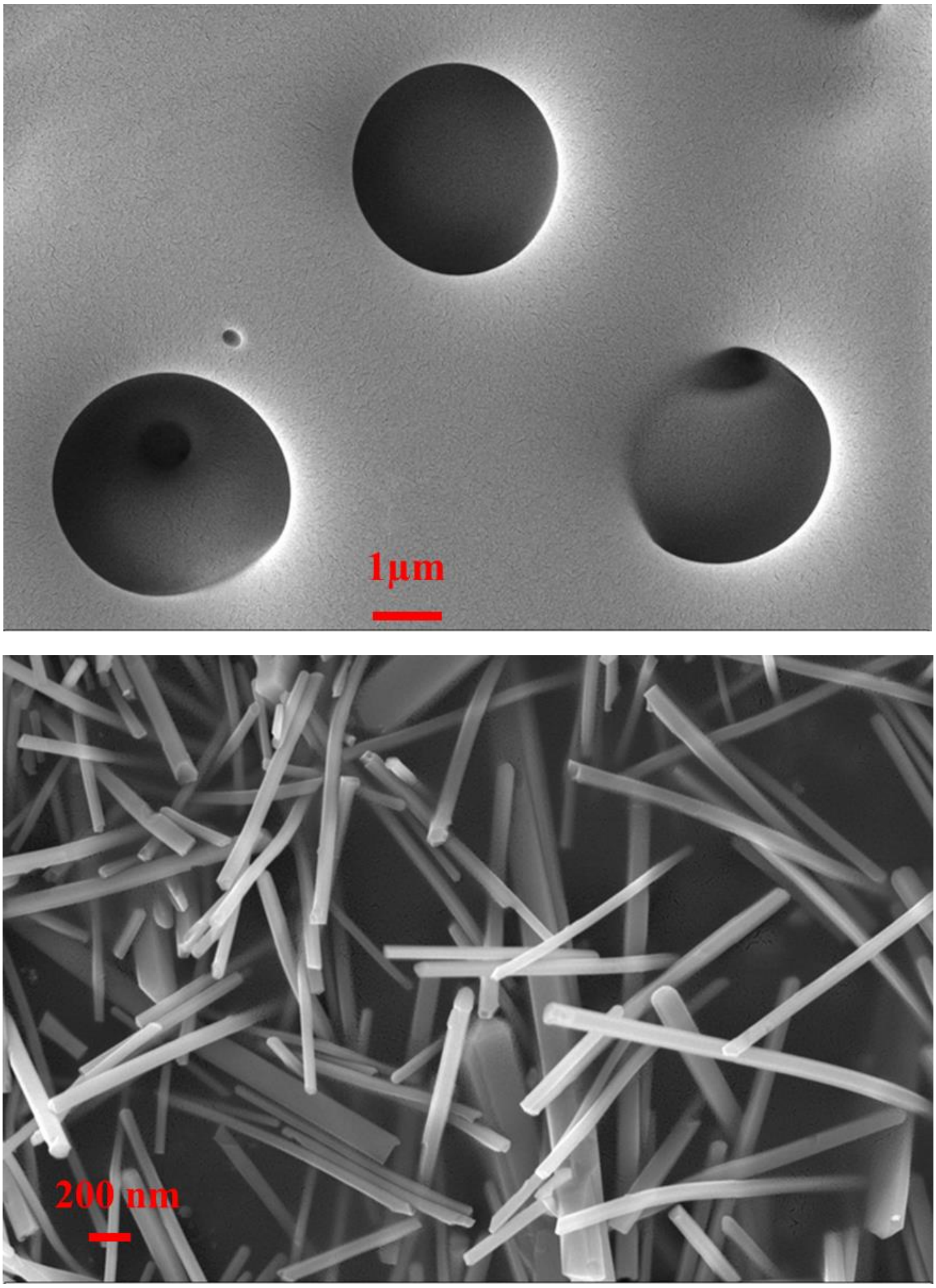

Fig. 3.6. (a) FESEM images of voids exhibited by PMMA polymer matrix **(b)**Tubular hospots exhibited PBT 650 film.

The incorporation of Barium Titanate (BT 650) nanoparticles into a Poly (methyl methacrylate) (PMMA) matrix result in a significant alteration in morphology, notably observed in PBT films. These films showcase densely packed nanotube-like structures within the voids of the PMMA matrix shown in fig. 3.6. This unique morphology holds crucial importance, particularly concerning adsorption properties. The formation of nanotube structures provides a high surface area-to-volume ratio, significantly amplifying the available surface area for adsorption processes. Additionally, the tubular morphology offers an interconnected network of channels, facilitating the diffusion of adsorbates throughout the material and enhancing adsorption efficiency. Furthermore, the presence of nanotube-like structures introduces additional active sites and defects on the surface, which can enhance the interaction between the adsorbate molecules and the substrate, further improving adsorption capacity and selectivity. Overall, the tube-like morphology exhibited by PBT films enhances the structural integrity and significantly boosts the adsorption performance.

3.3.5 Design and analysis of BT as SERS substrates for DMP detection.

Clear and distinct Raman peaks in Surface-Enhanced Raman Scattering (SERS) allow for unambiguous identification and precise analysis of molecular species. The non-overlapping Raman peaks between the SERS substrate and the probe molecule are crucial for accurately identifying and monitoring molecular changes in the presence of the probe molecule. As demonstrated previously, the absence of significant peaks for the BT and PBT film beyond 1000 cm^{-1} enhances the SERS effect, thereby amplifying the Raman peaks of the target probe molecule with Raman fingerprint bands beyond 1000 cm^{-1}.

Effective adsorption of the probe molecules, specifically DMP, on the surfaces of BT is crucial for utilizing these materials as SERS substrates for phthalate detection. Analyzing the adsorption profile of DMP on the substrate, as illustrated in Fig.3.7, reveals that within the first 30 minutes, 92% of the DMP molecules (from a 1 ppm solution) were effectively adsorbed onto the BT surface. Complete adsorption of DMP, reaching 99%, was achieved within 60 minutes.

The Raman spectra of the BT SERS substrate, exhibiting distinguishable Raman fingerprint bands, are presented in Fig. 3.4(a). The obtained Raman peaks of DMP are shown in Fig. 3.8(a), and the Raman peaks of DMP coated on BT SERS substrate are shown in 3.8(a). The Raman spectra of DMP reveal a series of characteristic peaks that offer valuable insights for their identification and analysis. Each molecule exhibits unique characteristic peaks in its Raman spectrum, serving as distinctive signatures. For DMP, the Raman fingerprint bands typically include a strong peak around 745 cm^{-1}, corresponding to the C-H out-of-plane bending vibration, peaks around 1030 cm^{-1} and 1070 cm^{-1} associated with C-H in-plane bending vibrations, a significant peak near 1285 cm^{-1} due to the C-H in-plane bending vibration, and a peak around 1610 cm^{-1} attributed to the C=C stretching vibration. The distinctive Raman fingerprint bands of DMP provide valuable information for its precise identification and analysis when coated on SERS substrates such as BT. These bands enable enhanced detection and monitoring of phthalate molecules by leveraging the increased and non-coinciding Raman signal, allowing for accurate and sensitive analysis.

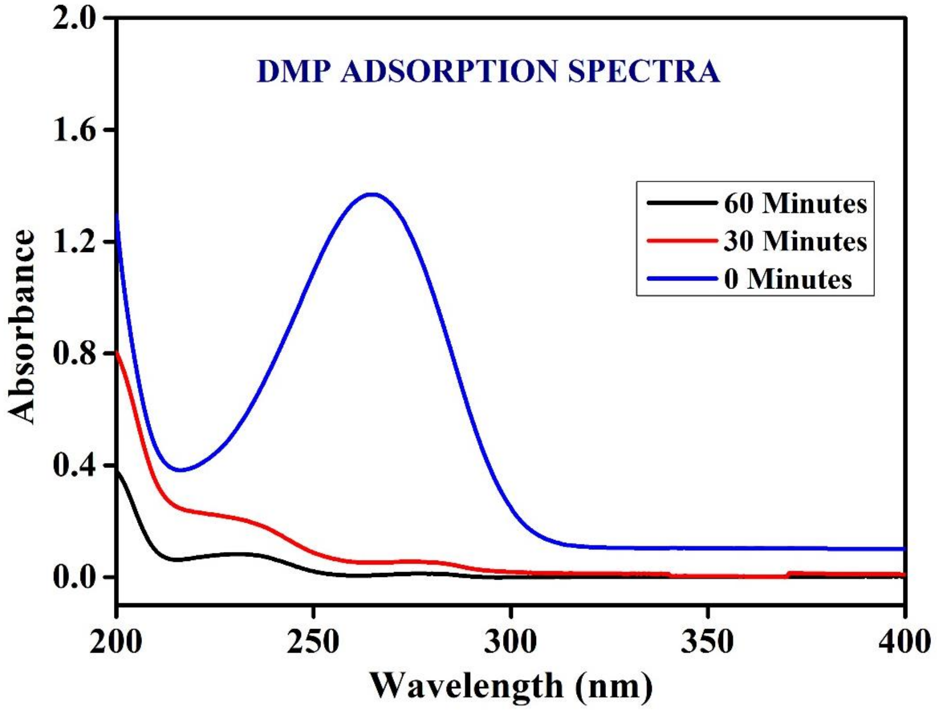

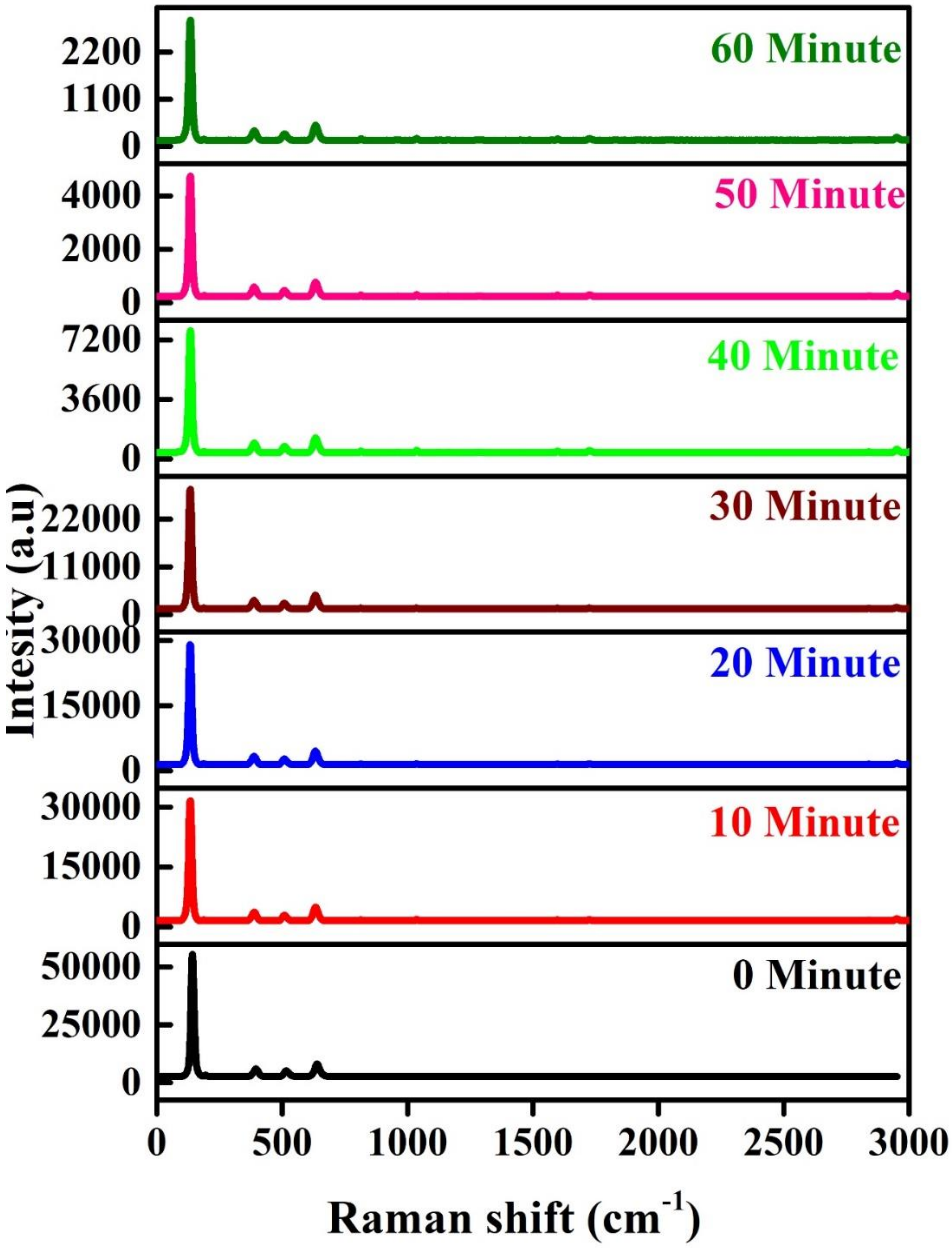

Fig.3.7 (a) and (b) UV- Visible absorbance spectra and Raman spectra showing that the BT substrate in DMP solution adsorbed 92% of the DMP molecules got adsorbed onto BT substrate in 30 mins. 99% of the DMP got adsorbed within 60 minutes. The experiment demonstrates desirable affinity between BT SERS substrate and DMP probe molecule.

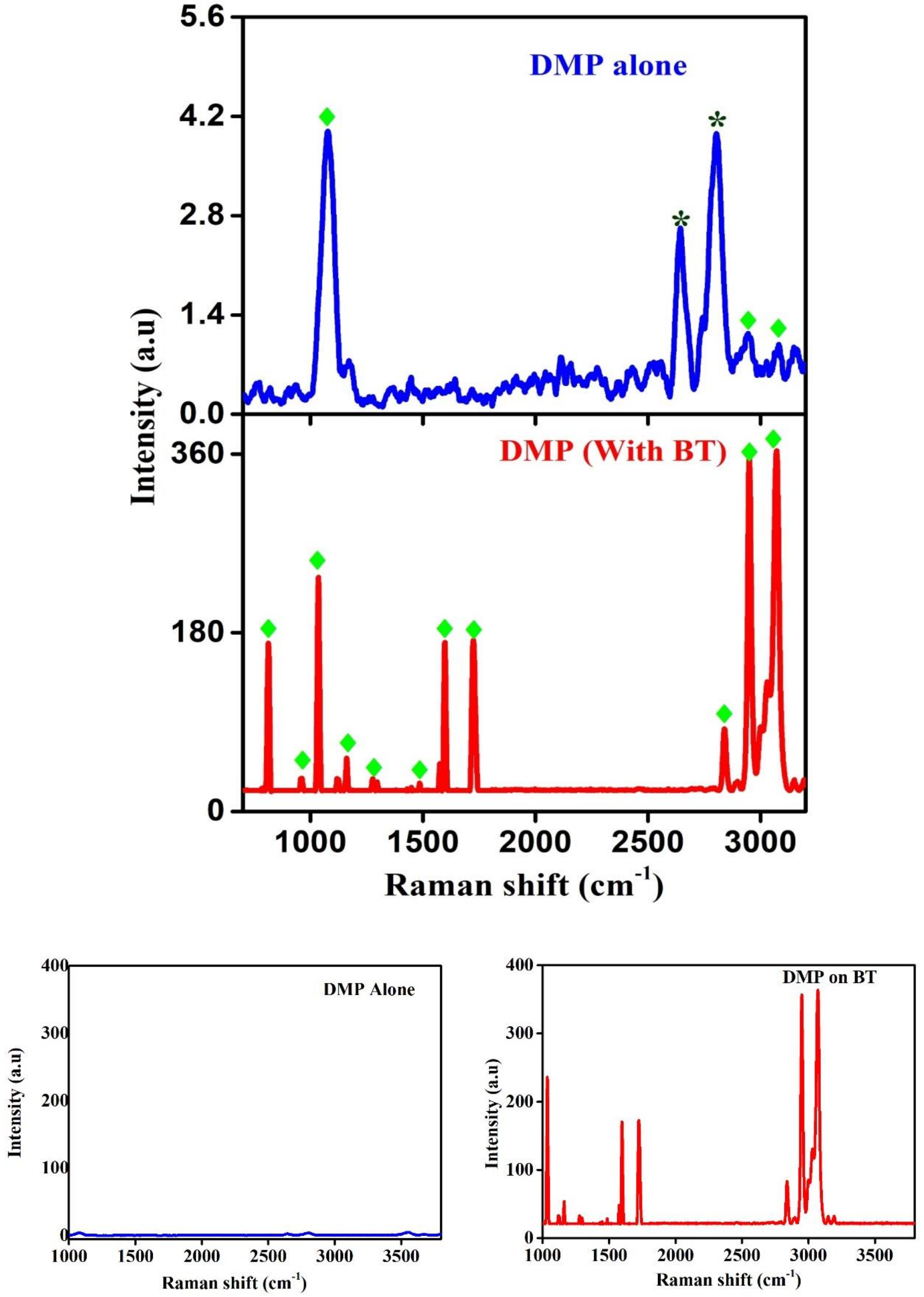

Fig. 3.8 (a) and (b) Raman spectra of DMP probe molecules and SERS spectra of DMP on BT with a Comparison plot showing the enhancement in DMP Raman fingerprint bands. (In Fig.(a), * denotes Raman peaks of glass, and ♦ denotes Raman peaks of DMP.

3.3.6 Design and analysis of BT and PBT films as SERS substrates for DMP and DEP phthalate detection.

Effective adsorption of probe molecules, particularly DEP, onto the surfaces of PBT films is essential for their use as SERS substrates for phthalate detection. Analyzing the adsorption profiles of DEP on these substrates, as depicted in Fig. 3.9 (a), shows that within the first 30 minutes, 95% of the DEP molecules (from a 1 ppm solution) were successfully adsorbed onto the PBT surface. Full adsorption of DEP, reaching 99%, was achieved within 60 minutes.

The Raman spectra of the PBT SERS substrate, with distinguishable Raman fingerprint bands, are shown in Fig.3.4(b). The corresponding Raman peaks for DEP are displayed in Fig. 3.9(a), while the Raman spectra of DEP coated on the PBT SERS substrate are also presented in Fig. 3.9(b). The Raman spectra of DEP reveal a series of characteristic peaks that provide valuable insights for its identification and analysis. Each molecule exhibits unique characteristic peaks in its Raman spectrum, serving as distinctive signatures. For DEP, the characteristic bands include a strong peak near 630 cm^{-1} corresponding to the C-H out-of-plane bending vibration, peaks around 1125 cm^{-1} and 1170 cm^{-1} associated with C-H in-plane bending vibrations, a prominent peak near 1280 cm^{-1} due to the C-H in-plane bending vibration, and peaks around 1600 cm^{-1} attributed to the C=C stretching vibration [26]. These distinctive Raman fingerprint bands are crucial for the precise identification and analysis of DEP when coated on PBT SERS substrates, enabling enhanced detection and monitoring of these phthalate molecules through the amplified Raman signal for accurate and sensitive analysis.

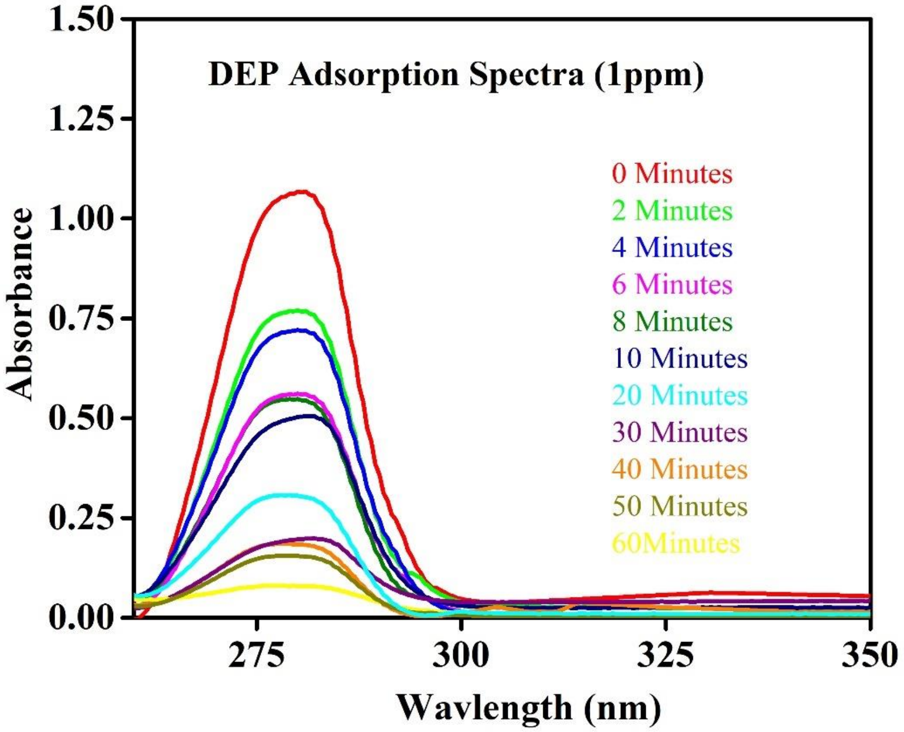
DEP Adsorption Spectra (1ppm)
Absorbance
Wavlength (nm)
1.50
1.25
1.00
0.75
0.50
0.25
0.00
275
300
325
350
0 Minutes
2 Minutes
4 Minutes
6 Minutes
8 Minutes
10 Minutes
20 Minutes
30 Minutes
40 Minutes
50 Minutes
60Minutes

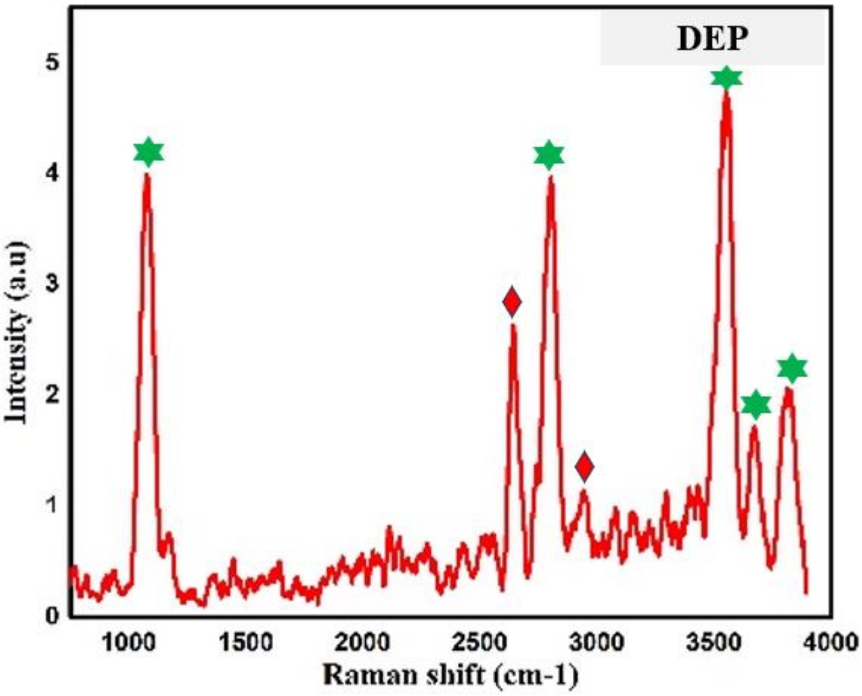
DEP
Intensity (a.u)
Raman shift (cm-1)
0
1
2
3
4
5
1000
1500
2000
2500
3000
3500
4000

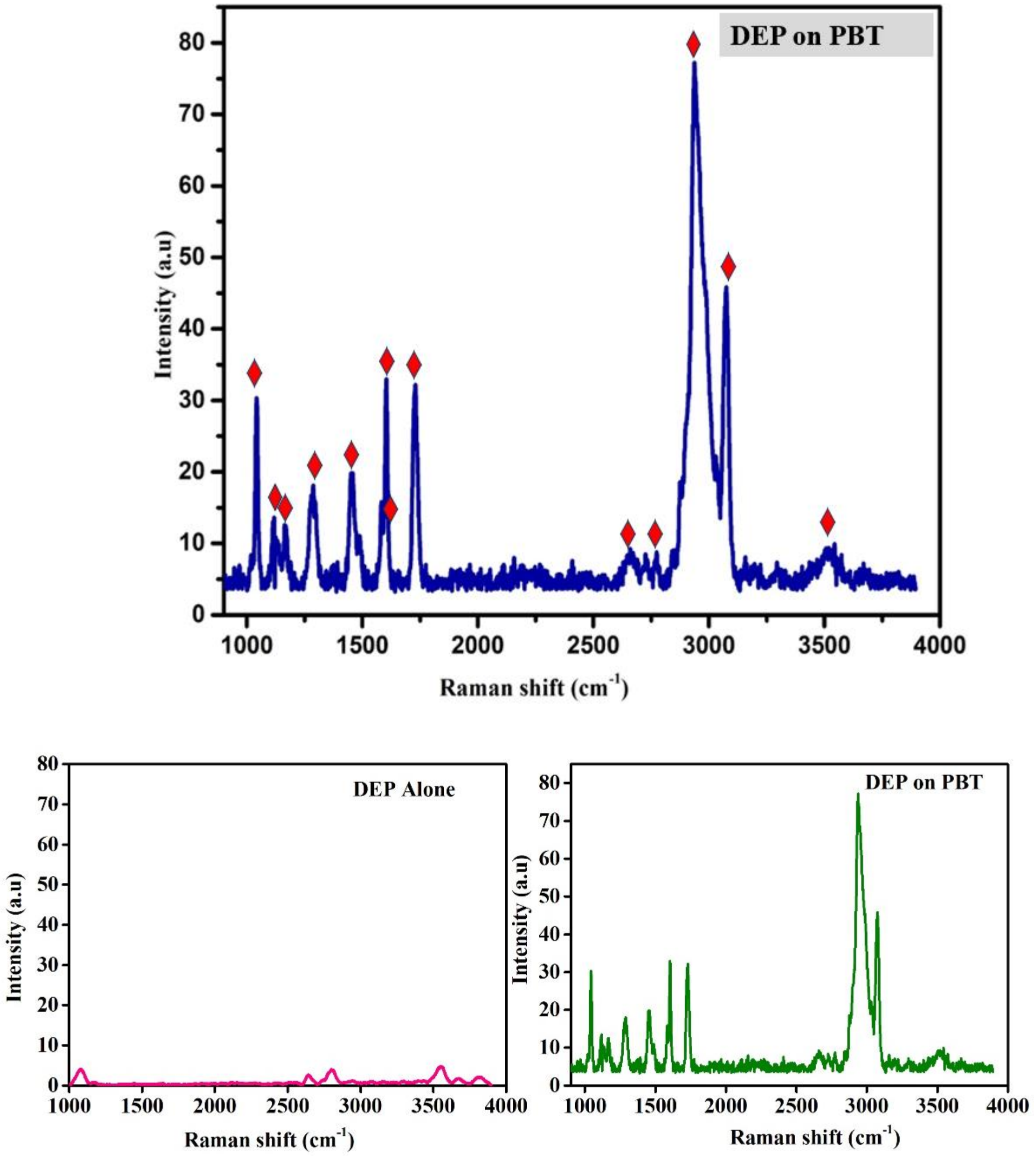

Fig.3.9 (a) UV- Visible absorbance showing that the PBT substrate in DEP solution adsorbed 95% of the DEP molecules got adsorbed onto PBT film in 30 mins. 99% of the DEP got adsorbed within 60 minutes. The experiment demonstrates desirable affinity between PBT SERS substrate and DEP probe molecule. **(b)** Raman spectra of DEP probe molecules and **(c)** SERS spectra of DEP on PBT with a Comparison plot showing the enhancement in DEP Raman fingerprint bands. **(d)** Comparison plot showing the enhancement in DEP Raman fingerprint bands. (In Fig.(c), * denotes Raman peaks of glass,and ♦ denotes Raman peaks of DEP,

3.3.7 Mechanism behind the SERS activity

The enhancement in Raman peak intensity in Surface-Enhanced Raman Scattering (SERS) is primarily attributed to electromagnetic and chemical enhancement mechanisms. In semiconductor-based SERS substrates, like $BaTiO_3$, the plasmon resonance typically occurs in the long-wavelength infrared region, unlike metal-based substrates, where it is in the visible and near-IR range. The primary mechanism for semiconductor-enhanced Raman scattering in $BaTiO_3$ is charge transfer resonances. This process involves charge transfer between the analyte molecule and the semiconductor substrate, which can be better understood through bandgap analysis and electronic transitions.

When $BaTiO_3$ is exposed to UV-visible light, electron-hole pairs are generated. The photo-excited electrons from these pairs migrate to the surface and transfer to the adsorbed analyte molecule. This electron transfer is facilitated by the alignment of energy levels between the conduction band (CB) of the semiconductor and the electronic states of the analyte, shown in fig 3.10. This alignment modifies the electronic structure of the analyte, potentially forming charged species or altering its vibrational or electronic states, which can cause shifts or broadening of energy levels. These modifications enhance the Raman scattering efficiency by changing the polarizability, vibrational modes, or electronic transitions, thus intensifying and altering the Raman scattering signals.

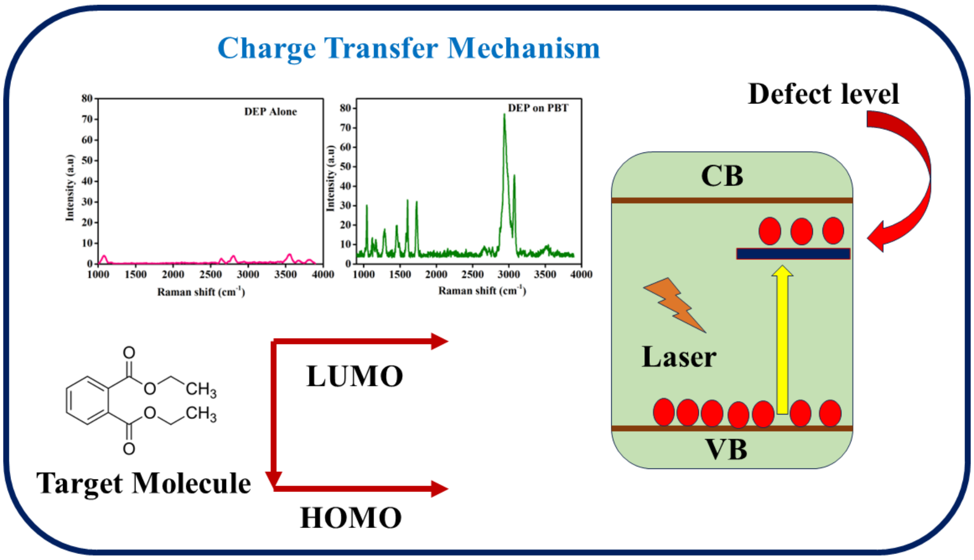

Fig. 3.10. Charge transfer mechanism responsible for Raman enhancement. The defect level originates from DEP (or DMP) -facilitating enhanced charge transfer resonance in the DEP_PBT system (or DMP_BT system).

Therefore, the SERS enhancement of DMP and DEP peaks observed with BT and PBT substrates can be primarily attributed to the charge transfer (CT) mechanism. As shown in Fig. 3.7(a) and 3.8(a), DMP and DEP exhibit a strong affinity towards their respective substrates. The cuboid-like and tubular morphology offers unique advantages for enhancing adsorption and Surface-Enhanced Raman Scattering (SERS) performance. Cuboid-like structures provide increased surface area and diverse adsorption sites, facilitating efficient adsorption of analyte molecules onto the substrate. The flat surfaces and defined edges of cuboids offer stable platforms for molecule adsorption, while the corners and edges create localized "hotspots" for intensified electromagnetic fields, crucial for SERS enhancement. Additionally, the tubular morphology exhibited by the PBT film enhances adsorption by providing channels and voids that effectively trap and hold molecules, increasing the concentration of analytes on the substrate surface. The tubular structure promotes better interaction between the substrate and analyte molecules, optimizing orientation and interaction for enhanced SERS signals. Moreover, combining cuboid-like and tubular morphologies facilitates efficient charge transfer processes between the substrate and analytes, enhancing Raman signal intensity through chemical enhancement mechanisms. Overall, the synergistic effects of cuboid-like and tubular morphologies result in a highly effective SERS substrate with improved adsorption capabilities and enhanced sensitivity for analytical applications. Phthalate molecules confined within these tubes interact via electrostatic interactions and hydrogen bonding with the hotspots. Consequently, the desired Raman peak enhancement occurs through the charge transfer mechanism.

3.4 Conclusions

We have introduced a novel approach employing a noble metal-free SERS substrate for the sensitive detection of phthalates, such as DMP and DEP. The design of this substrate hinges on the creation of "hotspots" derived from the morphology of the semiconductor $BaTiO_3$ integrated into a PMMA polymer matrix. This design strategy ensures distinct Raman bands for the substrate and probe molecules, eliminating potential spectral overlap and enabling precise detection.

Unlike conventional methods involving high-temperature processes exceeding 1000°C, we utilized a low-temperature sol-gel route to synthesize phase-pure $BaTiO_3$. The incorporation of PMMA facilitated the formation of densely packed $BaTiO_3$ tubular hotspots, as evidenced by FESEM images, crucial for enhancing the weak Raman signals of DEP. The underlying mechanism driving the SERS phenomenon relies on charge transfer resonance, supported by the demonstrated strong interaction between the phthalates DMP and DEP with BT and PBT, respectively. The direct interaction of metal nanostructures and analytes is responsible for the chemical enhancement mechanism (CM). The effect of CM requires direct contact between substrate and analyte. The chemical interaction between metal nanostructures and analyte molecules forms a new surface complex. The photo-induced charge transfer in a newly formed surface complex leads to polarizability change in the adsorbed analyte molecule. The shift in polarizability further enhances the Raman scattering cross-section and subsequent SERS enhancement. Hence, BT and PBT systems can be proposed as novel noble metal-free SERS substrates for the detection of DMP and DEP.

NB: The next chapter discusses the sensitive and selective detection of another significant pollutant, DEHP, using a different SERS substrate.

3.5 References

[1] Muhammad Ali Tahir† a, Nicoleta E. Dina† ORCID logo*b, Hanyun Cheng a, Ventsislav K. Valev ORCID logo*c and Liwu Zhang, Surface-enhanced Raman spectroscopy for bioanalysis and diagnosis, *Nanoscale*, 2021, **13**, 11593-11634, DOI: 10.1039/D1NR00708D.

[2] K. Anju, K. Roopitha, L.K. Alexander, BaTiO3 SERS substrates for Dimethyl phthalate detection, Materials Today: Proceedings, Volume 46, Part 8, 2021, Pages 3044-3050, ISSN 2214-7853, https://doi.org/10.1016/j.matpr.2021.01.843.

[3] X. Tan, J. Melkersson, S. Wu, L. Wang, and J. Zhang, "Noble-Metal-Free Materials for SERS Detection."

[4] Manoj B. Gawande, Anandarup Goswami§, François-Xavier Felpin, Tewodros Asefa, Xiaoxi Huang, Rafael Silva, Xiaoxin Zou, Radek Zboril, and Rajender S. Varma, Cu and Cu-Based Nanoparticles: Synthesis and Applications in Catalysis, hem. Rev. 2016, 116, 6, 3722–3811, https://doi.org/10.1021/acs.chemrev.5b00482.

[5] Jie Li, Huamin Zeng, Zhaowu Zeng, Yiying Zeng, and Tian Xie, Promising Graphene-Based Nanomaterials and Their Biomedical Applications and Potential Risks: A Comprehensive Review, ACS Biomater. Sci. Eng. 2021, 7, 12, 5363–5396, https://doi.org/10.1021/acsbiomaterials.1c00875.

[6] Wang, B. X., Duan, G., Xu, W., Xu, C., Jiang, J., Yang, Z., … Pi, F. Flexible surface-enhanced Raman scatting substrates: recent advances in their principles, design strategies, diversified material selections and applications. Critical Reviews in Food Science and Nutrition, 2022, 64(2), 472–516. https://doi.org/10.1080/10408398.2022.2106547.

[7] Zhuyuan Wang, Shenfei Zong, Lei Wu, Dan Zhu, and Yiping Cui, SERS-Activated Platforms for Immunoassay: Probes, Encoding Methods, and Applications, Chemical Reviews 2017 117 (12), 7910-7963, DOI: 10.1021/acs.chemrev.7b00027.

[8] K. Y. S. Hayashi, R. Koh, Y. Ichiyama, "Evidence for surface-enhanced Raman scattering on nonmetallic surfaces: Copper phthalocyanine molecules on GaP small particles," Phys. Rev. Lett., vol. 60, 1085, 1988.

[9] Y. Y. H. Yamada, "Surface-enhanced Raman scattering (SERS) of chemisorbed species on various kinds of metals and semiconductors," Surf. Sci., 1983, vol. 134, 71,.

[10] K. Y. S. Hayashi, R. Koh, Y. Ichiyama, "Evidence for surface-enhanced Raman scattering on nonmetallic surfaces: Copper phthalocyanine molecules on GaP small particles," Phys. Rev. Lett., 1988, vol. 60, 1085,.

[11] B. H. Loo, Observation of the surface enhanced raman scattering effect from the semiconductor—electrolyte interface J. Electroanal. Chem., 1982, vol. 136, 209.,.

[12] Ibrahim Khan, Khalid Saeed, Idrees Khan, Nanoparticles: Properties, applications and toxicities, Arabian Journal of Chemistry, Volume 12, Issue 7, 2019, Pages 908-931, ISSN 1878-5352, https://doi.org/10.1016/j.arabjc.2017.05.011.

[13] W. Ji and Y. Ozaki, "Semiconductor materials in analytical applications of surface-enhanced Raman scattering," 2016, November 2015, pp. 51–58 , doi: 10.1002/jrs.4854.

[14] Xue-Jiao Chen, Gema Cabello, De-Yin Wu, Zhong-Qun Tian, Surface-enhanced Raman spectroscopy toward application in plasmonic photocatalysis on metal nanostructures, Journal of Photochemistry and Photobiology C: Photochemistry Reviews, 2014, Volume 21,Pages 54-80, ISSN 1389-5567, https://doi.org/10.1016/j.jphotochemrev.2014.10.003.

[15] Xiaotian Wang, Wensheng Shi, Guangwei She, and Lixuan Mu, Using Si and Ge Nanostructures as Substrates for Surface-Enhanced Raman Scattering Based on Photoinduced Charge Transfer Mechanism, Journal of the American Chemical Society 2011 133 (41), 16518-16523DOI: 10.1021/ja2057874.

[16] K. M. Gani and A. A. Kazmi, "Phthalate contamination in aquatic environment: A critical review of the process factors that influence their removal in conventional and advanced wastewater treatment," Crit. Rev. Environ. Sci. Technol., ,2016, vol. 46, no. 17, pp. 1402–1439, doi: 10.1080/10643389.2016.1245552.

[17] J. D. Meeker, S. Sathyanarayana, and S. H. Swan, "Phthalates and other additives in plastics: human exposure and associated health outcomes," Philos. Trans. R. Soc. B Biol. Sci., , 2009, vol. 364, no. 1526, pp. 2097–2113, doi: 10.1098/rstb.2008.0268.

[18] A. Gonsioroski, V. E. Mourikes, and J. A. Flaws, "Endocrine disruptors in water and their effects on the reproductive system," Int. J. Mol. Sci., 2020, vol. 21, no. 6, doi: 10.3390/ijms21061929.

[19] Kumar, M., Sarma, D. K., Shubham, S., Kumawat, M., Verma, V., Prakash, A., & Tiwari, R. (2020). Environmental Endocrine-Disrupting Chemical Exposure: Role in Non-Communicable Diseases. *Frontiers in Public Health*,2020, *8*. https://doi.org/10.3389/fpubh.2020.553850.

[20] Y. I. and Y. T. T. Nakamura, T. Sakudo, J. Matt. Sci., vol. 40, pp. 1289–1292.

[21] N. K. Shabina Kappadan, Tesfakiros Woldu Gebreab, Sabu Thomas, "Tetragonal $BaTiO_3$ nanoparticles: An efficient photocatalyst for the degradation of organic pollutants," Mater. Sci. Semicond. Process., 2016.

[22] M. V. N. and R. N. U. Venkateswaran, Phys. Rev. BCondens. Matt.B x, vol. 58, pp. 14256–14260.

[23] B. D. S. Z. Z. Lazarevic, M. Vijatovic, Z. Dohcevic Mitrovic, N. Z. Romcevic, M.J.Romcevic, N.Paunovic, The characterization of the barium titanate ceramic powders prepared by the Pechini type reaction route and mechanically assisted synthesis J. Eur. Ceram. Soc., vol. 30, pp. 623–628.

[24] K. S. and K. K. Japan, J. App. Phys., vol. 44 4A, pp. 2081–2082.

[25] Pallikari, F., Chondrokoukis, G., Rebelakis, M., & Kotsalas, Y. (2001). Raman spectroscopy: A technique for estimating extent of polymerization in PMMA. Materials Research Innovations, 4(2–3), 89–92. https://doi.org/10.1007/s100190000076.

[26] Guodong Fang, Cun Liu, Yujun Wang, Dionysios D. Dionysiou, Dongmei Zhou, Photogeneration of reactive oxygen species from biochar suspension for diethyl phthalate degradation, Applied Catalysis B: Environmental, Volume 214, 2017, Pages 34-45, ISSN 0926-3373, https://doi.org/10.1016/j.apcatb.2017.05.036.

CHAPTER 4

Surface-engineered flexible PMMA_SrTiO$_3$ as a SERS substrate for detection of Di(2-ethylhexyl) phthalate

Contents

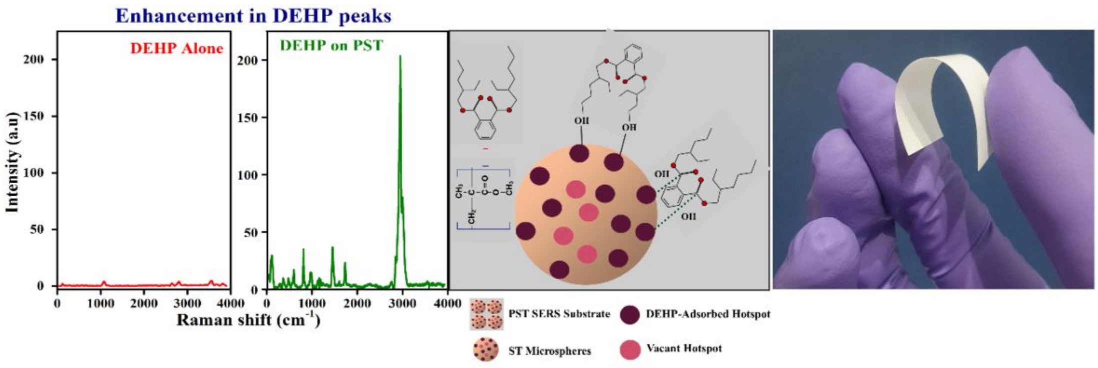

Abstract: *Di(2-ethylhexyl) phthalate (DEHP), used widely in manufacturing everyday artificial items, has severely harmful health effects. The reported DEHP detectors lack cost-effective, real-time detection. Surface-enhanced Raman spectroscopy (SERS) technique holds enormous promise for detecting environmental pollutants. This work demonstrated an effective tool for sensitively detecting a phthalate, DEHP - based on a flexible noble metal-free polymer-based SERS substrate. The successful design of the SERS substrate is based on the hotspot created on the pores of a semiconductor,* $SrTiO_3$*, coated on a polymer PMMA. Unlike the conventional high-temperature route (above 1000 °C), a low-temperature sol-gel route was adapted to synthesise* $SrTiO_3$*. Significant enhancement of feeble Raman peaks of DEHP is ensured by the dense arrangement of microspherical pore hotspots facilitated by the PMMA platform. Also, the design choice of the active SERS element and the platform ensured the non-coincidence of Raman bands of the SERS substrate and the probe molecule. The predominant mechanism behind the SERS activity is the charge transfer resonance, backed by the substantial affinity between* $SrTiO_3$ *and DEHP. Unlike conventional chromatographic techniques, the cost-effective, real-time sensitive detection of a phthalate demonstrated here using noble metal-free flexible SERS substrate adds an efficient route for sensing environmental pollutants.*

4.1 Introduction

In Chapter 1, sections 1.2.1 and 1.2.2, we discussed phthalates and their toxicity. This chapter reports our work on a significant phthalate, Bis (2-ethylhexyl) phthalate (DEHP). DEHP is a widely employed phthalate, which is utilised in manufacturing various everyday items, including cosmetics, medical devices, beverage bottles, infant formulas, food packages, and PVC tubes. Because DEHP is not chemically bonded to plastics, it can readily seep from the plastic materials into the contents they come into direct contact with, posing a high risk of exposure [1-5]. Adverse health effects linked to exposure to DEHP include shortened human pregnancy duration, reduced anogenital distance in male infants, sperm abnormalities, and decreased sperm motility in adult males [6-9].

Multiple methods are proposed for the sensitive detection of DEHP. Each technique offers diverse approaches with specific constraints. Chromatographic and mass spectrometric methods often demand specialised equipment and large amounts of organic solvents, limiting their suitability for rapid on-site analysis. Immunoassays may face challenges with cross-reactivity, impacting specificity [10], while electrochemical methods may have sensitivity limitations. Details regarding the various detection methods and their drawbacks are discussed in Section 1.2.3. [11]. Also we have introduced and discussed the advantages of Surface-enhanced Raman Spectroscopy (SERS) technique in section 1.2.4. As mentioned in section 1.2.4, the SERS excels in significantly amplifying Raman signals, delivering outstanding sensitivity and selectivity for detecting molecules at low concentrations, thereby proving its worth as a valuable tool across various analytical applications. Another advantage of SERS sensors is their rapid on-site analysis capability. The standard category of SERS substrate involves noble metals, particularly gold and silver. However, a notable disadvantage of noble metal SERS substrates is their susceptibility to oxidation and degradation over time, reducing SERS performance and signal reproducibility [12-15]. Maintaining the stability and longevity of noble metal-based SERS substrates remains a challenge. Additional challenges include the difficulty of creating optimal hot spots, the potential risk of coinciding Raman bands of the probe molecule and substrate, and substrate rigidity. Addressing these issues remains a key challenge in ensuring SERS substrates' enduring stability and longevity based on noble metals. Therefore, a demand exists to design and fabricate a **surface-engineered flexible noble metal-free SERS substrate with indispensable Raman peaks** for DEHP detection.

In this study, we developed a flexible SERS substrate using a PMMA polymer matrix, integrating morphologically customised hotspots through the low-temperature synthesis of $SrTiO_3$ - offering better characteristics than the one prepared through the conventional high-temperature route. The resulting substrate exhibits distinctive Raman peaks attributed to strontium titanate. These SERS substrates, adorned with microspherical hotspots, show a pronounced chemical enhancement effect based on charge transfer resonance, which is particularly advantageous for detecting DEHP.

4.2. Materials and methods

4.2.1 Choosing PMMA_$SrTiO_3$ combination for a SERS substrate.

The selection of PMMA (Polymethyl methacrylate) as the polymeric matrix for surface-enhanced Raman spectroscopy (SERS) in detecting DEHP (Di (2-ethylhexyl) phthalate) is grounded in its advantageous properties such as (i) The flexibility of PMMA enables the fabrication of versatile SERS substrates that are adaptable to various surfaces and shapes, aided by its ease of processing into controlled configurations [16] and (ii) The compatibility of PMMA with the synthesis process of semiconductor materials like $SrTiO_3$ can possibly facilitate the creation of micro-spherical pore hotspots crucial for SERS, enhancing detection sensitivity.

$SrTiO_3$ is chosen as the prime filler for our SERS substrate due to (i) its high dielectric constant, promoting electromagnetic field amplification near its surface for enhanced Raman signals, (ii) the chemical stability of $SrTiO_3$ ensures compatibility with diverse experimental conditions and large bandgap enables efficient excitation of surface plasmons or other localised surface modes that can augment Raman scattering signals. Moreover, $SrTiO_3$'s tunable properties offer optimisation avenues for enhanced SERS performance, making it a cost-effective and versatile option for research and industrial applications in SERS detection.

4.2.2 Low-temperature synthesis of strontium titanate nanoparticles.

Conventional approaches to strontium titanate synthesis often necessitate elevated calcination and sintering temperatures between 1000°C and 1300°C, leading to challenges such as agglomeration, the presence of phase impurities, limited control over morphology, large particle sizes (2-5μm), and notable impurity content [17-19]. To overcome these drawbacks, we designed an alternative modified two-step sol–gel route with a stepwise sintering procedure. Strontium carbonate, dissolved in acetic acid, undergoes partial hydrolysis at low temperatures in the presence of 2-propanol and titanium tetra isopropyl alkoxide. The resulting sol undergoes gelation, drying, calcination at 800°C, and sintering (600°C to 850°C) to achieve phase-pure nanocrystalline $SrTiO_3$.

4.2.3 Synthesis of PMMA_$SrTiO_3$ nanocomposite substrates.

Flexible self-standing polymer matrix films were prepared using PMMA crystals in an acetone solvent. As the solution turns into a white, viscous consistency, $SrTiO_3$ nanoparticle filler is gradually introduced, with continuous stirring. This process forms a thick, white gel that can be moulded into any desired shape for a composite film with a thickness of 100 microns- coined as PST film/substrate hereafter.

4.2.4 Bis (2-ethylhexyl) phthalate stock solution preparation.

A meticulous process is followed to prepare DEHP stock solution – considering the ultra-low concentration desired for SERS investigation. Only 10.10 μl of Bis (2-ethylhexyl) phthalate ($C_{24}H_{38}O_4$, molecular weight: 390.50) is needed to create a standard 100-ppm solution. This implies that a one-ppm DEHP solution contains an exceedingly low quantity of DEHP. Consequently, a one ppm DEHP solution is meticulously prepared by thoroughly blending the standard stock solution with distilled water in a standard flask.

4.2.5 Experimental procedure for adsorption

Adsorption experiments assessed the interaction between DEHP (Bis(2-ethylhexyl) phthalate) and the synthesised PST substrate. A 1 cm x 1 cm PST film was immersed in 100 ml of 1 ppm phthalate solution, and the mixture was stirred for 60 minutes at room temperature. Every 30 minutes, 30 ml of the solution was withdrawn for analysis. UV-Vis spectrophotometry (using a JASCO V-750 spectrometer) was employed to analyse the initial and post-adsorption solutions at the wavelength of maximum absorbance.

4.2.6 Raman and SERS property analysis

The micro-Raman measurements were performed using a Laser Micro Raman Spectrometer (532 nm excitation wavelength, ×50 L magnification, 1 mW excitation power) for precise Raman band identification of PST film and DEHP. SERS sensitivity was measured using the DEHP probe molecule stock solution coated onto a 1X1 cm PST film aligned on a clean glass slide.

4.3. Results and Discussion

4.3.1 Structural and morphological analysis

The elemental composition of the prepared, assessed using the EDX technique, confirms the expected formation of the PST. The X-ray diffraction peaks of the PMMA film, $SrTiO_3$ synthesised at low temperature (ST 600), and the PST film are shown in Fig. 4.1A. The peaks of ST 600 match with JCPDS card number 01-089-4934 confirming the single-phase formation of tetrogonal $SrTiO_3$. X-ray diffractogram of the ST 600 coated on the PMMA film (PST film) shows both PMMA and ST 600 peaks.

FE-SEM micrographs of the PST films are shown in Fig. 4.1B and 4.1C. The low-temperature synthesis route led to non-agglomerated morphology for strontium titanate (ST) nanoparticles. As seen in the images, the PST film exhibits a densely packed structure interspersed with uniform 3D microspheres of $SrTiO_3$. The attractive morphology for a semiconductor-based potential SERS substrate is formed through (i) deposition of the ST microspheres on the voids offered by PMMA and (ii) the affinity between closely arranged ST microspheres on PMMA. The resultant PST morphology enhances the specific surface area - facilitating a potential enrichment of the Raman peaks of the probe molecules.

4.3.2 Raman spectra of ST nanoparticles and PST film.

The Raman spectrum of strontium titanate sintered at 600 °C (ST 600) is shown in Fig 4.1D (1). The peak at ~ 148 cm^{-1} in the spectrum of ST is often attributed to lattice phonon mode [20]. The peak in the range 345-390 cm^{-1}, originating from the symmetric stretching of the Ti-O bonds, can be attributed to the A1g mode. Slightly higher in frequency, the Eg mode appears at 490-520 cm^{-1}, attributed to the symmetric stretching of both Sr-O and Ti-O bonds, revealing essential structural information. A secondary, albeit crucial, feature is the 2TO mode in the region 610-640 cm^{-1}, which arises from the second-order scattering of the A1g mode. On close examination, the B1g mode can be seen in the range 650-680 cm^{-1}, associated with the stretching vibrations of the Ti-O and Sr-O bonds. At even higher frequencies, around 735-750 cm^{-1}, the Eg and A1g modes combined created another distinctive peak. It's worth noting that, in addition to these primary modes, strontium titanate may exhibit transverse optical (TO) and longitudinal optical (LO) phonon modes. However, they are typically weaker and may overlap with other peaks in the Raman spectrum. The Raman spectrum of the PST film (Fig 4.1D (2)) is a mixture of the distinctive features from both PMMA and $SrTiO_3$. The peaks attributed to PMMA are observable in PST alongside the peaks associated with ST 600. On close examination, the signature peaks of PMMA can be seen at around 1700-1725 cm^{-1} (stretching vibration of the carbonyl group (C=O)). Between 1000 and 1500 cm^{-1}, the mid-frequency range showcases peaks associated with the bending vibrations of methylene (CH_2) groups. In the high-frequency region, vibrations of methyl (CH_3) groups are apparent, with symmetric stretching around 2950 cm^{-1} and asymmetric stretching around 2980 cm^{-1}.

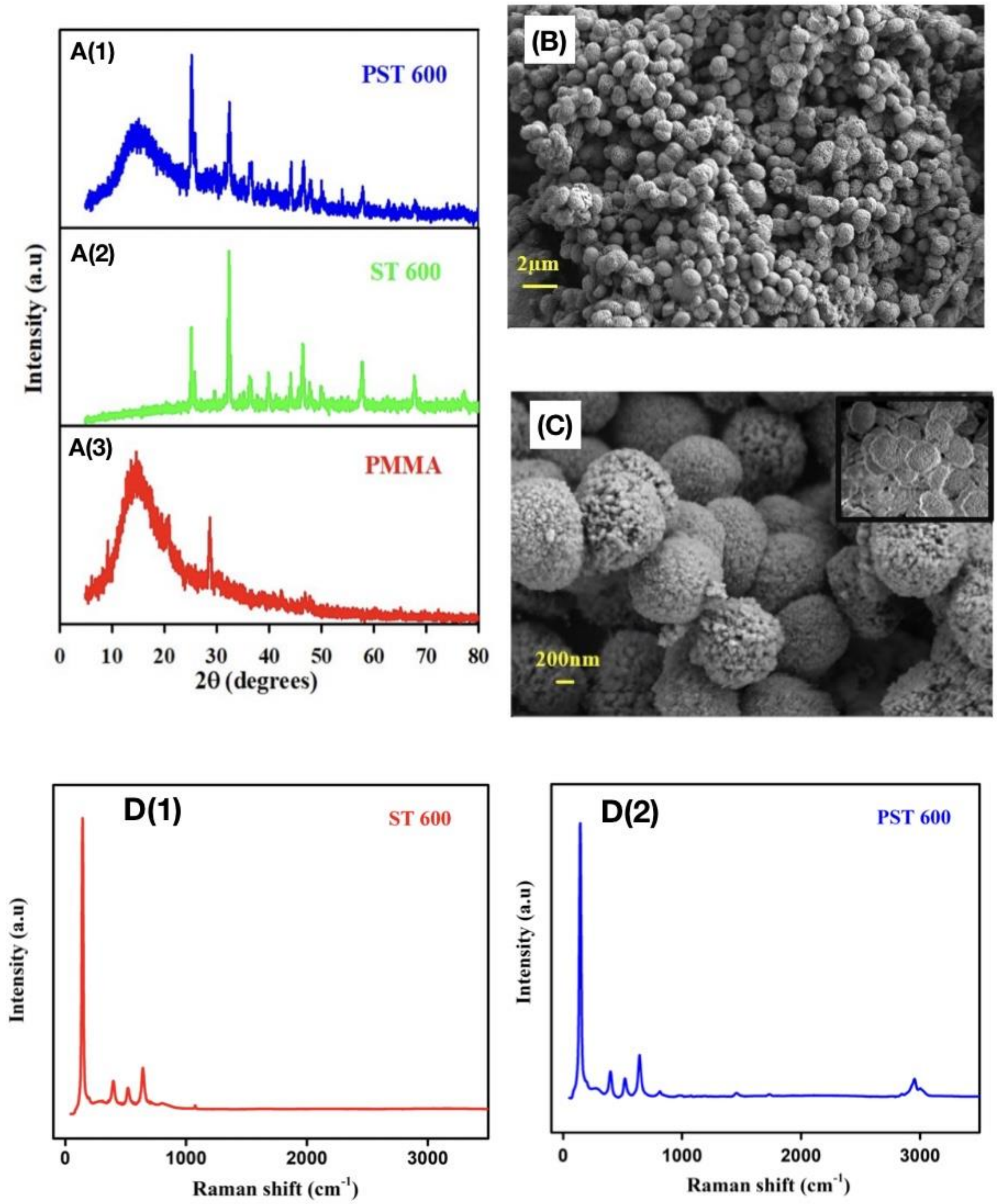

Fig. 4.1. **(A)** The XRD patterns of the PMMA, ST 600 and PST 600; **(B)** SEM image of the SERS substrate. **(C)** SEM image showing a magnified view of the ST microspheres with the cross-sectional view of the SERS substrate projecting pores. **(D)** The Raman spectra of the ST 600 and PST 600. The absence of any significant peak for PST film beyond 1000 cm^{-1} facilitates SERS enhancement of Raman peaks of the potential probe molecule.

4.3.3 Design and analysis of PST film as a SERS substrate for DEHP detection

Clear and distinct Raman peaks in SERS ensure unambiguous identification and precise analysis. The non-coinciding Raman peaks between the SERS substrate and the probe molecule ensure accurate identification and monitoring of molecular changes in the presence of the probe molecule. As shown in the previous subsection, the absence of any significant peak for PST film beyond 1000 cm^{-1} facilitates SERS enhancement of Raman peaks of the potential probe molecule.

Effective adsorption of the probe molecule (here, DEHP) on the surface of the PST film is critical for the methodology for employing PST film as an SERS substrate for detecting DEHP. Analysing the adsorption profile of the DEHP on the substrate, as shown in Fig 4.2A, we noticed that within the first half-hour, 92% of the DEHP molecules (1 ppm solution) got effectively attached to the PST film. 99.95% adsorption of the DEHP was achieved within 60 minutes.

Raman spectra of PST SERS substrate with distinguishable Raman fingerprint bands are shown in Fig. 2B. The obtained Raman peaks of DEHP are shown in Fig.4.2C, and the Raman peaks of DEHP coated on PST SERS substrate are shown in Fig.4.2D. The Raman spectrum of DEHP (Bis(2-ethylhexyl) phthalate) reveals a series of characteristic peaks that provide valuable insights for its identification and analysis. The peak observed in the 800-1180 cm^{-1} range corresponds to the stretching vibration of the C-O bond in the ester group of DEHP. The peak at 1290-1310 cm^{-1} represents the stretching vibration of the C-C bonds within the long alkyl chains of DEHP, substantiating the existence of these extensive alkyl chains. The 1460-1470 cm^{-1} peak is attributed to the bending vibration of methyl ($-CH_3$) groups in DEHP. The peak at 1600-1620 cm^{-1} corresponds to the stretching vibration of the C=C double bonds from the benzene rings of DEHP. The stretching vibration of the C=O bond in the ester group is represented by the peak at 1720-1740 cm^{-1}. The 3000-3100 cm^{-1} peak signifies the stretching vibration of the C-H bond in the aromatic group of DEHP [21,22]. On contact with the PST SERS substrate, selected peaks of DEHP were enhanced in intensity. Therefore, as demonstrated in Fig 4.2E, the distinctive Raman peaks of DEHP visible in combination with the substrate suggest the utility of PST as a commendable detection SERS substrate for DEHP. Further appreciation of the utility is discussed in the following subsection.

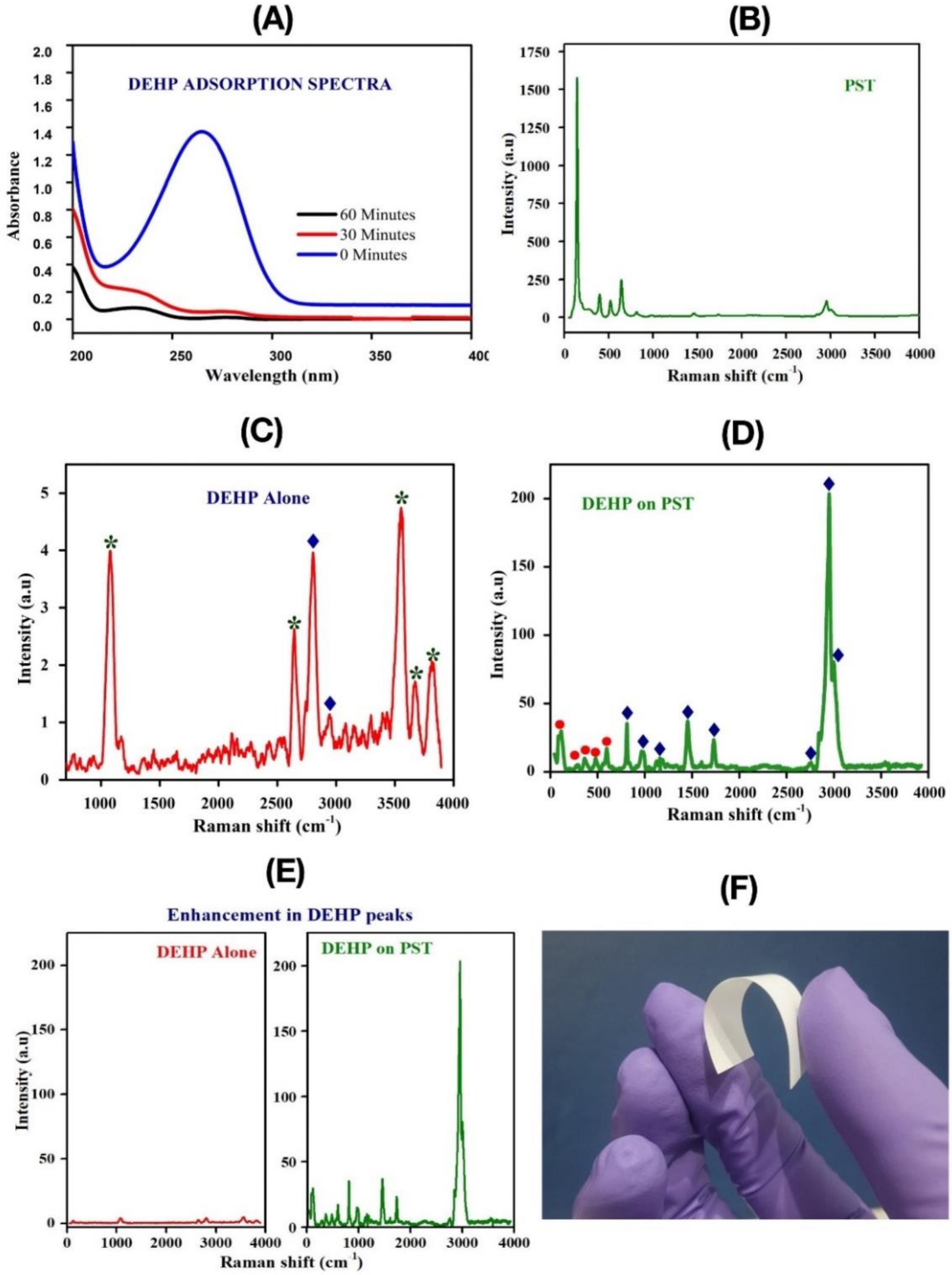

Fig. 4.2. (A) UV- Visible absorbance spectra showing that the PST film in DEHP solution adsorbed 92% of the DEHP molecules got adsorbed onto PST film in 30 mins. 99.95% of the DEHP got adsorbed within 60 minutes. The experiment demonstrates desirable affinity between PST SERS substrate and DEHP probe molecule. **(B)** Raman spectra of PST SERS substrate with distinguishable Raman fingerprint bands. **(C)** Raman spectra of DEHP probe molecules **(D)** SERS spectra of DEHP on PST. **(E)** Comparison plot showing the enhancement in DEHP Raman fingerprint bands. (In Fig. C & D, * denotes Raman peaks of glass, ♦ denotes Raman peaks of DEHP, and ● Denotes Raman peaks of PST). **(F)** The photograph shows the flexibility of the PST SERS substrate we fabricated.

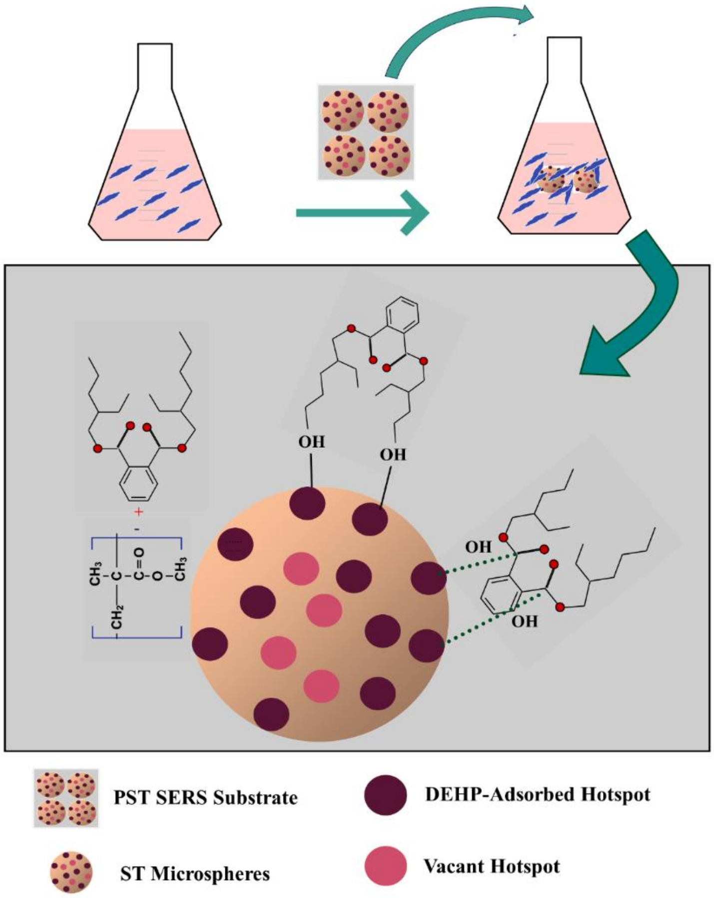

Fig. 4.3. Schematic representation depicting how porous microsphere hotspots contribute to the charge transfer resonance. Electrostatic interactions and hydrogen bonding link the DEHP molecules attracted to the pores.

Generally, the mechanism behind the enhancement in the Raman peak intensity in SERS is mainly attributed to electromagnetic and chemical enhancement. The plasmon resonance in most semiconductor-based SERS substrates is located in the long-wavelength infrared region (unlike the metal-based ones with LSRP in visible and near-IR). The charge transfer resonances are considered the leading mechanism for semiconductor-enhanced Raman scattering - here, in this case, due to $SrTiO_3$. Charge transfer between the analyte molecule and the semiconductor substrate, such as $SrTiO_3$, is elucidated through bandgap analysis and electronic transitions. The UV-visible light generates electron-hole pairs on the $SrTiO_{3.}$ The photo-excited electrons (generated as part of the electron-hole pairs) migrate to the surface and get transferred to the adsorbed analyte molecule. Such a transfer is made possible by the alignment of energy levels between the semiconductor CB and the analyte's electronic states. Consequently, the analyte's electronic structure undergoes modification, potentially forming charged species or altering vibrational or electronic states, accompanied by shifts or broadening of energy levels. These modifications enhance Raman scattering efficiency, attributed to changes in polarizability, vibrational modes, or electronic transitions, thus intensifying and altering Raman scattering signals. Ultimately, this charge transfer mechanism contributes significantly to the enhancement observed in semiconductor-enhanced Raman spectroscopy, driven by energetic alignment and substrate-analyte affinity. Thus, the SERS enhancement of the DEHP peaks due to the PST substrate can be attributed to the charge transfer (CT) mechanism. As seen in Fig 4.2A, DEHP and PST have a strong affinity aided by the porous morphology. The ST microsphere arrangement facilitated by PMMA voids yields a higher surface area featuring densely distributed porous "hotspots," These hotspots serve as accumulation centres for DEHP, and their increased surface area, along with a high-density configuration and molecular affinity, augments the adsorption capacity. DEHP molecules confined within the pores establish connections via electrostatic interactions and hydrogen bonding with hotspots, as illustrated in Fig.4.3. Consequently, the desired Raman peak enhancement happens via the charge transfer mechanism.

4.3.3 (c). Utility of the PMMA_SrTiO$_3$ SERS for detection of DEHP.

Sensitivity: Our study achieved a significant milestone by successfully credibily detecting DEHP presence in a one ppm solution (0.091 µl). The Environmental Protection Agency (EPA) in the United States has established stringent guidelines for DEHP in drinking water, maintaining a maximum contaminant level (MCL) of 6 micrograms per litre (µg/L) [23]. In blood products stored in plastic bags for transfusions, DEHP concentrations vary from 4.3 to 1,230 ppm. Our report on the SERS-based detection of DEHP based on a one-ppm stock solution brings out a new and better tool for monitoring environmental and health-related concentrations of DEHP.

Quick Analysis: The chromatographic methods, such as gas chromatography-mass spectrometry (GC-MS) and high-performance liquid chromatography (HPLC), are highly sensitive but often involve time-consuming sample preparation and analysis. The PST SERS DEHP detector emphasises its application for detection purposes rather than quantification of DEHP. Beyond that, the PST SERS DEHP detector offers real-time rapid detection capabilities - overcoming the time constraints associated with traditional methods.

Cost-effectiveness: The flexible PMMA_$SrTiO_3$ substrate offers distinct advantages for DEHP Raman detection compared to the existing materials. The substrate provides an economical alternative to noble metals typically used in traditional Raman spectroscopy setups.

4.4 Conclusion

We have demonstrated an effective tool based on a flexible noble metal-free polymer-based SERS substrate for sensitively detecting a phthalate, DEHP. The successful design of the SERS substrate was based on the hotspot created on the pores of a semiconductor, $SrTiO_3$, coated on the polymer PMMA. The design choice of the SERS substrate avoided an overlap between Raman bands of the substrate and DEHP molecules, ensuring accurate detection without ambiguity. Unlike the conventional high-temperature route (above 1000 °C), a low-temperature sol-gel route was adapted to synthesise phase-pure $SrTiO_3$. The PMMA effectively ensured the highly dense presence of $SrTiO_3$ microspherical pore hotspots- as seen in the FESEM images- needed for significant enhancement of feeble Raman peaks of DEHP. The mechanism behind the SERS behaviour is based on charge transfer resonance – backed by the demonstrated substantial affinity between $SrTiO_3$ and DEHP. Unlike conventional chromatographic techniques, the cost-effective, real-time sensitive detection of a phthalate demonstrated here using noble metal-free flexible SERS substrate adds a potent route for sensing environmental pollutants.

4.5 References

[1] Chang, W.H., Herianto, S., Lee, C.C., Hung, H., Chen, H.L., The effects of phthalate ester exposure on human health: a review. Sci. Total Environ. 2021, 786, 147371. PMID: 33965815. https://doi.org/10.1016/j.scitotenv.2021.147371.

[2] Fang, L., Huang, T., Lu, H., Wu, X.L., Chen, Z., Yang, H., et al., Biochar-based materials in environmental pollutant elimination, H2 production, and CO2 capture applications. 2023, Biochar 5 (1). https://doi.org/10.1007/s42773-023-00237-7.

[3] Chi, C.C., Xia, M., Zhou, C., Wang, X.Q., Weng, M.L., Shen, X.Y.,. Determination of 15 phthalate esters in air by gas-phase and particle-phase simultaneous sampling. J. Environ. Sci. 2017, (5), 9.

[4] Luo, Q., Liu, Z.H., Yin, H., Dang, Z., Wu, P.X., Zhu, N.W., Lin, Z., Liu, Y. Migration and potential risk of trace phthalates in bottled water: a global situation. Water Res., 2018, 147, 362–372.

[5] Wang, W.L., Wu, Q.Y., Wang, C., He, T., Hu, H.Y., Health risk assessment of phthalate esters (PAEs) in drinking water sources of China. Environ. Sci. Pollut. Res. 2015, 22, 3620–3630.

[6] Duan, C.H., Fang, Y.J., Liang, J., Gao, Z.X., In vitro cytotoxicity evaluation of phthalate plasticisers, 06 Asian J. Ecotoxicol. 2019, 14, 23–31 (in Chinese).

[7] Swan, S.H., 2008. Environmental phthalate exposure in relation to reproductive outcomes and other health endpoints in humans. Environ. Res. 108 (2), 177–184.

[8] Wu, W., Zhou, F., Wang, Y., Ning, Y., Yang, J.Y., Zhou, Y.K. Exposure to phthalates in children aged 5-7 years: associations with thyroid function and insulin like growth factors. Sci. Total Environ., 2017, 579, 950–956.

[9] Xiangle Meng, Ao Huang, Yuye Li, Xiuxiu Dong, Tianyan You, Highly sensitive and selective photoelectrochemical detection of bis (2-ethylhexyl) phthalate on broad-spectrum responsive and interfacial electronic interaction induced p− n BiOI/ZnO nanoarrays heterojunction. j.bios. 2024, 116121, 251. https://doi.org/ 10.1016/ j.bios.2024.116121

[10] Jill Tate, Greg Ward 2004 Interferences in Immunoassay, Clin Biochem Rev Vol 25 May 2004 105-120

[11] Ziqiao Zhu, Renzhi Rao, Zhenyuan Zhao, Jinfeng Chen, Wenlong Jiang, Fukun Bi, Yang Yang, Xiaodong Zhang, 2022. Research progress on removal of phthalates pollutants from environment. Journal of Molecular Liquids, 2022, 355 ,118930.

[12]. Kosslick, H.; Sauer, H.; Just, T.; Vick, U.; Fulda, G.; Jonas, L. Biodegradation of gold and platinum implants in rats studied by electron microscopy. Int. J. 2019, 2766, 2748.

[13]. Lu, Z.; Si, H.; Li, Z.; Yu, J.; Liu, Y.; Feng, D.; Zhang, C.; Yang, W.; Man, B.; Jiang, S. Sensitive, reproducible, and sTable 3D plasmonic hybrids with bilayer

WS2 as nanospacer for SERS analysis. Opt. Express 2018, 26, 21626–21641.

[14]. Palaghias, G.; Eliades, G.; Vougiouklakis, G. In vivo corrosion behavior of gold-plated versus titanium dental retention pins. J. Prosthet. Dent. 1992, 67, 194–198.

[15]. Ying Gu , Yonghui Li , Huimin Qiu , Yukun Yang , Qiyue Wu , Xuejing Fan , Yangyue Ding , Lunzhao Yi , Kun Ge , Yizhong Shen, Recent progress on noble-free substrates for surface-enhanced Raman spectroscopy analysis. j.ccr , 2023, 215425, 497. https://doi.org/10.1016/j.ccr.2023.215425

[16] Anju K Libu K. Alexander, Extremely low-frequency plasmonic state achieved in AC-ZnO polymer composite for tuned negative permittivity applications. j.materresbull. April 2024, 112649, 172. https://doi.org/ 10.1016/ j.materresbull.2023.112649.

[17] P. Balaya, M. Ahrens, L. Kienle, J. Maier, B. Rahmati, S. B. Lee and W. Sigle, Synthesis and characterisation of nanocrystalline $SrTiO_3$, *J. Am. Ceram. Soc.*, (2006), **89**, 2804.

[18] X. Fan, Y. Wang, X. Chen, L. Gao, W. Luo, Y. Yuan, Z. Li, T. Yu, J. Zhu and Z. Zou, Facile method to synthesise mesoporous multimetal oxides ($ATiO_3$, A = Sr, Ba) with large specific surface areas and crystalline pore walls, *Chem. Mater.*, 2010, **22**, 1276.

[19] F. Zou, Z. Jiang, X. Qin, Y. Zhao, L. Jiang, J. Zhi, T. Xiao and P. P. Edwards, Template-free synthesis of mesoporous N-doped $SrTiO_3$ perovskite with high visible-light-driven photocatalytic activity, *Chem. Commun.*, 2012, 48, 8514.

[20] Raman Spectra of Strontium Titanate June 2006 Journal of the American Ceramic Society 65(4):c54 - c56 10.1111/j.1151-2916.1982.tb10417.x

[21] Yuan Xiang, Menghua Li, Xiaoyu Guo, Yiping Wu, Ye Ying, Ying Wen, Haifeng Yang, 2018 Raman rapid detection of environmental hormone, Sensors and Actuators B 262 44–49.

[22] He Xu, Jianhao Zhu , Yuxiao Cheng , Dongqing Cai , 2021. Functionalised UIO-66@Ag nanoparticles substrate for rapid and ultrasensitive SERS detection of di-(2-ethylhexyl) phthalate in plastics, Sensors and Actuators: B. Chemical 349 130793.

[23] https://www.epa.gov/sdwa/drinking-water-regulations-and-contaminants.

CHAPTER 5

A novel PPy_ZnO polymer nanocomposite system for rapid removal of Dimethyl phthalate.

Contents

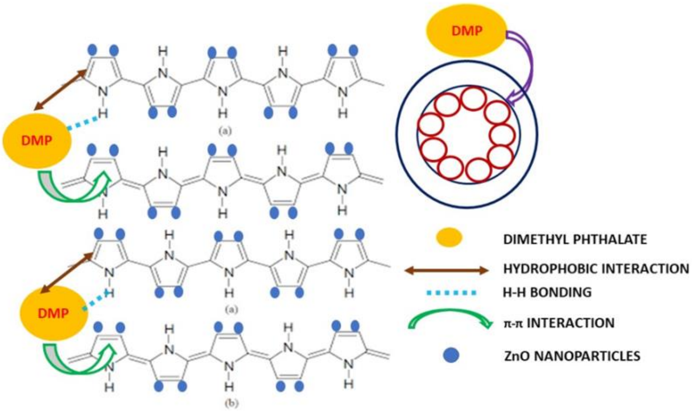

Abstract: *Industrial manufacturing processes using Dimethyl Phthalate (DMP) based plasticizers contribute significantly to the growing issue of water pollution. The processes that can remove DMP at lower concentrations (~ 1ppm) are seriously lacking for real-world application. The study aims for efficient adsorptive removal of DMP using a facilely synthesised zinc oxide incorporated polypyrrole (PPy_ZnO) polymer nanocomposites. A high-yield synthesis of PPy_ZnO was achieved through the oxidative polymerisation method. XRD, FESEM, and BET-BJH characterised the synthesised samples. The study found PPy_ZnO composite with 0.03 g of ZnO as a novel adsorbent for DMP. The PPy_ZnO removed 91.84% of DMP from a 1 ppm aqueous solution in 10 minutes – a rarity with lower concentrations of phthalate. Also, the results demonstrate that PPy_ZnO is an attractive and feasible material for removing higher and lower DMP concentrations. The enhanced adsorption phenomena are explained based on the synergetic effect of slit-like micropores and conjugated benzene rings in the PPy_ZnO. The DMP molecules become trapped inside the pores and are held there primarily by electrostatic attraction, H-bonding, and π-π interactions. This research shows that engineered surface functional groups of polymer nanocomposites could be used to make high-performance phthalate adsorbents.*

5.1. Introduction

Phthalic acid esters (PAEs) serve as critical plasticizers and softening agents in various industrial applications, including construction materials, food packaging, medical devices, and cosmetics [1,2]. These compounds, classified as endocrine-disrupting chemicals (EDCs), pose significant environmental and health risks due to their ability to disrupt hormone balance and reproductive systems [3-6]. Properties and sources of phthalates are explained in detail in section 1.2. PAEs, such as dimethyl phthalate (DMP), exhibit persistence in the environment and bioaccumulation tendencies, leading to their widespread presence in indoor dust [3-6], food [7,8], air [9,10], soil [11], and water sources [12,13]. The migration of phthalates into food and beverages from packaging materials or manufacturing processes highlights the pervasive nature of this environmental pollutant and its potential for human exposure [14,15]. Studies have reported elevated levels of phthalates in various matrices, including fatty foods and drinking water, underscoring the urgency for effective remediation strategies [16-19].

DMP specifically leaches into water sources, such as coolers and mineral water, and poses health risks even at low concentrations, with implications for DNA damage and organ irritation [23-25]. The widespread contamination of aquatic environments with DMP necessitates immediate action to mitigate its adverse effects [26]. Various advanced technologies exist for removing phthalates from contaminated sources, described in detail in section 1.2.5, including adsorption, advanced oxidation processes (AOPs), membrane filtration, biological treatments, chemical precipitation, and advanced sorption technologies [27-35]. Each method offers distinct advantages depending on the concentration and matrix of the contaminant.

Chemical oxidation has emerged as an efficient method for DMP degradation, utilizing oxidants like Fenton's reagent, ozone, and potassium permanganate, among others [30-34]. However, these methods may encounter drawbacks such as secondary pollution or inefficiencies in lower concentrations. Adsorption, on the other hand, stands out for its simplicity, cost-effectiveness, and versatility in removing PAEs like DMP from water [15,24]. Novel adsorbents, including molecularly imprinted polymers (MIPs) and surface-modified materials, enhance selectivity and efficiency but may require more complex synthesis processes [30,31].

Despite advancements, many existing methods struggle with effectively removing DMP at lower concentrations typical of real-world environmental conditions [36-42]. To address these challenges, this study focuses on developing novel polymer-metal oxide nanocomposites with amphiphilic properties tailored for efficient DMP removal. A novel oxidative polymerization method combined with a solution suspension technique at room temperature facilitates high-yield production of the PPy_ZnO nanocomposites, ensuring scalability and exceptional surface properties. The study evaluates the adsorption capacity of these nanocomposites across low (~1 ppm) and higher concentrations (>5 ppm) of DMP, aiming to bridge the gap between laboratory efficacy and practical application in environmental remediation. The adsorption mechanism is elucidated, emphasizing electrostatic attraction, hydrogen bonding, and π-π interactions as key factors contributing to the nanocomposites' effectiveness in removing DMP from aqueous solutions.

5.2. Materials and Methods

The synthesis of polymer nanocomposites mainly includes three stages: the first one is the oxidative polymerization of pyrrole monomer units into Polypyrrole (PPy); the second one is the ZnO nanoparticle synthesis; and the third stage is combining them into a PPy_ZnO composite.

5.2.1 Materials

Pyrrole (C_4H_5N) monomer (Spectrochem) stored in dark at 23 °C, Iron (III) chloride Hexahydrate ($FeCl_3 \cdot 6H_2O$ - analytical grade; Merck) used as a radical oxidant in the aqueous medium, Zinc acetate hexahydrate ($Zn(CH_3COO)_2.2H_2O$; purity 98.5%; SRL), methanol (99.9% purity; Spectrochem) and H_2O_2 (Merck) were used in this work. Double-distilled water was used for synthesis procedures.

5.2.2 Synthesis of Polypyrrole

Polymerization of pyrrole monomer was carried out in a chemical oxidative environment. About 0.2 moles of pyrrole was added dropwise to a 0.6 M aqueous solution of $FeCl_3 \cdot 6H_2O$ and ethylene glycol under constant magnetic stirring at very low speed for 30 minutes. The resultant solution was vigorously stirred for 4 hrs, leading to the formation of polypyrrole. To remove all soluble impurities, including $FeCl_3$ and $Fe(OH)_2$, the obtained black precipitate was filtered under vacuum and washed repeatedly with copious amounts of distilled water, ethanol, and ethylene glycol, respectively. The obtained PPy was dried in an oven at 60 °C. The yield of PPy with respect to monomer was found to be 85%. The higher yield can be attributed to the suitability of ethylene glycol for synthesizing cyclic polymers. The cyclisation reaction involving PEG or EG through its tosylate intermediate is well-established [29]. This cyclisation reaction improved the yield of cyclic raw products. The washing process allowed an efficient ring closure reaction, increasing PPy yield.

5.2.3 Synthesis of ZnO nanoparticles

8.5 g of zinc acetate hexahydrate (Zn $(CH_3COO)_2.2H_2O$ - 98.5% purity; SRL) is stirred for 30 minutes in double-distilled water at 30°C. The resultant white-coloured suspension is stirred continuously for 3 hours in 400 ml of methanol (99.9% purity, Spectrochem). Then, 4 ml of H_2O_2 is added dropwise to the solution, setting a white turbidity. The solution is kept at room temperature for 24 hours without any agitation. Volatile impurities are removed by drying the solution at 80 °C. The resultant white powder was then washed with double distilled water to remove acetate impurities. The residue is dried at 80 °C [4], then calcinated at 600 °C for 1 hour to remove all left-over volatile impurities present in the obtained sample.

5.2.4. Synthesis of PPy_ZnO composites.

Polypyrrole_ZnO nanocomposites were synthesized using the chemical suspension reaction method. Initially, a mixture of zinc oxide (0.05 g) dispersed in a 0.6 M aqueous solution of $FeCl_3 \cdot 6H_2O$ in distilled water was left undisturbed for 30 minutes. Subsequently, 0.2 moles of polypyrrole were gradually added to the above mixture, followed by stirring for 3 hours to obtain a PPy_ZnO composite called PPy_5% ZnO. Additional samples of PPy with varying weight percentages of ZnO (10, 15, and 20) were obtained by adding 0.1 g, 0.15 g, and 0.2 g of zinc oxide to the oxidant solution, resulting in the formation of PPy_10% ZnO, PPy_15% ZnO, and PPy_20% ZnO, respectively.

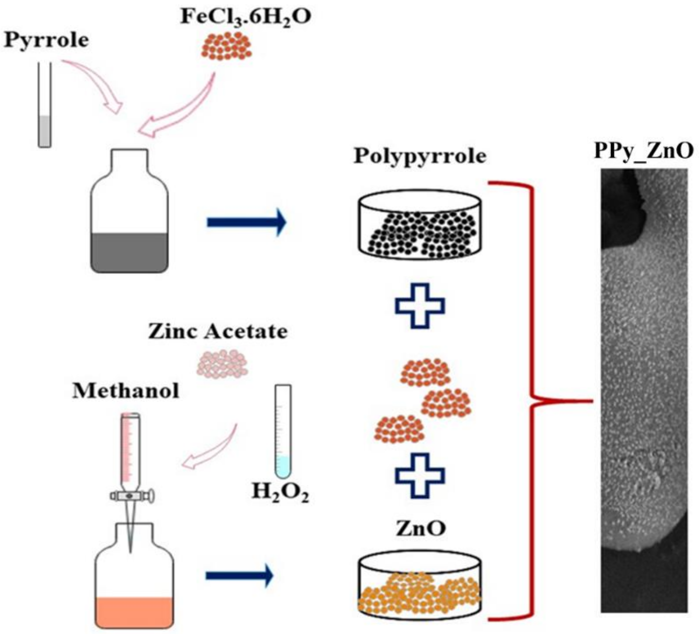

Scheme 5.1: Schematic illustration of PPy_ZnO preparation

5.2.5. Adsorption experiment

Adsorption experiments were carried out while stirring at a constant temperature (RT) and speed. The effect of adsorbent dose was studied by treating varying amounts of Polypyrrole_ZnO composite (adsorbent) with a 1 ppm solution (0.084 mL in 100 mL) of DMP (adsorbate). The corresponding adsorption efficiency was determined as

$$Adsorption\ efficiency = \left[\frac{(C_0 - C_e)}{C_0}\right] * 100$$

Where C_0 and C_e are the initial and equilibrium concentrations of the DMP in the reaction medium. The adsorption capacity at equilibrium condition (q_e) was determined as:

$$q_e = \left[\frac{(C_0 - C_e)}{m}\right] * V$$

Where m is the amount of adsorbent (g), and V is the volume of the DMP solution. The effect of other important parameters like contact time, ZnO concentration within the polypyrrole matrix, and the DMP concentration on the adsorption was performed using the optimized concentration of adsorbate - 30 mg in 100 ml of adsorbate phthalate solution. The DMP concentration was quantified every 10 minutes using a UV-Vis spectrometer (Jasco V-750).

5.3. Results and discussion

5.3.1 Crystal structure of PPy_ZnO composites.

The XRD pattern of pure PPy film shows an amorphous peak at 26.22°, which indicates a low degree of molecular ordering, as expected for a typical polymer. For PPy_ZnO nanocomposites, the reduced intensity of ZnO diffraction peaks suggests that the PPy matrix fully encapsulates the ZnO nanoparticles. It is a sign of a high degree of dispersion [43] of ZnO – a desirable feature towards adsorption capacity.

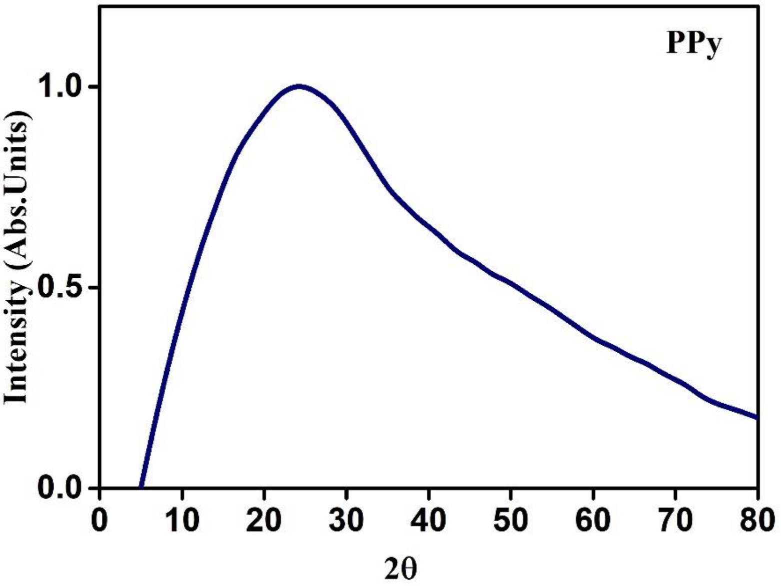
PPy
Intensity (Abs.Units)
1.0
0.5
0.0
0
10
20
30
40
50
60
70
80
2θ

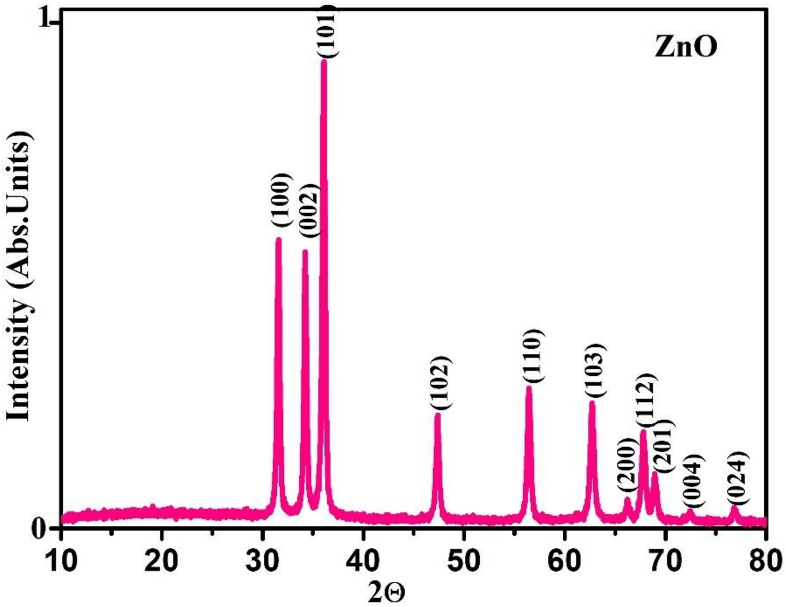
ZnO
Intensity (Abs.Units)
1
0
(100)
(002)
(101)
(102)
(110)
(103)
(200)
(112)
(201)
(004)
(024)
10
20
30
40
50
60
70
80
2Θ

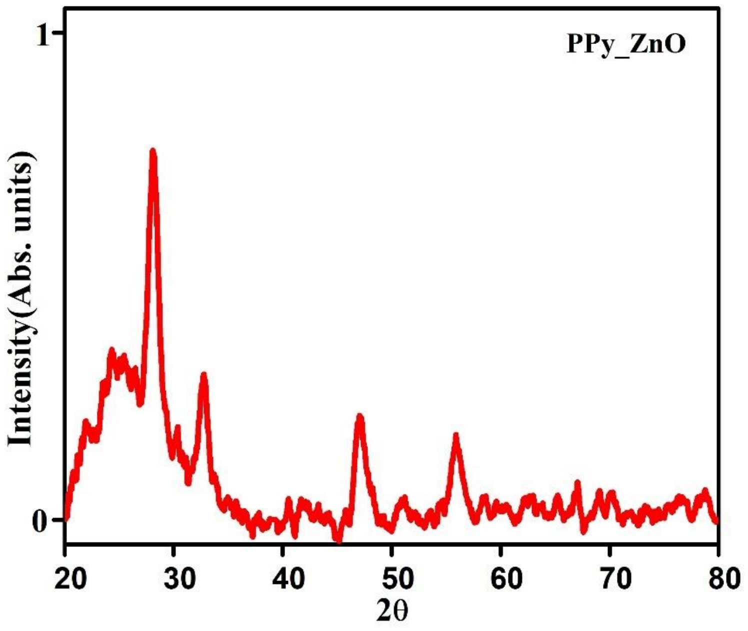

Fig 5.1. XRD pattern of synthesized PPy, ZnO, and PPy_ZnO polymer nanocomposites.

5.3.2 Morphology of PPy_ZnO composite

Fig 5.2 displays the SEM image of PPy_ZnO composites. The pure PPy and its polymer composites demonstrate a particulate structure with a reasonably even distribution. The SEM predicts a significant dependence of morphology on filler concentration. An effective ZnO nanoparticle dispersion is essential for improved polymer nanocomposite properties. The images of PPy show a uniform granular skeletal morphology. Polymer composite films are comparatively closely packed. Hence, it gives polymer-metal oxide composites with well-dispersed nanoparticles as a coating layer on the skeletal structure.

.

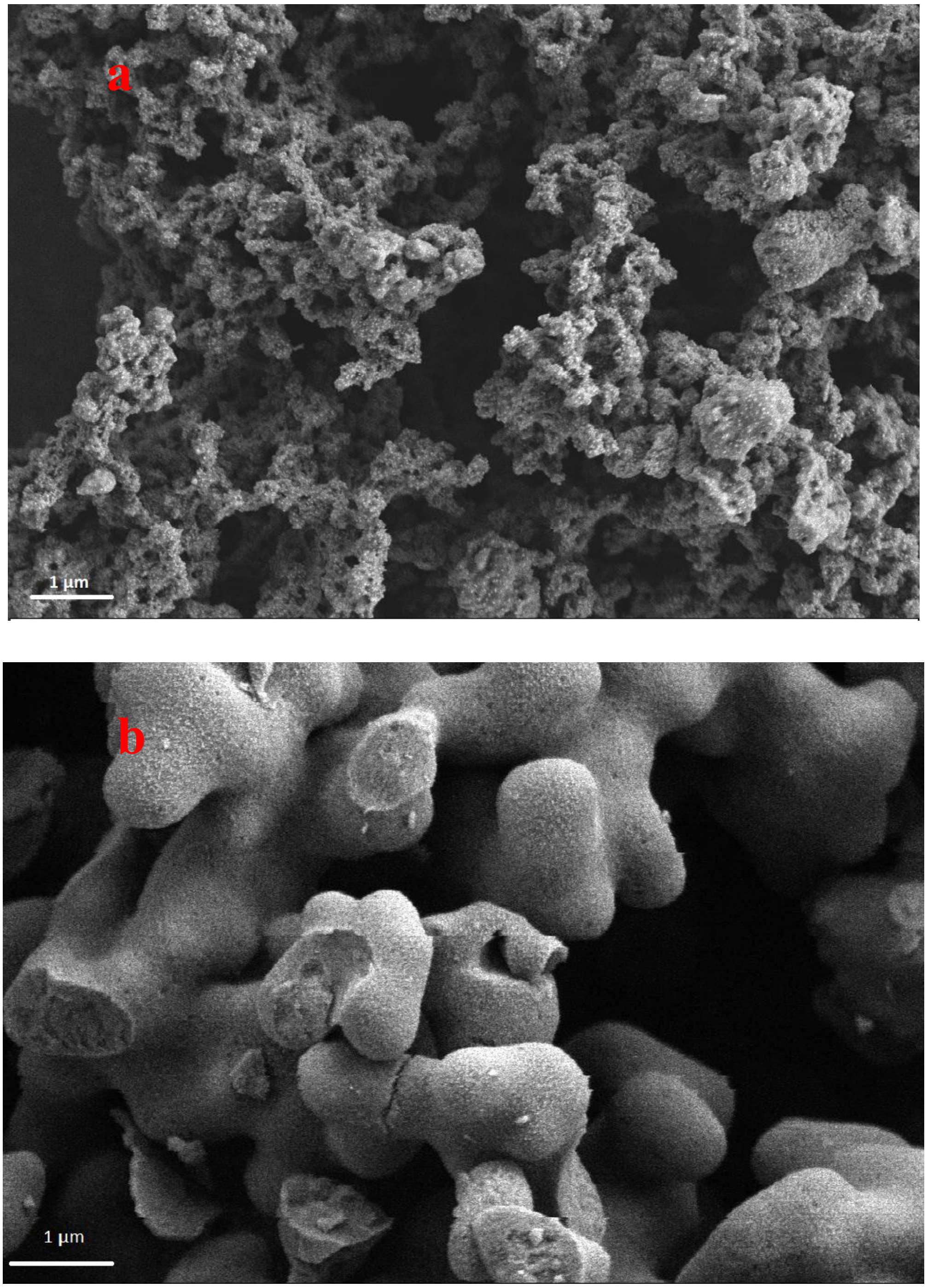

Fig 5.2. FESEM image of **(a)** synthesized Polypyrrole and **(b)** PPy_ZnO polymer nanocomposite.

5.3.3 BET Analysis

Fig. 5.3 shows the BET result obtained from sample PPy_ZnO. The nitrogen adsorption-desorption isotherms of the Polypyrrole_ZnO composite show a type IV isotherm. Also, the loop hysteresis can be identified as an H4 type, pointing to open, narrow slit pores in the micropore region. Fig. 3 demonstrates that most pores are microporous with a 5-10 nm range. Using N_2 adsorption-desorption isotherms and a BET plot, the surface area (S_{BET}) and average pore diameter (Dp) were calculated to be around 59 $m^2 g^{-1}$ and 9 nm, respectively. The slit-like pores on the sample surface can be assumed to contribute substantially to the adsorption process.

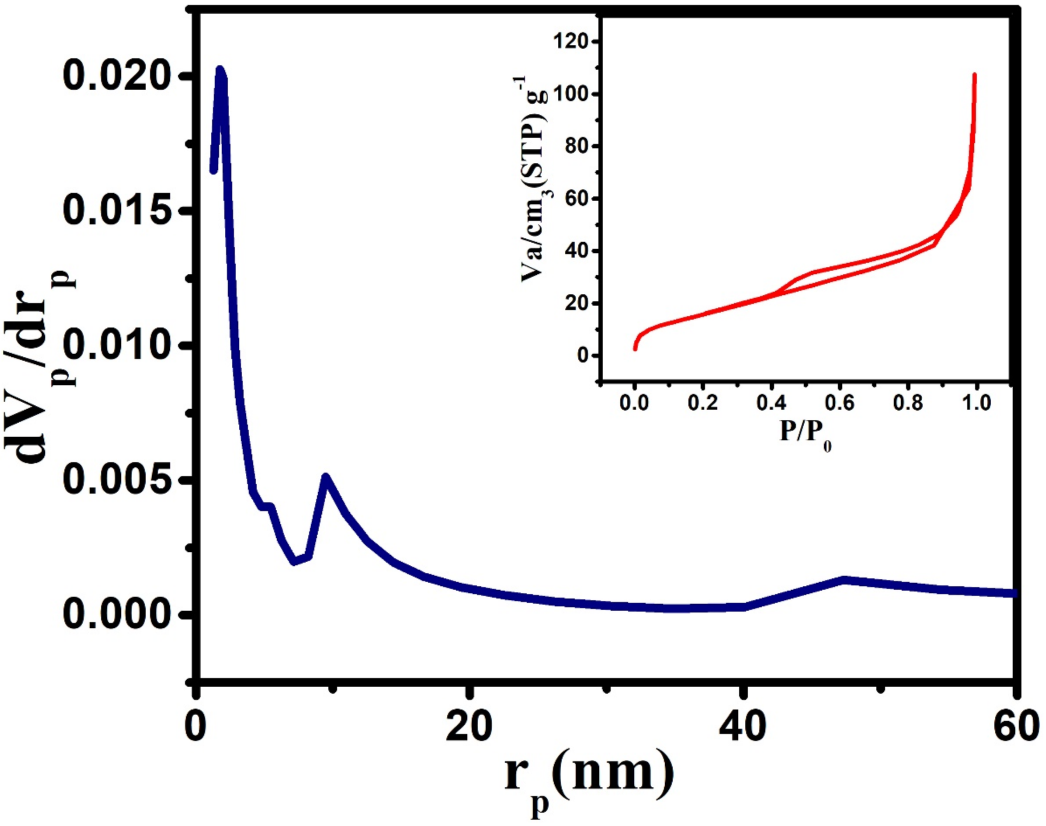

Fig. 5.3. BET adsorption and desorption isotherm and pore distribution of synthesized PPy_ZnO polymer nanocomposite.

5.3.4. Adsorption studies

As mentioned in section 5.2, all the adsorption experiments in the rest of the paper were made using 30 mg of PPy_ZnO nanocomposite in 100 mL of water-based (adsorbate) solution.

5.3.4.1. Effect of concentration of ZnO in the adsorbent

The amount of DMP adsorbed on PPy_ZnO powder was investigated. In the 1ppm DMP solution with a natural solution pH and an initial concentration of 0.1 mg L^{-1}, 0.03 g of each adsorbent was added and stirred for 1 hr. The adsorption capacity of the pure polypyrrole polymer matrix was observed to be meagre. However, as the ZnO concentration increased (0.01 to 0.05 g), the DMP sorption improved significantly, as demonstrated in Fig. 5.4. PZ1, PZ2, PZ3, PZ4, and PZ5 represent the polymer composites with various ZnO concentrations. The adsorption capacity was either maximum or found to be saturated for the batch of Polypyrrole_ZnO, which corresponds to 0.03g of ZnO. All further DMP adsorption studies are performed using an optimized PPy_ZnO (0.03g) batch.

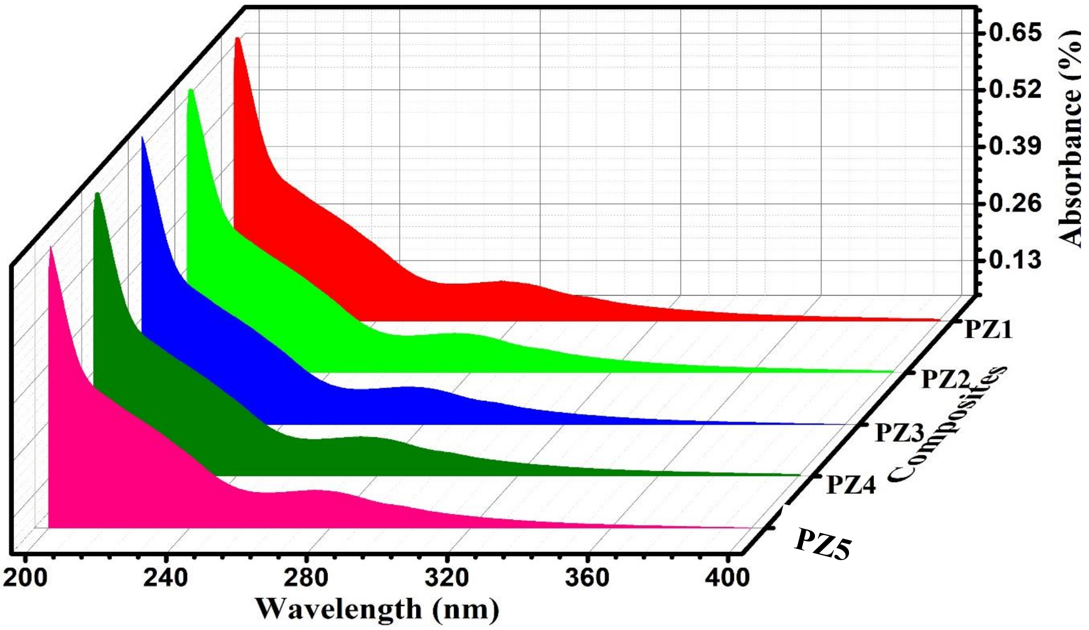

Fig 5.4: Adsorption of 1 ppm DMP solution on various PPy_ZnO composites. The area under the absorption peak is a measure of DMP present in the medium after 30 minutes.

5.3.4.2. Effect of contact time

The influence of contact time on the adsorption of DMP was studied using a 1 ppm DMP solution (0.1 mg L^{-1}) in contact with PPy_ZnO (0.03g) in the natural pH - while the solution was kept agitated throughout the experiment. Fig 5.5 shows that by increasing the contact time from 0 minutes to 10 minutes, the removal percentage increases rapidly from 0 to 98.15%. Then, it shows a very slow adsorption tendency for the remaining 50 minutes. However, the amount of DMP adsorbed increases from 95.18 to 99.19% in 60 minutes. The enhanced removal percentage in the initial stage of batch adsorption is due to the availability of increased surface area and adsorption sites. Furthermore, when the adsorption of DMP reaches a state of saturation equilibrium, no significant further removal of DMP is observed. However, an increase in the adsorbent dosage increased the presence of unsaturated adsorption sites, reducing the number of occupied adsorption sites. This leads to a decrease in the amount of DMP adsorbed. Based on the obtained results, a dosage of 0.03 g was selected as the optimal amount of adsorbent. This dosage demonstrated the highest removal percentage, and the most effective amount of DMP adsorbed within 10 minutes.

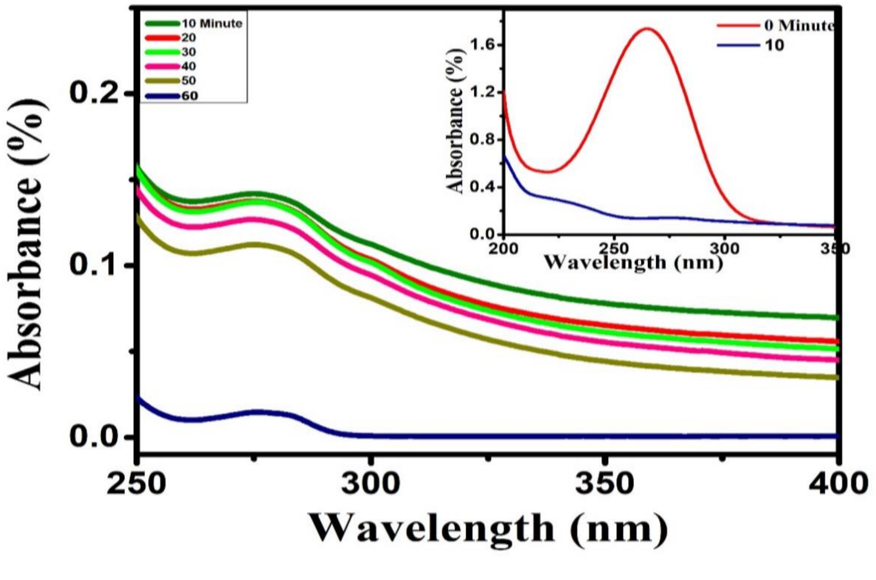

Fig.5.5: Contact time-dependent adsorption of DMP 1 ppm solution. More details of

the behaviour are shown in a figure of one of the following subsections

The adsorption capacity of the Polypyrrole_ZnO nanocomposite adsorbent in this study was compared with other adsorbents mentioned in prior research to remove Dimethyl Phthalate from aqueous solutions. A compilation of these comparisons can be found in Table 5.1. Notably, there are significant variations in the adsorption time values among different adsorbents. The adsorbent developed in this study demonstrates a higher adsorption capacity for removing Dimethyl Phthalate within a shorter time frame than certain previously developed adsorbents.

Table 5.1: Comparison of adsorption potential of various adsorbents for DMP removal from aqueous solutions. (1 ppm is equivalent to 1 mg/L)

Adsorbent	Concentration of DMP	degradation efficiency (%)	Time (min)	Ref
DMP imprinted Activated iron-doped carbon aerogel (AFeC)	50 ppm	98	150	[30]
MWCNTs	40 mg/L	70		[31]
Fe3O4/MWCNTs	40 mg/L	42.25		[31]
organo-vermiculites with imidazolium-based Gemini surfactants.		60		[32]
Fe/Al electrode pairs	100 mg/L	91.5%	60	[33]
Fe/Fe electrode pairs	100 mg/L	38%	60	[33]
Al/Al electrode pairs	100 mg/L	26.8%	60	[33]
Al/Fe electrode pairs,	100 mg/L	20.3%	60	[34]
Present Study	**1 ppm**	**91.84%**	**10**	

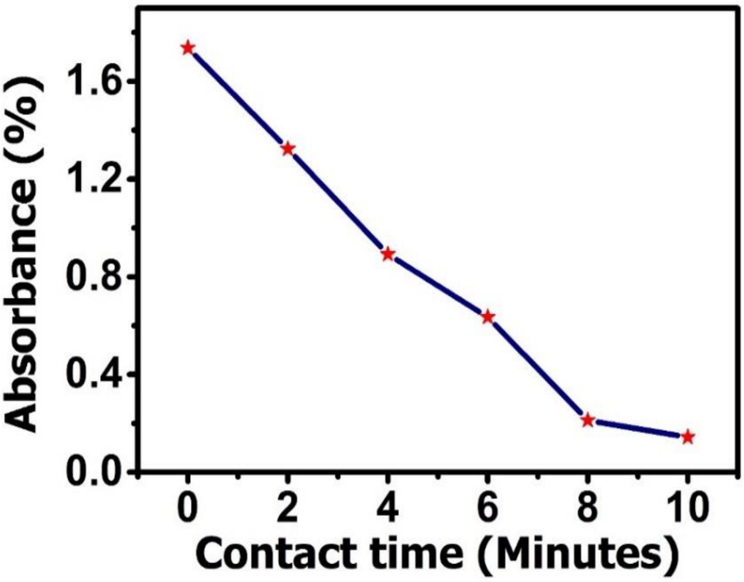

Fig 5.6: Effect of contact time on adsorption experiments.

5.3.4.3. Effect of adsorbate concentration

To display the effect of adsorbate concentration in the adsorption process, the optimum amount of adsorbent dosage of 0.03g of PPy_ZnO (0.03g) batch was added to the ppm level DMP solution maintained at pH = 7. The adsorption of dimethyl phthalate is carried out under normal room temperature by varying the concentration of DMP from 1 ppm to 5 ppm. The adsorption experiments show that polymer nanocomposites with 0.03g of ZnO show a greater adsorption tendency towards the DMP. It can adsorb 91.84% of phthalate within 10 minutes. And the removal efficiency is 99.15% for DMP (1ppm). The removal efficiency decreased with increased phthalate concentration, which is optimum for 30 mg of the adsorbent. It is shown in Fig.5.7. The removal efficiency is higher for a lower concentration of DMP solution. This indicates that PPy_ZnO composites can be considered a suitable adsorbent for the ppb level of DMP removal because the intraparticle diffusion and the presence and availability of mesopores within the sample help the fast adsorption on the sample surface. In our present study, the adsorption of the DMP molecule is affected by the concentration of adsorbate and adsorbent. Due to their favourable adsorption capacity, straightforward synthesis process, and affordability of polymer precursors, these adsorbents exhibit promise and cost-effectiveness. Therefore, they are highly recommended for removing DMP from aqueous solutions.

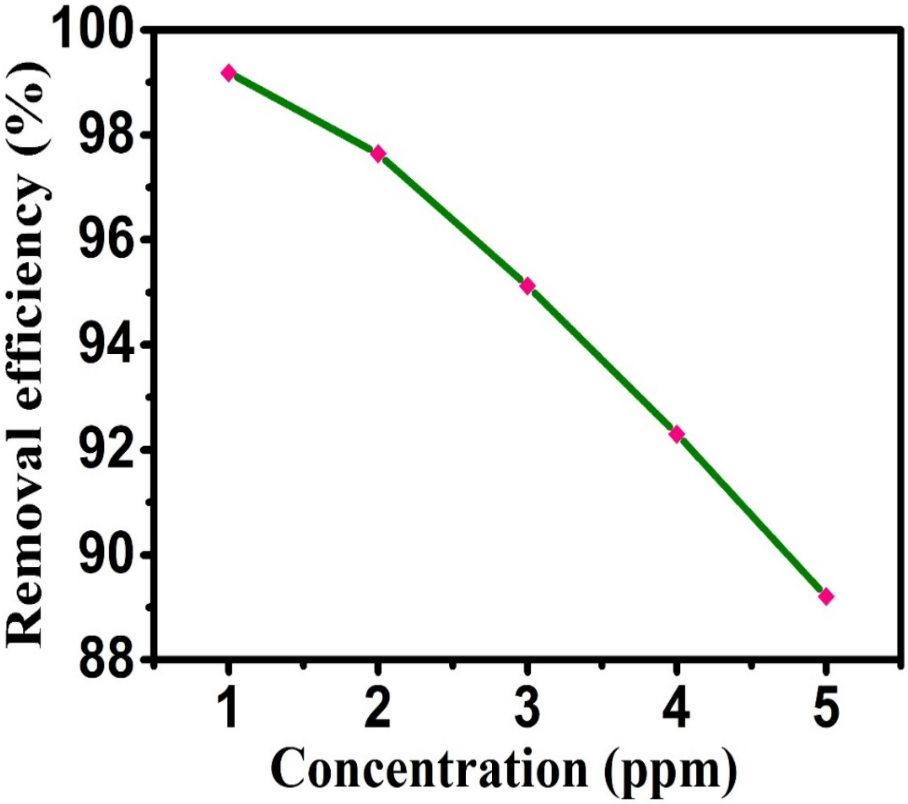

Fig 5.7: Effect of adsorbate concentration on adsorption experiments.

5.3.5 Utility of PPy_ZnO as a phthalate adsorbate

It is crucial to assess the efficiency of PPy_ZnO nanocomposites in removing DMP at both lower and higher concentrations, considering their applicability in real-world situations.

5.3.5.1 Utility at lower concentrations of DMP

The detection and removal of DMP at its lower concentrations is quite significant. As illustrated in Table 5.1, studies on detection and removal primarily focus on eliminating DMP at elevated concentrations. The current treatment method adopted for DMP removal at lower concentrations is ICPMS, but this process is highly time-consuming and not cost-effective. Large amounts of organic solvents are required for the removal process. Hence, it is more critical that DMP be found and removed when it is present in its lowest concentrations. From Fig. 5.8, it is very clear that in low concentrations, PPy_ZnO performs effectively. Within 10 minutes, it could adsorb 91.84% of phthalate. The inset of the figure 5.8 shows the variation in absorbance at smaller intervals within 0 to 12 minutes of contact between DMP and PPy-ZnO. (There is a slight difference in the shapes of the plots between the main plot and the inset plot. The difference is because of a better resolution UV-Vis spectrometer for experiments in the inset plot. However, the decline in intensity of the characteristic peak for DMP is drastically reduced in 10 minutes). The removal efficiency at 60 minutes is 99.15% for 1 ppm DMP solution.

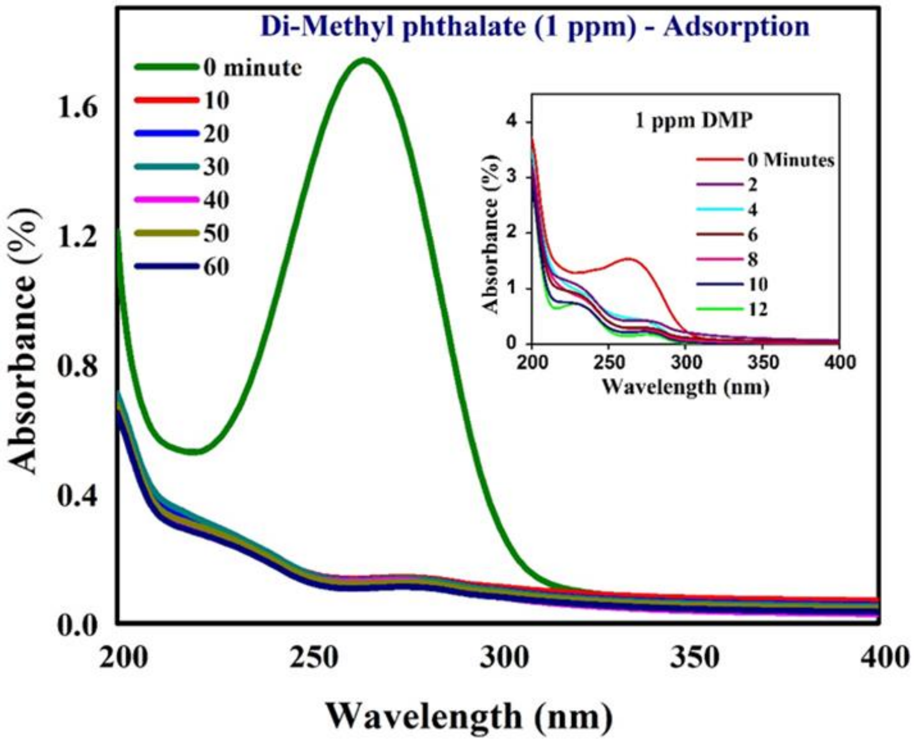

Fig. 5.8: Adsorption of DMP at lower concentration. The inset shows the variation in absorbance at smaller intervals within 0 to 12 minutes of contact between DMP and PPy-ZnO. This figure is also an extension of Figure 5.5.

5.3.5.2 Utility at higher concentrations of DMP

There is great industrial demand for the removal of DMP at higher concentrations. Organic pollution occurs when large amounts of organic compounds are introduced into the environment. This type of pollution originates from sources such as domestic sewage, industrial discharges, urban runoff, and agricultural wastewater. As a result, sewage treatment plants are often integrated with industrial operations. Among organic pollutants, plasticizers represent a significant category. The need for effective methods to remove these highly toxic plasticizers from water has garnered considerable attention. Among various water treatment methods, the use of solid adsorbents in the adsorption process has emerged as a promising and highly effective technique for treating and removing organic contaminants from wastewater. Adsorption stands out due to its simple design, low initial cost, and minimal time investment compared to other methods. The search for low-cost adsorbents with pollutant-binding capacities has intensified in recent years. Here, the attempt to adsorb higher concentrations of DMP present in the water samples is reported. From Fig. 5.9, it is very clear that within 10 minutes, 30 mg of PPy_ZnO composites can be able to adsorb 71.6% DMP at 5 ppm, 10 ppm, and 20 ppm. The relevance of the present work compared to previously reported data is tabulated in Table 5.1.

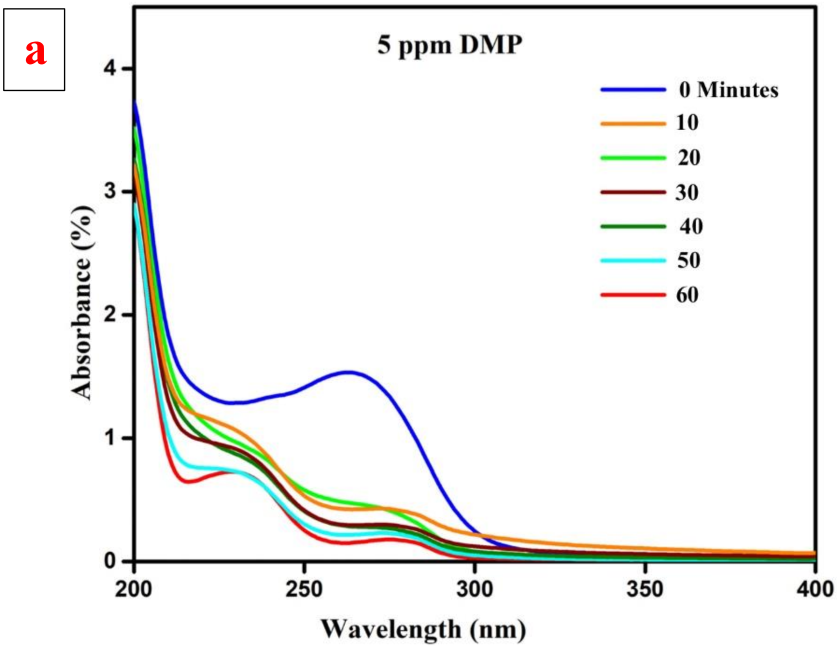
a
5 ppm DMP
0 Minutes
10
20
30
40
50
60
Absorbance (%)
4
3
2
1
0
200
250
300
350
400
Wavelength (nm)

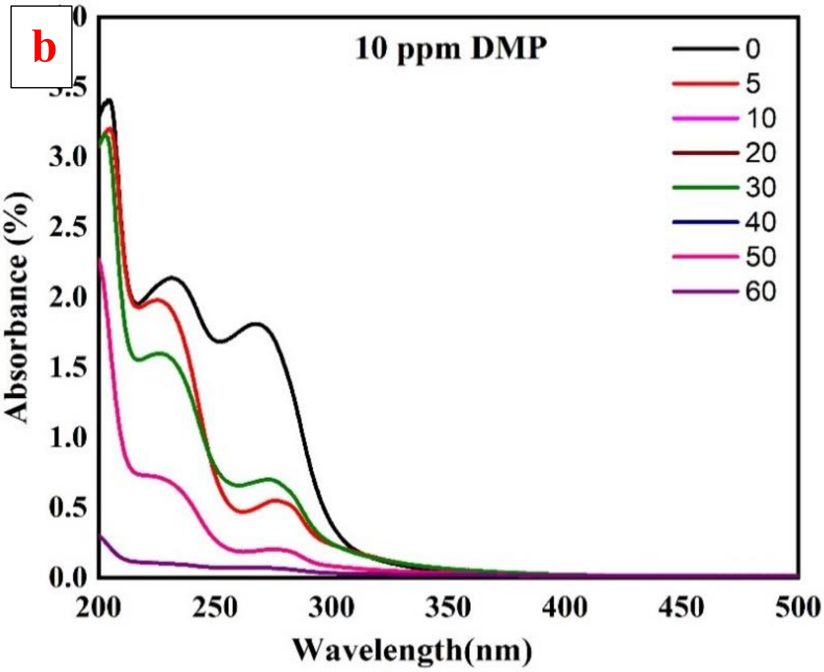
b
10 ppm DMP
0
5
10
20
30
40
50
60
Absorbance (%)
3.0
2.5
2.0
1.5
1.0
0.5
0.0
200
250
300
350
400
450
500
Wavelength(nm)

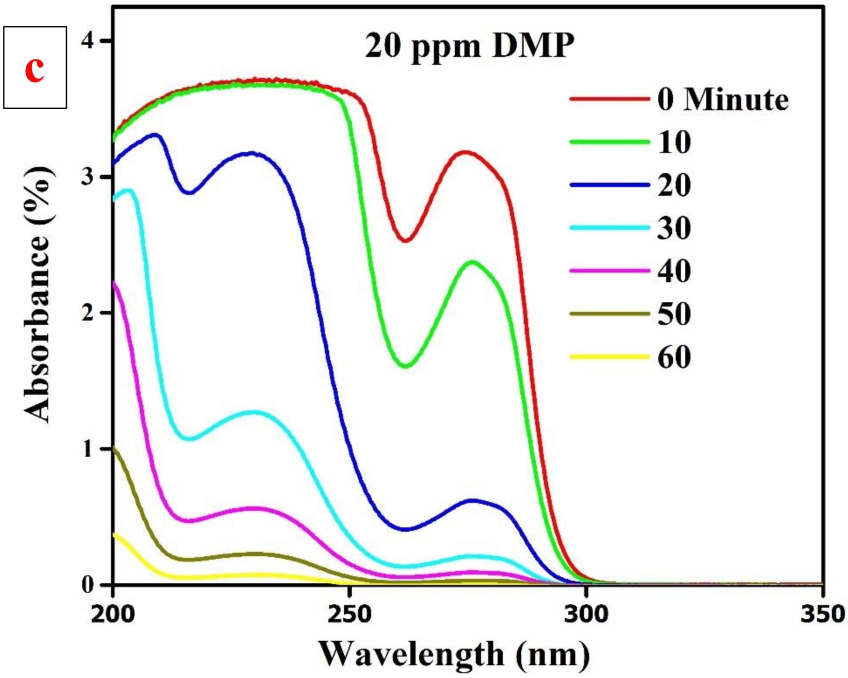

Fig. 5.9: Adsorption spectra of DMP at higher concentrations **(a)** 5 ppm, **(b)**10 ppm, and **(c)** 20 ppm respectively.

5.3.6 Adsorption mechanism

It has been reported that the adsorption of PAEs containing benzene rings in the adsorbate is facilitated by π-π interactions, which are recognized as significant mechanisms [36, 37]. Given that the PPy_ZnO nanocomposite possesses conjugated benzene rings, it is reasonable to speculate that it can form strong bonds with DMP through π-π interactions. Furthermore, previous studies have indicated that adsorbents with long-chain structures can establish hydrophobic interactions with similar functional groups present in the target contaminants [38, 39]. Additionally, hydrogen bonding may play a crucial role in the adsorption of organic compounds, particularly those containing oxygenated functional groups or carbonyl groups [40]. Wang et al. [41] have emphasized the formation of hydrogen bonds between the hydroxyl groups of the adsorbent and the carbonyl groups of DMP during the adsorption process. In the case of the PPy_ZnO nanocomposite, the surface features hydroxyl and amino groups. Therefore, it can be anticipated that three types of interactions (π-π interaction, hydrophobic interaction, and hydrogen bonding) are involved in the adsorption of DMP on the PPy_ZnO nanocomposite. PPy_ZnO consist of oxygen atoms and hexagonal conjugation rings. The presence of non-bonding electron pairs on nitrogen and oxygen atoms enables hydrogen bonding with analytes. The conjugated rings within the structure facilitate π-π interactions with the analytes. Typically, the composite is non-polar, rendering it unable to dissolve in an aqueous medium, causing it to float on the surface of solutions. This hydrophobic characteristic allows nonpolar analytes to preferentially transfer from polar aqueous media to the nonpolar extraction phase of PPy_ZnO. The HPLC chromatographs of standard DMP and extracted DMP solution with composites confirm the absence of adsorbent within the solution after filtration. In addition to that, the presence of slit-like micropores and mesopores in the adsorbent surface, as suggested by BET, can provide suitable binding sites for the DMP analyte molecules. The trapped analyte DMP molecules have strong, nonpolar interactions with the adsorbent surface. It makes the adsorption process efficient.

Based on our findings, as depicted schematically in Fig. 5.10, we can deduce that the combined effect of π-π interaction, hydrophobic interaction, and hydrogen bonds, along with the presence of slit-like mesopores on the surface of the adsorbent and the π-π interaction is the crucial mechanism for the adsorption of DMP.

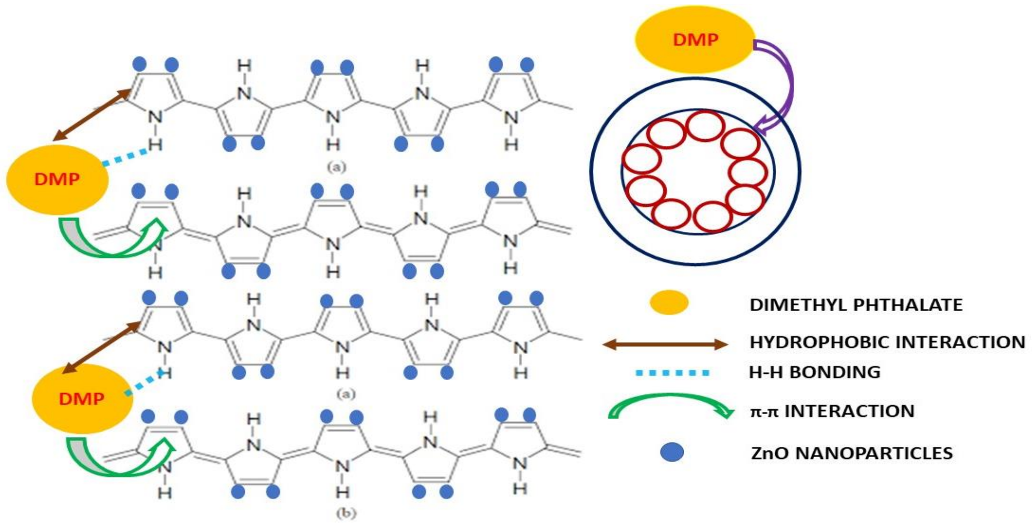

Fig. 5.10: Adsorption mechanism of DMP on PPy_ZnO nanocomposites

5.4. Conclusion

In summary, a novel, straightforward method involving oxidative polymerization and a solution suspension technique at room temperature has been developed to synthesize PPy_ZnO polymer-metal oxide nanocomposites with exceptional surface properties. The synthesis approach resulted in high-yield production of the PPy_ZnO through a cyclic chain reaction. The PPy_ZnO rapidly and efficiently eliminated DMP from high and low-concentration aqueous solutions. The removal of DMP at a lower concentration of 1 ppm, as reported here, is a remarkable upgrade compared to previous reports. The demonstration of adsorption at low concentrations of DMP is critical for the real-world adoption of any phthalate removal technique. The enhanced DMP adsorption is attributed to the synergistic effects of slit-like micropores and conjugated benzene rings in the PPy_ZnO, where DMP molecules are trapped and held primarily by electrostatic attraction, hydrogen bonding, and π-π interactions. This research underscores that engineered surface functional groups in polymer nanocomposites can be utilized to develop high-performance phthalate adsorbents, offering a promising solution for water pollution.

5.5 References

[1] Y. Guo, L. Wang, K. Kannan, Phthalates and parabens in personal care products from China: concentrations and human exposure, Arch. Environ. Con. Tox. 2014, 66 113-119.

[2] Y. Ji, F. Wang, L. Zhang, C. Shan, Z. Bai, Z. Sun, L. Liu, B. Shen, A comprehensive assessment of human exposure to phthalates from environmental media and food in Tianjin, China, J. Hazard. Mater.2014, 279,, 133-140.

[3] Y. Kang, Y.B. Man, K.C. Cheung, M.H. Wong, Risk assessment of human exposure to bioaccessible phthalate esters via indoor dust around the Pearl River Delta, Environ. Sci. Technol., 2012, 46, 8422-8430.

[4] J. Yang, R. Hauser, R.H. Goldman, Taiwan food scandal: the illegal use of phthalates as a clouding agent and their contribution to maternal exposure, Food. Chem. Toxicol. 58, 2013, 362-368.

[5] Mehrnaz Gharagozlou, Narges Elmi Fard, Mehdi Ghahari, Mohammad Tavakkoli Yaraki, Bimetal Cu/Ni-BTC@SiO2 metal-organic framework as high performance photocatalyst for degradation of azo dyes under visible light irradiation, Environmental Research, 2024, Volume 256, 119229, ISSN 0013-9351, https://doi.org/10.1016/j.envres.2024.119229.

[6] Narges Elmi Fard, Ilnaz Raeisi, Zivar Yousefipour, and Rashid Mosavin, Review of Metal Sulfide-Based MXene Nanocomposites for Environmental Applications, Gas Sensing, Energy Storage, and Photothermal Therapy, *ACS Applied Nano Materials* ,2024, *7* (6), 5698-5728, DOI: 10.1021/acsanm.3c05455.

[7] A. Saini, J.O. Okeme, E. Goosey, M.L. Diamond, Calibration of two passive air samplers for monitoring phthalates and brominated flame retardants in indoor air, Chemosphere, 2015, 137 166-173.

[8] T.M. Tran, K. Kannan, Occurrence of phthalate diesters in particulate and vapor phases in indoor air and implications for human exposure in Albany, New York, USA, Arch. Environ. Con. Tox., 2015, 68, 489-499.

[9] K.K. Selvaraj, G. Sundaramoorthy, P.K. Ravichandran, G.K. Girijan, S. Sampath, B.R. Ramaswamy, Phthalate esters in water and sediments of the Kaveri River, India: environmental levels and ecotoxicological evaluations, Environ. Geochem. Hlth. 37, 2015, 83-96.

[10] A. Musolff, S. Leschik, M. Moder, G. Strauch, F. Reinstorf, M. Schirmer, Temporal and spatial patterns of micropollutants in urban receiving waters, Environ. Pollut. 157, 2009, 3069-3077.

[11] K. Khosravi, G.W. Price, Determination of phthalates in soils and biosolids using accelerated solvent extraction coupled with SPE cleanup and GC–MS quantification, Microchem. J., 2015, 121, 205-212.

[12] Y. Guo, H. Alomirah, H.S. Cho, T.B. Minh, M.A. Mohd, H. Nakata, K. Kannan, 26 Occurrence of phthalate metabolites in human urine from several Asian countries, Environ. Sci. Technol. 2011, 45, 3138-3144.

[13] B. Wang, H. Wang, W. Zhou, Y. Chen, Y. Zhou, Q. Jiang, Urinary excretion of phthalate metabolites in school children of China: implication for cumulative risk assessment of phthalate exposure, Environ. Sci. Technol. 2015, 49, 1120-1129.

[14] Fan, J.-C., Jin, Q., He, H.-L., Ren, R., & Wang, S.-T. Detection of 20 phthalate esters in different kinds of food packaging materials by GC-MS/MS with five internal standards. Journal of AOAC International, 2019, 102(1), 255–261. https://doi.org/10.5740/jaoacint.18- 0005

[15] Brar, S. K., Verma, M., Tyagi, R. D., Valéro, J. R., & Surampalli, R. Y. Concurrent degradation of dimethyl phthalate (DMP) during production of Bacillus thuringiensis based biopesticides. *Journal of Hazardous Materials*, 2009, *171*(1–3), 1016–1023. https://doi.org/10.1016/j.jhazmat.2009.06.108

[16] Kan, H., Wang, T., Yang, Z., Wu, R., Shen, J., Qu, G., & Jia, H. (2020). High frequency discharge plasma induced plasticizer elimination in water: Removal performance and residual toxicity. *Journal of Hazardous Materials*, 2019, *383*, 121185. https://doi.org/10.1016/j.jhazmat.2019.121185

[17] Schmidt N, Castro-Jimenez J, Fauvelle V, Ourgaud M, Sempere R (2020) Occurrence of organic plastic additives in surface waters of the Rhone River (France). Environ Pollut , 2019, 257.https://doi.org/ 10.1016/j.envpol.2019.113637.

[18] Berardi C, Fibbi D, Coppini E, Renai L, Caprini C, Scordo CVA, Checchini L, Orlandini S, Bruzzoniti MC, Del Bubba M (2019) Removal efciency and mass balance of polycyclic aromatic hydrocarbons, phthalates, ethoxylated alkylphenols and alkylphenols in a mixed textile-domestic wastewater treatment plant. Sci Total Environ, 2019, 674:36–48. https://doi.org/10.1016/j.scitotenv. 2019.04.096.

[19] Le TM, Nguyen HN, Nguyen VK, Nguyen AV, Vu ND, Yen NTH, Hoang AQ, Minh TB, Kannan K, Tran TM (2021) Profles of phthalic acid esters (PAEs) in bottled water, tap water, lake water, and wastewater samples collected from Hanoi, Vietnam. Sci Total Environ 788.https://doi.org/10.1016/j.scitotenv.2021.147831.

[20] Ayamba, A. A., Ali, M., Carboo, D., & Awuku, F. J. Extraction and determination of phthalates content in polyethylene food contact materials on the Ghanaianmarket.Journal of Natural Sciences Research, 2018, 8,1–6.

[21] X. Wei, Y. Shi, Y. Fei, J. Chen, B. Lv, Y. Chen, H. Zheng, J. Shen, L. Zhu, Removal of trace phthalate esters from water by thin-film composite nanofiltration hollow fiber membranes, Chem. Eng. J.2016, 292, 382-388.

[22] A. Hassani, M. Malhotra, A.V. Karim, S. Krishnan, P.V. Nidheesh Recent progress on ultrasound-assisted electrochemical processes: A review on mechanism, reactor strategies, and applications for wastewater treatment Environ. Res.,2022, 205, Article 112463

[23] Surhio MA, Talpur FN, Nizamani SM, Talpur MK, Afridi HI, Khaskheli AA, et al. Leaching of phthalate esters from different drinking stuffs and their subsequent biodegradation. *Environ Sci Pollut Res Int*. 2017;**24**(22):18663-71.

[24] Al-Saleh I, Al-Rajudi T, Al-Qudaihi G, Manogaran P. Evaluating the potential genotoxicity of phthalates esters (PAEs) in perfumes using in vitro assays. *Environ Sci Pollut Res Int*. 2017;**24**(30):23903-14.

[25] Benson R. Hazard to the developing male reproductive system from cumulative exposure to phthalate esters--dibutyl phthalate, diisobutyl phthalate, butylbenzyl phthalate, diethylhexyl phthalate, dipentyl phthalate, and diisononyl phthalate. *Regul Toxicol Pharmacol*. 2009;**53**(2):90-101.

[26] Mathieu-Denoncourt J, Martyniuk CJ, Loughery JR, Yargeau V, de Solla SR, Langlois VS. Lethal and sublethal effects of phthalate diesters in Silurana tropicalis larvae. *Environ Toxicol Chem*. 2016;**35**(10):2511-22.

[27]. Liu Y.; Wu D.; Peng S.; Feng Y.; Liu Z. Enhanced mineralization of dimethyl phthalate by heterogeneous ozonation over nanostructured Cu-Fe-O surfaces: Synergistic effect and radical chain reactions. Sep. Purif. Technol. 2019, 209, 588–597. 10.1016/j.seppur.2018.07.016.

[28] Wang G.; Chen Q.; Liu Y.; Ma D.; Xin Y.; Ma X.; Zhang X. In situ synthesis of graphene/WO_3 co-decorated TiO_2 nanotube array photoelectrodes with enhanced photocatalytic activity and degradation mechanism for dimethyl phthalate. Chem. Eng. 2017, J. 2018, 337, 322–332. 10.1016/j.cej.2017.12.058.

[29] Ku Y.; Shiu S.; Wu H. Decomposition of dimethyl phthalate in aqueous solution by UV-LED/TiO_2 process under periodic illumination. J. Photochem. Photobiol., A 2017, 332, 299–305. 10.1016/j.jphotochem.2016.09.011

[30] Zhao H.; Wang Q.; Chen Y.; Tian Q.; Zhao G. Efficient removal of dimethyl phthalate with activated iron-doped carbon aerogel through an integrated adsorption and electro-Fenton oxidation process. Carbon 2017, 124, 111–122. 10.1016/j.carbon.2017.08.034.

[31] Wang Z.; Deng D.; Yang L. Degradation of dimethyl phthalate in solutions and soil slurries by persulfate at ambient temperature. J. Hazard. Mater. 2014, 271, 202–209. 10.1016/j.jhazmat.2014.02.027.

[32] Fard, N.E., Fazaeli, R., Yousefi, M. *et al.* Oxidative Desulfurization of Dibenzothiophene Using M/TiO_2/MWW (M = Cu, Ag, and Au) Composite. *Russ. J. Phys. Chem.* 95 (Suppl 1), S23–S32 (2021). https://doi.org/10.1134/S0036024421140065.

[33] Vandani, S., Kalaee, M., Saravani, M.G. *et al.* Preparation of Magnetic Fe_3O_4/MoO_3/MCM-22 Photocatalyst and Its Study on Metronidazole Adsorption, Degradation, and Process Optimization. *Russ. J. Phys. Chem.2023,* **97**, 618–632. https://doi.org/10.1134/S003602442304026X

[34] Pasdar, H., Elmi Fard, N. & Rezvani, M. Fabrication of MoS_2/Bi_2S_3 heterostructure for photocatalytic degradation of Metronidazole and Cefalexin and antibacterial applications under NIR light: experimental and theoretical approach. *Appl. Phys. A, 2023,* **129**, 380. https://doi.org/10.1007/s00339-023-06663-5.

[35] Brar, S. K., Verma, M., Tyagi, R. D., Valéro, J. R., & Surampalli, R. Y. (2009). Concurrent degradation of dimethyl phthalate (DMP) during production of Bacillus thuringiensis based biopesticides. *Journal of Hazardous Materials*, 2009, *171*(1–3),

1016–1. https://doi.org/10.1016/j.jhazmat.2009.06.108

[36] Claas H. Hö velmann, Sebastian Gooßen, and Jü rgen Allgaier: Scale-Up Procedure for the Efficient Synthesis of Highly Pure Cyclic Poly(ethylene glycol). *Macromolecules* 2017, 50, 11, 4169–4179.

[37] Brar, S. K., Verma, M., Tyagi, R. D., Valéro, J. R., & Surampalli, R. Y. (2009). Concurrent degradation of dimethyl phthalate (DMP) during production of Bacillus thuringiensis based biopesticides. *Journal of Hazardous Materials*, 2023, *171*(1–3), 1016–1023. https://doi.org/10.1016/j.jhazmat.2009.06.108.

[38] Y. Xiang, M. Gao, F. Ding, and T. Shen, "The efficient removal of dimethyl phthalate by three organo-vermiculites with imidazolium-based gemini surfactants in aqueous media," *Colloids and Surfaces A: Physicochemical and Engineering Aspects*, vol. 580, Nov. 2019, doi: 10.1016/j.colsurfa.2019.123726.

[39] K. Y. Huang, W. L. Chou, C. T. Wang, Y. C. Chang, and C. M. Shu, "Electrochemically assisted coagulation for the adsorptive removal of dimethyl phthalate from aqueous solutions using iron hydroxides," *J Taiwan Inst Chem Eng*, vol. 50, pp. 236–241, May 2015, doi: 10.1016/j.jtice.2014.12.028.

[40] H. Zhao, Q. Wang, Y. Chen, Q. Tian, and G. Zhao, "Efficient removal of dimethyl phthalate with activated iron-doped carbon aerogel through an integrated adsorption and electro-Fenton oxidation process," *Carbon, 2017, N Y,* vol. 124, pp. 111–122, Nov. 2017, doi: 10.1016/j.carbon.2017.08.034.

[41] Ozay Y, Canli O, Unal BO, Keskinler B, Dizge N (2021) Investigation of plasticizer production industry wastewater treatability using pressure-driven membrane process. Water Supply 21:1994–2007. https://doi.org/10.2166/ws.2020.268.

[42] S. Zhuang, X. Zhu, and J. Wang, "Adsorptive removal of plasticizer (dimethyl phthalate) and antibiotic (sulfamethazine) from municipal wastewater by magnetic carbon nanotubes," *Journal of Molecular Liquids*, vol. 319, Dec. 2020, doi: 10.1016/j.molliq.2020.114267.

[43] Islam, Md. K., & Sharif, A. (2015). Nanocharacterization of interface between natural fiber and polymer matrix: an overview. *Composite Interfaces*, *23*(2), 2016,105–123. https://doi.org/10.1080/09276440.2016.1103082.

CHAPTER 6

Extremely low-frequency plasmonic state achieved in AC-ZnO polymer composite for tuned negative permittivity applications.

Contents

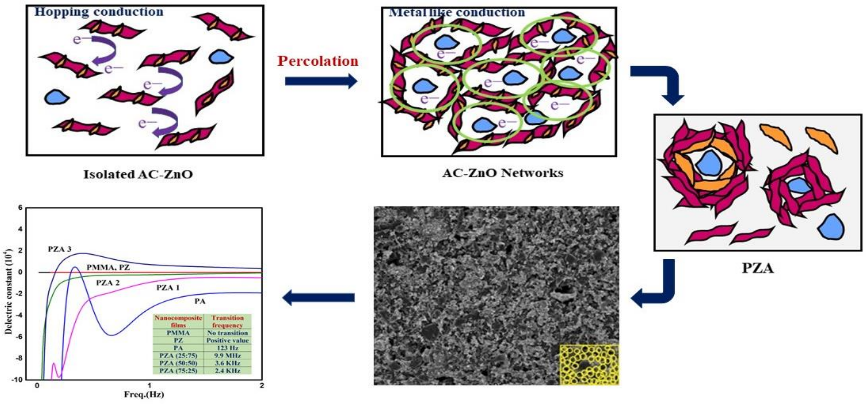

Nanocomposite films	Transition frequency
PMMA	No transition
PZ	Positive value
PA	123 Hz
PZA (25:75)	9.9 MHz
PZA (50:50)	3.6 KHz
PZA (75:25)	2.4 KHz

Abstract: *Flexible composites with negative permittivity behaviour have generated a lot of attention due to their potential applications in the electromagnetic field and novel capacitance. This work aimed to design and explore surface microstructure-induced negative permittivity flexible composites for their metamaterial properties. The composites were synthesised using Poly (methyl methacrylate) or PMMA, Activated Carbon (AC), and Zinc Oxide (ZnO) through an in-situ polymerisation process. The composite was designed to acquire negative permittivity in the extremely low-frequency regime by increasing the AC and ZnO filling content. The microstructure formation, real permittivity, and ac conductivity of the composites were investigated, and it was observed that the negative permittivity and its magnitude could be controlled by changing the amount of the filler, AC_ ZnO. Flexible composites with suitable permittivity values for ELF applications can create heavy industrial demand. The objectives and ethos behind the research are highlighted as an important part of this chapter.*

6.1 Introduction

Metamaterials have drawn attention due to their unique and extraordinary physical properties, such as negative refractive index values, permittivity, and permeability. Properties make metamaterials suitable for a wide range of novel applications that are difficult to realise with natural materials [1]. Materials exhibiting negative permittivity have gotten an enormous interest because of their possible usage in antennas [3, 4], electromagnetic invisibility [5-7], novel capacitors with extraordinary negative capacitance [8, 9], field transistors with negative capacitance [2-13], etc. Earlier in chapter 1, in sections 1.3.1 to 1.3.3, we provided a general introduction to metamaterials, the theory behind metamaterials and the characteristics of metamaterials. In section 1.3.4, we have drawn attention to a class of metamaterials characterised by their negative permittivity.

Literature reports compounds with negative permittivity at various frequency ranges, from X-ray to radio waves, as shown in Fig 6.1. For example, Ni/Al_2O_3 material systems offer a negative permittivity window at 10 MHz to 530 MHz [14], C/Si_3N_4 systems at 10 MHz to 1 GHz [15], and Ni/PVDF metasystems at 100 Hz to 100 kHz [16], respectively.

Based on the literature, the reported results show no significant advancement in metamaterials suitable for extra low frequency (ELF) regime applications. In the present study, we focus on ELF metasystems (101 to 10-2 electromagnetic waves belonging to the Extremely low frequency (ELF) regime, considered the lowest frequency waves regularly utilised for wireless transmission and communication. Their capability to cover the fundamental requirements with less transmitted power and penetrate deeply into the conducting (electrical) material makes them crucial in various applications. The critical application belongs to the communication channels connected with submerged submarines [17]. One of the potential applications of metamaterials below 10 Hz is in the development of antennas and other components for communication in underground environments where traditional radio waves cannot penetrate. Metamaterials could be used to develop low-frequency antennas that are more efficient and compact than conventional antennas. Another great application is the requirement of sensors for geophysical exploration. Low-frequency electromagnetic waves can detect underground mineral deposits and other geological features. In addition, low-frequency electromagnetic waves can penetrate the body, making them useful for imaging and therapy of internal organs. Metamaterials could be used to develop more effective devices for manipulating these waves, allowing for improved imaging and medical therapy. Since transmitting regulated electromagnetic power at such long wavelengths can be challenging, there is a high demand for ELF field materials.

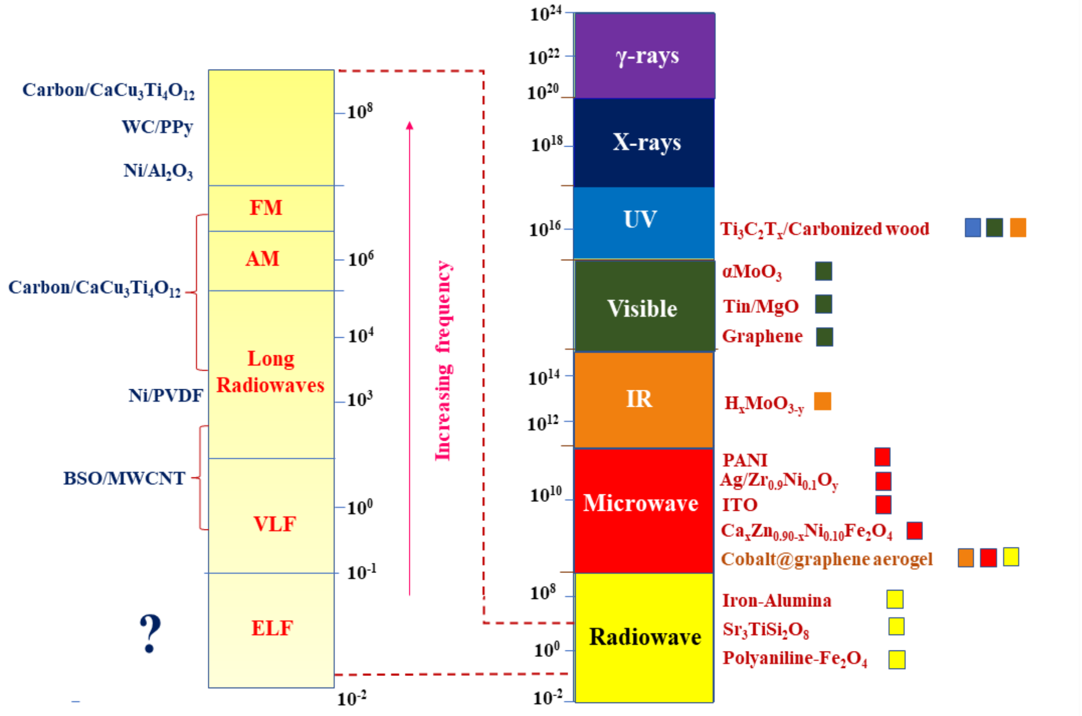

Fig 6.1. Electromagnetic spectra with reported metamaterials.

Metallic fillers like Cu, Fe, Ag, or Ni and carbon materials were often used to make meta-composites. These materials were used as the conducting functional fillers in insulating matrixes. Negatively valued parameters like permittivity, refractive index, or permeability of a metamaterial correspond to the tuning based on the chemical composition and microstructure formation of the composite [18-20]. Negative permittivity could also be observed in meta-composites composed of metallic or amorphous alloys (e.g., $Fe_{50}Ni_{50}$, FeNiMo, or $Fe_{78}Si_9B_{13}$) [21]. However, the application of metal-based meta composites is limited by the excessive power dissipation in composites and electromagnetic interference (EMI) to neighbouring metal electronics [22,23]. To overcome these limitations, meta composites containing non-metallic conductive functional phases known as "MAX" phases are in demand.

Designing of micro capacitors for ELF Regime:

(i) Structure-defining microstructure: Microstructure creation on regular, patterned void structures provides a possible foundation for metamaterial composites. In this context, polymers are apt candidates because of their flexibility. In this work, a non-conducting polymer, PMMA, is chosen.

(ii) Availability of delocalised electrons: The likelihood of exhibiting a negative dielectric constant increase with the number of delocalised electrons. In addition, entities with many free electrons have a high chance of getting arranged around the attractive ends (Voids). For negative permittivity, activated carbon provides an abundance of delocalised electrons.

(iii) Metallic filler: Filler acts as a conducting pathway for every meta composite. For this purpose, we selected ZnO in this study.

Thus, designing a flexible ternary meta-composite made of zinc oxide and activated carbon embedded in a PMMA polymer matrix is intended to create a new paradigm for microstructures with tunable and ELF regime-negative properties.

We tried to design an extremely low-frequency negative permittivity metamaterial with a structure-defining polymer matrix and a 3D conducting network generated from the fillers. The microstructure formed from this will create densely packed, single tiny micro-capacitor units. Here, the weight percentage of activated carbon and metal oxide nanoparticles provides a tunable negative permittivity in the extra low-frequency regime. Hence, radio wave applications can be extended up to a large wavelength with less dielectric loss.

This work reports a flexible polymer material designed to behave as a metamaterial at extra low-frequency radio waves. The PMMA_AC_ZnO nanocomposites were synthesised by the low-temperature in situ polymerisation process. The composition and microstructure of the PMMA_AC_ZnO nanocomposites were characterised. The dielectric property studies were carried out by Broadband Dielectric Spectroscopy. The observed plasma-type epsilon negative state in AC_ZnO networks is attributed to the extremely low-frequency radio wave. The plasmonic state with negative permittivity is explained using the appropriate model.

6.2. Materials and Methods

The synthesis of ternary meta-composite PZA mainly includes two stages: the ZnO nanoparticle is synthesised in the first stage; in the second stage, the polymer composite is synthesised in situ via the polymerisation reaction of PMMA, Activated Carbon, and the ZnO

6.2.1 Synthesis of ZnO nanoparticles:

8.5 g of zinc acetate hexahydrate (Zn $(CH3COO)_2.2H_2O$ - 98.5% purity; SRL) was stirred for 30 minutes in double-distilled water at 30 °C. The resultant white-coloured suspension was stirred continuously for 3 hours in 400 ml of methanol (99.9% purity, Spectrochem). Then 4 ml of H_2O_2 was added dropwise to the solution, which resulted in white turbidity. The solution was kept at room temperature for 24 hours without any agitation. Impurities were removed by drying the solution at 80 °C for 6 hours. The resultant white powder was washed with double distilled water to remove acetate impurities. The obtained residue is dried at 80 °C and then calcinated at 600 °C for 1 hour to remove all the left-over volatile contaminants in the sample.

6.2.2. Synthesis of PMMA_AC_ZnO Nanocomposite.

PMMA polymer matrix films were fabricated using commercially available transparent PMMA crystals. To synthesise the polymer nanocomposite film, 1 g of PMMA crystals were dissolved in 50 ml of acetone solvent and stirred for 90 minutes at 60 ° C. Once the solution turned white and viscous, varying proportions of activated carbon and ZnO nanoparticles were gradually added while stirring. The stirring continued for 1 hour, resulting in a viscous black gel. When poured into a petri dish, it formed a self-standing polymer composite film with a thickness of 0.1 mm (100 microns). The entire synthesis procedure is shown in Scheme 6.1.

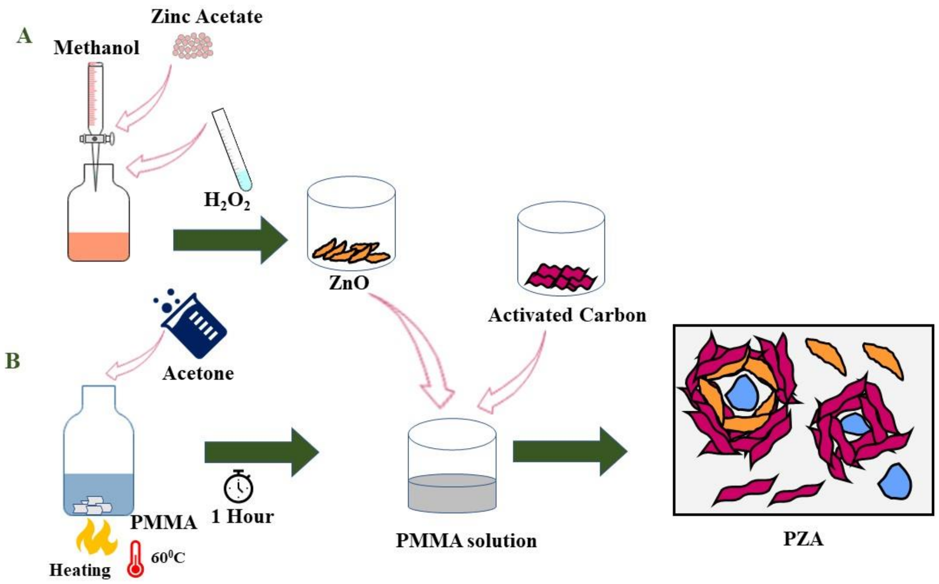

Scheme 6.1: Schematic illustration of PZA preparation

Table 6.1 Summary of composition of the prepared films.

Nanocomposite films	**Relative composition (PMMA: ZnO: AC)**
PMMA	**1.00: 0.00: 0.00**
PZA (25:75)	**1.00: 0.25: 0.75**
PZA (50:50)	**1.00: 0.50: 0.50**
PZA (75:25)	**1.00: 0.75: 0.25**

6.2.3 Characterisations and Measurements

At room temperature, the phase composition of the synthesised PMMA_AC_ZnO composites was determined using X-ray diffraction (XRD, RIGAKU, MiniFlex) with Cu-K radiation (λ = 1.5406). The microstructures and morphologies of materials were examined using field emission scanning electron microscopy (FE-SEM; Carl Zeiss; Gemini SEM 300). Surface topological studies were carried out by Atomic Force Microscope (Bruker, Multimode 8). The conductivity, permittivity, and capacitance of PMMA_AC_ZnO composites were measured with Broadband Dielectric Spectroscopy (Novocontrol Technologies, BDS 50) in the frequency range 10^{-2} Hz-10^{7}Hz.

6.3. Results and discussion:

6.3.1 Phase composition

The structure and formation of synthesised PMMA_ZnO_AC were confirmed using X-ray diffraction patterns, as shown in Fig. 6.2**.** The pure ZnO particles exhibit a polycrystalline wurtzite structure. The crystalline size of the prepared samples is (determined using the Scherrer equation) 18.02±0.02 nm. The calculated lattice parameters are a = 3.26 Å and c = 5.23 Å, consistent with JCPDS Data File no 5-0664. When these nanoparticles are incorporated in the PMMA polymer matrix, a broad and relatively weak reflection is found at $2\theta = 15.67^{o}$, further confirming the presence of PMMA chains in the polymer-metal oxide nanocomposites. The intensity of the characteristic peaks of ZnO increases as the filler loading increases, but the intensity of the diffraction peaks of PMMA decreases.

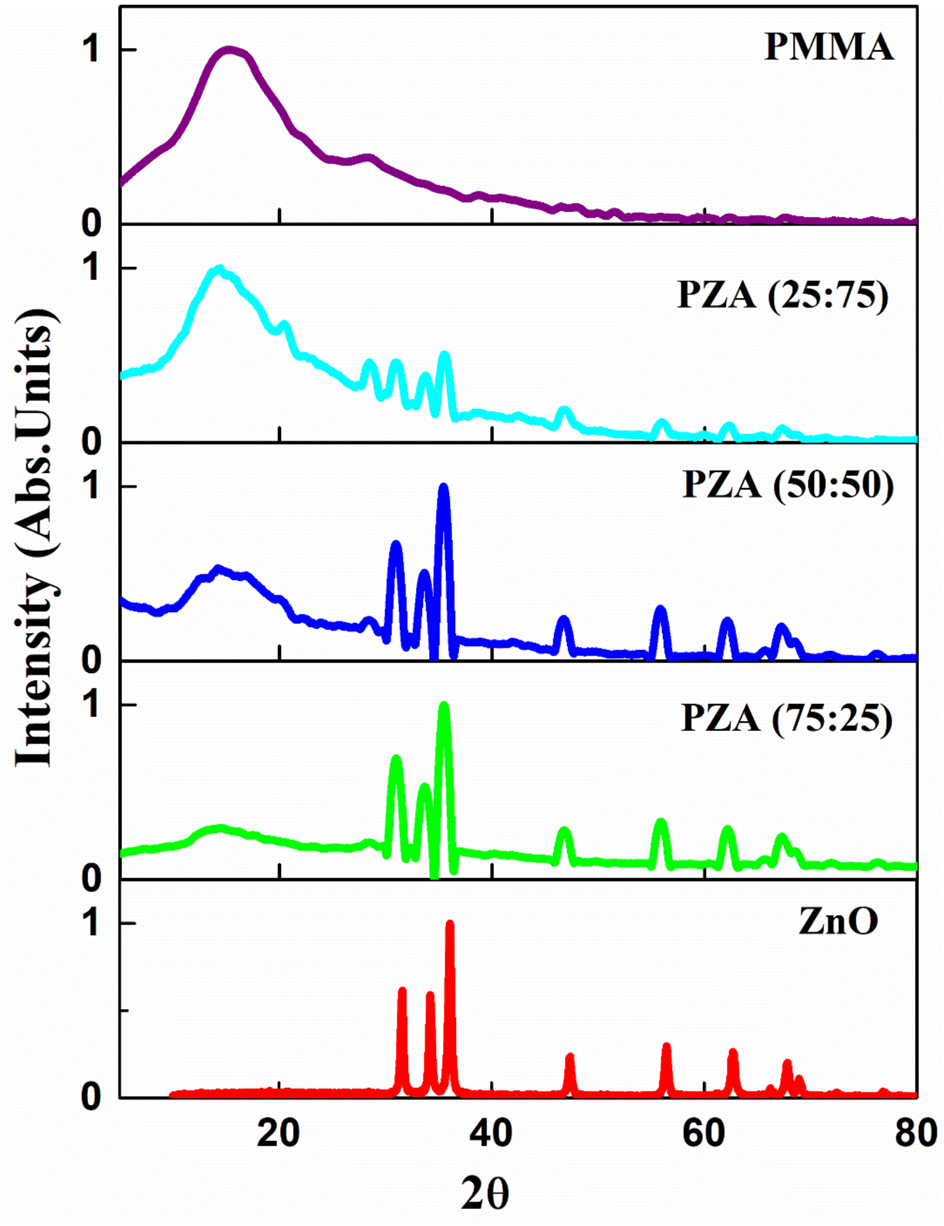

Fig 6.2. XRD pattern of the synthesised PMMA, ZnO, and PZA polymer nanocomposites, consistent with JCPDS Data File no 5-0664

6.3.2 Formation of tiny capacitors- Morphological investigation:

The surface morphologies of AC_ZnO_PMMA nanocomposites with increasing AC-ZnO concentration are shown in Fig 6.3. The neat, plane PMMA sheets show void-like structures throughout the film. During the incorporation of ZnO nanoparticles, they show a tendency to fall inside the void structures. While incorporating AC nanoparticles, they tend to occupy the edges of voids. Fig. 6.3d, with the yellow circled region, demonstrates the formation of the interconnected AC_ZnO networks around the voids that are complimented by the active carbon present in the matrix. This formation leads to the development of tiny capacitors at the attractive ends of the PMMA matrix. PMMA_AC units are weakly coupled with one another at lower concentrations of activated carbon and subsequently form three-dimensional PMMA_AC networks adorned with ZnO by raising the AC_ZnO content. As can be noticed, the PMMA voids have developed well, and the AC_ZnO units are densely inserted in PMMA voids. The distribution of AC_ZnO clusters is unsystematic and isolated at the edges of polymer voids with a low AC_ZnO content. As the AC_ZnO concentration increases, the AC_ZnO clusters are partly coupled to create three-dimensional (3D) AC-ZnO networks. A schematic representation of the microstructural evolution of AC_ZnO_PMMA nanocomposites is shown in Fig. 6.4. According to the percolation hypothesis, the microstructural development of AC_ZnO_PMMA nanocomposites strongly tends to be associated with their electrical and dielectric characteristics, which will be discussed later.

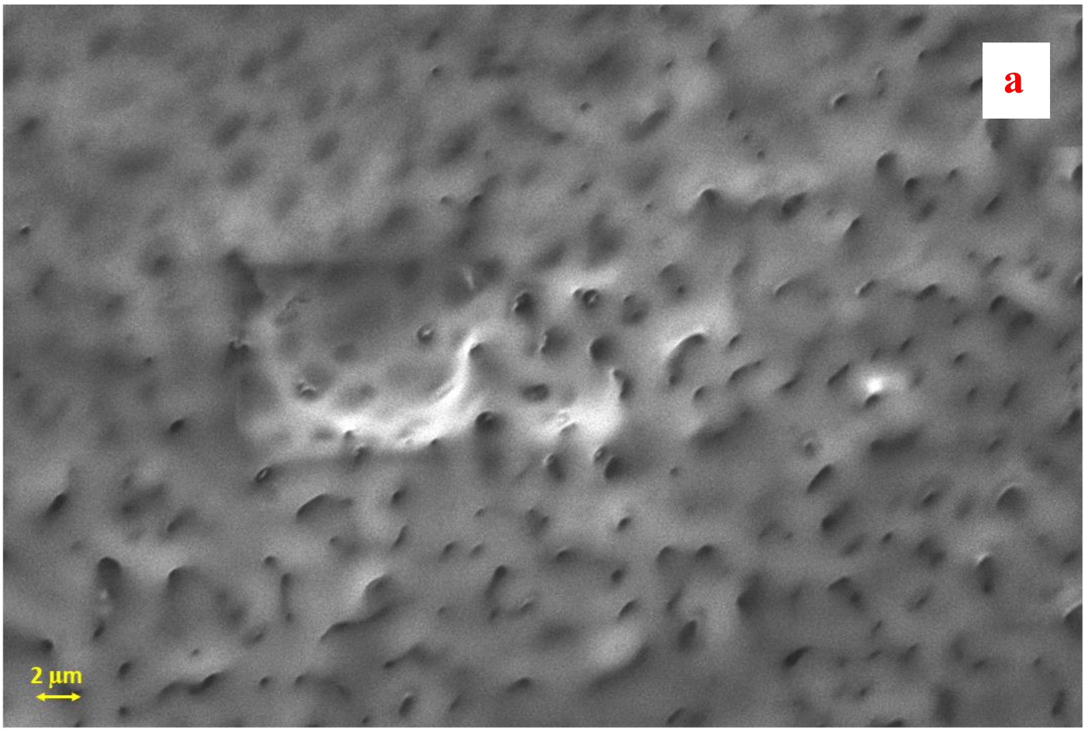

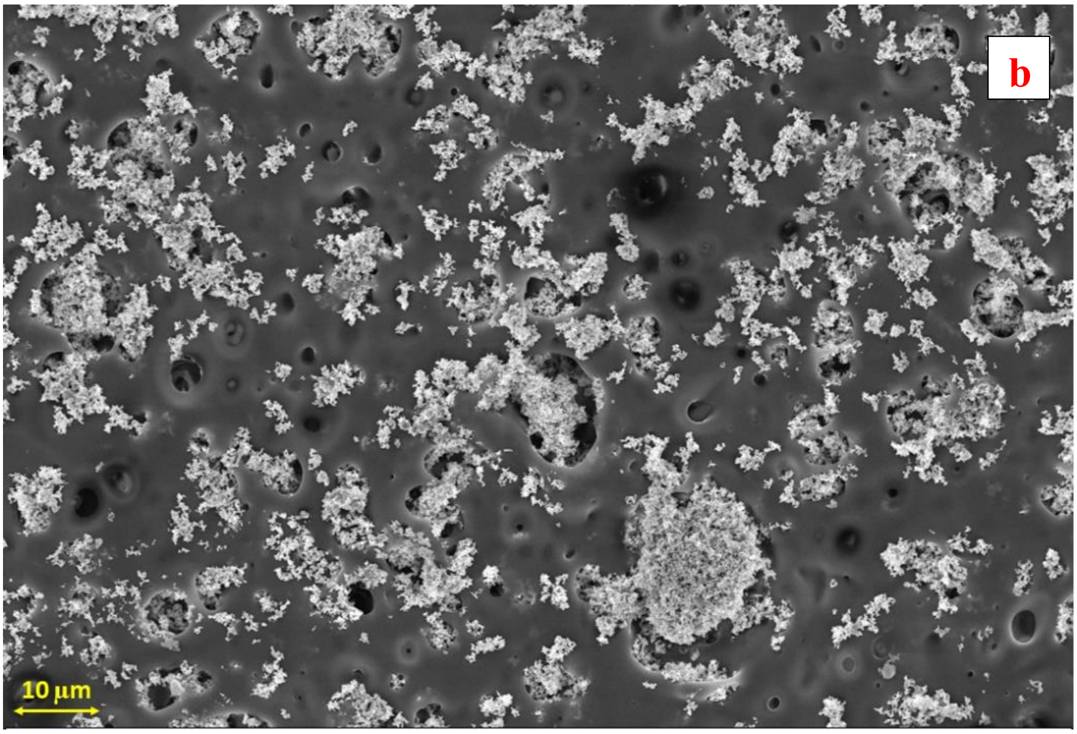
b
10 μm

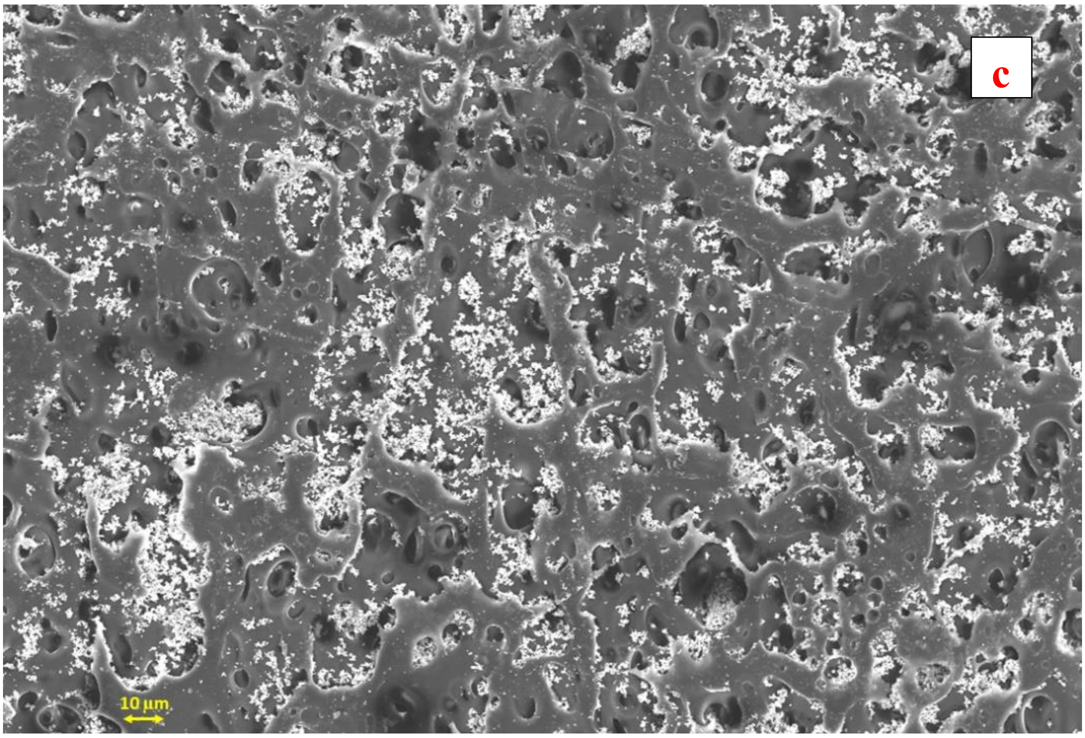
c
10 μm

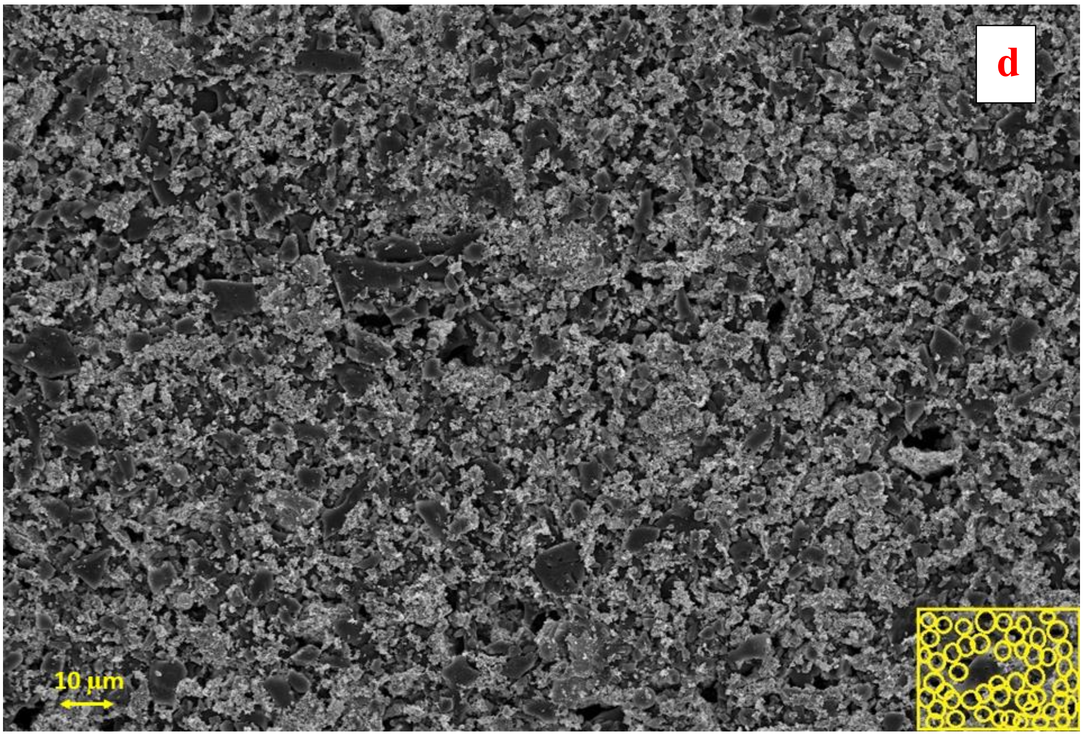

Fig. 6.3. SEM images of PMMA_ZnO_AC composites with **(a)** Pure PMMA, **(b)** PMMA_ZnO Composite, **(c)** PMMA_AC composite, **(d)** PMMA_AC_ZnO composite with interconnected conducting networks,

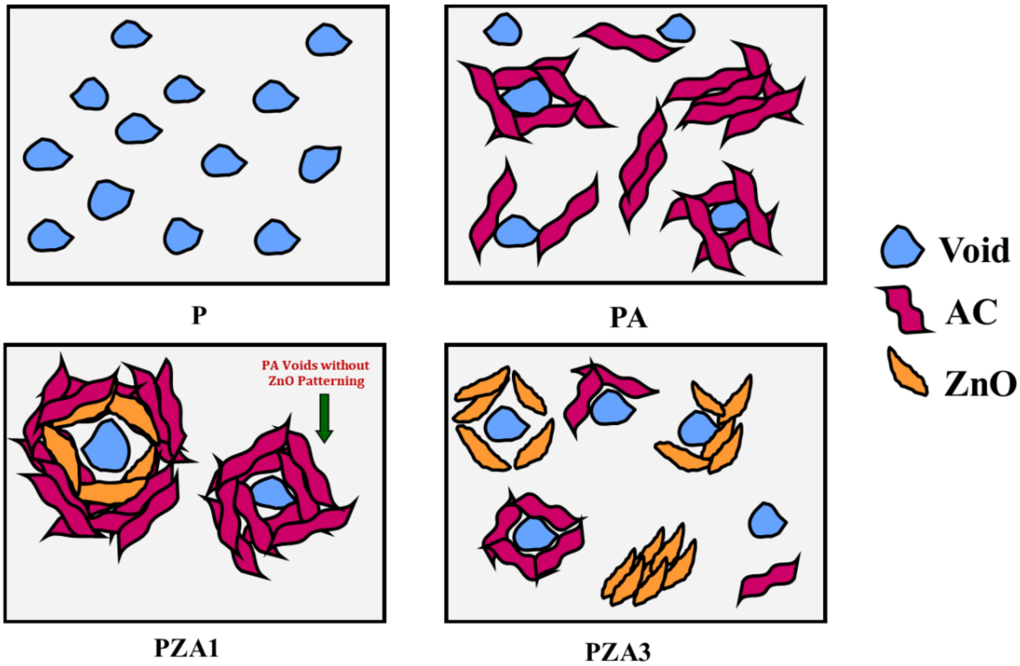

Fig.6.4. Schematic representation of the microstructural evolution of AC_ZnO_PMMA nanocomposites with (P) pure PMMA films with voids, (PA) Activated carbon decorated at the edges of voids, (PZA1) ZnO deposition complimented by AC_PMMA voids.

6.3.3 Conductivity and negative permittivity behaviour

The frequency dispersions associated with ac conductivity for AC_ZnO nanocomposites at (10^{-2} Hz to 10^{7} Hz) are shown in Fig. 6.5. Pure PMMA film exhibits nearly zero conductivity, which implies the non-conducting nature of voids. With the incorporation of ZnO nanoparticles, there is no significant improvement in conductivity, while with the addition of activated carbon, surprisingly, the conductivity values become substantial. The availability of free electrons makes it possible. In the case of PZA (25:75), it shows a rapid increase in conductivity due to the evolution of well-distinguished conductive 3D networks throughout the sample. As mentioned in the previous section, as the concentration of ZnO increases, the chances of ZnO agglomeration and the tendency for void filling by ZnO increase; this makes the composite less conducting. The ac conductivity (σ_{ac}) of composites shows a rising trend at low AC_ZnO content, suggesting a transition from hopping to metallic conduction behaviour, as schematically shown in Fig 6.7.

The dependence of conductivity on microstructural evolution can be explained based on the classical percolation theory. According to classical percolation theory for metamaterials, a significant impact of percolation on the conductivity is associated with the 3D conducting networks organised by the inextricable link between neighbouring conductive phases, which has a substantial effect on the electrical properties of compounds [24,25]. Since all the observations are collected at the same ambient temperature, just the geometrical and physical connection between the conducting fillers is considered [26, 27]. Before the percolation threshold, the internetwork of neighbouring fillers in composites is relatively weak; hence, the conductivity is not remarkable due to the reduced contribution from the hopping mechanism. While increasing the filler content, most of the conduction electrons are unbounded and significantly contribute to the conductivity through the metallic conduction mechanism. In the case of the composite containing 25% ZnO and 75% activated carbon content, the clusters establish direct contact with each other, allowing electrons to be lifted by metallic conduction as free-moving electrons [28], hence the conductivity.

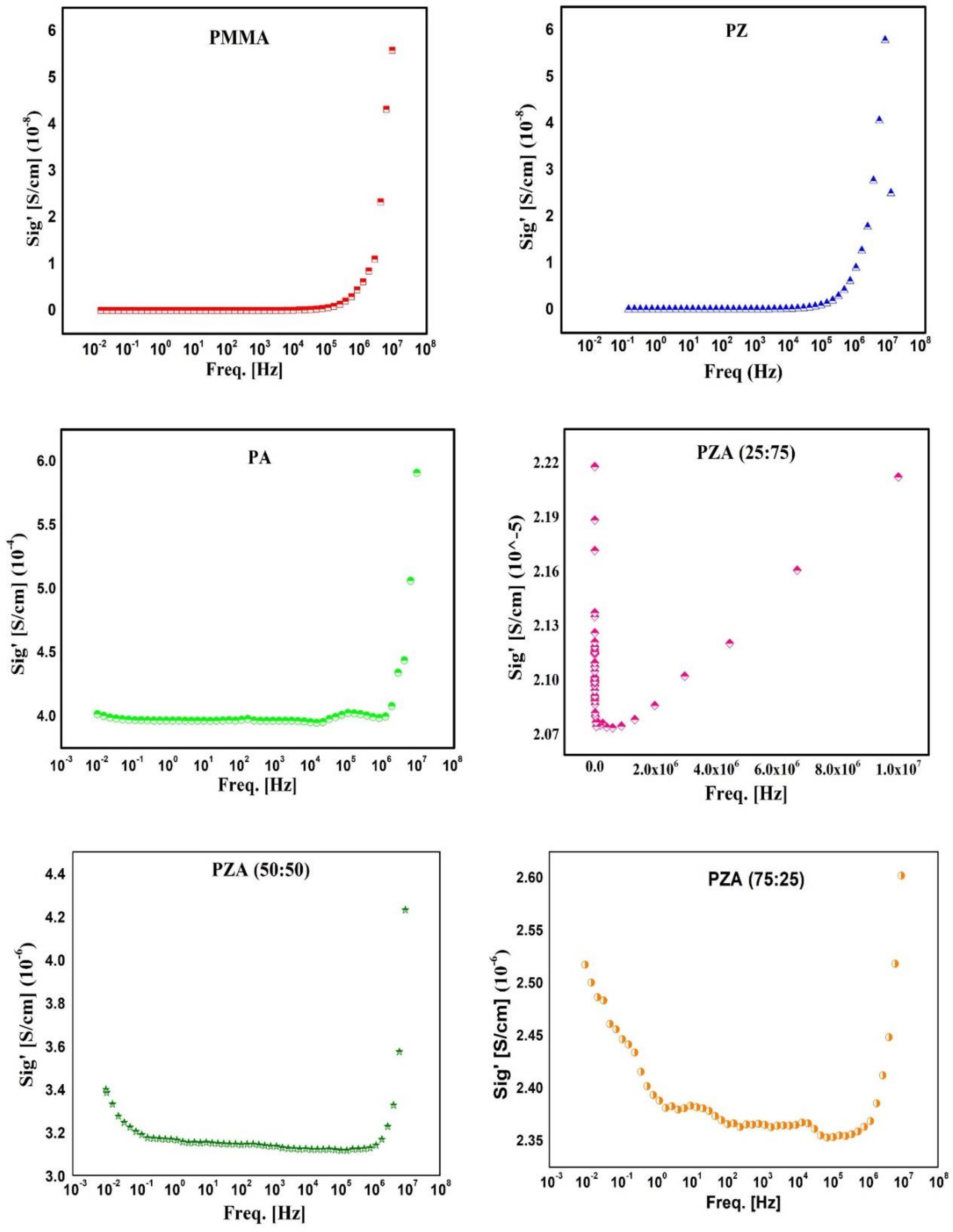

Fig. 6.5. Frequency spectra of conductivity for the **(a)** PMMA, **(b)** PMMA_ZnO Composite, **(c)** PMMA_AC composite, **(d)** PMMA_ZnO_AC (25:75), **(e)**PMMA_ZnO_AC (50:50), and **(f)** PMMA_ZnO_AC (75:25) composites

Fig. 6.6 depicts the frequency-dependence of real permittivity for percolated PMMA_ZnO_AC composites. Interestingly, the sign of real permittivity switches to negative at a lower frequency regime when filler content reaches 25% of ZnO and 75% of activated carbon. The plasma-like negative permittivity is achieved when the filler content is sufficiently high. The permittivity value decreases drastically with an increase in external frequency, exposing the plasmonic state at low radio frequency [25].

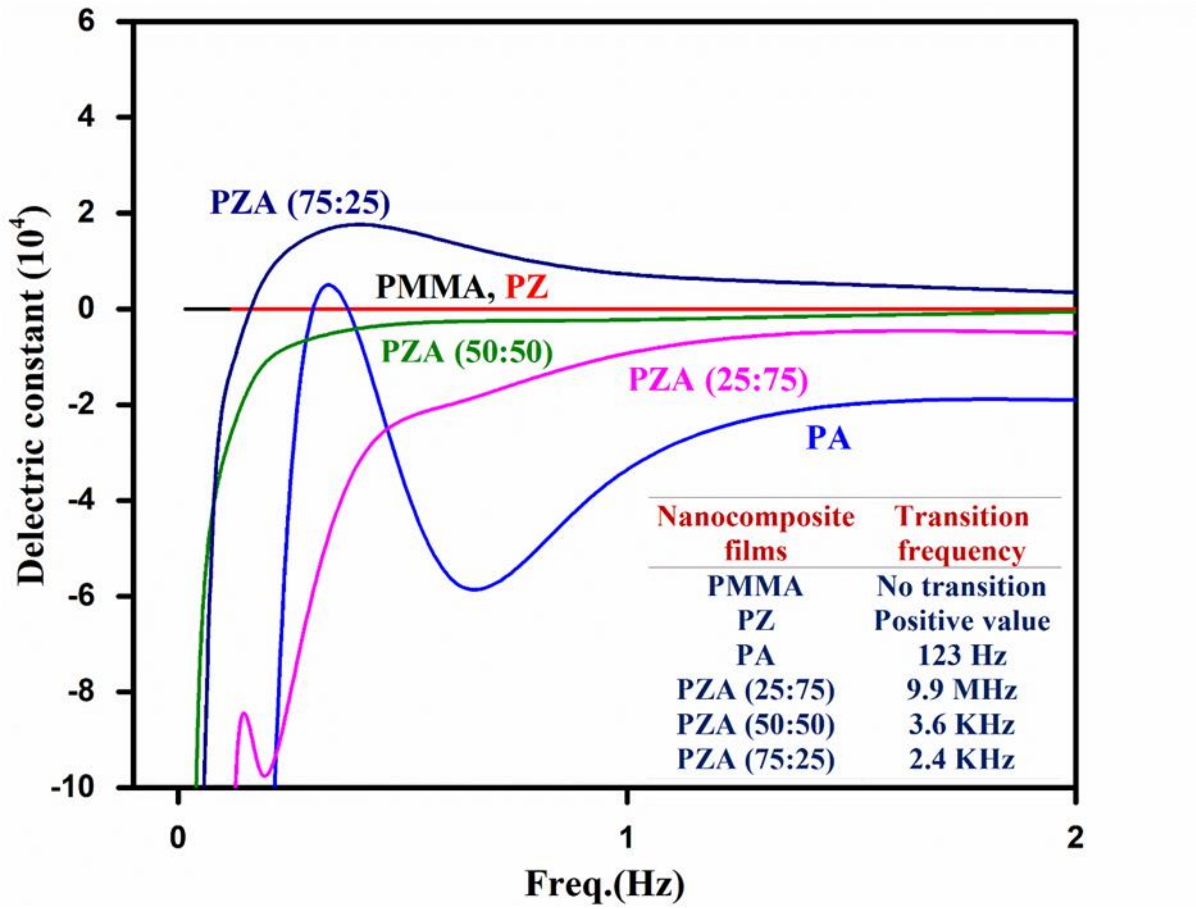

Nanocomposite films	Transition frequency
PMMA	No transition
PZ	Positive value
PA	123 Hz
PZA (25:75)	9.9 MHz
PZA (50:50)	3.6 KHz
PZA (75:25)	2.4 KHz

Fig. 6.6. Frequency spectra of permittivity for the PMMA and PZA composites.

6.3.4 Micocapacitor formation and percolation of charge carriers.

The SEM image Fig. 6.3d suggests the formation of micro capacitors. The interconnected micro capacitors must be the main reason behind the enhanced negative permittivity shown by the composite PZA (25:75). Now, we must unravel the formation mechanism of interconnected conductive networks. The hopping can be considered a mechanism to achieve charge transfer between the isolated micro capacitors. But at a particular threshold composition, the micro capacitors get interconnected and form a conductive network with each other through a mechanism similar to that in metals. Based on the observed density of micro capacitors in PZA, we can suggest that PZA belongs within the regime of classical percolation theory.

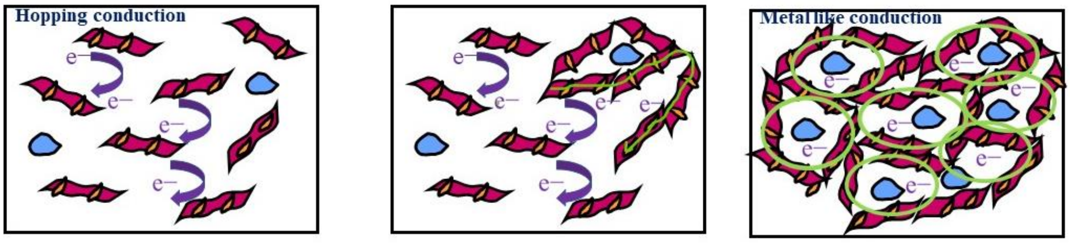

Isolated AC-ZnO

Interconnected AC-ZnO

AC-ZnO Networks

Fig. 6.7. Schematic representation of conduction mechanisms.

The preceding studies and discussions reveal that localised and delocalised electrons coexist within the composites, resulting in distinct behaviours to the applied external electric field. The negative permittivity observed in composites underneath the percolation threshold is attributed to the formation of densely packed micro capacitors and the interfacial polarisation of electrons [27]. Noticeably, the sign of permittivity changes from positive to negative at a lower frequency regime when filler content reaches 25% of ZnO and 75% of activated carbon. The lowest conductivity value is necessary for metal-based composites to achieve a low-frequency plasmonic state.[28], When filler content is high enough, a plasma-like negative permittivity is developed. After that, the permittivity value rapidly decreases with increasing external frequency, which results in the development of a plasmonic state in the regime of extremely low radio frequency.

The behaviour is theoretically related to the collective oscillation of delocalised electrons. The permittivity can analyse the collective oscillation and plasma frequency state. ε'_r can be analysed by the Drude model [29,30]:

$$m\frac{d^2x}{dt^2} + m\gamma\frac{dx}{dt} = q\varepsilon_0\cos(\omega t + \varphi) \quad (1)$$

$$\varepsilon'_r(\omega) = 1 - \omega^2{}_p / (\omega^2 + \omega^2{}_t) \ (2)$$

When, $\omega_p > \omega \quad \varepsilon_r < 0$

$\omega_p < \omega \quad \varepsilon_r > 0$

where ω_p is angular plasma frequency, ω_τ is the damping parameter, e is the electron charge, and n_{eff} and m_{eff} are the average concentration and effective mass of delocalised electrons, respectively [25]. The accumulation of AC_ZnO clusters just above the percolation threshold (PZA 25:75) and the development of microstructure with 3D conducting networks can be observed. The 3D conducting network contains significant amounts of delocalised electrons. Under an applied external electric field, plasma oscillation generates at a specific applied external frequency, and the transition of permittivity value occurs from positive to negative [32]. This permittivity transition can be described entirely by the combination of the Drude model and Lorentz model of free electron theory, which can be represented as follows by equation (3):

$$\varepsilon_r = 1 + \frac{{\omega_p}^2({\omega_0}^2 - \omega^2)}{({\omega_0}^2 - \omega^2) + \omega^2{\gamma_L}^2} + \frac{K{\omega_p}^2}{\omega^2 + {\gamma_D}^2} \qquad (3)$$

As seen in **Fig. 6.6**, the pure PMMA self-standing films exhibit near-to-zero permittivity for the entire frequency range. During the addition of zinc oxide nanoparticles, ε'_r again becomes slightly positive throughout the range. The isolated dispersion of AC_ZnO's or AC alone in the PMMA matrix leads to electrical dipole resonance within the composites. As the content of ACs increases, it shows a tendency to occupy the walls of the voids created by PMMA. This, in turn, increases the density of micro-capacitors within the material, increasing the sample's actual permittivity. It means by tuning the weight percentages of AC and ZnO, we can tune the transition region from positive to negative permittivity.

There are two types of resonance mechanisms: (i). electrical dipole resonance generated from isolated AC_ZnO clusters, and (ii). low-frequency electron plasma oscillation resonance in interconnected AC_ZnO networks. The slight dip in frequency responses is associated with dielectric polarisation transitions- which is observed in other high-frequency materials, also PVA-CB systems (MHz), Ag/$Zr_{0.9}Ni_{0.1}O_y$ (microwave), and Polyaniline- Fe_3O_4 (Radio wave). According to the Drude and Lorentz free electron model, the free electron concentration can be considerably correlated to the negative permittivity. In the case of AC_ZnO cluster-based meta composites belonging to the percolation region, negative permittivity property arises from the combinational effect of interfacial polarisation, electrical dipole resonance, and extremely low-frequency plasmonic state. Furthermore, when the amount of AC increased, the effective electron concentration increased, resulting in more conductive channels and an increase in negative permittivity's real value. Hence the percolative conducting 3D networks are formed in 25 and 75 wt. % ternary composites, which means there seem to be a lot of relaxed free electrons. Thus, the epsilon-negative characteristic in composites is governed by the low-frequency plasmonic state of unpaired electrons.[40]. As external field frequency rises, plasma-type ε -negative spectra exhibit a rising trend, which indicates that the ε -negative is weaker the closer external field frequency is near plasma oscillation frequency. Thus, the combined contribution of dipole-type, plasma-type, and inter-facial type polarisation mechanisms might open a beneficial and significant path to extremely low-frequency negative permittivity [31-39].

The combination of the Lorentz and Drude models matches the experimental data of real permittivity to understand the underlying mechanism of ε-negative property better. The Lorentz model explains the dielectric response at a higher frequency range. In contrast, at a low-frequency regime, the combination of the Drude model and theory of plasma oscillation explains the negative permittivity behaviour. The solid lines representing the fitting curves shown in Fig. 6.8 agree with the measuring outcomes of ε'_r, which indicates that the combination of the Drude model, Lorentz model, and theory of plasma oscillation could explain the negative permittivity behaviour. The fitted results for the composites are shown in Fig. 6.8**.**

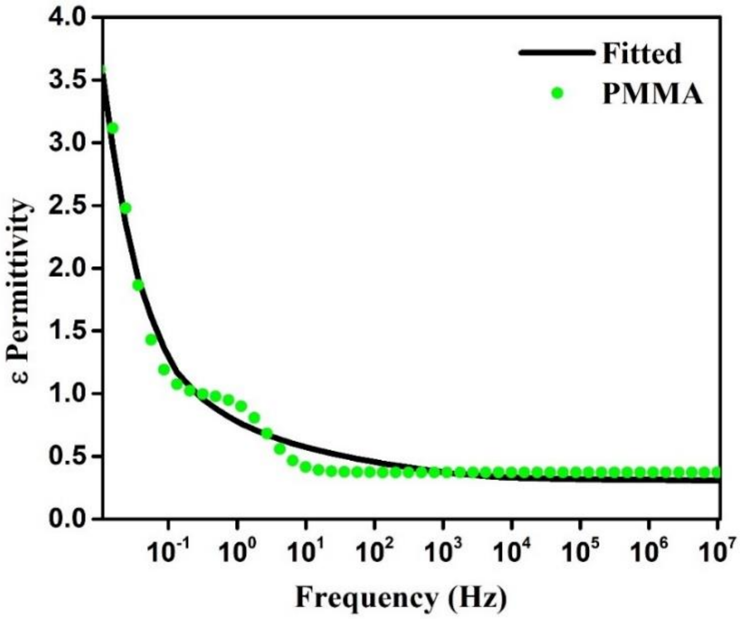

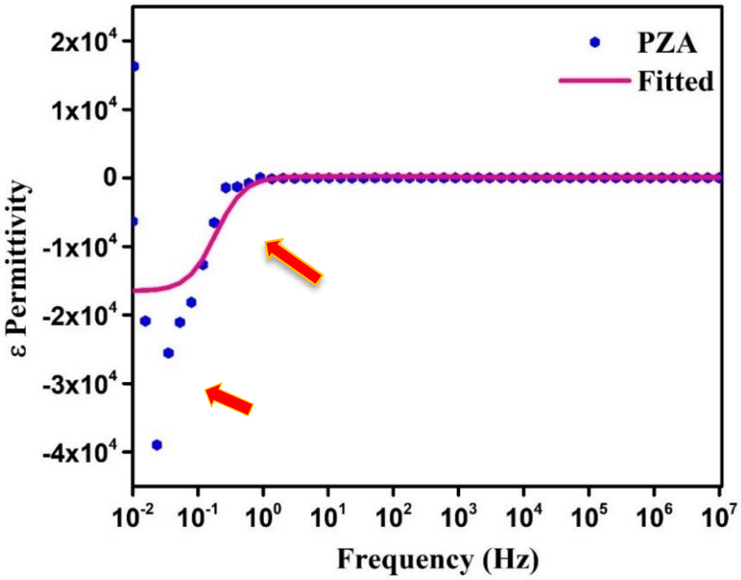

Fig. 6.8. The fitted frequency response spectra of composites using equation (3). Deviation from the fitted curve corresponds to the transitions in polarisation mechanisms. The discrepancy in the fitted result is attributed to the transition that occurs in polarisation mechanisms.

To summarise, PMMA_ZnO_AC percolating ternary composites with varying filler content were successfully designed and prepared. As filler content increases, three-dimensional metallic conducting networks are generated throughout the composites, leading to the emergence of percolation and the alteration of electronic transport mechanisms from localisation (hopping) to delocalisation (metallic). Furthermore, composites exhibit a positive-to-negative permittivity transition at the percolation threshold. Surprisingly the point of transition belongs to extremely low-frequency radio waves. The development of enhanced interfacial polarisation is attributable to the rise in permittivity below the percolation threshold. When the system attains the percolation threshold, delocalised electrons and ions develop an extremely low-frequency plasmonic state, resulting in a plasma-like negative permittivity. The negative permittivity behaviour is well explained using the Drude and Lorentz model for free electrons.

6.4. Conclusion:

In summary, PMMA_AC_ZnO, a flexible composite with surface microstructure-induced negative permittivity composites, is designed and explored for its metamaterial properties. The PMMA_AC_ZnO composites exhibited extra low frequency adjustable negative permittivity behaviours and were successfully designed and fabricated by the in-situ polymerisation method. Interestingly, the microstructural evolution of composites made from the combined effects of PMMA voids and AC_ZnO filler concentration significantly impacts the material's dielectric characteristics. Because of the plasmonic state created from free-moving ions and delocalised electrons inside the 3D conductive networks generated via percolation, the permittivity value of the ternary meta composites undergoes a transition from positive to negative. Meanwhile, composites' negative permittivity transition region could be tuned by controlling the content of activated carbon and ZnO nanoparticles. PZA composites with tailorable negative permittivity at extra low radio frequency regimes are anticipated to be critical in less dissipative low frequency, long wavelength range applications.

6.5 References

[1]. Urzhumov YA, Shvets G, Optical magnetism and negative refraction in plasmonic metamaterials. Solid State Commun, 2008, 146(5–6):208–220

[2]. Zhongyang Wang, Kai Sun, Peitao Xie, Qing Hou, Yao Liu, Qilin Gu, Runhua Fan. Design and analysis of negative permittivity behaviors in barium titanate/nickel metacomposites, Acta Materialia, 2020, 85, 2020, 412-419,1359-6454, https://doi.org/10.1016/j.actamat.2019.12.034.

[3]. Valentine J, Zhang S, Zentgraf T, Ulin-Avila E, Genov DA, Bartal G, Zhang X Three-dimensional optical metamaterial with a negative refractive index. Nature, 2008, 455(7211):376–379

[4]. Cheng C, Fan R, Ren Y, Ding T, Qian L, Guo J, Li X, An L, Lei Y, Yin Y, Guo Z, Radiofrequency negative permittivity in random carbon nanotubes/alumina nanocomposites. Nanoscale, 2017, 9(18):5779–5787.

[5] Zhang Y, Huang Y, Zhang T, Chang H, Xiao P, Chen H et al, Broadband and tunable high-performance microwave absorption of an ultralight and highly compressible graphene foam. Adv Mater, 2015, 27(12):2049–2053

[6] Nan C, Shen Y, Ma J, Physical properties of composites near percolation. Annu Rev Mater Res 2010, 40:131–151

[7] B. Wang, K.H. Teo, t. Nishino, W. Yerazunis, J. Barnwell, J. Zhang, Experiments on wireless power transfer with metamaterials. Appl. Phys. Lett. 2011, 98, 254101-254103.

[8] N. Engheta, An idea for thin subwavelength cavity resonators using metamaterials with negative permittivity and permeability, IEEE Anten. Wirel. Propag. Lett. 2002, 1 10–13.

[9] D. Schurig, J. Mock, B. Justice, S.A. Cummer, J.B. Pendry, A. Starr, D. Smith, Metamaterial electromagnetic cloak at microwave frequencies, Science, 2006, 314 (5801) 977–980.

[10] J. Wang, Z. Shi, F. Mao, S. Chen, X. Wang, Bilayer polymer metacomposites containing negative permittivity layer for new high-k materials, ACS Appl. Mater. Interfaces, 2017, 9 (2) 1793–1800.

[11] Z. Shi, J. Wang, F. Mao, C. Yang, C. Zhang, R. Fan, significantly improved dielectric performances of sandwich-structured polymer composites induced by alternating positive-k and negative-k layers, J Mater. Chem. A, 2017, 5 (28) 14575–14582.

[12] M. Hoffmann, M. Pešic', K. Chatterjee, A.I. Khan, S. Salahuddin, S. Slesazeck, U. Schroeder, T. Mikolajick, Direct observation of negative capacitance in polycrystalline ferroelectric HfO_2, Adv. Funct. Mater. ,2016, 26 (47) 8643–8649.

[13] Y.-F. Hou, W.-L. Li, T.-D. Zhang, Y. Yu, R.-L. Han, W.-D. Fei, Negative capacitance in $BaTiO_3/BiFeO_3$ bilayer capacitors, ACS Appl. Mater. Interfaces 2016, 8 (34) 22354–22360.

[14] Z. Shi, R. Fan, Z. Zhang, L. Qian, M. Gao, M. Zhang, L. Zheng, X. Zhang, L. Yin, Random composites of nickel networks supported by porous alumina toward double negative materials, Adv. Mater., 2012, 24 2349e2352.

[15] C. Cheng, R. Fan, Z. Wang, Q. Shao, X. Guo, P. Xie, Y. Yin, Y. Zhang, L. An, Y. Lei, J. Ryu, A. Shankar, Z. Guo, (2017) Tunable and weakly negative permittivity in carbon/ silicon nitride composites with different carbonising temperatures, Carbon 125 103e112.

[16] B. Zhao, C. Park, (2017) Tunable electromagnetic shielding properties of conductive poly (vinylidene fluoride)/Ni chain composite films with negative permittivity, *J. Mater. Chem. C*, 2017,5, 6954-6961. https://doi.org/10.1039/C7TC01865G.

[17] Steven Cummer. "Extremely Low Frequency (ELF) Electromagnetic Wave PropagationExtremely Low Frequency (ELF) Electromagnetic Wave Propagation", Wiley Encyclopedia of Telecommunications, 04/15/2003.

[18] Z. Zhang, R. Fan, Z. Shi, S. Pan, K. Yan, K. Sun, J. Zhang, X. Liu, X.L. Wang, S.X. Dou, Tunable negative permittivity behavior and conductor–insulator transition in dual composites prepared by selective reduction reaction. J. Mater. Chem., 2013, C 1, 79–85.

[19] Z. Zhang, K. Sun, Y. Liu, Z. Kuang, S. Sun, X. Ji, The negative permittivity behavior and magnetic property of $FeNi/Al_2O_3$ composites in radio frequency region. Ceram. Int. 2016, 42, 19063–19065.

[20] Yao Liu, Yunpeng Qu, Jiahao Xin, Zezhong Wang, Guohua Fan, Peitao Xie, Kai Sun. Weakly Radio-Frequency Negative Permittivity of Poly (vinylidene fluoride)/Ti3SiC2 MAX Phase Metacomposites, *J Inorg Organomet Polym* 2018, 29, 248–257 (2019). https://doi.org/10.1007/s10904-018-0983-8.

[21] M. Chen, M. Gao, F. Dang, N. Wang, B. Zhang, S. Pan, Tunable negative permittivity and permeability in $FeNiMo/Al_2O_3$ composites prepared by hot-pressing sintering. Ceram. Int. ,2016, 42, 6444–6449.

[22] M. Chen, R.H. Fan, M. Gao, S.B. Pan, M.X. Yu, Z.D. Zhang, Negative permittivity behavior in Fe50Ni50/Al2O3 magnetic composite near percolation threshold. J. Magn. Magn. Mater. 2015,381, 105–108.

[23] X.A. Wang, Z.C. Shi, M. Chen, R.H. Fan, K.L. Yan, K. Sun, S.B. Pan, M.X. Yu, Tunable electromagnetic properties in Co/Al_2O_3 cermets prepared by wet chemical method. J. Am. Ceram. Soc. 2014, 97, 3223–3229.

[24] Dong Y, Liu Z, Pang L, Han Y, Yao S, Wang X, Preparation of Y2O3–

ZrO2–CeO2 solid solution by co-precipitation and its electrical property. Physica B, 2021, 612:412972.

[25] Zaixin Wei, Zhongyang Wang, Guohua Fan, Ciqun Xu, Guangyue Shi, Guodong Zhang, Yao Liu, Runhua Fan. Low-frequency plasmonic state and negative permittivity in copper/titanium dioxide percolating composites", Ceramics International. 2020, 47, Issue 2, 2021, 2208-2213, ISSN 0272-8842, https://doi.org/10.1016/j.ceramint.2020.09.060.

[26]. Dong Y, Liu Z, Qiu G, Pang L, Han Y, Yao S et al. A limiting current oxygen sensor with 8YSZ solid electrolyte and $(8YSZ)_{0.9}(CeO_2)_{0.1}$ dense diffusion barrier. J Alloy Compd 2021, 885:160903.

[27]. Wang Z, Sun K, Xie P, Fan R, Liu Y, Gu Q et al, Low-loss and temperature-stable negative permittivity in La0.5Sr0.5MnO3 ceramics. J Eur Ceram Soc 2020, 40(5):1917–1921.

[28]. Kittel C, McEuen P, McEuen P (1996) Introduction to solid state physics. Wiley, New York 23. Pendry J, Holden A, Stewart W, Youngs I, extremely low-frequency plasmons in metallic mesostructures. Phys Rev Lett 1996, 76(25):4773.

[29]. Kou X, Yao X, Qiu Negative permittivity and negative permeability of multi-walled carbon nanotubes/polypyrrole nanocomposites. Org Electron J 2016, 38:42–47.

[30]. Wang Z, Sun K, Xie P, Liu Y, Gu Q, Fan R, Permittivity transition from positive to negative in acrylic polyurethane aluminum composites. Compos Sci Technol 2020, 188:107969.

[31] Sun, K.; Wang, L.; Wang, Z.; Wu, X.; Fan, G.; Wang, Z.; Cheng, C.; Fan, R.; Dong, M.; Guo, Z.Flexible Silver Nanowire/Carbon Fiber Felt Metacomposites with Weakly Negative Permittivity Behavior. Phys. Chem. Chem. Phys. 2020, 22, 5114−5122.

[32] Jinke Song, Guangyue Shi, Xiaoting Song, Zidong Zhang, Yao Liu, Runhua Fan. ,Tunable negative permittivity behavior in percolated MWCNTs/PVDF composites, Materials Letters, 2022,318,2022,132051, ISSN 0167-577X,https://doi.org/10.1016/j.matlet.2022.132051.

[33] Cheng, C.; Jiang, Y.; Sun, X.; Shen, J.; Wang, T.; Fan, G.; Fan, R. Tunable Negative Permittivity Behavior and Electromagnetic Shielding Performance of Silver/Silicon Nitride Metacomposites. Composites, 2020, Part A, 130, 105753.

[34] Wang, Z.; Sun, K.; Xie, P.; Liu, Y.; Gu, Q.; Fan, R. Permittivity Transition from Positive to Negative in Acrylic Polyurethane Aluminum Composites. Compos. Sci. Technol., 2020,188, 107969.

[35] Fan, G.; Zhao, Y.; Xin, J.; Zhang, Z.; Xie, P.; Cheng, C.; Qu, Y.; Liu, Y.;

Sun, K.; Fan, R. Negative Permittivity in Titanium Nitride Alumina Composite for Functionalized Structural Ceramics. J. Am. Ceram. Soc. 2020, 103, 403−411.

[36] Shi, Z.-c.; Fan, R.-h.; Yan, K.-l.; Sun, K.; Zhang, M.; Wang, C.- g.; Liu, X.-f.; Zhang, X.-h. Preparation of Iron Networks Hosted in Porous Alumina with Tunable Negative Permittivity and Permeability. Adv. Funct. Mater., 2013, 23, 4123−4132.

[37] Shi, Z.-c.; Fan, R.-h.; Zhang, Z.-d.; Qian, L.; Gao, M.; Zhang, M.; Zheng, L.-t.; Zhang, X.-h.; Yin, L.-w., Random Composites of Nickel Networks Supported by Porous Alumina toward Double Negative Materials. Adv Mater, 2012,24, 2349−2352.

[38] Zheng, X.; Smith, W.; Jackson, J.; Moran, B.; Cui, H.; Chen, D.; Ye, J.; Fang, N.; Rodriguez, N.; Weisgraber, T.; Spadaccini, C. M. Multiscale Metallic Metamaterials. Nat Mater, 2016, 15, 1100−1106.

[39] Sun, K.; Xin, J.; Li, Y.; Wang, Z.; Hou, Q.; Li, X.; Wu, X.; Fan, R.; Leong Choy, K. Negative Permittivity Derived from Inductive Characteristic in the Percolating Cu/EP Metacomposites. J. Mater. Sci. Technol., 2019,35, 2463−2469.

[40] Yunpeng Qu, Jiamin Lin, Jiada Wu, Zongxiang Wang, Kai Sun, Min Chen, Binbin Dong, Zhanhu Guo, Runhua Fan. Graphene– Carbon Black/CaCu Ti O Ternary Metacomposites toward a Tunable and Weakly ε-Negative Property at the RadioFrequency Region, *Phys. Chem. C* 2020, 124, 42, 23361-23367 https://doi.org/10.1021/acs.jpcc.0c07544

CHAPTER 7

Design and analysis of negative permittivity behaviours in PMMA_Calcium Titanate_Graphite Composites at Extremely Low Frequencies.

Contents

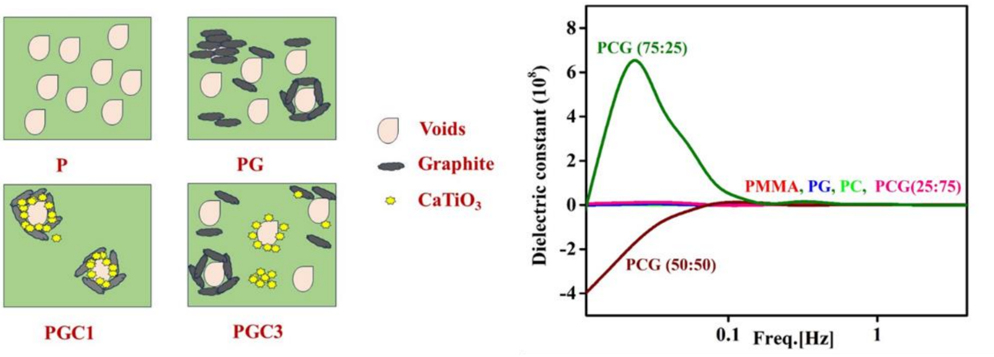

Abstract: *Carbon-ceramic composites with adjustable electrical properties are promising candidates for electromagnetic metamaterials featuring negative permittivity. Here, ceramic fillers composed of calcium titanate and graphite (CG) were incorporated into a PMMA matrix. The distribution of fillers around voids facilitated by the polymer significantly influenced the microstructure, electrical conductivity, and dielectric behaviour of the metamaterials. The composite exhibited dielectric conductivity and a capacitive nature with positive permittivity at lower filler content. The increased CG content led to better filler contact formation of 3D networks. As a result, a plasma-type negative permittivity behaviour was observed in those ceramics. It is attributed to the low-frequency plasmonic state of free electrons within the CG networks. Remarkably, increasing CG content shifted the plasma frequency to extremely low frequencies, significantly enhancing the absolute magnitude of negative permittivity (~ 10^8). Our findings could propel the development of more ceramic-based metamaterials with tunable negative permittivity.*

7.1 Introduction

The development of metamaterials has opened new pathways for achieving negative permittivity across a broad spectrum of frequencies. In Chapter 6, we successfully designed and fabricated a flexible ternary metasystem with metallic fillers to address the gap in the extremely low-frequency regime. In this study, we propose an alternative design strategy to enhance the order of dimensionality of negative permittivity for ELF applications.

It is widely acknowledged that composites consist of multiple components, with their properties being determined by both the matrix and the fillers [1-5]. The selection of fillers in meta-composites significantly influences their dielectric properties. The diverse composition of negative dielectric materials offers greater flexibility in regulating electromagnetic parameters and enhances the concept of metamaterials. Typically, these composites are made up of conductive fillers and an insulating matrix, which can be either ceramics or polymers. The conductive fillers are crucial for imparting negative dielectric properties, as the final dielectric characteristics depend heavily on the composition and distribution of these conductive fillers within the heterogeneous composites [6-8]. Although metallic conducting fillers are widely accepted for their ability to induce negative permittivity in metamaterials, they also come with several significant drawbacks. One significant issue is their tendency to lead to heavier and bulkier materials, potentially limiting their practical applications in lightweight or flexible devices. Additionally, metals are prone to oxidation and corrosion, which can degrade their conductive properties over time and reduce the long-term reliability and durability of the metamaterials. Another drawback is the potential for increased energy loss due to eddy currents and joule heating, especially at higher frequencies, which can impair the efficiency of electromagnetic applications. Furthermore, the dispersion and uniform distribution of metallic fillers within the matrix can be challenging to achieve - leading to inconsistent material properties and performance. These challenges necessitate careful consideration and innovative approaches to mitigate the drawbacks of metallic conductive fillers in metamaterials.

To address these drawbacks, we are exploring the incorporation of ceramic fillers instead of metallic ones. These ceramic fillers also provide pathways for conducting free electrons.

Designing of micro capacitors based on ceramics for ELF Regime:

(i) Structure-defining microstructure: Microstructure creation on regular, patterned void structures provides a possible foundation for metamaterial composites. In this context, polymers are apt candidates because of their flexibility. Polymers are increasingly being utilised in the development of metamaterials due to their versatile properties and ease of fabrication. They offer several advantages, including inherent flexibility and lightweight, which allow for the creation of metamaterials that can be easily shaped, stretched, and integrated into various devices, particularly useful for wearable technologies and flexible electronics [9,10]. The properties of polymers can be tailored through chemical modification, blending, and the incorporation of nanoparticles or other fillers, enabling the design of metamaterials with specific optical, electrical, and mechanical characteristics. Polymers can be processed using techniques such as moulding, extrusion, and 3D printing, facilitating the mass production of metamaterials with complex structures at relatively low costs. Polymers typically exhibit low dielectric losses and can be engineered to have specific permittivity values, making them suitable for applications in radiofrequency (RF) and microwave devices. In this work, a non-conducting polymer, PMMA, is chosen.

(ii) Availability of delocalised electrons: The likelihood of exhibiting a negative dielectric constant increase with the number of delocalised electrons. In addition, entities with many free electrons have a high chance of getting arranged around the attractive ends (Voids). Carbon materials are gaining significant attention in the development of metamaterials due to their exceptional properties and wide range of applications. These materials, such as graphene, carbon nanotubes (CNTs), and graphite, exhibit high electrical conductivity [11,13], essential for electromagnetic applications and the development of electrically responsive metamaterials. For negative permittivity, graphite provides an abundance of delocalised electrons.

(iii) Ceramic filler: Filler acts as a conducting pathway for every meta composite. Ceramic materials have become essential metamaterials, leveraging their unique dielectric, magnetic, and thermal attributes [14,15]. In contrast to traditional metallic counterparts, ceramics offer many advantages, ranging from exceptional temperature stability and low electrical conductivity to finely tuning their electromagnetic properties through compositional adjustments and structural modifications. These qualities position ceramics as ideal candidates for applications in extreme environments and tailored electromagnetic functionalities. With high dielectric permittivity and low loss. For this purpose, we selected $CaTiO_3$ in this study.

This study introduces a flexible polymer material engineered to exhibit metamaterial properties at extra-low-frequency radio waves. The PMMA_$CaTiO_3$_Graphite (PCG) nanocomposites were synthesised via a low-temperature in situ polymerisation process. The composition and microstructure of the PMMA_$CaTiO_3$_Graphite nanocomposites were characterised, and their dielectric properties were analysed using Broadband Dielectric Spectroscopy. The observed plasma-like epsilon negative state in $CaTiO_3$_Graphite networks is linked to their interaction with extremely low-frequency radio waves. Notably, the magnitude of negative permittivity reaches a remarkably high value of 10^8. This observation underscores the robustness of the material's ability to exhibit strong negative permittivity, which is crucial for its application in manipulating electromagnetic fields at extremely low frequencies.

7.2. Materials and Methods

The synthesis of ternary meta-composite PCG mainly includes two stages: the $CaTiO_3$ nanoparticle is synthesised in the first stage; in the second stage, the polymer composite is synthesised in situ via the polymerisation reaction of PMMA/Graphite, and the $CaTiO_3$.

7.2.1 Synthesis of $CaTiO_3$ nanoparticles:

The synthesis of calcium titanate involves using calcium carbonate ($CaCO_3$), titanium Isopropoxide (TTIP) [Ti $(OC_3H_7)_4$], ethylene glycol ($C_2H_6O_2$), and anhydrous citric acid ($C_6H_8O_7$) as starting materials. Initially, 1g of TTIP is added to 40 ml of an aqueous citric acid solution and heated to 353K for 3 hours with continuous stirring. After this period, 1g of calcium carbonate is introduced into the solution, which is then heated for an additional hour. Subsequently, 60ml of ethylene glycol is added, and the solution is gradually heated to 373K with constant stirring to facilitate the evaporation of water and the formation of a resin. This resin is then transferred to a conventional furnace and subjected to heat treatment at 473K for approximately 23 hours. Finally, the resulting product is ground into calcium titanate powder. The entire synthesis procedure is shown in Scheme 7.1

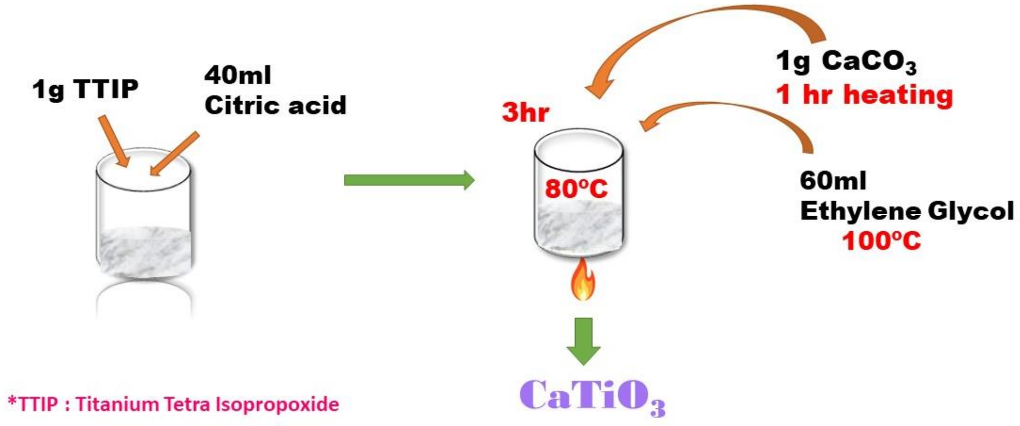

Scheme 7.1: Schematic illustration of $CaTiO_3$ nanoparticles preparation**.**

7.2.2. Synthesis of PMMA_Graphite_$CaTiO_3$ Nanocomposite.

PMMA polymer matrix films were fabricated using commercially available transparent PMMA crystals. To synthesise the polymer nanocomposite film, 1 g of PMMA crystals were dissolved in 50 ml of acetone solvent and stirred for 90 minutes at 60 ° C. Once the solution turned white and viscous, varying proportions of graphite and $CaTiO_3$ nanoparticles were gradually added while stirring. The stirring continued for 1 hour, resulting in a viscous black gel. When poured into a petri dish, it formed a self-standing polymer composite film with a thickness of 0.1 mm (100 microns). The entire synthesis procedure is shown in Scheme 7.2

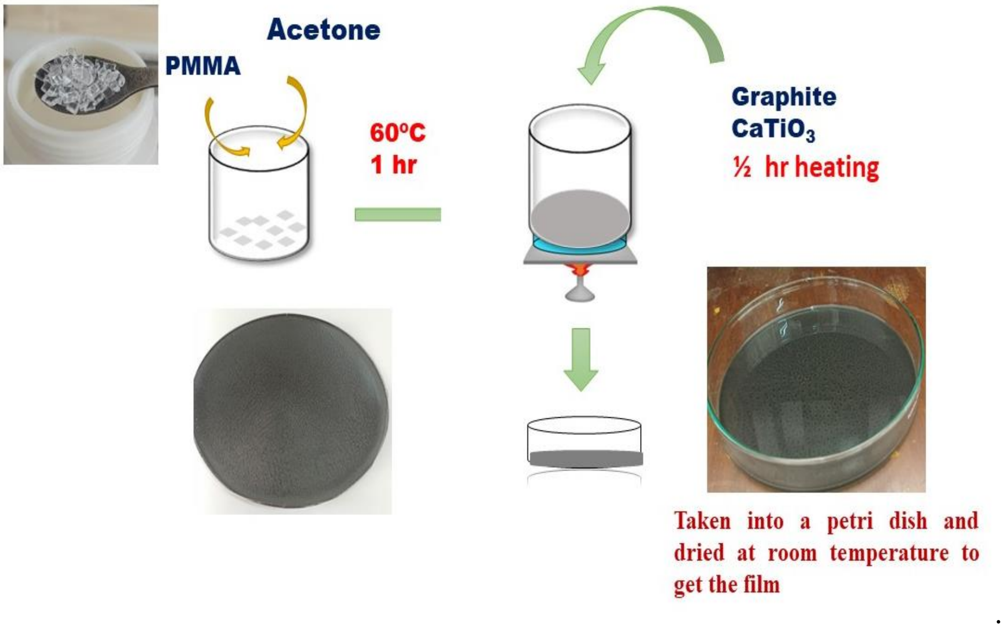

Scheme 7.2: Schematic illustration of PCG preparation**.**

7.2.3 Characterisations and Measurements

At room temperature, the microstructures and morphologies of materials were examined using field emission scanning electron microscopy (FE-SEM; Carl Zeiss; Gemini SEM 300). Surface topological studies were carried out using an Atomic Force Microscope (Bruker, Multimode 8). The conductivity, permittivity, and capacitance of PMMA_$CaTiO_3$_Graphite composites were measured with Broadband Dielectric Spectroscopy (Novocontrol Technologies, BDS 50) in the frequency range 10^{-2} Hz-10^7Hz.

7.3 Results and Discussions

7.3.1 Formation of tiny capacitors- Morphological investigation:

The surface morphologies of PMMA_$CaTiO_3$_Graphite nanocomposites with increasing concentrations of $CaTiO_3$_Graphite are illustrated in Fig. 7.1. The pristine PMMA sheets exhibit void-like structures throughout the film. Upon incorporating $CaTiO_3$ nanoparticles, they tend to settle within these void structures. Conversely, when graphite nanoparticles are incorporated, they primarily occupy the edges of the voids. Fig.7.1d, highlighted by the red circled region, shows the formation of interconnected $CaTiO_3$_Graphite networks around the voids, supplemented by the graphite in the matrix. This configuration leads to the development of tiny capacitors at the attractive ends of the PMMA matrix. PMMA_Graphite units are weakly coupled at lower graphite concentrations, but as the graphite_$CaTiO_3$ content increases, they form three-dimensional PMMA_Graphite networks embellished with $CaTiO_3$.

It is evident that the PMMA voids are well-formed, and the $CaTiO_3$_Graphite units are densely packed within these voids. With a low graphite_$CaTiO_3$ content, the distribution of $CaTiO_3$_Graphite clusters is unsystematic and isolated at the polymer void edges. As the concentration of $CaTiO_3$_Graphite increases, these clusters partially couple, creating three-dimensional (3D) $CaTiO_3$_Graphite networks. Fig. 7.2 presents a schematic representation of the microstructural evolution of PMMA_$CaTiO_3$_Graphite nanocomposites. According to the percolation theory, the microstructural development of these nanocomposites is closely related to their electrical and dielectric properties, which will be discussed subsequently.

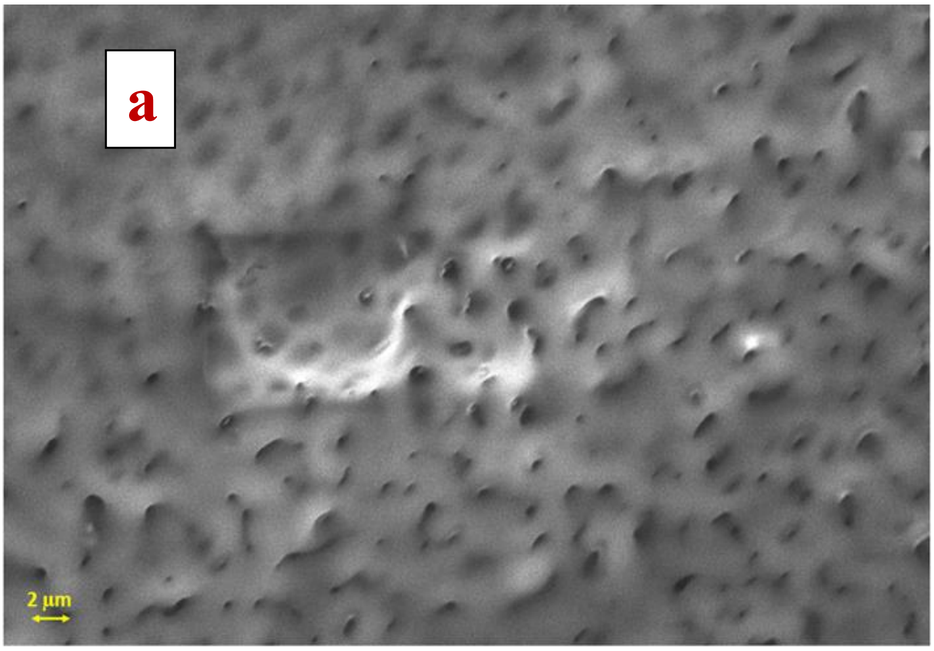
a
2 µm

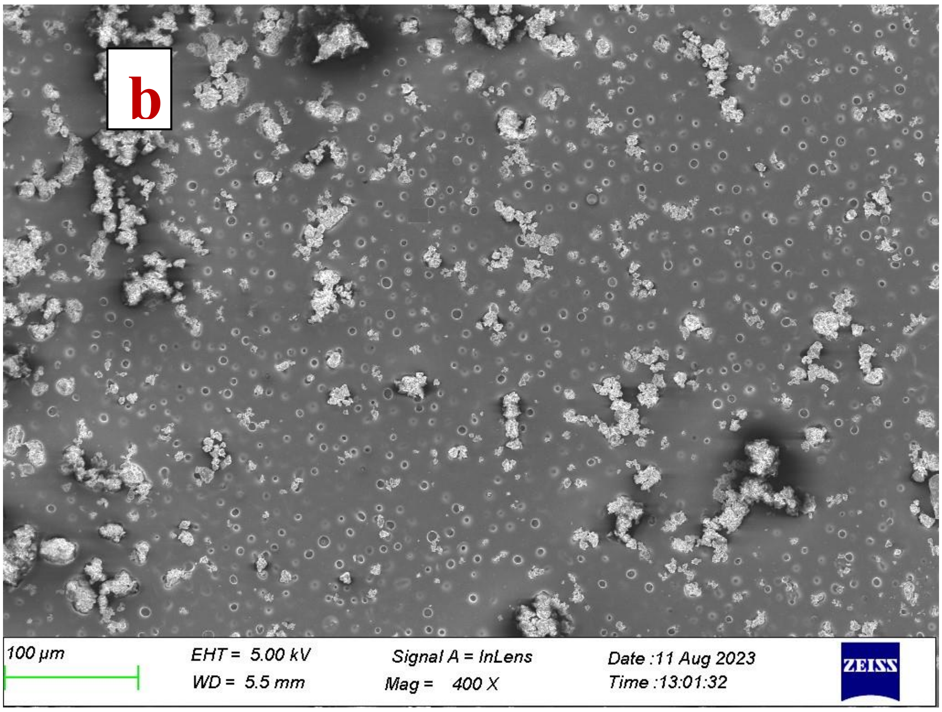
b
100 µm
EHT = 5.00 kV
WD = 5.5 mm
Signal A = InLens
Mag = 400 X
Date :11 Aug 2023
Time :13:01:32
ZEISS

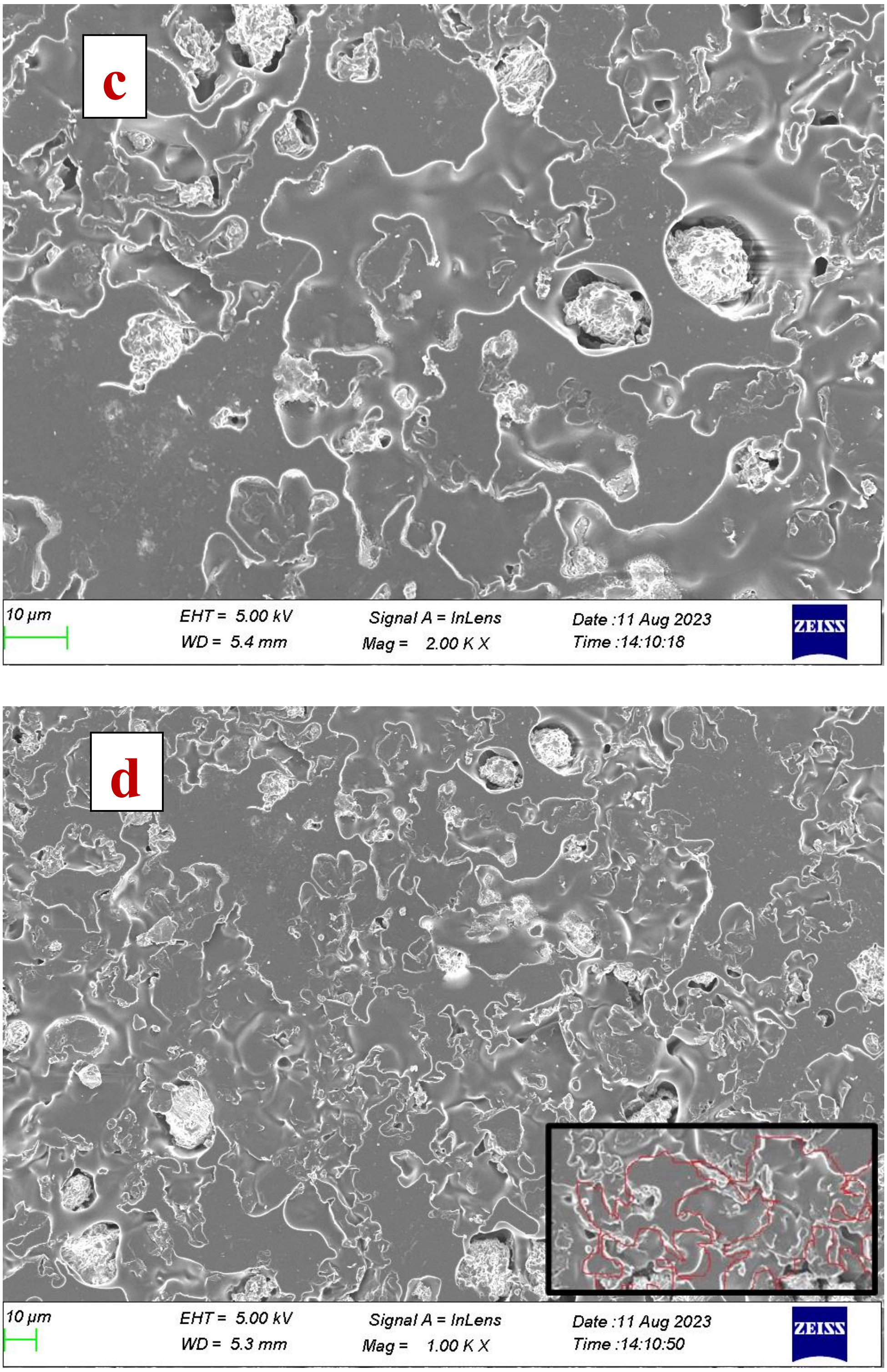

Fig.7.1. SEM images of PMMA_CaTiO_3_Graphite composites with **(a)** Pure PMMA; **(b)** PMMA_CaTiO_3Composite; **(c)** PMMA_Graphite composite; **(d)** PMMA_CaTiO_3_Graphite composite with interconnected conducting networks.

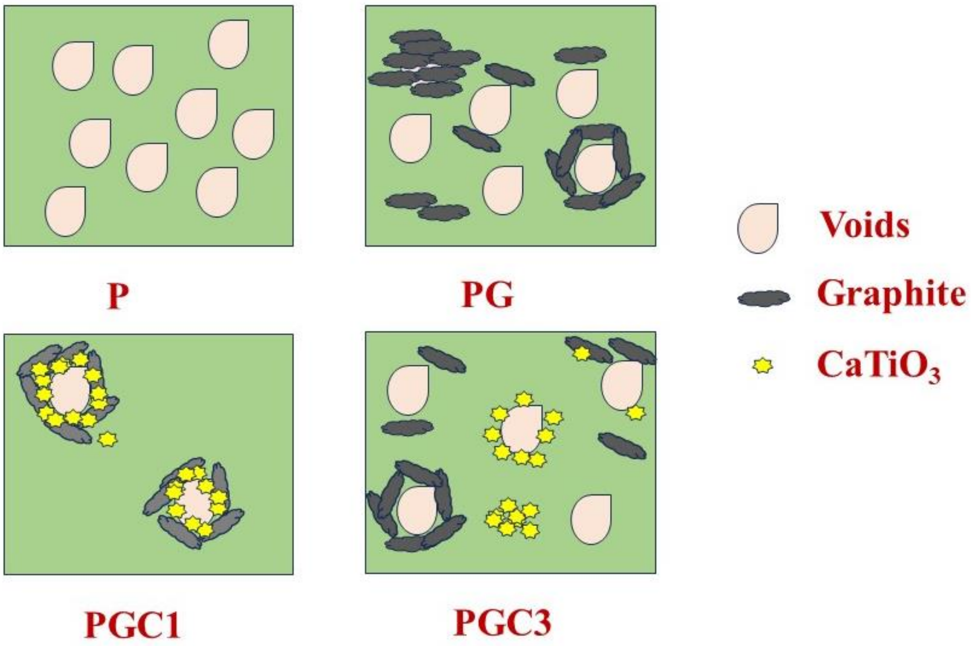

Fig.7.2: Schematic representation of the microstructural evolution of PMMA_CaTiO$_3$_Graphite nanocomposites. P - Pure PMMA films with voids; PG- Graphite decorated at the edges of PMMA voids; PGC1- CaTiO$_3$ deposition complimented by Graphite_PMMA voids (25:75); PGC3 – PMMA_CaTiO$_3$_Graphite (75:25) composites.

7.3.2. Conductivity and negative permittivity behaviour

The frequency dispersion plots giving the variation of AC conductivity of Graphite_CaTiO$_3$ nanocomposites, with AC field frequency ranging from 10^{-2} Hz to 10^7 Hz, are illustrated in Fig. 7.3. Pure PMMA film demonstrates nearly zero conductivity, indicating the non-conductive nature of its voids. When CaTiO$_3$ nanoparticles are incorporated, there is no significant increase in conductivity. However, the addition of graphite markedly enhances conductivity, attributed to the availability of free electrons. In the PCG (25:75) sample, conductivity rapidly increased due to well-defined conductive 3D networks forming throughout the material. As previously mentioned, increasing the concentration of CaTiO$_3$ leads to greater agglomeration and void filling by CaTiO$_3$, resulting in reduced conductivity. The AC conductivity (σ_{ac}) of the composites shows an upward trend at low CaTiO$_3$_Graphite content – representing the transition from hopping to metallic conduction behaviour.

Classical percolation theory can elucidate the relationship between conductivity and microstructural evolution. This theory posits that percolation significantly influences conductivity in metamaterials, as it is linked to the formation of 3D conducting networks formed by interconnected conductive phases, thereby affecting the electrical properties of the materials [16,17]. Since all observations were collected at the same ambient temperature, only the geometrical and physical connections between the conducting fillers were considered. Before reaching the percolation threshold, the internetwork of neighbouring fillers in the composites is relatively weak, resulting in unremarkable conductivity due to the minimal contribution from the hopping mechanism. As the filler content increases, most conduction electrons become unbound, significantly enhancing conductivity through the metallic conduction mechanism. In composites with 50% $CaTiO_3$ and 50% Graphite content, clusters establish direct contact, allowing electrons to move freely through metallic conduction, thereby increasing conductivity.

Fig. 7.4 depicts the frequency-dependence of real permittivity for percolated PMMA_$CaTiO_3$_Graphite composites. Interestingly, the sign of real permittivity switches to negative at a lower frequency regime when filler content reaches 50% $CaTiO_3$ and 50% Graphite. Plasma-like negative permittivity is achieved when the filler content is sufficiently high. The permittivity value decreases drastically with an increase in external frequency, exposing the plasmonic state at low radio frequency.

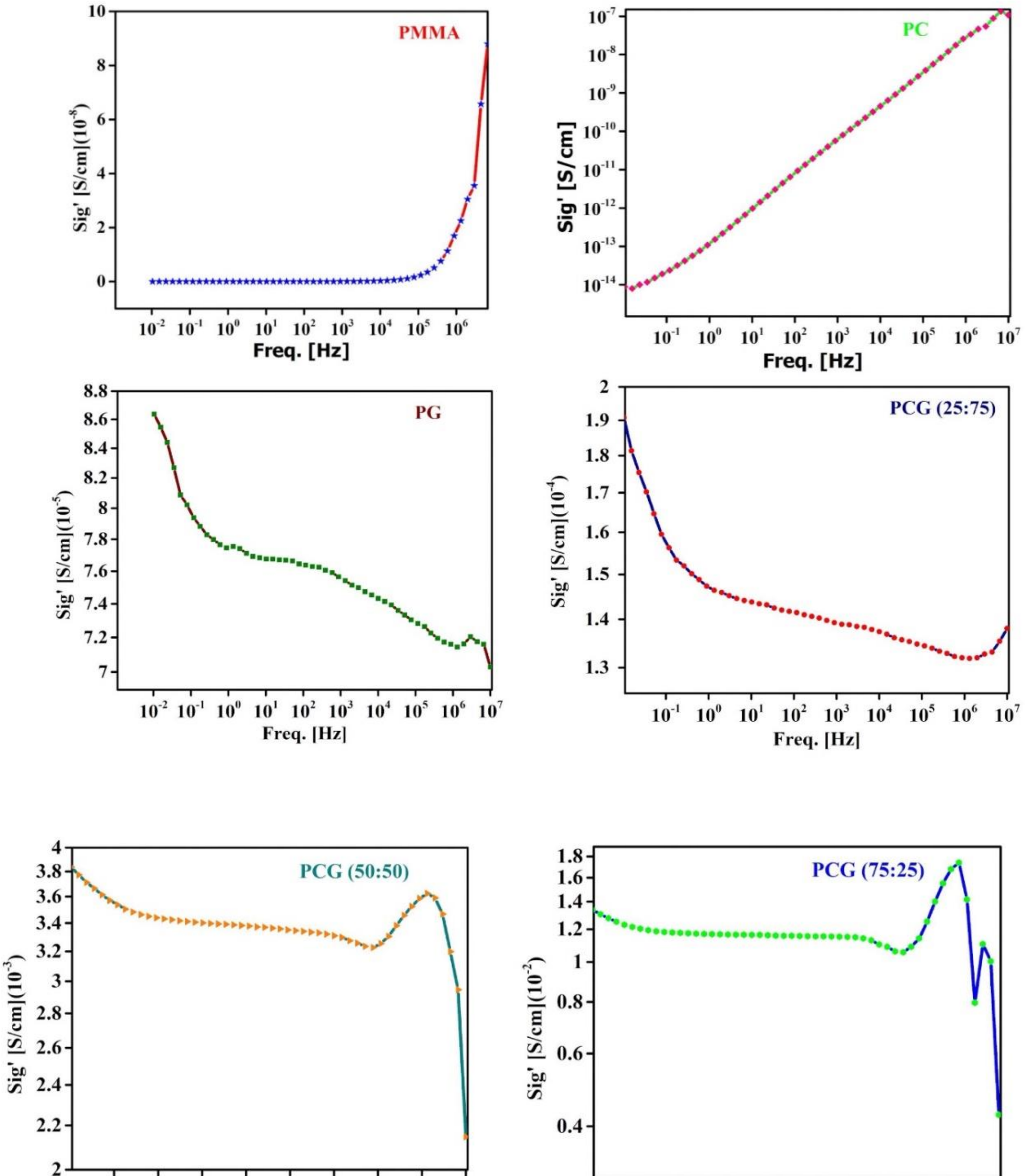

Fig.7.3. Frequency spectra of conductivity for the **(a)** PMMA, **(b)** PMMA_CaTiO$_3$ Composite**; (c)** PMMA_Graphite composite; **(d)** PMMA_CaTiO$_3$_Graphite (25:75), **(e)** PMMA_CaTiO$_3$_Graphite (50:50); and **(f)** PMMA_CaTiO$_3$_Graphite (75:25) composites.

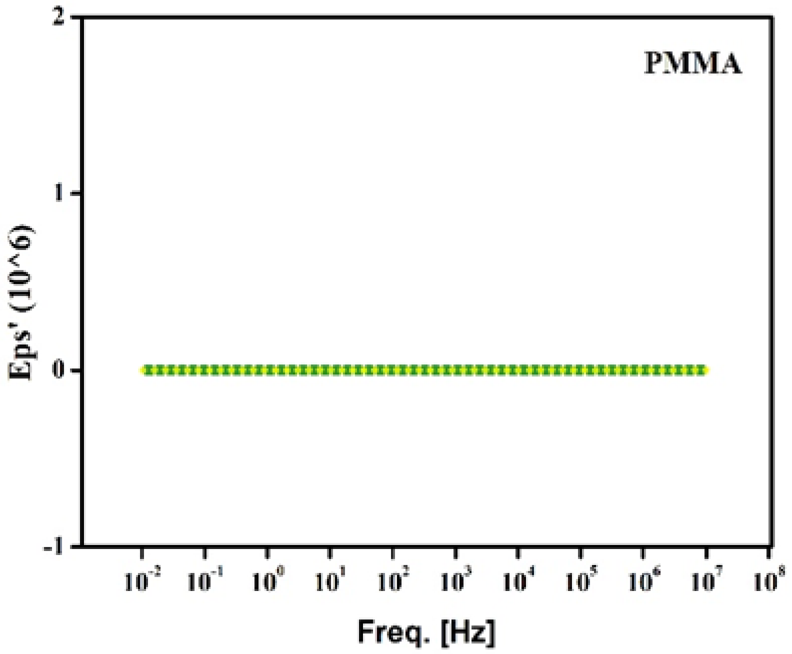

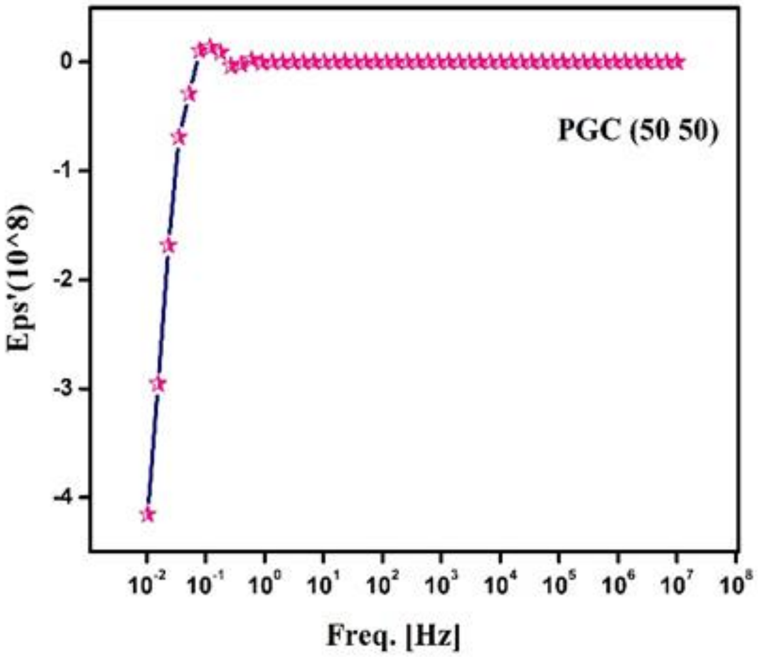

Fig.7.4. Frequency spectra of permittivity for the PMMA and PCG (50:50) composites.

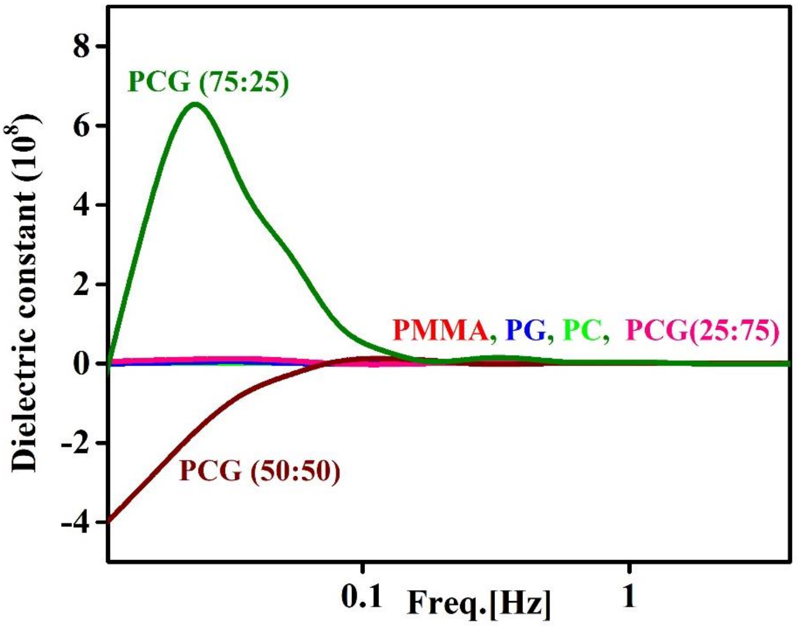

Fig. 7. 5. Frequency spectra of permittivity for the PMMA and PCG composites.

7.3.3 Micocapacitor formation and percolation of charge carriers.

The SEM image in Fig. 7.1(d) indicated the formation of microcapacitors. These interconnected microcapacitors are likely the primary reason for the enhanced negative permittivity observed in the composite PCG (50:50). To understand this better, we need to explore the formation mechanism of these interconnected conductive networks. Initially, hopping can be considered a mechanism for charge transfer between the isolated microcapacitors. However, the microcapacitors interconnect at a particular threshold composition, forming a conductive network through a mechanism akin to that in metals. Given the observed density of microcapacitors in PCG, it can be suggested that PCG operates within the framework of classical percolation theory.

Previous studies and discussions indicate that localised and delocalised electrons coexist within the composites, leading to distinct responses to an applied external electric field. The negative permittivity observed in composites below the percolation threshold is attributed to the formation of densely packed microcapacitors and the interfacial polarisation of electrons. Notably, the permittivity shifts from positive to negative in the lower frequency range when the filler content reaches 50% $CaTiO_3$ and 50% Graphite. Metal-based composites must have the lowest possible conductivity value to achieve a low-frequency plasmonic state. When the filler content is sufficiently high, a plasma-like negative permittivity emerges. Subsequently, as the external frequency increases, the permittivity value rapidly decreases, leading to the development of a plasmonic state in the extremely low radio frequency regime.

Fig. 7.4 and 7.5 illustrate that the pure PMMA self-standing films exhibit nearly zero permittivity across the entire frequency range. Upon adding zinc oxide nanoparticles, ε'_r becomes slightly positive throughout the range. The isolated dispersion of Graphite_$CaTiO_3$ or Graphite alone in the PMMA matrix induces electrical dipole resonance within the composites. As the graphite content increases, it tends to occupy the walls of the voids created by PMMA, thereby raising the density of micro capacitors within the material and consequently increasing the actual permittivity of the sample. Graphite significantly influences the negative permittivity of metamaterials due to its unique electronic and structural properties. Its high electrical conductivity is essential for supporting plasmonic resonances across various frequencies, which can lead to negative permittivity in specific frequency ranges. The delocalised π-electrons in graphite's structure contribute to its metallic-like behaviour, allowing free electrons to oscillate in response to an external electromagnetic field, thereby facilitating conditions for negative permittivity. The tunable electronic properties of graphite, achieved through layer thickness or defect engineering modifications, enable the design of metamaterials with specific negative permittivity characteristics. Additionally, when incorporated into composites, graphite forms interconnected networks that enhance the overall electrical conductivity of the material, aiding in achieving and sustaining negative permittivity over a broader frequency range. Graphite's high electron density enhances plasmonic resonances, which is crucial for negative permittivity. They allow the material to exhibit a negative response to the electric field component of incident electromagnetic waves [18]. At frequencies below the plasma frequency, the material exhibits negative permittivity, with graphite's free electrons playing a pivotal role in this behaviour, enabling the composite material to demonstrate negative permittivity at specific frequencies. At the same time, Calcium titanate ($CaTiO_3$) significantly impacts the negative permittivity of metamaterials through its unique dielectric properties and interaction with other composite materials. $CaTiO_3$'s high dielectric constant enhances the overall dielectric properties of the composite, which is crucial for achieving negative permittivity, especially at low frequencies. When included in a polymer matrix like PMMA, $CaTiO_3$ induces significant interfacial polarisation effects at the particle-matrix interfaces, bolstering the dielectric response and enhancing negative permittivity. The formation of micro capacitors by $CaTiO_3$ particles supports localised electric fields countering the external field, further contributing to negative permittivity. At higher concentrations, $CaTiO_3$ particles tend to agglomerate, forming interconnected networks that facilitate electron conduction, enhancing conductivity and negative permittivity. According to percolation theory, the composite exhibits weak conductivity and negligible negative permittivity below a certain threshold, but beyond this threshold, improved conductivity and pronounced negative permittivity occur due to conductive pathway formation. In composites combining $CaTiO_3$ with conductive materials like graphite, plasmonic resonances are essential for negative permittivity, as they enable the material to exhibit a negative response to the electric field component of incident electromagnetic waves. Thus, the combination of high dielectric constant, interfacial polarisation, micro-capacitor formation, and plasmonic resonances allows $CaTiO_3$ to influence the negative permittivity in metamaterials significantly. This implies that by adjusting the weight percentages of graphite and $CaTiO_3$, we can fine-tune the transition region from positive to negative permittivity.

Two primary types of resonance mechanisms exist: (i) electrical dipole resonance arising from isolated $CaTiO_3$_Graphite clusters and (ii) low-frequency electron plasma oscillation resonance in interconnected $CaTiO_3$_Graphite networks. For $CaTiO_3$_Graphite cluster-based meta composites within the percolation region, the negative permittivity property results from the combined effects of interfacial polarisation, electrical dipole resonance, and an extremely low-frequency plasmonic state. Additionally, as the graphite content increases, the effective electron concentration rises, creating more conductive channels and enhancing the real value of negative permittivity. Consequently, percolative conducting 3D networks are formed in composites with 50% $CaTiO_3$ and 50% graphite, indicating a significant contribution of free electrons. Therefore, the epsilon-negative characteristic in these composites is governed by the low-frequency plasmonic state of unpaired electrons. As the external field frequency increases, the plasma-type ε-negative spectra exhibit a rising trend, indicating that the ε-negative effect weakens as the external field frequency approaches the plasma oscillation frequency. Thus, the combined contribution of dipole-type, plasma-type, and interfacial polarisation mechanisms may provide a valuable and significant pathway to achieving extremely low-frequency negative permittivity.

To summarise, PMMA_$CaTiO_3$_Graphite percolating ternary composites with varying filler content were successfully designed and synthesised. As filler content increases, three-dimensional metallic conducting networks are generated throughout the composites, leading to the emergence of percolation and the alteration of electronic transport mechanisms from localisation (hopping) to delocalisation (metallic). Furthermore, composites exhibit a positive-to-negative permittivity transition at the percolation threshold. Surprisingly, the transition point belongs to extremely low-frequency radio waves, and the value of permittivity is 10^8. The development of enhanced interfacial polarisation is attributable to the rise in permittivity below the percolation threshold. When the system attains the percolation threshold, delocalised electrons and ions develop an extremely low-frequency plasmonic state, resulting in a plasma-like negative permittivity.

7.4. Conclusion.

In conclusion, the development of carbon-ceramic composites with adjustable electrical properties represents a significant advancement in the field of electromagnetic metamaterials. Incorporating Calcium Titanate and Graphite (CG) fillers into a PMMA matrix has effectively demonstrated the ability to manipulate microstructure, electrical conductivity, and dielectric behaviour. The PMMA_$CaTiO_3$_Graphite ternary composites represent a significant advancement in metamaterial design, demonstrating a clear transition from positive to negative permittivity as filler content increases. This transition occurs at the percolation threshold, where three-dimensional ceramic conducting networks are formed within the composites. The evolution from localised (hopping) to delocalised (metallic) electronic transport mechanisms enhance the conductivity and facilitates the emergence of negative permittivity, particularly evident at extremely low-frequency radio waves. The permittivity values achieved, reaching orders of magnitude around 10^8, underscore the effectiveness of these composites in manipulating electromagnetic responses. Below the percolation threshold, enhanced interfacial polarisation contributes to the rise in permittivity. In contrast, beyond this threshold, developing an extremely low-frequency plasmonic state further enhances the negative permittivity, akin to a plasma-like behaviour. These findings highlight the complex interplay between material composition and electromagnetic properties and suggest promising avenues for developing advanced metamaterials based on ceramic fillers tailored for specific applications in communications, sensing, capacitance and beyond.

7.5 References

[1] D.G. Papageorgiou, I.A. Kinloch, R.J. Young, Mechanical properties of graphene and graphene-based nanocomposites, Prog. Mater. Sci. 90 ,2017, 75e127.

[2] G. Fan, Y. Jiang, J. Xin, Z. Zhang, X. Fu, P. Xie, C. Cheng, Y. Liu, Y. Qu, K. Sun, R. Fan, Facile synthesis of Fe@Fe3C/C nanocomposites derived from bulrush for excellent electromagnetic wave-absorbing properties, ACS Sustain. Chem. Eng. 7, 2019, 18765e18774.

[3] C. Hou, Z. Tai, L. Zhao, Y. Zhai, Y. Hou, Y. Fan, F. Dang, J. Wang, H. Liu, High performance MnO@C microcages with a hierarchical structure and tunable carbon shell for efficient and durable lithium storage, J. Mater. Chem. 6, 2018, 9723e9736.

[4] C. Hou, J. Wang, W. Du, J. Wang, Y. Du, C. Liu, J. Zhang, H. Hou, F. Dang, L. Zhao, Z. Guo, One-pot synthesised molybdenum dioxide-molybdenum carbide heterostructures coupled with 3D holey carbon nanosheets for highly efficient and ultrastable cycling lithium-ion storage, J. Mater. Chem. 7, 2019, 13460e13472.

[5]] C. Hou, J. Wang, W. Zhang, J. Li, R. Zhang, J. Zhou, Y. Fan, D. Li, F. Dang, J. Liu, Y. Li, K. Liang, B. Kong, Interfacial superassembly of grape-like MnO-Ni@C frameworks for superior lithium, Storage, ACS Appl. Mater. Interf. 12, 2020, 13770e13780.

[6] u Y, Wang Z, Xie P, Wang Z, Fan R, Ultraweakly and fine-tunable negative permittivity of polyaniline/nickel metacomposites with high-frequency diamagnetic response. Compos Sci Technol, 2022, 217:109092

[7] Qu Y, Wu J, Wang Z, Liu Y, Xie P, Wang Z et al, Radio-frequency epsilon-negative property and diamagnetic response of percolative Ag/CCTO metacomposites. Scripta Mater, 2021, 203:114067

[8] Wu H, Zhong Y, Tang Y, Huang Y, Liu G, Sun W et al, Precise regulation of weakly negative permittivity in $CaCu_3Ti_4O_{12}$ metacomposites by synergistic effects of carbon nanotubes and grapheme. Adv Compos Hybrid Mater. (2021) https://doi.org/10.1007/s42114-021-00378-y

[9] Soyeon Park, Wan Shou, Liane Makatura, Wojciech Matusik, Kun (Kelvin) Fu, 3D printing of polymer composites: Materials, processes, and applications, Matter, Volume 5, Issue 1, 2022, Pages 43-76, ISSN 2590-2385, https://doi.org/10.1016/j.matt.2021.10.018.

[10] D. W. Hatchett and M. Josowicz, Composites of intrinsically conducting polymers as sensing nanomaterials, *Chem. Rev.*, 2008, 108, 746 —769.

[11] ernardo Marinho, Marcos Ghislandi, Evgeniy Tkalya, Cor E. Koning, Gijsbertus de With, Electrical conductivity of compacts of graphene, multi-wall carbon nanotubes, carbon black, and graphite powder, Powder Technology, Volume 221, 2012, Pages 351-358, ISSN 0032-5910, https://doi.org/10.1016/j.powtec.2012.01.024.

[12] Yoo, D.-Y.; You, I.; Lee, S.-J. Electrical Properties of Cement-Based Composites with Carbon Nanotubes, Graphene, and Graphite Nanofibers. *Sensors* **2017**, *17*, 1064. https://doi.org/10.3390/s17051064.

[13] Ian A. Kinloch et al. Composites with carbon nanotubes and graphene: An outlook. Science 362,547-553(2018). DOI:10.1126/science.aat7439.

[14] Zhongyang Wang, Kai Sun, Peitao Xie, Qing Hou, Yao Liu, Qilin Gu, Runhua Fan, Design and analysis of negative permittivity behaviors in barium titanate/nickel metacomposites, Acta Materialia, Volume 185, 2020, Pages 412-419,,ISSN 1359-6454, https://doi.org/10.1016/j.actamat.2019.12.034.

[15] Zhuo Wang, Jiahao Fana, Xu Guoa, Jiamin Jia and Zixiong Sunb, Enhanced permittivity of negative permittivity middle-layer sandwich polymer matrix composites through conductive filling with flake MAX phase ceramics, RSC Adv., 2020, 10, 27025-27032, DOI: 10.1039/D0RA03493B.

[16] Y. Dong and T. Itoh, "Metamaterial-Based Antennas," in *Proceedings of the IEEE*, vol. 100, no. 7, pp. 2271-2285, July 2012, doi: 10.1109/ JPROC. 2012.2187631.

[17] Zaixin Wei, Zhongyang Wang, Ciqun Xu, Guohua Fan, Xiaoting Song, Yao Liu, Runhua Fan, Defect-induced insulator-metal transition and negative permittivity in La1-xBaxCoO3 perovskite structure, Journal of Materials Science & Technology, Volume 112, 2022, Pages 77-84, ISSN 1005-0302, https://doi.org/10.1016/j.jmst.2021.11.002.

[18] Anju K, Libu K. Alexander, Extremely low-frequency plasmonic state achieved in AC-ZnO polymer composite for tuned negative permittivity applications, Materials Research Bulletin, Volume 172, 2024, 112649, ISSN 0025-5408, https://doi.org/10.1016/j.materresbull.2023.112649.

CHAPTER 8

SUMMARY AND CONCLUSIONS

8.1 Summary and Conclusions

The thesis titled ***"Polymer Nanocomposites for Phthalate Detection, Remediation, and Metamaterial Applications"*** is a product of our motivation to extend the microstructure tuning capabilities of polymers to relevant environmental and dielectric applications. For environmental applications, we focused on detecting and removing phthalates. For dielectric applications, we addressed a significant gap in the availability of suitable metamaterials for extremely low-frequency (10^1 to 10^{-2} Hz) applications. We also explored, in detail, the mechanisms behind the enhanced activity of polymer nanocomposites for the application we reported. Our investigation primarily focused on the five objectives in Chapter 1, Section 1.5. Guided by these objectives, we explored the surface-tuning properties of polymers and their composites for our applications of interest.

In this thesis, Chapter 3 is focused on the successful synthesis of semiconductor-based Surface-Enhanced Raman Scattering (SERS) substrates tailored for ultra-sensitive and selective detection of phthalates viz dimethyl phthalate (DMP) and diethyl phthalate (DEP). We developed two novel noble metal-free SERS substrates based on $BaTiO_3$ and PMMA_$BaTiO_3$. Unlike traditional high-temperature synthesis methods exceeding 1000 °C, a low-temperature sol-gel route was employed to synthesise $BaTiO_3$. Structural and morphological analyses were done using X-ray diffraction (XRD), Scanning Electron Microscopy (SEM), and Micro-Raman spectroscopy. As demonstrated by the SEM images, the dense arrangement of cuboidal and tubular morphology hotspots on the substrate significantly enhanced the weak Raman signals of DMP and DEP. Moreover, our substrate design ensured that the Raman bands of the SERS substrate and the probe molecule do not coincide, enabling precise and unambiguous detection. The primary mechanism behind the SERS activity of $BaTiO_3$ (BT) and PMMA_$BaTiO_3$ films (PBT) is charge transfer resonance, bolstered by the strong affinity between BT and

DMP and between PBT and DEP.

Chapter 4 describes our subsequent efforts to utilise a flexible noble metal-free SERS substrate for detecting phthalates- this time, DEHP. We successfully designed and fabricated PMMA_$SrTiO_3$ substrates featuring morphologically created micro-spherical hotspots. These densely packed porous hotspots significantly enhanced the affinity towards the probe molecule, leading to increased Raman scattering. We proposed a mechanism for DEHP detection based on charge transfer-mediated chemical enhancement. The distinguishable, non-coinciding bands corresponding to DEHP and PMMA_$SrTiO_3$ simplify the detection process, making it more efficient and effective. These investigations could pave the way for the future design and fabrication of surface-engineered, flexible, noble metal-free SERS substrates with indispensable Raman peaks using semiconductor-modified noble metals for environmental applications.

Our research to remove low-density phthalates from the water system by a metal oxide-incorporated polymeric matrix is reported in Chapter 5. Persuaded by the remarkable efficiency of ZnO nanoparticles, we have explored the capability of Polypyrrole_ZnO (PPy_ZnO) polymer nanocomposites in removing low-density phthalate from aqueous systems. The synthesis approach suggests high-yield production of the composites through a cyclic chain reaction. The nanocomposite is effective for both high and low concentrations of plasticizer removal from aquatic systems. The nanocomposite rapidly and efficiently eliminated DMP from solutions, with substantial removal achieved within a short time frame. The enhanced DMP adsorption is attributed to the synergistic effects of slit-like micropores and conjugated benzene rings in the PPy-ZnO, where DMP molecules are trapped and held primarily by electrostatic attraction, hydrogen bonding, and π-π interactions. This research underscores that engineered surface functional groups in polymer nanocomposites can be utilized to develop high-performance phthalate adsorbents, offering a promising solution for water pollution. Considering their impressive adsorption capacity, ease of synthesis, and cost-effective availability of polymer precursors, these adsorbents show great potential for removing DMP from aqueous solutions.

Chapter 6 of this thesis addresses the significant need for metamaterials suitable for extremely low-frequency (ELF - 10^1 to 10^{-2} Hz) applications. The objective was to design and investigate flexible composites with surface microstructure-induced negative permittivity, essential for metamaterial properties. Ternary flexible composites were successfully designed and synthesised using poly (methyl methacrylate) (PMMA), activated carbon (AC), and zinc oxide (ZnO) through an in-situ polymerisation process. The evolution of composite microstructure, influenced by PMMA voids and AC_ZnO filler concentration, notably affected the material's dielectric characteristics. The presence of free-moving ions and delocalised electrons within the 3D conductive networks formed via percolation induced a plasmonic state, leading the permittivity of the ternary meta-composites to transition from positive to negative. Furthermore, the transition region of the composites' negative permittivity was controlled by adjusting the content of activated carbon and ZnO nanoparticles. The permittivity and AC conductivity of the composites were analysed using a BDS Analyzer, revealing that the magnitude and negative permittivity can be tailored by varying the AC_ZnO filler content. Flexible composites engineered to achieve optimal permittivity values for extremely low-frequency (ELF) applications are primed to fulfil substantial industrial needs.

In Chapter 7 of this thesis, we adopted an efficient strategy to enhance the magnitude of negative dielectric constant values of flexible ternary composites by incorporating a ceramic component. Specifically, we successfully designed and synthesised a poly (methyl methacrylate) (PMMA), graphite, and $CaTiO_3$ ternary nanocomposite through an in-situ polymerisation process. The evolution of microstructure in these composites is influenced by the presence of PMMA voids, which play a crucial role in shaping their dielectric properties. In particular, the incorporation of ceramics promoted percolation pathways for charge carriers and polarisation mechanisms, which collectively amplified the material's ability to exhibit negative permittivity. This enhancement is crucial for developing advanced metamaterials capable of manipulating electromagnetic waves in novel and efficient ways, particularly in applications requiring tailored dielectric properties at extremely low frequencies.

Throughout our thesis, we successfully achieved our objectives by employing innovative approaches to synthesise nanocomposite materials harnessing the unique structural properties of polymers. We addressed both environmental and dielectric challenges, tailoring our polymer nanocomposites to effectively detect and remove phthalates in water sources. In this thesis we have developed noble metal-free flexible SERS substrates with expansive surface areas and adaptable surface chemistry, significantly boosting sensitivity and selectivity for detecting low concentrations of phthalates. The exceptional adsorption capacity and chemical functionality demonstrated in the polymer nanocomposite enabled efficient capture and removal of phthalate molecules from polluted water sources. The successful creation of hotspots in polymer nanocomposite led to bridging a critical gap in metamaterial application, specifically for extremely low-frequency dielectric applications.

CHAPTER 9

RECOMMENDATIONS

Recommendations for future studies

Based on the comprehensive findings and conclusions drawn from the thesis, we propose the following future research directions and applications:

- Advancing SERS substrate technology: Future research holds promise in advancing the technology of noble metal-free flexible SERS substrates, aiming to enhance their sensitivity and selectivity for detecting a wide range of environmental contaminants. Further exploration into novel nanocomposite configurations and innovative synthesis methods is crucial to expanding the applicability of these substrates beyond phthalates, thereby addressing emerging environmental challenges. Commercialising these advanced SERS substrates could enable their deployment in real-time applications, revolutionising environmental monitoring and offering robust solutions for sustainable resource management.

- Broadening Environmental Remediation Techniques: Expanding on the success of polymer-metal oxide nanocomposites in Chapter 5, future studies could investigate their efficacy in removing a wider range of pollutants from water systems. This could involve optimising adsorption capacities, exploring new floating flexible functional materials, and scaling up processes for practical environmental applications.

- Innovations in Metamaterial Development: Building on the advancements in metamaterials for ELF applications discussed in Chapter 6, future research could focus on refining the design parameters and material compositions. Exploring new filler materials, optimising percolation pathways, and integrating advanced characterisation techniques could further tailor these materials for specific dielectric applications.

- Integration of Ceramic Components in Composites for Dielectric Applications: Continuing from Chapter 7, future investigations could delve deeper into the role of ceramics in enhancing the dielectric properties of polymer composites. Research could explore new ceramic-polymer combinations, investigate their impact on percolation thresholds and polarisation mechanisms, and study their applicability in advanced metamaterial designs.
- Mechanistic Understanding and Modelling: Further studies could aim to deepen the understanding of the underlying mechanisms governing the enhanced functionalities observed in polymer nanocomposites. Utilising advanced modelling and simulation techniques could provide insights into structure-property relationships, aiding in the rational design of next-generation materials with tailored properties.
- Validation in Real-world Applications: Collaborations with industry partners and environmental agencies could facilitate pilot testing and verification of developed technologies in real-world settings. This would assess their scalability, cost-effectiveness, and environmental impact, paving the way for practical implementation and commercialisation.

By pursuing these recommendations, the thesis work can contribute significantly to advancing environmental monitoring technologies, improving water quality management strategies, and fostering innovations in metamaterials for under-sea communication and sensing applications. These efforts not only promise scientific advancement but also hold the potential for addressing pressing global challenges related to environmental sustainability and innovations in communication.